

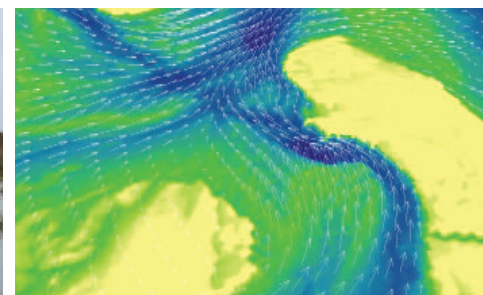
RP# 2020-09

---

# FINAL REPORT

## Monitoring and Modeling Sound-Side Erosion near Oregon Inlet to Support Feasibility Level Transportation Planning

AUGUST 2022



**ORIGINAL**

**SUBMITTED BY**

Elizabeth J. Sciaudone, Ph.D., P.E.  
North Carolina State University  
Raleigh, North Carolina

Liliana Velásquez-Montoya, Ph.D.  
Anna Wargula, Ph.D.  
Tori Tomiczek, Ph.D.  
United States Naval Academy  
Annapolis, Maryland

Elizabeth Smyre, P.E.  
Dewberry  
Raleigh, North Carolina

---

**Technical Report Documentation Page**

1. Report No. FHWA/NC/2020-09		2. Government Accession No.		3. Recipient's Catalog No.	
4. Title and Subtitle  Monitoring and Modeling Sound-Side Erosion near Oregon Inlet to Support Feasibility Level Transportation Planning				5. Report Date August 2022	
				6. Performing Organization Code	
7. Author(s) Elizabeth J. Sciaudone, Ph.D., P.E. <a href="https://orcid.org/0000-0003-2313-2172">https://orcid.org/0000-0003-2313-2172</a> Liliana Velásquez-Montoya, Ph.D. <a href="https://orcid.org/0000-0001-6703-6217">https://orcid.org/0000-0001-6703-6217</a> Anna Wargula, Ph.D. <a href="https://orcid.org/0000-0002-2736-2656">https://orcid.org/0000-0002-2736-2656</a> Tori Tomiczek, Ph.D. <a href="https://orcid.org/0000-0003-4116-7547">https://orcid.org/0000-0003-4116-7547</a> Elizabeth Smyre, P.E.				8. Performing Organization Report No.	
9. Performing Organization Name and Address  North Carolina State University, CCEE, Box 7908, Raleigh NC 27695 United States Naval Academy, 590 Holloway Road, Mail Stop 11D, Annapolis, MD 21402-5042 Dewberry, 2610 Wycliff Road, Suite 410, Raleigh, NC 27607-3073				10. Work Unit No. (TRAIS)	
				11. Contract or Grant No.	
12. Sponsoring Agency Name and Address North Carolina Department of Transportation Research and Development Unit 104 Fayetteville Street Raleigh, North Carolina 27601				13. Type of Report and Period Covered Final Report  August 1, 2019-July 31, 2022	
				14. Sponsoring Agency Code 2020-09	
Supplementary Notes:					
16. Abstract NCDOT Research Project 2020-09 "Monitoring and modeling sound-side erosion near Oregon Inlet to support feasibility level transportation planning" used field observations, numerical modeling, fragility curves, and engineering analysis to (1) assess the hydrodynamics and erosion processes near Oregon Inlet, (2) estimate the potential for roadway failure based on marsh conditions, and (3) evaluate potential erosion mitigation options for NCDOT. Field measurements were collected over three years to inform the site conditions and the erosion processes at the marsh shoreline and the adjacent flood channel, and a classification system was developed to visually assess the erosion condition of the marsh shoreline. Bathymetric observations show that the flood channel is rapidly migrating landward. The locations where the channel is closest to the shoreline correspond to the highest short-term erosion (0.7 m to 2.7 m (2.3 ft to 8.9 ft) during storms) and long-term erosion rates (2 m/yr to 4 m/yr (6.6 ft/yr to 13 ft/yr)), as well as a severely eroded shoreline condition observed in the field. Observation data and numerical modeling results were used to develop a series of fragility curves (i.e., probability curves predicting damage, given environmental conditions), which quantify the conditions likely to lead to shoreline erosion or roadway flooding impacts. The fragility curve analysis was used to develop an online vulnerability indicator, which correlates water levels and wave heights measured at the Oregon Inlet Marina and Oregon Inlet Waverider to potential flooding conditions along N.C. 12. A series of erosion mitigation alternatives, including structural, natural or nature-based, and hybrid options, were reviewed to determine the potential engineering, environmental, and regulatory considerations associated with each. Based on the initial screening, six of these options were simulated in a numerical model of the project area to determine the ability of each option to reduce erosive flow velocities. Three alternatives - terminal groin extension, channel relocation, and island restoration - displayed the most effectiveness at reducing flow velocities at the shoreline. The results of this effort provide a feasibility-level review of potential engineering alternatives to address the documented marsh erosion within the project study area as well as insight on the engineering, environmental, and regulatory constraints associated with these alternatives.					
17. Key Words Estuarine Erosion Numerical Modeling Coastal Erosion Mitigation			18. Distribution Statement		
19. Security Classif. (of this report) Unclassified	20. Security Classif. (of this page) Unclassified	21. No. of Pages 223	22. Price		

## **DISCLAIMER**

The contents of this report reflect the views of the author(s) and not necessarily the views of the University. The author(s) are responsible for the facts and the accuracy of the data presented herein. The contents do not necessarily reflect the official views or policies of either the North Carolina Department of Transportation or the Federal Highway Administration at the time of publication. This report does not constitute a standard, specification, or regulation.

# Executive Summary

NCDOT Research Project 2020-09 “Monitoring and modeling sound-side erosion near Oregon Inlet to support feasibility level transportation planning” used field observations, numerical modeling, fragility curves, and engineering analysis to (1) assess the hydrodynamics and erosion processes near Oregon Inlet, (2) estimate the potential for roadway failure based on marsh conditions, and (3) evaluate potential erosion mitigation options for NCDOT. The summary of these results is as follows:

- (1) Currents inside the flood channel adjacent to the eroding shoreline are ebb-dominated, with observed 0.91 m/s (1.8 knot) ebbing currents to the northwest and 0.49 m/s (1.0 knot) flooding currents to the southeast. The tides (0.46 m (1.5 ft) amplitude) are semidiurnal, and the processes unrelated to tides (e.g., sustained winds and ocean-side waves) are significant, leading to sustained ebbing or flooding currents in the flood channel over several tidal cycles. Elevated oceanside wave heights (> 3 m (10 ft)) increase flood levels in the marsh. Bathymetric observations show that the flood channel adjacent to the shoreline is rapidly migrating landward (**Figure 11**). The locations where the channel is closest to the shoreline correspond to the highest short-term erosion (0.7 m to 2.7 m (2.3 ft to 8.9 ft) during storms, **Table 3**) and long-term erosion rates (2 m/yr to 4 m/yr (6.6 ft/yr to 13 ft/yr), **Figure 10**), as well as a severely eroded shoreline condition observed in the field (**Table 4**).
- (2) Observation data and numerical modeling results were used to develop a series of fragility curves (*i.e.*, probability curves predicting damage, given environmental conditions), which quantify the conditions likely to lead to shoreline erosion or roadway flooding impacts. The fragility curves were developed using three different methodologies, using both water level gauge and NCDOT TIMS roadway closure datasets. The results provided insight on the potential for roadway transect flooding (**Figure 14**) as well as the likelihood of roadway closure due to flooding (**Figure 13**). An additional fragility curve established the probability of the marsh shoreline being classified as either “severely eroded” or “eroded” (**Figure 15**), increasing the potential vulnerability of the marsh and adjacent infrastructure to bay-side flooding.

The results indicated that there is at least a 20 percent chance of flood-related closure for any measured wave heights above 6 m (20 ft); however, any increases in water level could lead to increased chances of flooding for lower wave heights (**Figure 13, Table 11, Table 12**). Within the study area, the chance of flooding increases with both an increase in water level at the marina combined with a decrease in distance from the marsh shoreline to the road. For any water levels greater than 2 m (6.7 ft), there is at least a 20 percent chance of sound-side flooding for locations where the road is within 100 m (328 ft) of the marsh shoreline (**Figure 14, Table 13**). Based on the importance of marsh buffer distance in numerical model-based fragilities, the condition and vulnerability of the marsh shoreline within the study area was also investigated. Areas of marsh that were classified as “eroded” or “severely eroded” (**Table 4**) were correlated to an increase in long-term erosion rates and shoreline proximity to the nearby flood channel.

- (3) A series of erosion mitigation alternatives, including structural, natural or nature-based, and hybrid options, were reviewed to determine the potential engineering, environmental, and regulatory considerations associated with each. Based on the initial screening, six of these options

(seawalls, bendway weirs, terminal groin extension, jetties, channel relocation, and island restoration) were simulated in a numerical model of the project area to determine the ability of each option to reduce erosive flow velocities. Three alternatives - terminal groin extension, channel relocation, and island restoration - displayed the most effectiveness at reducing flow velocities at the shoreline (**Table 9**), which would be required to reduce marsh shoreline erosion. Channel relocation was shown to impact velocities throughout the flood delta, while island restoration resulted in localized hydrodynamic changes near the estuarine shoreline. Seawall and bendway weirs demonstrated minimal changes in flow velocities at the estuarine shoreline, while jetties caused significant changes in the velocities throughout the inlet system. All the options assessed are expected to require extensive federal and state permitting and associated environmental review, though they represent a range of potential environmental impacts to the inlet system and the adjacent federal lands. A summary of the six options included in the modeling review, along with the advantages and disadvantages of each, is presented in **Table 10**.

The data collection effort and literature review was used to establish a marsh shoreline classification system, which provides a set of criteria for the visual classification of marsh conditions. The system is illustrated in **Table 4** and establishes a methodology for NCDOT and other stakeholders to assess the potential health of the estuarine marsh and to estimate the likelihood of further marsh degradation.

The fragility curve analysis was also used to develop an online vulnerability indicator, which correlates water levels and wave heights measured at the Oregon Inlet Marina and Oregon Inlet Waverider to potential flooding conditions along N.C. 12 (**Figure 21**). Should any of the indicators exceed a threshold (**Tables 11, 12, 13**), an email alert is sent to interested parties to allow for preparedness and mitigation response.

This project was intended to provide a feasibility-level review of potential engineering alternatives to address marsh erosion within the project study area as well as insight on the engineering, environmental, and regulatory constraints associated with potential mitigation alternatives. Combinations of alternatives could also be considered to balance the engineering and environmental considerations, allowing for alternatives that are both effective in high velocity environments and beneficial to local ecology.

Continued collection and review of data on the marsh shoreline position and condition within the project area will be critical to the identification, development, and implementation of erosion mitigation alternatives as well as options for transportation infrastructure. This dataset will provide a robust basis for future engineering and environmental assessments.

# Table of Contents

<b>Introduction and Research Questions</b>	<b>5</b>
<b>Research Methodology</b>	<b>7</b>
<b>Field observations and site characterization</b>	<b>9</b>
Hydrodynamics: Water Levels, Waves, and Currents	13
Morphology and shoreline and marsh erosion classification	15
<b>Fragility curves and potential erosion mitigation alternatives.</b>	<b>21</b>
Numerical model of existing conditions and bay-side storms	21
Development of fragility curves	24
Fragility Curve Development Methodology	24
Results of Fragility Curve Derivations	25
Implications of Fragility Curves	28
Considerations for Fragility Models	29
Compilation and Qualitative Review of Mitigation Options	30
Compilation of nature-based, structural, and hybrid options for assessment	30
Simulation of potential erosion mitigation alternatives	31
Simulation Conditions and Proposed Alternative Assessment Rating	35
<b>Decision making tools and information</b>	<b>37</b>
Alternative Modeling and Effectiveness Assessment	37
Alternatives Effectiveness at Reducing Erosive Flows at the Shoreline	37
Spatial Changes in Velocities Across the Inlet During Peak Tidal Flows	39
Assessment of Alternatives	43
Online vulnerability indicator/notification system	46
Field Database Description	48
<b>Recommendations and Next Steps</b>	<b>49</b>
Considerations for future assessments	49
Research implications	50
<b>Acknowledgements</b>	<b>51</b>
<b>References</b>	<b>51</b>
<b>Attachments/Appendices</b>	<b>56</b>
A. Field reports	
B. Summary of Erosion Mitigation Options	
C. Vulnerability Indicator	
D. Submitted Paper: Modeling the hydrodynamics of a tidal inlet during bay-side storms.	
E. Submitted Paper: Hydrodynamics of a tidal inlet under gray to green coastal protection interventions	
F. Field Data Database File Descriptions	

# I. Introduction and Research Questions

The ongoing southward migration of Oregon Inlet was interrupted in the early 1990s after the construction of the terminal groin on Hatteras Island for the protection of the southern abutment of the Herbert C. Bonner Bridge. Although the terminal groin stabilized the shoreline as designed, the inlet channels and shoals have continued to adjust and respond to ongoing oceanographic and meteorological conditions, as well as human activities. These activities include ongoing dredging as well as actions associated with construction of the Basnight Bridge, which opened in 2019, and removal of the Bonner Bridge.

Ongoing monitoring along the Pea Island National Wildlife Refuge (Velasquez-Montoya et al. 2021) identified high rates of inner-bank erosion (up to 4 m/year) along the marsh at the north end of Hatteras Island (Figure 1). Continued erosion along this estuarine shoreline could increase the vulnerability of the existing and future N.C. 12 roadway from the sound side. This project was designed to study the possible drivers of this erosion, including the migration and curvature of the southernmost flood channel of the inlet, flow velocities, inundation depths, and locally-generated waves, as well as to explore potential mitigation options to support feasibility level transportation planning for NC 12. This information has implications for both NCDOT's future infrastructure planning decisions as well as stakeholders' (including the U.S. Fish and Wildlife Service and National Park Service) estuarine shoreline management decisions.



**Figure 1.** Eroding shoreline edge on the estuarine side of the Pea Island National Wildlife Refuge near the abutment of the Marc Basnight Bridge (Pictures taken in March, 2021)

The research questions addressed in this project are:

1. *What are the ranges of flow velocities, wave, and wind conditions causing estuarine shoreline erosion near Oregon Inlet in the short-term (storms) and long-term (months to years)?*
2. *Are there technically feasible mitigation options that could be implemented at this location that could help slow down or stop estuarine shoreline erosion?*

This final report provides an overview of the research methodology (Section II), a summary of the field observations and site characterization (Section III), a description of fragility curves developed to describe the probability of roadway and marsh impacts from given wave and water level conditions (Section IV), numerical modeling and evaluation of potential mitigation alternatives (Section IV), a summary of the decision-making tools developed as part of this project (Section V), and finally the recommendations and next steps (Section VI).

## II. Research Methodology

The methodology outlined in Figure 2 summarizes the approach taken to answer the research questions. To identify the conditions leading to estuarine erosion in the study area (Question 1), field measurements of currents, water levels, wave heights, and wind conditions were performed, as well as analyses of existing data sets. Details of the field investigations are provided in previously submitted interim reports, included here in Appendix A. This information was used along with numerical modeling to develop fragility curves, which quantify the conditions likely to lead to shoreline or roadway “failure” as defined in Section III.B. To identify technically feasible mitigation options that could potentially be implemented in the study area (Question 2), a literature review of a wide range of erosion mitigation projects was used to establish a list of potential mitigation measures (Appendix B). A subset of these measures were evaluated using numerical modeling techniques.

The primary outcomes of this research are tools and information for decision-making and future planning. The results of the literature review and numerical modeling are presented in a table listing the advantages and disadvantages as well as the performance of each mitigation alternative. This table can be used to decide whether various mitigation options merit further investigation. The threshold storm conditions identified using the fragility curves, can be implemented with an online tool, which will provide an email alert when conditions likely to cause roadway flooding thresholds occur.

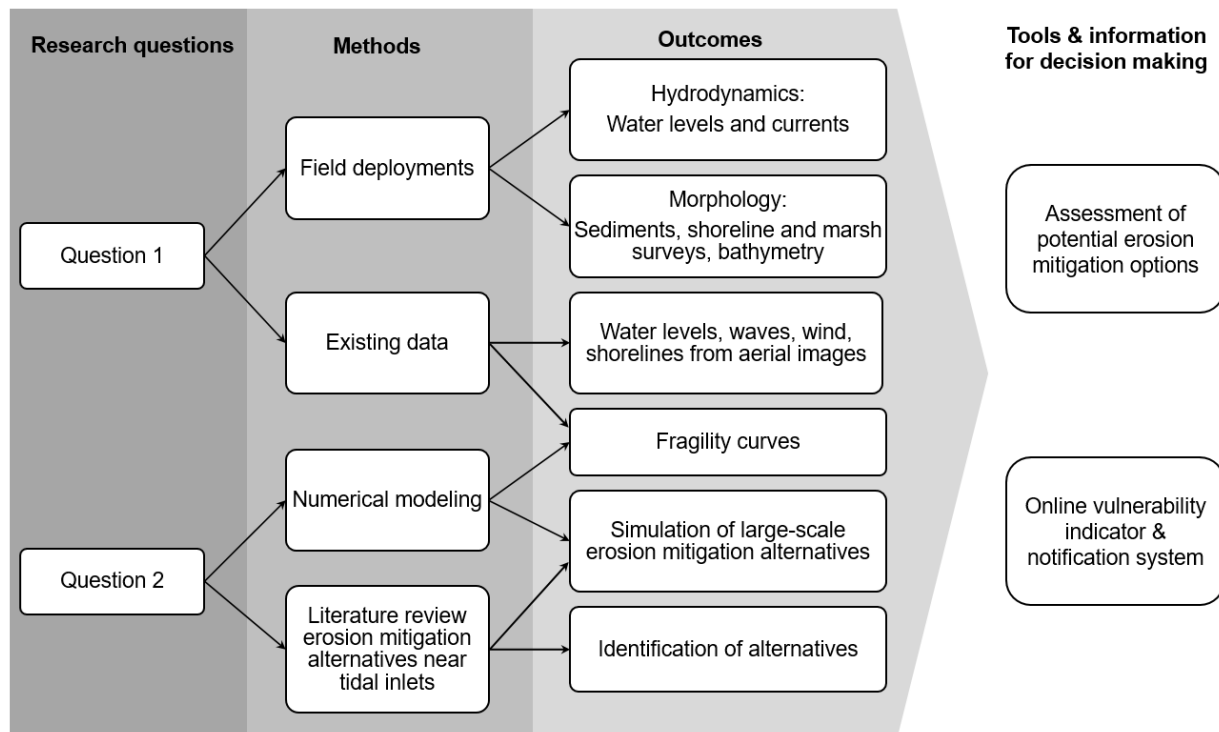


**Figure 2.** Schematic of the research project approach and outcomes.

The focus of the study is the roadway, marsh, and adjacent tidal channel on the estuarine side of the north end of Hatteras Island, shown in Panel C of Figure 3. Bathymetric contours shown were developed from data collected by Woods Hole Oceanographic Institute researchers in April 2021 (Over et al., 2022). This figure also shows the locations of the NOAA stations Oregon Inlet Marina (water levels and meteorological data) and the Oregon Inlet Waverider (wave height, period, and direction). Data at these stations are publicly available via the National Oceanic and Atmospheric Administration (NOAA).

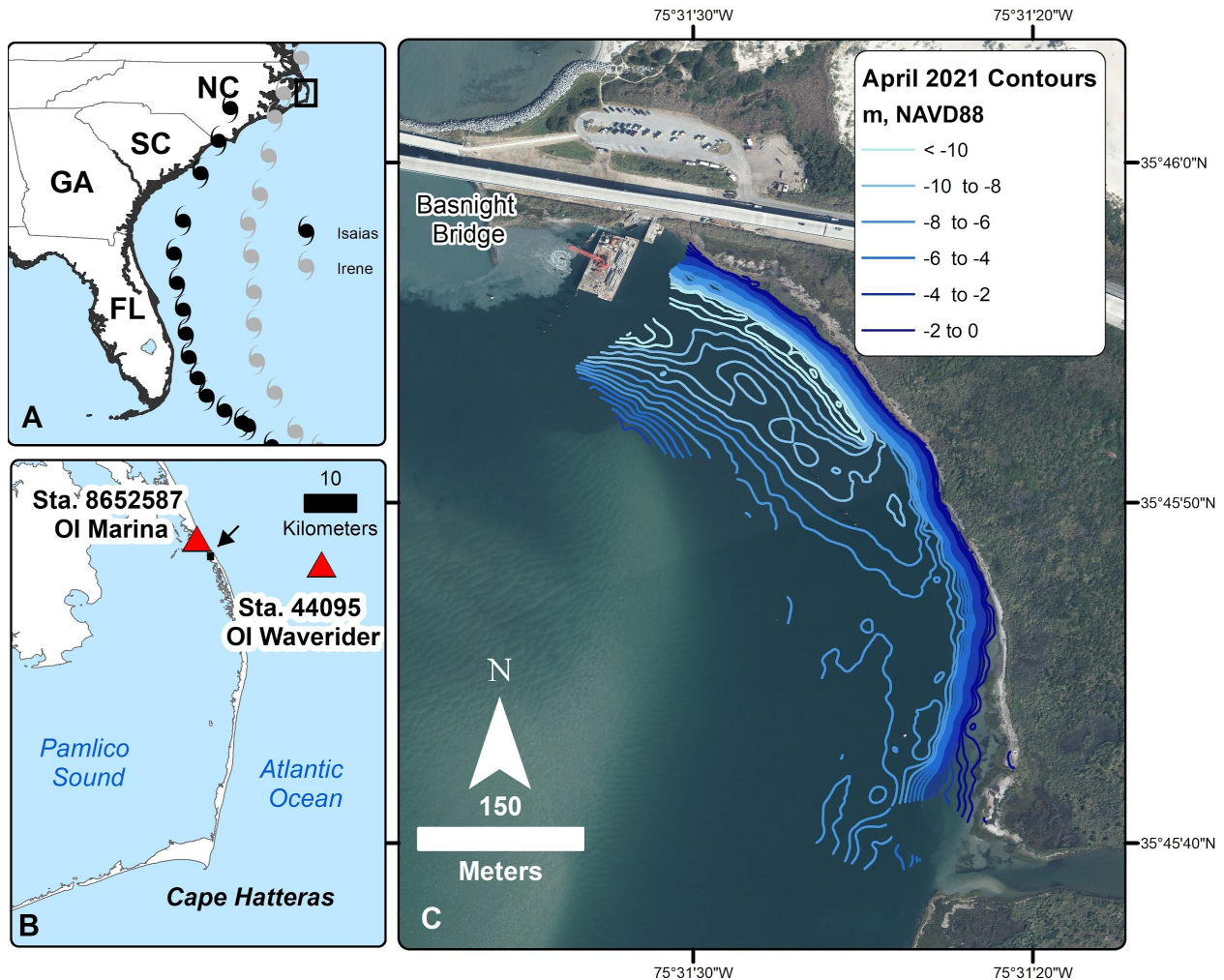


**Figure 3.** Panel A indicates the region of Panel B along with the paths of the two most recent bay-approaching hurricanes (Hurricane Irene in 2011 and Hurricane Isaias in 2020). Panel B shows the location of the two permanent data collection stations near the study area. Panel C shows the region of focus for this study, including the estuarine shoreline, adjacent channel, and marsh at the north end of Hatteras Island. NCDOT photo: 30 September 2021.

### III. Field observations and site characterization

Field measurements conducted under auspices of this project took place from October 2019 to November 2021 (Table 1) and are outlined in four reports included in Appendix A. Field measurements from 2019 included measurements of marsh flooding, water levels, boat-mounted currents during the flood tide, bathymetry, and sediment samples (Appendix A-01) as well as pre- and post-storm shoreline surveys (Appendix A-02). Field measurements from 2020 included marsh flooding, water levels, currents, two shoreline surveys, and a wrackline survey (Appendix A-03). Field measurements from 2021 included marsh flooding, water levels, boat-mounted currents during flood and ebb, and five shoreline and wrackline surveys (Appendix A-04).

**Table 1.** Schedule of fieldwork. Shaded cells indicate measurements taken continuously over several weeks, and check marks indicate measurements taken in a single visit to the site. See Appendix A for detailed field reports.

	2019			2020											2021												
	Oct	Nov	Dec	Jan	Feb	Mar	Apr	May	Jun	Jul	Aug	Sep	Oct	Nov	Dec	Jan	Feb	Mar	Apr	May	Jun	Jul	Aug	Sep	Oct	Nov	
Marsh Flooding																											
Water Levels																											
Currents	✓																										
Shoreline Survey		✓																									
Wrackline Survey		✓																									
Bathymetry	✓																										
Sediment Samples	✓																										

Currents were measured using an acoustic Doppler current profiler (ADCP, a Nortek Signature1000<sup>1</sup>), which was fixed to the side of a boat to measure spatial variability in currents in 2019 and 2021 (left hand panel of Figure 4) and two ADCPs (a Nortek Signature1000 and a Nortek Aquadopp<sup>2</sup>) fixed to the seafloor to measure temporal variability in currents in 2020 (right hand panel of Figure 4).

<sup>1</sup> <https://www.nortekgroup.com/products/signature-1000>

<sup>2</sup> <https://www.nortekgroup.com/products/aquadopp-profiler-2-mhz>



**Figure 4.** Spatial variability in currents were measured from a boat in 2019 and 2021 (left hand image, October 2019) and temporal variability in currents were measured from a bottom structure in 2020 (right hand image, August 2020).

Water levels and marsh flooding were measured with Onset HOBO pressure gauges<sup>3</sup> fixed to the seafloor on concrete structures or onto the land on a metal base (Figure 5). These hydrodynamic measurements of marsh flooding levels, water levels, and currents from 2019 to 2021 were used to understand the drivers of flood events and to compare local hydrodynamics with those measured at existing monitoring stations, the results of which informed the development of fragility curves (Section IV) and the online vulnerability indicator (Section V). The hydrodynamic measurements in 2019 and 2020 were also used to calibrate and validate the numerical model (Section IV).



**Figure 5.** To measure water levels, pressure gauges were deployed in PVC cases on concrete structures near the shoreline edge (left hand image, September 2021). Marsh flood depth was measured by a pressure gauge in a PVC case fixed to the ground (right hand image, March 2020).

<sup>3</sup> <https://www.onsetcomp.com/products/data-loggers/u20-001-01/>

Shoreline and wrackline positions were measured with a Trimble R10 GNSS GPS system<sup>4</sup> (Figure 6). Shoreline position surveys informed shoreline fragility curve development, and wrackline surveys were used to understand the spatial extent of flooding during extreme events.



**Figure 6.** Trimble GPS System and Shoreline Surveys (August 2020).

Two bathymetric datasets were collected in the study area as part of a collaboration made possible via the During Nearshore Event eXperiment (DuNEX), a multi-institutional research program organized by the US Coastal Research Program (Cialone et al., 2019). The initial survey was conducted on 10 October 2019 by staff from the National Science Foundation (NSF) Natural Hazards Engineering Research Infrastructure (NHERI) Rapid Response Research (RAPID) program (Berman et al., 2020). The survey was performed using the NHERI RAPID program’s ZBoat 1800 with a single-beam echo sounder (left hand image in Figure 7). The Z-Boat was remotely controlled by NHERI staff and performed soundings, which were located using an onboard Digital Global Positioning System (D-GPS). A second bathymetric survey was conducted on 20 April 2021 by Woods Hole Oceanographic Institution researchers (Over et al., 2022; right hand image in Figure 7). The survey was completed using a single-beam echo sounder with an onboard GPS locator mounted on a remotely driven vessel (Traykovski and Francis, 2021). For the initial survey, vertical elevations were adjusted to NAVD88 using VDatum and validated using water level data from the Marina tide gauge. For the second survey, Post-Processed Kinematic (PPK) processing methodologies were used with the CORS reference station (NCBI) located 10 km from the site to measure the vessel’s position with 3 cm to 5 cm vertical and horizontal accuracy. These data were used to update and refine the numerical model bathymetry near the shoreline (Section IV) and to determine the change in bathymetry during the study, a measurement which informed development of shoreline fragility curves (Section IV).

---

<sup>4</sup> <https://geospatial.trimble.com/products-and-solutions/trimble-r10>



**Figure 7.** Z-boat measuring channel bathymetry using a single-beam echosounder (left hand image, October 2019); remotely-driven kayak measuring bathymetry (right hand image, April 2021).

Sediment samples were collected throughout the area with a grab sampler and a trowel in the flood channel and on land, respectively (Figure 8). Sediment samples were used to estimate median sediment sizes ( $D_{50}$ ) throughout the marsh and in the inlet's flood channel. The  $D_{50}$  was then used to determine the erosion velocity thresholds used to define the effectiveness of erosion mitigation solutions (Section V).



**Figure 8.** Seafloor sediment samples were taken with a grab sampler (left hand image, October 2019) and sediment samples on land were gathered with a trowel (right hand image, October 2019).

The following sections describe the main results of the field campaigns. Section III.A provides an overview of the water level and current conditions observed in the study area, and Section III.B details the observed shoreline, marsh, and sediment characteristics. Detailed information on all field campaigns may also be found in Appendix A. Data collected during the field campaigns is provided to NCDOT as text and GIS format files. Details on file formats and locations are available in Section V.C.

## A. Hydrodynamics: Water Levels, Waves, and Currents

The hydrodynamics (water levels and currents) near the sound-side of Hatteras Island are dynamic, owing to proximity to an inlet as well as the large back bay. This section overviews 1) the water levels near Hatteras Island, 2) inundation depths on the marsh, and 3) currents in the south flood channel. In particular, these hydrodynamic measurements are compared with water levels, winds, and waves measured at long-term, real-time monitoring stations nearby to illustrate the drivers of hydrodynamics at Hatteras Island.

There are several long-term, real-time monitoring stations near Oregon Inlet. At the Oregon Inlet Marina, the National Oceanic and Atmospheric Administration (NOAA) maintains a meteorological station measuring wind speed, wind direction, and atmospheric pressure and a tidal gauge measuring water levels, herein referred to as the “Marina” (Figure 3B). Offshore of Oregon Inlet, the University of North Carolina (UNC) Coastal Studies Institute maintains a buoy, herein referred to as the “Waverider Buoy,” measuring wave heights, period, and direction (Figure 3B). However, our field studies have shown that the hydrodynamics at the eroding estuarine shoreline are complex and not easily predictable by these readily available measurements.

Water levels at the eroding shoreline are more strongly influenced by tides than those at the Marina, with tidal constituents accounting for more than 50% of the signal variance (compared to 14% of the signal variance at the Marina tidal gauge). The tidal amplitude is also nearly 3 times greater at the eroding shoreline compared to the Marina tidal gauge, owing to the attenuation of tidal amplitude as the tide travels away from the inlet. Tide-subtracted (i.e., wind- and wave-driven) water levels are similar in amplitude at the two sites and have a low correlation ( $R^2 = 0.27$ ), suggesting that there are also differences in the impacts of winds and waves on water levels. Specifically, the difference in tide-subtracted water level between the Marina and the eroding shoreline is correlated with the north-south wind velocity ( $R^2 = 0.79$ ), consistent with southerly winds pushing water northward to the Marina and northerly winds pushing water southward to Hatteras Island. In addition, non-tidal (e.g., wind and wave) processes near the inlet may impact the water levels on the soundside of Hatteras Island more strongly than those at the Marina.

Flooding along the eroding shoreline varies alongshore, owing to the change in topography and elevation. In the northern part of the marsh, the shoreline elevation is roughly 0.03 m (0.10 ft) NAVD88 and floods during the majority of the tidal cycle. Shoreline elevations increase to roughly 0.34 m (1.12 ft) NAVD88 in the narrow marsh north of the pocket beach, and flooding becomes more infrequent - only occurring during the peaks of higher high tides and high water level events driven by storms. Ocean-side waves, in particular, are important in driving flooding on the marsh; daily peak flood levels on the marsh are correlated with wave heights at the waverider buoy ( $R^2 = 0.42$ ). Flood levels increase in time if there is a sustained duration of large waves over several tidal cycles.

Currents inside the flood channel are ebb-dominated, ranging from -0.91 m/s to 0.49 m/s (-1.77 knots to 0.95 knots), where negative currents are towards the northwest (ebbing) and positive currents are towards the southeast (flooding). Although the tides are semi-diurnal, non-tidal (e.g., wind and wave) processes are significant, leading to sustained ebbing or flooding currents in the flood channel over several tidal cycles. During marsh inundation, which typically occurs when the south flood channel currents are

southeastward (i.e., flooding from the ocean to the bay), the channel flows decrease, potentially owing to increased drag by the vegetation on land.

Table 2 presents a summary of the hydrodynamic measurements during the three years of field campaigns near the eroding shoreline. For each year, the average, maximum, and minimum measurements are presented for total inundation depth on the island marsh, mean-subtracted water level in the flood channel, depth-averaged currents in the flood channel, water level relative to NAVD88 at the Oregon Inlet Marina tidal gauge, wind speed at the Oregon Inlet Meteorological Station, and wave height at the waverider buoy. Minimum values are not presented for total inundation depths on the marsh, since a “minimum” indicates no flooding. Further details and figures showing the measurements can be found in the individual field reports in Appendix A.

**Table 2.** Summary of hydrodynamic (water levels and flow velocities) and wind and wave conditions during field surveys completed in the years 2019, 2020, and 2021.

Year	Dates	Variable (units)	Location	Average	Max	Min
2019 (Appx A-01)	10/11 - 10/22	Total water depth (NAVD88, m) Deployed -0.2 m NAVD88	Hatteras Island marsh	0	0.4	--
	10/11 - 11/10	Total water level (NAVD88, m)	Marina	0.2	0.7	-0.2
	10/11 - 11/10	Total water level (mean-subtracted, m)	Flood channel	0	0.6	-0.4
	10/08	Depth-averaged currents (m/s)	Flood channel	0.5	1.0	0.1
	10/11 - 11/10	Offshore wave heights (m)	Offshore	1.6	4.2	0.5
	10/11 - 11/10	Wind speed (m/s)	Marina	4.6	13.4	0
2020 (Appx A-03)	06/22 - 10/01	Total water depth (NAVD88, m) Deployed 0.3 m NAVD88	Hatteras Island marsh	0.4	0.8	--
	06/22 - 10/01	Total water level (NAVD88, m)	Marina	0.2	0.9	-0.1
	08/26 - 10/01	Total water level (mean-subtracted, m)	Flood channel	0	0.2	-0.2
	08/26 - 10/01	Depth-averaged currents (m/s)	Flood channel	0.4	0.9	0
	06/22 - 10/01	Offshore wave heights (m)	Offshore	1.1	4.9	0.3
	06/22 - 10/01	Wind speed (m/s)	Marina	4.7	18.4	0.2
2021 (Appx A-04)	03/08 - 10/29	Total water depth (NAVD88, m) Deployed 0.1 m NAVD88	Hatteras Island marsh	0.2	0.6	--
	03/08 - 10/29	Total water level (NAVD88, m)	Marina	0.1	0.6	-0.4
	09/23 - 10/29	Total water level (mean-subtracted, m)	Flood channel	0	0.6	-0.4
	10/26, 10/28	Depth-averaged currents (m/s)	Flood channel	0.3	0.6	0
	03/08 - 10/29	Offshore wave heights (m)	Offshore	1.1	5.0	0.4
	03/08 - 10/29	Wind speed (m/s)	Marina	5.1	16.9	0

## B. Morphology and shoreline and marsh erosion classification

The shoreline in the study area consists of intermittent sections of eroding marsh shoreline, sandy pocket beaches, and healthy marsh. In general, the highest erosion rates are in the northern portion of the study area, and healthy marsh growth is observed in the southern portion. This section summarizes findings from 1) sediment sampling, 2) shoreline surveys and shoreline characterization, 3) bathymetric surveys, and 4) long-term shoreline change rates from aerial photography. This section illustrates that Oregon Inlet's flood channel is rapidly migrating landward and that the locations where the channel is closest to the shoreline correspond to the highest short- and long-term erosion rates, as well as a severely eroded shoreline condition observed in the field.

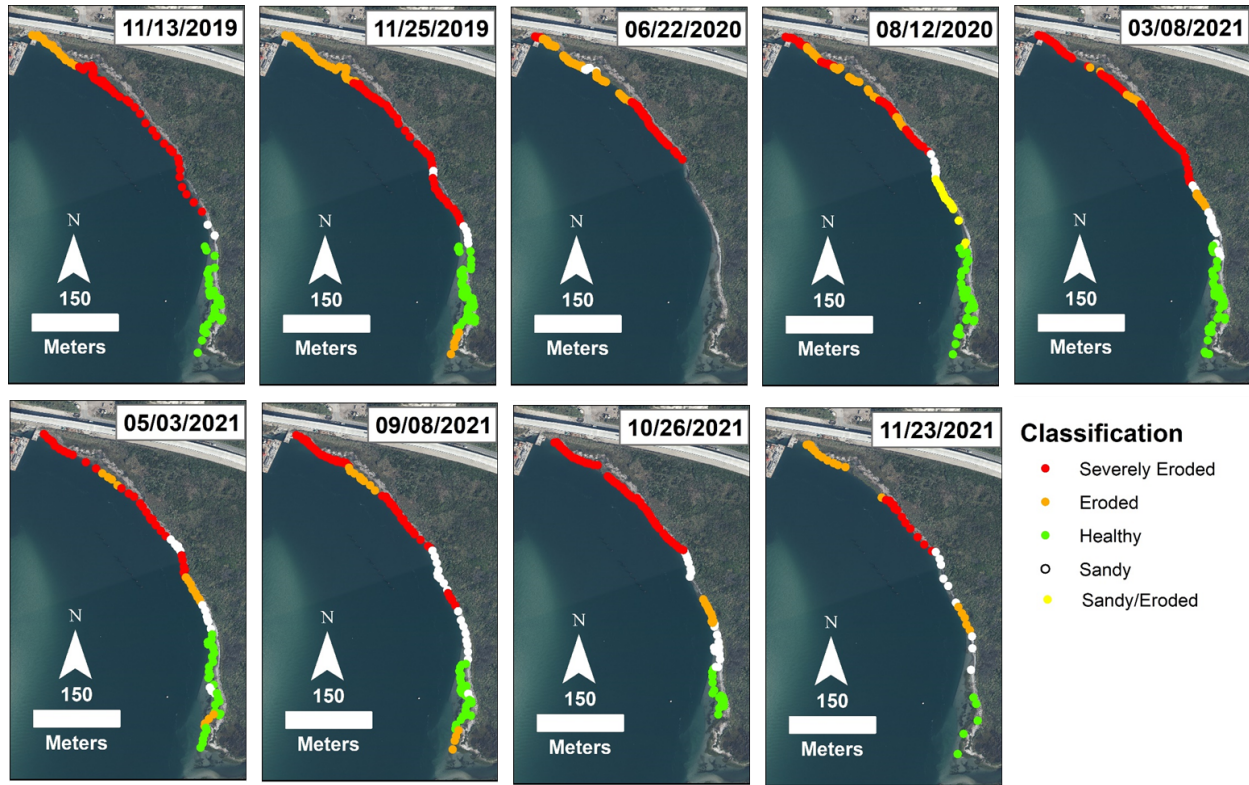
Median sediment grain sizes ( $D_{50}$ ) inside the flood channel ranged from 63  $\mu\text{m}$  to 350  $\mu\text{m}$ , classified as very fine to medium sand on the Wentworth scale. Sediment grain sizes generally increased from north to south along the channel and with cross-channel distance from the shoreline edge. On the marsh,  $D_{50}$  ranged from 31  $\mu\text{m}$  to 63  $\mu\text{m}$  (coarse silt) in the northern part of the marsh and 250  $\mu\text{m}$  to 350  $\mu\text{m}$  (medium sand) in the southern pocket beach. See Appendix A-01 for more details.

Table 3 summarizes the shoreline surveys conducted as a part of this research project. If a storm event occurred between surveys, the event as well as the maximum water level at the Marina and the maximum wave height at the Waverider Buoy are also shown, along with the average and range of shoreline change rate between surveys. As shown in the table, the shoreline is consistently eroding on average over the study time period, with periods of more severe erosion interspersed with less erosion or, in the case of the March to May 2021 time period, there was one survey period with slight accretion on average. Following that short accretional period, the shoreline receded significantly between May and September 2021. After that, there was slight erosion observed between October and November 2021.

**Table 3.** Summary of shoreline survey dates, largest event, water level, and wave height between surveys, and the average and range of shoreline change measured.

Survey Dates	Purpose/Event	Max Water Level at Marina between surveys (m NAVD)	Max Wave Height at Waverider Buoy between surveys (m)	Average Shoreline Change Between Surveys (m)	Range of Shoreline Change (m)
11/13/2019 (pre-storm)	Nor'easter (11/16 - 20/2019)	0.6 (11/24/2019)	7.6 (11/16/2019)	-2.7 (erosion)	[-10.1, -0.6]
11/25/2019 (post-storm)					
06/22/2020	2020 Baseline	0.9	4.4	-0.8	[-3.2, 0.9]
08/12/2020 (post-storm)	Hurricane Isaias (08/04/2020)	(08/04/2020)	(08/04/2020)	(erosion)	
03/08/2021	2021 Baseline	0.5	5.2	0.2	[-2.1, 3.1]
05/03/2021	Nor'easter (03/19/2021)	(04/29/2021)	(03/19/2021)	(accretion)	
09/08/2021	TS Elsa (07/09/2021)	0.6 (07/29/2021)	2.9 (07/09/2021)	-2.2 (erosion)	[-11.0, 2.6]
10/26/2021 (pre-storm)	Eastern Storm (10/29/2021)	0.9 (10/29/2021)	5.1 (11/07/2021)	-0.7 (erosion)	[-3.9, 1.1]
11/23/2021 (post-storm)					

In addition to the shoreline position surveys, a classification system was developed to determine whether the marsh shoreline condition was healthy, eroded, or severely eroded (Table 4). During each of the surveys, the shoreline was assessed using this system and a category assigned to each survey point. In addition to the marsh shoreline classification, another category for a sandy shoreline was used, where the marsh was not adjacent to the sound. The most severely eroded shoreline was consistently observed in the northern portion of the study area (see Figure 9).



**Figure 9.** Marsh shoreline surveys with classifications for each survey date. Note that due to access and time constraints there were portions of the shoreline that were not surveyed on some of the dates.

**Table 4.** Shoreline and marsh classification scheme

System Rating	Shoreline Condition	Marsh Condition	Example
<b>Healthy</b>	Gentle slope; plant growth on or adjacent to shoreline; minimal to no exposed root mat	Slope < 1:30*; all or majority of marsh above 2' elevation; consistent plant growth throughout marsh, including juvenile plants; intact root mat	
<b>Eroded</b>	Scarp < 1'; evidence of offshore (in-water) plant growth  <i>May include:</i> Evidence of undercutting or cracks, chunks of marsh breaking off along shoreline	Slope between 1:30 and 1:10*; 50% of marsh above 2' elevation; evidence of dead or otherwise removed plants; intact or exposed root mat.  May also show signs of semi-regular flooding, evidence of channel incursion or paleo inlets.	
<b>Severely Eroded</b>	Scarp > 1'; evidence of offshore (in-water) plant growth  <i>May include:</i> Visible chunks of marsh sloughed off into water	Slope > 1:10*; less than 50% of marsh above 2' elevation; significant evidence of dead plants/ no plant growth; exposed root mat, or no evidence of root mat present.  May also show signs of regular flooding, evidence of channel incursion or paleo inlets.	

\*Slope parameter as defined in FHWA, Nature-Based Solutions for Coastal Highway Resilience

In order to supplement the data collected by the marsh shoreline surveys with a longer-term comparison, estuarine shoreline changes were computed using shorelines digitized using aerial photography provided by NCDOT. The photographs span the timeframe September 2003 to April 2021, with images available approximately bimonthly. Figure 10 shows the linear regression shoreline change rates determined using the aerial photo shorelines. Long-term erosion rates over 2 m/year were observed along the northern portion of the study area, with localized rates over 4 m/year.

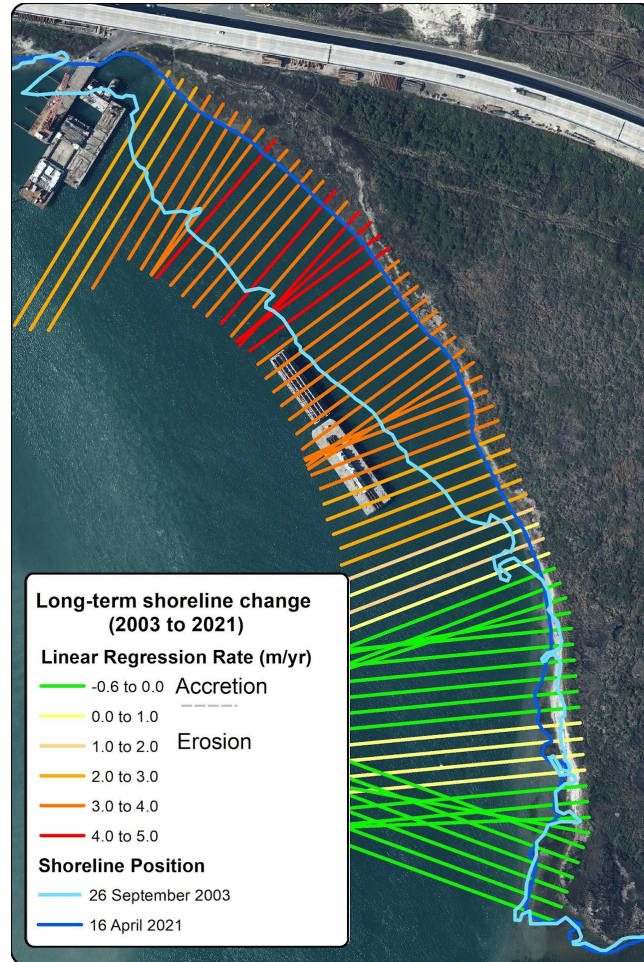


**Figure 10.** Long-term linear-regression shoreline change rate (m/year) at each transect (shore-perpendicular green-to-red lines), determined using bimonthly aerial imagery. 26 September 2003 shoreline position (light blue) and 16 April 2021 shoreline position (darker blue) are shown to illustrate the severity of ongoing erosion in the study area. Note that the shoreline change and the classifications shown in Figure 9 follow the same patterns.

The bathymetric surveys collected during the project were used to determine the position of the deepest part of the channel and to track channel migration along the study area via changes in the 5 m NAVD88 depth contour adjacent to the estuarine shoreline. This contour was chosen because it marks the boundary of the deeper portions of the channel, where velocities are higher. Figure 11 illustrates the channel migration observed in the surveys. As the channel moves closer to the shoreline, particularly in the northern part of the study area, the shoreline also recedes. This supports the conclusion that ongoing channel migration has contributed to the high rates of erosion.

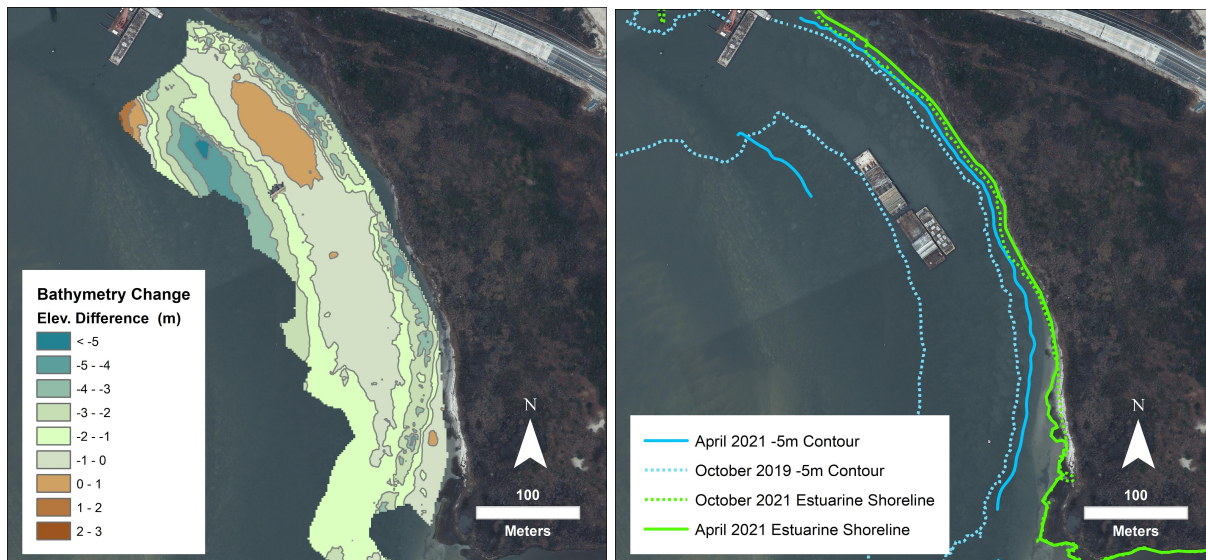


**Figure 11.** Left panel shows the change in bathymetry from 2019 to 2021. Brown colors indicate infilling of the channel to the west with deepening shown by blue colors near the shoreline. Right panel shows the changes in the -5 m elevation contour from 2019 to 2021 along with the shoreline positions. Both panels show that the channel is rapidly migrating closer to the shoreline.

## IV. Fragility curves and potential erosion mitigation alternatives.

Three sets of empirical fragility curves were developed to investigate the vulnerability of N.C. 12 to flood-related closures and the vulnerability of the marsh shoreline to erosion and severe erosion, per Table 4. Two sets of curves were derived to predict roadway vulnerability to flooding based on either publicly available data or numerical model outputs. Publicly available data from the Marina tide gauge, Waverider buoy (Figure 3B), and the NCDOT Traveler Information Management System (TIMS) were synthesized to evaluate the vulnerability of any section of N.C. 12 along the Pea Island National Wildlife Refuge to closure due to flooding from either the ocean or bay-side. Numerical modeling was performed to more thoroughly investigate the potential of bay-side storm events to cause flooding on the section of N.C. 12 passing through the study area near the eroding shoreline of the Pea Island National Wildlife Refuge. Finally, one set of fragility curves was developed to identify marsh vulnerability to erosion based on channel proximity and long-term and short-term stressors. Fragility curves were derived by fitting available data to the Gaussian probability distribution, consistent with previous studies for engineering applications that have fit damage data to normal or lognormal probability distributions (Padgett et al. 2012, Tomiczek et al. 2014, Ellingwood et al. 2004, van de Lindt et al. 2020). Additional details about the fragility model derivations are presented in Tomiczek et al., 2022.

### A. Numerical model of existing conditions and bay-side storms

A two-dimensional depth-averaged numerical model based on Delft3D (Lesser et al., 2004) was set up to simulate the hydrodynamic conditions at Oregon Inlet under 2019 or “present” conditions. The hydrodynamic model extends 35 km alongshore and 27 km cross-shore, including mainland N.C. to the west and ocean depths of about 25 m to the east (Figure 12). The hydrodynamic model has two subdomains that allow for increased resolution near the inlet, where the computational cells reach 15 m in length. Water level boundary conditions are obtained from large-scale simulations of the Advanced Circulation Model (ADCIRC) (Westerink et al., 2008; Luetlich and Westerink, 2004) part of Coastal Emergency Risk Assessment (CERA) archives.

The hydrodynamic model is coupled with the third generation wave model Simulating WAVes Nearshore (SWAN) (Booij et al., 1999). The wave model extends 70 km alongshore with Oregon Inlet located in the middle of the domain to prevent boundary artifacts from reaching the area of interest. Wave boundary conditions are extracted from the Waverider buoy (Figure 3B). Spatially constant, time-varying wind speed and direction are extracted from the Oregon Inlet Marina meteorological station (Figure 3B), and are used for wind- wave growth in SWAN and wind-driven flows in Delft3D.

The bathymetry and topography of the model were obtained from different sources. The bathymetry of the ocean-side was obtained from the 10 m resolution digital elevation model of the North Carolina Floodplain Mapping Project (Blanton et al., 2008). The bathymetry of the Albemarle-Pamlico Sound was extracted from NOAA’s H11032 hydrographic survey and the depths from the inlet channels and shoals were obtained from the 2019 U.S. Army Corps of Engineers (USACE) hydrographic survey (Figure 12). All depths and elevations were converted to meters and referenced from the NAVD88 vertical datum. The

terminal groin in the south shoulder of Oregon Inlet is schematized as a thin dam, which is an infinitely thin object that prevents flow between adjacent computational cells (Deltares, 2022). The piles of the Marc Basnight Bridge are schematized as porous plates using spatially varying energy loss coefficients ranging from 0.03 to 3.75 dependent on the bridge pile sizes relative to the size of the computational cells (Deltares, 2022).

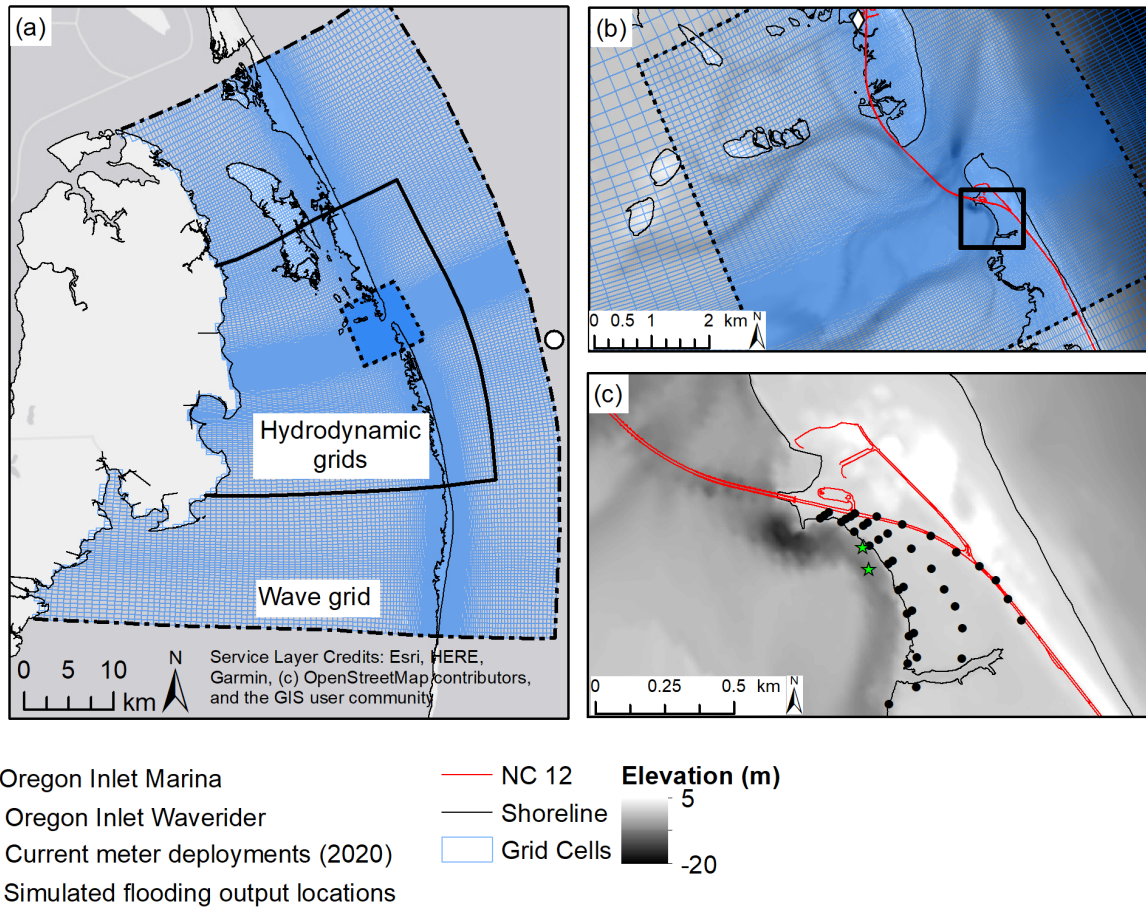


**Figure 12.** (a) Numerical model domain. (b) Hydrodynamic grid and bathymetry near Oregon Inlet. (c) Location of numerical modeling outputs in the study site

The numerical model was calibrated and validated by comparing simulation outputs with measured water levels and depth-averaged velocities near the study site for the periods with field observations collected in 2019 (Appendix A-01) and 2020 (Appendix A-03). Model skill metrics are shown in Table 5, along with the root-mean-square (RMS) magnitudes of the observed and modeled mean-subtracted water levels. Observed and modeled water levels have good agreement (high Pearson Correlation Coefficient (CC), low Root-Mean Square Deviation (RMSD), positive Brier Skill Score (BSS), and Willmott Skill (WS) score over 0.9) at most locations, although the modeled RMS water levels are somewhat smaller than observed RMS water levels. During the validation period (2020 field survey), the model reproduced water level magnitudes and temporal fluctuations in mean-subtracted water levels with reasonable accuracy at the Marina and shoreline (Table 5). Observed and simulated depth-averaged velocity components at the

locations of current meter deployments in 2020 (green stars Figure 12C) were also compared. The model shows excellent agreement with observed major-axis flows (WS score over 0.90) and a high correlation and BSS (Table 5). More details about the model calibration and validation process can be found in Appendix D.

**Table 5.** Skill scores of time-varying water levels during the 2019 and 2020 field surveys.

Year	Location	RMS Observed (m)	RMS Modeled (m)	CC	RMSD (m)	BSS	WS
2019	Marina	0.17	0.14	0.82	0.10	0.68	0.90
	Shoreline South	0.21	0.20	0.85	0.11	0.71	0.92
2020	Marina*	0.12	0.12	0.76	0.08	0.48	0.87
	Shoreline North*	0.16	0.17	0.89	0.08	0.76	0.94
	Thalweg North†	0.41	0.34	0.86	0.22	0.64	0.90
	Thalweg South†	0.40	0.44	0.89	0.22	0.69	0.93

\*Mean-subtracted water level (m), †Major-axis velocity (m/s)

After the model was successfully calibrated and validated, it was applied to study estuarine-side flooding during bay-side storms. Boundary conditions to simulate bay-side storms are based on the water levels observed in the bay and the ocean during Hurricane Irene (2011), which is the hurricane with the largest bay-side storm surge measured since 1979 (Clinch et al., 2012). This hurricane disturbed the water surface for nearly 24 hours, causing a larger change in water levels in the bay compared to the ocean, with peak surge occurring at the inlet during the start of the ebb tide. In the north region of the bay, NOAA’s Oregon Inlet Marina recorded a peak surge (i.e., measured water level minus tidal prediction) of 2.1 m. In the south region of the bay at station 8654467 USCG Station Hatteras, the surge reached 1.1 m. On the other hand, station 8651370 Duck, NC on the ocean side only reached a maximum total water level of 0.9 m, which was only 0.3 m higher than the expected tidal level. Significant wave height on the ocean side at station 44056 Duck FRF, NC located at 17.8 m water depth reached 7.0 m during the peak of the storm.

A set of synthetic storms were designed to have the same duration as Hurricane Irene; however the maximum water levels inside the bay and the wave conditions in the ocean were varied to account for potentially stronger and weaker storms. Given the small surge levels displayed on the ocean side during Hurricane Irene, the open ocean boundary is forced with tidal water levels only. Table 6 shows the range of maximum water levels forced at the lateral model boundaries in the Albemarle-Pamlico Sound. Each one of the water level cases shown in Table 6 is forced with six different maximum significant wave height conditions ranging in 1 m intervals from 2 m to 7 m during the peak of the storm. These values were selected based on historical wave records from the US Army Corps of Engineers Field Research Facility at Duck, NC and the analysis of the wave climate near Oregon Inlet by Velásquez-Montoya et al. (2020). These simulation settings resulted in seven water level cases, each forced with six wave conditions, for a total of 42 synthetic bay-side storm simulations. Flooding or no flooding conditions at the stations shown in Figure 12 were extracted for each storm and used for the development of roadway fragility curves described in the next section of this report.

**Table 6.** Maximum water levels at the bay boundaries and range of wave heights used for each storm case.

Storm	Max. water level at North Bay Boundary (m NAVD88)	Max. water level at South Bay Boundary (m NAVD88)	Wave heights at Ocean Boundary [minimum, maximum] (m)
Case 0 (No Storm)	0.20	0.10	0
Case 1	3.50	1.75	2, 3, 4, 5, 6, 7
Case 2*	2.00	1.00	2, 3, 4, 5, 6, 7
Case 3	0.50	0.25	2, 3, 4, 5, 6, 7

\*Closest case to Hurricane Irene when wave heights = 7 m

## B. Development of fragility curves

### *Fragility Curve Development Methodology*

As described above, fragility curves were developed using three methods. Fragility curves derived using Method 1 were based on publicly available data from 2017 to 2019 of daily environmental conditions from the marina tide gauge and waverider buoy and roadway closure and hazard information for N.C. 12 from the NCDOT TIMS data. Fragility curves created using Method 2 considered numerical outputs at the study site from bay-side storm scenarios. Finally, fragility curves were created to assess marsh vulnerability (Method 3) based on assessments (Section IV.A) of the marsh condition considering shoreline surveys following storm events, long-term erosion rates, and proximity of the nearby channel (Section III.B).

The fragility curves based on publicly available data (Method 1) defined failure as roadway designation as closed or hazardous in the TIMS data. Thus, curves assessed the vulnerability of the roadway to flooding or overwash, causing hazardous travel conditions affecting roadway functionality. Independent variables measured at the Marina tide gauge (Figure 3B) included the maximum daily water level  $WL_{max}$ , peak daily 5-second wind gust,  $V_{winds}$ , and corresponding wind direction  $\theta$ . Water levels were referenced with respect to NAVD88. These variables were considered in addition to the maximum daily significant wave height  $H_{s,max}$  and corresponding dominant wave period  $T_{pd}$  measured at the Waverider buoy (Figure 3B). While TIMS data provided the county and often near-by cities with information about reported incidents, the precise location of closures along N.C. 12 were not able to be determined, and all flood-driven closure events (from either the ocean or the bay) were considered. Therefore, landscape variables such as marsh or beach buffer distances to the roadway were not able to be disaggregated.

For Method 2, numerical model outputs from storm scenarios allowed for investigation of environmental conditions specifically leading to bay-side flooding. Roadway section failure was determined based on a numerical model output of whether a station was shown as flooded (failure) or remained dry over the duration of a storm scenario. Flooding was the most likely indicator of roadway closure in this situation, as the limited dimensions of the infrastructure (two-lane roadway with minimal shoulder) provide minimal opportunity to maintain traffic during inundation events. Variables considered in the numerical model-based fragility curves included significant wave height at the boundary  $H_{s,boundary}$ , peak water level at the Marina tide gauge  $WL_{max,marina}$ , significant wave height at the shoreline  $H_{s,shoreline}$ , and peak water

level at the shoreline  $WL_{max,shoreline}$ . The resolution of the numerical model outputs further allowed for consideration of the marsh buffer distance  $X_{marsh}$  as a potential predictor of roadway vulnerability, where  $X_{marsh}$  is defined as the perpendicular distance between the numerical model output station and the estuarine shoreline.

For fragility curves based on marsh condition (Method 3), two definitions of failure for marshes were considered: one considering failure when the marsh segment was classified as “severely eroded” and one considering failure when the marsh segment was classified as “eroded” or “severely eroded” per Table 4. These classifications were developed based on a literature review (Gittman et al. 2014, Tomiczek et al. 2020, Webb et al. 2019) and field observations at the study area. A detailed classification of the marsh shoreline was performed by the research team in May 2021 and is used in the fragility derivations. The marsh condition is important for both the persistence of the marsh and the performance of the vegetation in shoreline stabilization and infrastructure protection. Possible predictor variables influencing marsh failure included (i) distance from the marsh shoreline to the shore-line-adjacent 5-m depth contour in the channel  $X_{5mcontour}$  based on bathymetric measurements taken in either October 2019 or April 2021 (Figure 11), (ii) the slope of the channel between the 2-m contour and 5-m contour  $m_{2mto5m}$ , (iii) the rapid response erosion rate  $RR$  determined using a linear regression of shoreline positions between November 2019 and March 2021 (Table 3), (iv) the long term erosion rate  $LTR$  measured from satellite images of the shoreline at low tide taken between 2003-2021, and (v) the percentage of time  $T_{BSS} > 0.2$  that the modeled bed shear stress exceeded a critical threshold ( $0.2 \text{ N/m}^2$ ) near the marsh shoreline.

Backward multiple regression was used to determine fragility models for each track within each method, and variables were assessed for importance based on their statistical p-value considering the 99% percent significance level (Gauchi and Chagnon, 2001). Univariate regressions testing the significance of individual variables were also considered for roadway and marsh vulnerability. For the three sets of fragility curve derivations, multiple variable “tracks” were evaluated. Goodness of fit was assessed based on each model’s deviance and  $R^2$  value, which describes the proportion of the variance in the data that is explained by the predictor variables.

### *Results of Fragility Curve Derivations*

Results of the multivariate logistic regression for publicly available data (Method 1) indicate that the maximum daily water level at the Marina tide gauge and maximum significant wave height at the Waverider buoy are significant predictors ( $p < 0.01$ ) of roadway closure due to either ocean or bay-side flooding (Table 7). Figure 13 provides an example of fragility curves for Method 1, showing probability of roadway closure  $P(f)_1$  for four different water levels as a function of significant wave height. Larger significant wave heights and larger water levels cause increased probability of failure (i.e., roadway closure due to flooding). The ranges of water levels and significant wave heights considered in the fragility model are  $-0.20 \text{ m} < WL_{max} < 1.43 \text{ m}$  and  $0.44 \text{ m} < H_{s,max} < 7.59 \text{ m}$ , respectively. The  $R^2$  value for the fragility model is 0.26, indicating that 26% of the variance in the data is accounted for by maximum daily significant wave height and water level at the Waverider buoy and Marina tide gauge, respectively.

**Table 7.** Summary of Fragility Model Derivation Methods, Definition of Failure, Data Sources, Variables Considered, Significant Variables based on  $p < 0.01$ , and model  $R^2$  values.

Method	Failure Definition	Data Sources	Variables Considered	Significant Variables (p-value)	$R^2$
1	Roadway closure due to flooding	Publicly available from TIMS, marina tide gauge, waverider buoy	$H_{s,max}$ , $WL_{max}$ , $T_{pd}$ , $V_{wind}$ , $\theta$	$H_{s,max}$ (1.14e-12) $WL_{max}$ (1.17e-04)	0.26
2	Roadway transect flooding	Numerical model outputs	$H_{s,boundary}$ , $WL_{max,marina}$ , $H_{s,shoreline}$ , $WL_{max,shoreline}$ , $X_{marsh}$	$WL_{marina}$ (8.2e-09) $X_{marsh}$ (2.6e-06)	0.48
3	Marsh condition as severely eroded	Bathymetry data (2019, 2021), aerial shoreline imagery (2003 - 2021), rapid response shoreline measurements	$X_{5mcontour,2019}$ , $X_{5mcontour,2021}$ , $m_{2mto5m}$ , $RR$ , $LTR$ , $T_{BSS>0.2}$	$X_{5mcontour,2019}$ (2.48e-04)	0.46
	$LTR$ (1.39e-04)			0.52	
	$X_{5mcontour,2019}$ (3.11e-04)			0.35	
	Marsh condition as eroded or severely eroded			$LTR$ (1.39e-07)	0.52

The low  $R^2$  of the final model considering peak water levels and significant wave heights (0.26) may partially be owing to differences in local drivers of flooding (e.g., the water level at the shoreline of Hatteras Island (Wargula et al. 2021) from what was measured at publicly available gauges. In addition, other variables not able to be determined from publicly available data (e.g., buffer distance, elevation of flooded roadway) are likely to contribute to roadway vulnerability. Similarly, temporal considerations may also contribute to roadway inundation, such as previous flooding or rainfall events that saturate the soil, duration of sustained directional winds, or duration of flooding and elevated significant wave height conditions.

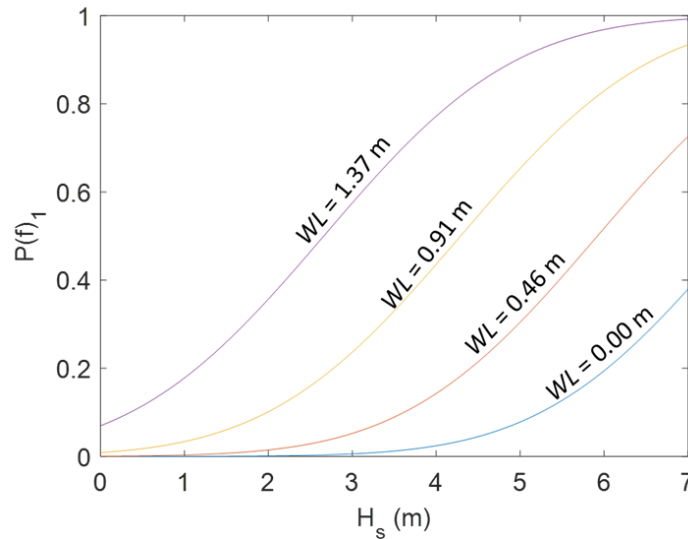


**Figure 13.** Probability of roadway failure  $P(f)_1$ , defined as roadway closure due to flooding based on TIMS data, as a function of peak significant wave height  $H_{s,max}$  (waverider buoy) for four peak water levels (NAVD88, marina tide gauge).

Considering the results of numerical model outputs for storm scenarios (Method 2), roadway vulnerability to bay-side flooding is dependent on peak water level at the marina tide gauge and buffer distance between the roadway transect and shoreline ( $p < 0.01$ ), for Marina water levels ranging from 0.4 m to 2.2 m NAVD88 and buffer distances ranging from 38 m to 563 m. Both water level at the Marina tide gauge and water level at the shoreline are found in separate models to be significant predictors of bay-side roadway flooding and exhibit similar performance ( $R^2 = 0.48$ ). Water level at the Marina tide gauge is selected as the predictor variable in Figure 14, owing to it being readily obtained from publicly available data.

Figure 14A shows the probability of roadway transect flooding  $P(f)_2$  as a function of water level at the Marina tide gauge for a buffer distance of 50 m. 95% confidence intervals are shown as dashed curves, and the solid fragility curve indicates that the probability of roadway flooding increases with increased water levels at the Marina tide gauge. Figure 14B shows the effect of buffer distance on roadway transect flood vulnerability, depicting fragility curves for four buffer distances from the roadway based on water level at the Marina tide gauge. Probability of roadway transect flooding increases with decreasing marsh buffer distance: for a water level at the Marina tide gauge of 2.5 m (NAVD88), the probability of a roadway transect flooding increases from 0.18 for a 200-m buffer to 0.95 for a 50-m buffer. These results highlight the importance of mitigating erosion to maintain large buffer distances between the bay-side shoreline and the roadway.

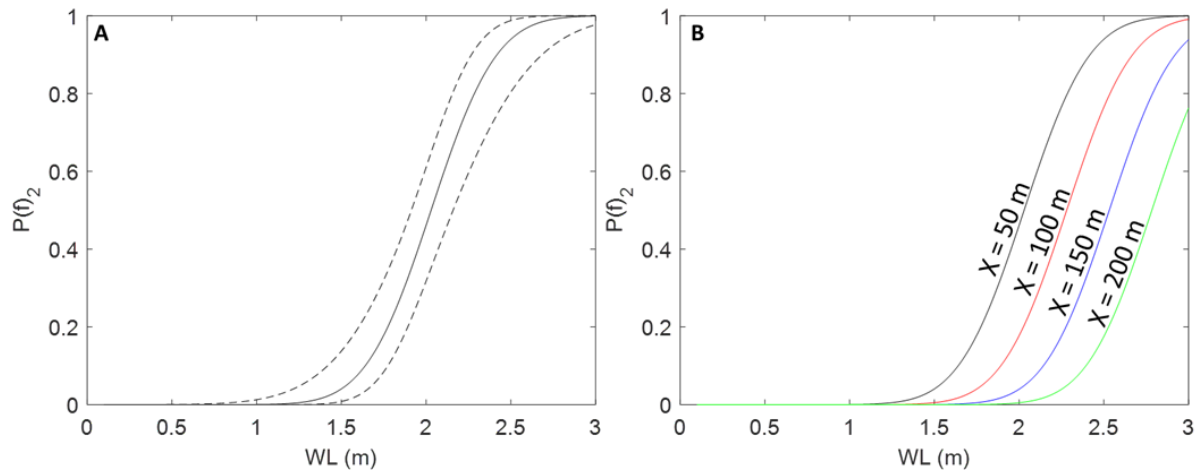


**Figure 14.** Probability  $P(f)_2$  of roadway transect flooding as a function of water level  $WL$  at the marina tide gauge (NAVD88) for (A) buffer distance  $X = 50$  m (black curve) and 95% confidence intervals (black dashed curves); (B) buffer distances  $X = 50$  m, 100 m, 150 m, and 200 m (black, red, blue, and green curves, respectively).

For fragility curves investigating marsh failure (Method 3), the horizontal distance from the marsh shoreline to the 5-m contour in the channel (ranging from 13.2 m to 66.5 m from 2019 data and 7.8 m to 49.5 m from 2021 data), long term erosion rate (ranging from -2.3 m/yr (accretion) to 5.6 m/yr), and slope between the 2-m and 5-m contours in the channel offshore of the marsh segment (ranging from 0.12 to 0.58) obtained from the 2021 bathymetry data are identified in univariate regression as significant variables predicting marsh failure ( $p < 0.01$ ). The fragility model using the 2019 bathymetry data provides a better description of the proportion of the variance in the data (severely eroded model,  $R^2 = 0.46$ ,

severely eroded or eroded model,  $R^2 = 0.35$ ) compared to that fragility model using the 2021 bathymetry data (severely eroded model,  $R^2 = 0.40$ , severely eroded or eroded model,  $R^2 = 0.22$ ). The better performance of the fragility model derived based on 2019 bathymetry data compared to the fragility model based on the more recent survey suggests a lag between channel proximity (determined from bathymetric measurements) and shoreline erosion on a temporal scale of several months to years.

The best overall predictor variable based on statistical significance and  $R^2$  value is the long-term erosion rate, determined from overhead imagery of the marsh shoreline obtained at low tide between 2003 and 2021 (severely eroded model,  $R^2 = 0.52$ , severely eroded or eroded model,  $R^2 = 0.52$ ). Fragility curves are shown in Figure 15 for marsh classification as severely eroded (black curve with markers) or eroded/severely eroded (black curve) as a function of (A) distance to the 2019 5-m contour  $X_{5mcontour,2019}$  and (B) long term erosion rate  $LTR$ . Shoreline data are shown as colored symbols, using a similar classification color scheme as in Figure 9. As indicated in Figure 10, many of the areas classified as severely eroded or eroded (red squares and orange triangles in Figure 15, respectively) are associated with locations of high long-term erosion rates in the northern to central sections of the study area. These areas, similarly, are associated with closer proximity to the channel as indicated by the 5-m depth contour (Figure 11).

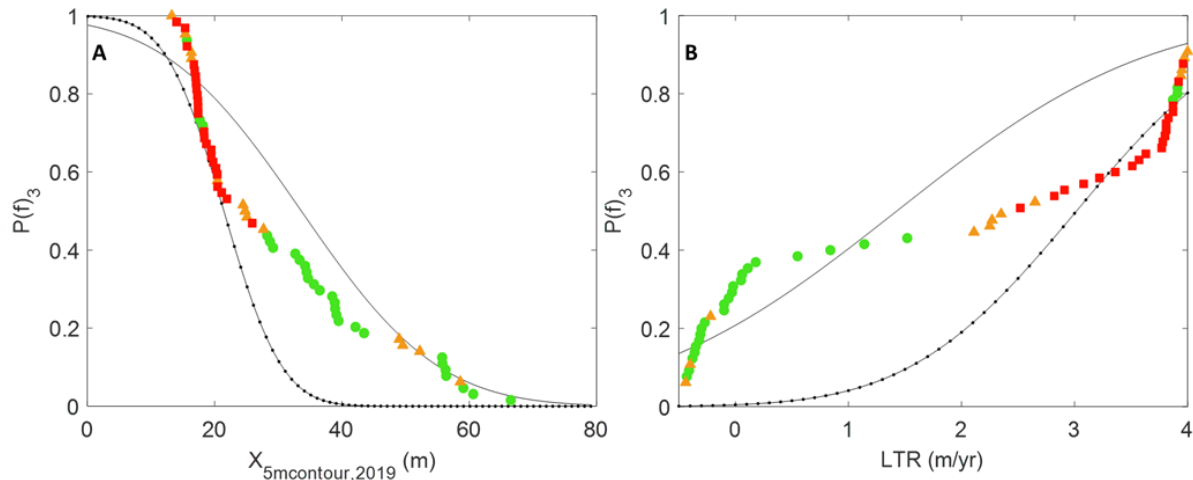


**Figure 15.** Probability  $P(f)_3$  of marsh being classified as severely eroded (black curve with markers), probability  $P(f)_3$  of marsh being classified as eroded/severely eroded (black curve), with empirical data showing shoreline classification as healthy (green circles), eroded (orange triangles), or severely eroded (red squares) as a function of (A) distance (m) to 2019 5-m contour  $X_{5mcontour,2019}$ ; (B) long term erosion rate  $LTR$  (m/yr).

### *Implications of Fragility Curves*

Empirical fragility curves derived from publicly available data and storm scenario simulations indicate the importance of measurements at nearby monitoring stations in predicting roadway inundation or closure due to flooding, particularly for bay-side events. Therefore, results of this study may contribute to risk management programs in the area to identify elevated water level conditions and take precautionary actions to mitigate roadway flooding or prevent unsafe travel conditions. Adaptation alternatives to improve the resilience and robustness of transportation infrastructure may also be identified. The fragility

curves based on numerical simulations identified marsh buffer distance as a significant predictor of bay-side roadway flooding, highlighting the importance of a healthy marsh buffer between the shoreline and the roadway for mitigating flooding impacts.

Sea level rise may exacerbate the vulnerability of coastal transportation infrastructure by inundating marshes and reducing the buffer distance between the shoreline and the roadway. Interactions between marshes and developed near-shore infrastructure must also be considered. While no adverse effects of the roadway on marsh erosion were observed at this study area (i.e., marsh erosion was driven more by proximity to the channel and long-term erosion rates related to channel velocity and/or sediment budget), effects of coastal squeeze by near-shore infrastructure may limit the ability of vegetation to adapt to rising sea levels (Borchert et al. 2017, Torio et al. 2013). Marsh condition is an essential component of roadway vulnerability (or robustness) to bay-side flooding for the ranges of hydrodynamic conditions considered here, in addition to its ecosystem services provided such as habitat for migratory birds and loggerhead turtles (U.S. Fish and Wildlife Service 2022) and carbon sequestration (Gulliver et al. 2020), which are particularly important for the location of the estuarine shoreline in a National Wildlife Refuge. Therefore, results indicate the importance of marsh monitoring and adaptive management through conservation, restoration, and erosion mitigation measures.

While the main drivers of shoreline condition are long term erosion rates associated with proximity of the inlet flood channel, episodic events can exacerbate existing erosion issues. A systems approach must be used to consider marsh vulnerability and its connection to the vulnerability of coastal transportation infrastructure.

### *Considerations for Fragility Models*

While the fragility models considered here identified significant variables influencing roadway flooding or marsh condition, several idealizations and assumptions were made in fragility model derivation. First, models were derived by fitting fragility data to a Gaussian distribution and assuming that data are normally distributed. Similarly, variables not considered in fragility model derivation owing to unavailability or insufficient data may be significant contributors to roadway or marsh fragility (i.e., event duration and timing, marsh vegetation properties, roadway design specifications). Sustained periods of high directional winds likely play an important role in bay-side roadway flooding, and wave direction may be important in driving flooding from the bay or ocean. While wind speed and direction are included in the fragility model based on publicly available data, fragility model derivations based on numerical model outputs indirectly account for wind speed and direction, considering only water levels at the marina tide gauge and at the shoreline and significant wave heights at the shoreline and boundary. However, peak directional wind speeds must be sustained for durations sufficient to generate significant fetch-generated waves and water level setup.

Other temporal considerations likely play a role in both roadway vulnerability to flooding and marsh vulnerability to erosion, such as duration of elevated water levels and/or wave heights and pre-storm marsh or roadway condition based on the timing and frequency of previous rainfall or inundation events. Longer-duration, lower intensity storms (e.g., 2019 nor'easter) may have a more significant effect on event-driven shoreline erosion (and flooding) than shorter duration, higher peak-intensity storms (e.g., 2020 Hurricane Isaias). Processes occurring at longer temporal scales such as climate change, sea level

rise, long-term scour, and infrastructure deterioration, as well as the occurrence of multiple hazards, should also be considered (Khandel and Soliman 2021, Li et al. 2020).

While this study identified key relationships between roadway and marsh vulnerability, environmental conditions, and landscape features, other considerations and vulnerabilities may make climate change adaptation in the area more complex. For example, the subsidence (Johnston et al. 2021) of the Outer Banks contributing to relative sea level rise may create long-term challenges for adaptation at the study area, particularly considering issues of coastal squeeze if the marsh is not able to retreat owing to the presence of the roadway. In addition, implications of interventions at regional scales must be considered for both updrift and downdrift locations.

## C. Compilation and Qualitative Review of Mitigation Options

### *Compilation of nature-based, structural, and hybrid options for assessment*

In order to develop recommendations on appropriate site-specific erosion mitigation options, a comprehensive review of relevant scientific and technical literature, regional erosion mitigation demonstration projects, and current federal regulatory guidance was conducted. This review provided insight on a range of mitigation strategies, accounting for structural alternatives, natural and nature-based solutions, and hybrid options.

The demonstration sites reviewed for this effort are summarized in Appendix B. The sites selected for review were considered based on their similarity to the project study area. Sites adjacent to existing tidal inlets, adjacent to deep channels, and located along either the Atlantic or Gulf coasts in the southeastern United States were prioritized based on the conditions of the study area. Additional consideration was given to sites completed within national parks or national wildlife refuges, to provide insight on options that would meet the regulatory requirements associated with these federal lands. Demonstration sites are at varying stages of development, ranging from recent (2020) implementation to up to 20 years post-construction.

In summary, potential mitigation options that could be considered for the project area include structural, natural or nature-based, or hybrid solutions. The initial ten options compiled for this effort are summarized below.

- **Channel relocation:** Use of dredging to redirect tidal currents away from an eroding shoreline, either by restoring a historic channel location, deepening other existing channels, or dredging a new channel while filling an old channel. This option may be combined with sediment placement and/or island restoration.
- **Living shoreline Type I:** (*vegetation only, biodegradable edging*): Use of constructed wetlands/vegetation to provide shoreline stabilization, possibly in combination with biodegradable edging.
- **Island or shoal creation and restoration:** Use of dredged materials to create or enhance islands or shoals in order to enrich habitat and reduce wave and current energy.

- **Thin layer placement:** Deposit additional sediment on existing shorelines; placement depths in project-scale applications typically range between 10 cm and 20 cm. This placement is designed to mimic natural sediment accretion in tidal marshes and mitigate sea level rise effects.
- **Living shoreline Type II:** (*vegetation with breakwater or sill*): Use of vegetation (marsh plantings), structural components (headland breakwater, sill), and possibly fill to diffract waves and reduce wave energy.
- **Soil bioengineering:** (*vegetated geogrids/ soft armor walls*): Construction of a soft, permanent structural system engineered to be vegetated for bank & shoreline stabilization, retaining wall, and erosion control applications using interlocking plates and geotextile bags.
- **Flow speed reduction:** (*root wad with footer*): Armament of a shoreline/bank with root wads, keeping the current off the bank. Can also be considered a soil-bioengineering alternative that assists at reducing erosive flows.
- **Flow speed reduction:** (*bendway weirs*): Construction of a low level, totally submerged rock structure that is positioned from the outside bankline of a riverbend, angled upstream toward the flow.
- **Jetties:** Construction of a rocky shore-perpendicular structure located adjacent to a tidal inlet to confine tidal flow and control migration and sediment deposition in the inlet. Jetties may be single or double.
- **Seawalls/bulkheads/revetments and terminal groin extension:** Construction along the shoreline of vertical hardened structures of rock, concrete, metal, or other non-native material. Structures may be held in place by tie-back rods or other anchoring devices and are typically built to protect slopes from wave action.

A review of each option, including potential engineering, environmental, and regulatory considerations, was considered in the determination of options to be included in the numerical model simulations. This initial review is summarized in Appendix B.

### *Simulation of potential erosion mitigation alternatives*

Based on the literature review of potential erosion mitigation alternatives near tidal inlets, a total of six engineering alternatives (pulled from the initial ten options listed previously) are considered and compared in their performance at reducing erosive flow velocities near the estuarine shoreline. The six alternatives were selected based on their historical use in tidal inlets, their potential to reduce constant high erosive flows near a deep channel, and the possibility to reasonably schematize them in the numerical model.

The alternatives that were discarded include living shorelines (with and without sills), thin layer placement, and soil bioengineering. Living shorelines typically require gentle slopes (Hardaway et al., 2017) that are not necessarily present near flood channels of tidal inlets. Thin layer placement, which is recommended to enhance vertical marsh resilience to sea level rise (Raposa et al., 2020), is not expected to enhance resilience to horizontal erosion as it cannot reduce fast, erosive flows along channel banks.

Some soil bioengineering techniques such as live posts and live cribwalls, which are extensively used in riverine systems to strengthen the soil in exposed banks and slow high flows (Mississippi Watershed Management Organization, 2010; U.S. Department of Agriculture, Forest Service, National Technology and Development Program, 2003), are not feasible in a submerged bank with brackish and cold water. It should be noted that although these alternatives are not considered here, their use in other environments have proven to be adequate. The remaining six alternatives considered in this study and their schematization within the numerical model are described in the following paragraphs.

Seawalls are a traditional option to stop erosion along banks and shorelines by hardening the edge between land and water. Seawalls (also known as bulkheads and revetments) are vertical, hardened structures made of rock, concrete, metal, or other non-native material and constructed along the eroding shoreline (Dean and Dalrymple, 2002; USACE, 1995; 2002). The seawall evaluated in this study extends 900 m along the eroding shoreline (red line in Figure 16A). The structure was schematized in the numerical model as a thin dam, in the same way the existing terminal groin is included in the model. The line of the thin dam follows the grid cell edges closest to the shoreline.

Bendway weirs are submerged rock structures positioned on the outside bankline of a riverbend, typically in a unidirectional-flow channel, angled upstream towards the flow in order to slow erosive velocities (Davinroy, 1990; Winkler, 2003). These structures have been built along bends in the Mississippi River (Derrick et al., 1994), the Rio Grande River (Scurlock et al., 2012), and other rivers in the US. Although bendway weirs have not been used in coastal channels with bi-directional tidal flow, this alternative was considered to explore potential flow reduction of the prevalent currents at the site. Inside the south flood channel of Oregon Inlet, ebb currents are nearly 3 times larger than the flood currents, leading to asymmetric forces along the channel banks. Bendway weirs angled into these strong ebb flows may help reduce the dominant cause of erosion. Following Winkler (2003), the dimension and angles of four bendway weirs were calculated, with alongshore spacing of 150 m, cross-channel lengths of 80 m (spanning the deepest part of the flood channel), and angled 20 degrees from the shoreline towards the ebb currents (red lines in Figure 16B). A 2D weir feature was added in Delft3D that results in energy loss due to constriction of the flow. The energy loss is converted into an effective friction coefficient and added in the momentum equation (Deltares, 2022). In the model, the weirs are defined by their start and end nodes in the domain. Weir heights meet local USACE navigation channel depths (4.5 m depth relative to NAVD88). The default friction coefficient of 1 was used as recommended in the Delft3D manual (Deltares, 2022).

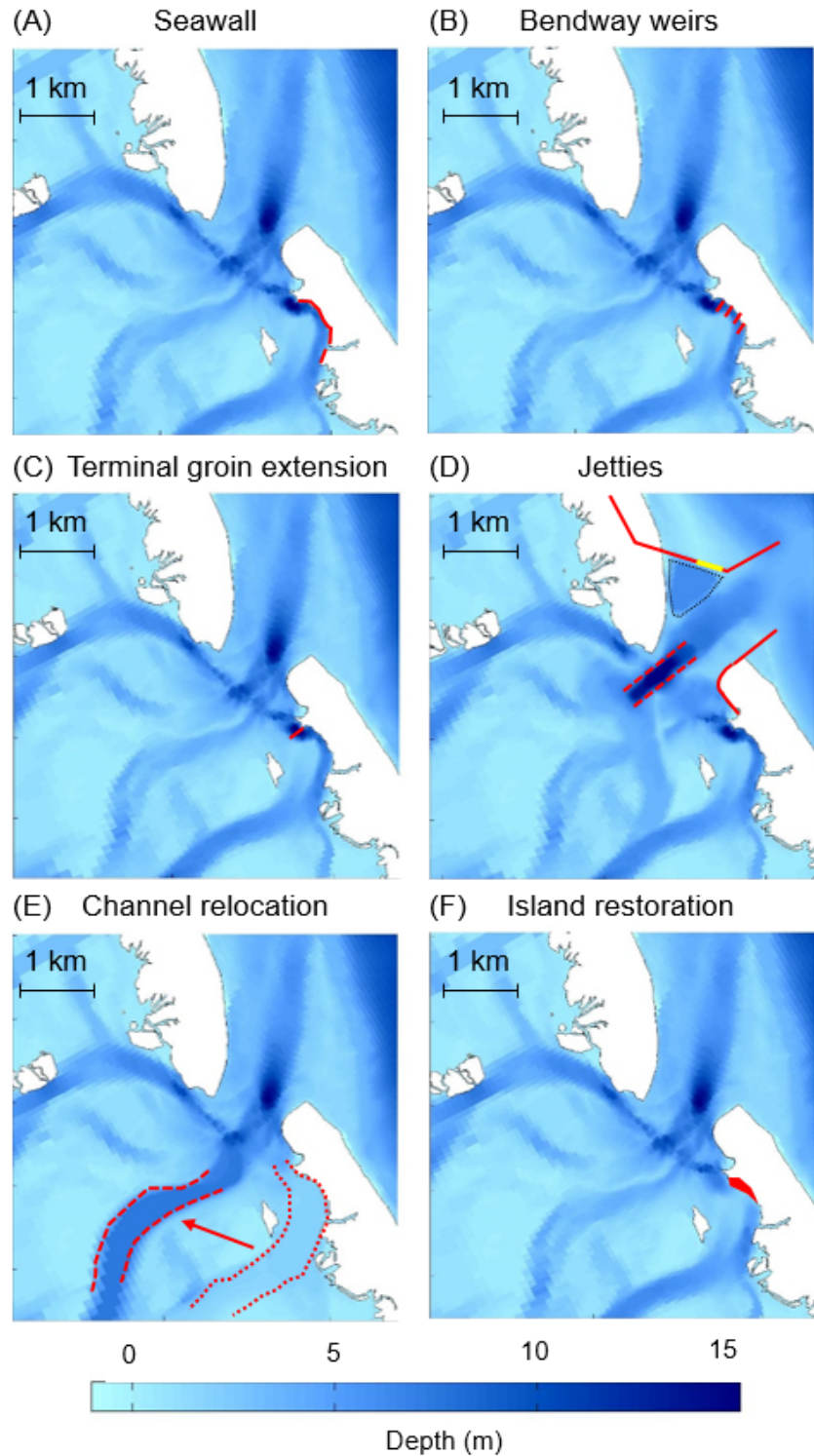


**Figure 16.** Coastal protection alternative (red highlights) on bathymetry (blue color contours) and the existing island shape (black outline) for (A) Seawall, (B) Bendway Weirs, (C) Terminal Groin Extension, (D) Jetties, where the dashed red line indicates the new position of central channel, the dotted black line indicates the area of the sedimentation basin, and the yellow line indicates the position of the weir (E) Channel Relocation, where dashed line indicates new flood channel position and dotted line indicates filled region (old channel) (F) Island Restoration.

Terminal groins are similar to jetties, but typically shorter and built on the tip of a barrier island to stabilize its position and interrupt inlet migration (Dean and Dalrymple, 2002). The terminal groin extension considered here was based on similar examples at Indian River Inlet, DE and Ocean City Inlet, MD, where shoreline armoring extends along the barrier island into the estuarine shoreline or the channels in the flood delta to redirect flows. A terminal groin extension was started at the existing revetment and extending perpendicular across the width of the deepest portion of the entrance to the south flood channel. In Delft3D, this alternative was schematized as a 240 m long thin dam (Deltares, 2022) (red line in Figure 16C), similar to the seawall, but located across the channel instead of along the shoreline. Different from the bendway weirs, this alternative completely blocks flow along its length.

Jetties are single or double rocky, shore-perpendicular structures built to confine tidal flow through and control migration of and sediment deposition in tidal inlets (Brunn, 1978; Kraus, 2008). The jetty system considered in this study was based on a dual jetty design for Oregon Inlet by the USACE (2001). The jetty system has a 3055-m long northern jetty and a southern jetty, which connects to the existing terminal groin for a total length of 2004 m (red lines in Figure 16D). In the north jetty, a 305-m long weir at mean sea level (-0.04 m NAVD88) is included to allow sedimentation in a 0.24 km<sup>2</sup> deposition basin with a depth of 6.13 m below NAVD88 (USACE, 2001). Within Delft3D, this alternative was schematized as a combination of thin dams for the jetties' extensions into the ocean, a 2D weir with a friction coefficient of 1 (default, Deltares, 2022) and a change in the bathymetry of the inlet based on that proposed by USACE (2001) to align the main channel with the center of the jetties (dashed red lines in Figure 16D).

Channel relocation involves changes to the inlet channels' locations through dredging and sediment placement with the aim to deepen some channels and close others (Rosgen, 2011) while increasing or maintaining a tidal prism that would keep the inlet open (Cleary and FitzGerald, 2003). This alternative was implemented in the numerical model by modifying the bathymetry in the domain. The south flood channel was filled to a depth of 1.80 m NAVD88 (dotted red lines, Figure 16E) and the center channel was deepened from depths ranging from 3.00 - 4.50 m (NAVD88) to a new maximum depth along the thalweg of 7.50 m NAVD88 (dashed red lines, Figure 16E). It should be noted that the change in bathymetry is instantaneous; in other words, the simulation is spun up with the bathymetric changes already in place, rather than accounting for dredging and sediment placement periods.

Island restoration (or shoal creation and restoration) is a method involving building back land lost to erosion (Berkowitz and Szimanski, 2020). Island restoration projects involve sediment placement as well as planting vegetation for the creation of habitat. The island restoration alternative investigated in this study entails rebuilding the back-barrier region in the north tip of Hatteras Island (just south of Oregon Inlet) that has been rapidly eroding. In the model, bathymetric and topographic changes were completed to account for this alternative; the addition of vegetation on the island is not accounted for. A total of 830 m of shoreline were considered to be restored. The new estuarine shoreline position was set to that of October 1989, prior to the construction of the terminal groin in Oregon Inlet. The location of this shoreline was obtained from georectified historical aerial images taken by NCDOT. The restored island has an elevation of 0.60 m NAVD88 (red area, Figure 16F); this elevation corresponds to the average elevation at which well-developed, healthy marsh vegetation is present at the site (Wargula et al., 2021). The topography of the back-barrier was leveled up to the 0.60 m contour, for a total restored area of 77,340 m<sup>2</sup>. At the edge of the restored shoreline, the bathymetry gets deeper up to a depth of 5 m

(NAVD88) with a slope into the flood channel of 12.5% (1:8). Similar to other alternatives, the simulation is spun up with the new bathymetry and topography already in place.

### *Simulation Conditions and Proposed Alternative Assessment Rating*

A 30-day period of typical oceanographic and atmospheric conditions in the absence of major storms in 2020 was selected to simulate the hydrodynamics of Oregon Inlet under the six estuarine erosion mitigation alternatives and present conditions. A calm period was selected, as it better represents the daily hydrodynamic conditions in the back barrier region and along the tidal inlet. All simulations were forced with tides, waves, and winds from August 12 to September 11, 2020 with a spin up period of 15 days to ensure hydrodynamic conditions have stabilized from initial conditions. A summary of the boundary conditions is shown in Figure 17. Water levels on the ocean boundary included neap and spring conditions with a maximum total water level of 1 m (NAVD88). Significant wave heights predominantly from the east quadrant ranged between 0.36 m and 1.86 m and wind speed reached a maximum of 12.5 m/s with varying directions.

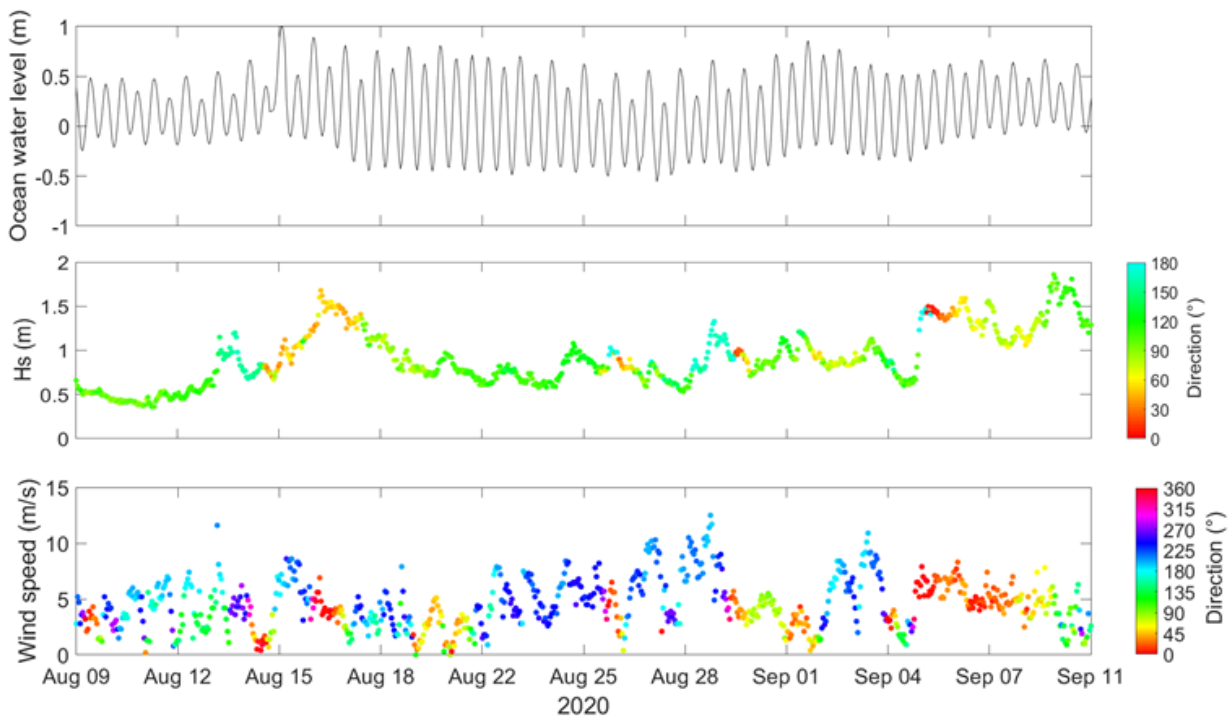


**Figure 17.** Water levels, waves, and wind speed boundary conditions used for the 30-day simulation period.

The “present condition” simulation includes the existing features at the inlet as of 2019 (e.g., terminal groin and Basnight Bridge piles) without any potential erosion mitigation alternative on the estuarine side of the inlet. The present condition simulation is used as a benchmark for comparison of depth-averaged velocities with simulations that include one inlet intervention at a time. Comparisons of time-series of depth-averaged velocities, herein referred to as “velocities,” for the sake of simplicity, are completed initially at the south flood channel to assess alternative performance.

The potential for the alternatives to mitigate erosion along the shoreline was quantified by examining the duration of along-channel velocities below an erosion threshold relative to the median sediment size as defined by Hjulström (1939). Median sediment grain size diameters ( $D_{50}$ ) in the flood channel, measured in 2019, range from 22 to 351  $\mu\text{m}$  (medium silt to medium sand on the Wentworth scale) (Wentworth, 1922), with fines typically close to the shoreline edge and coarser grains in the middle of the flood channel (Wargula et al., 2021). For this range of sediment grain sizes, the minimum velocity needed to erode the particles, according to the Hjulström diagram, is approximately 0.20 m/s. This velocity is therefore considered the threshold for comparison with simulations' outputs.

Along-channel velocities in the south flood channel were extracted for all alternatives and the present condition simulations. This point is located in the more convex section of the shoreline where the historical erosion rates are the highest (Tomiczek et al., 2022). Velocities in the south flood channel were rotated into along- and cross-channel velocity components using principal axes (Emery and Thomson, 2001). In the present condition simulation, the velocities near the shoreline are ebb-dominated, with a principal axis angle of 132 degrees (azimuthal) (Emery and Thomson, 2001). The principal axis angles for most alternatives were within 3 degrees of that in the present condition, except for the seawall and channel relocation alternatives, which had principal axis angles of 140 degrees and 110 degrees (azimuthal), respectively, resulting from veering of the flows compared to the present condition.

In the present condition, along-channel velocities at the south flood channel are below the 0.20 m/s erosion threshold 49% of the time. Given that historical data indicates that the shoreline suffers erosion under this condition, it is expected that a reduction in the duration of velocities greater or equal to 0.20 m/s, would result in a reduction of erosional processes at the shoreline. Based on this assumption, the main criterion to define the effectiveness of an alternative is the percentage of time that velocities are below the erosion threshold during typical flow conditions. To facilitate comparison and categorization between alternatives, three levels of effectiveness at reducing erosion were defined. The categories are Least Effective, Moderately Effective, and Highly Effective, corresponding to velocities below the erosion threshold (0.20 m/s) for less than 50% (almost no change in erosive flows relative to the present condition), 50% to 80%, and more than 80% of the time, respectively (Table 8). The results from this analysis are presented in Section V.A.

**Table 8.** Summary of the mitigation alternative effectiveness ratings based on the erosion threshold of 0.2 m/s.

<b>Effectiveness of Alternatives</b>	<b>% time along-channel velocity is below erosion threshold 0.2 m/s</b>
Least Effective	< 50%
Moderately Effective	50% to 80%
Highly Effective	> 80%

## V. Decision making tools and information

### A. Alternative Modeling and Effectiveness Assessment

#### *Alternatives Effectiveness at Reducing Erosive Flows at the Shoreline*

For the present condition simulation, along-channel (major axis) velocities ranged -0.58 to 0.33 m/s (positive to the southeast, during the flood), with a median velocity of -0.06 m/s, consistent with ebb-dominated flows. Cross-channel (minor axis) velocities were small, ranging from -0.03 to 0.02 m/s (positive to the southwest), suggesting strong channelization. The cross-channel (minor axis) flow magnitudes were less than 0.03 m/s for all alternatives except for the channel relocation and island restoration alternatives, which had cross-channel flows ranging -0.07 to 0.06 m/s and -0.12 to 0.05 m/s, respectively, potentially owing to the reduced channelization of flows in these alternatives.

Within each simulation, total velocity magnitude is less than 0.02 m/s greater than the maximum along-channel velocities at the south flood channel. The percentage of time below the erosion threshold for the total velocity magnitude and the along-channel velocity component is also similar for each model configuration. To preserve the flood/ebb asymmetry, the along-channel component of velocity was used to evaluate the performance of each alternative.

Figure 18 summarizes the along-channel velocities in the present condition and for all of the alternatives. The median flows for all alternatives are negative, consistent with ebb-dominant velocities in the south flood channel, except for the island restoration case, which has a median of 0 m/s, consistent with no flow (i.e., the island was dry) for the majority of the time series. The strongest median velocity, -0.06 m/s, is simulated in the present condition; all alternatives reduce the magnitude of this median velocity, with the seawall causing the least reduction in velocity (median velocity of -0.05 m/s) and island restoration causing the greatest reduction (median velocity of 0 m/s). Maximum flood and ebb flows are also reduced relative to present conditions for all cases except for the seawall case, which had maximum ebb flows of -0.61 m/s, slightly larger in magnitude than the maximum ebb flows of -0.58 m/s in the present condition.

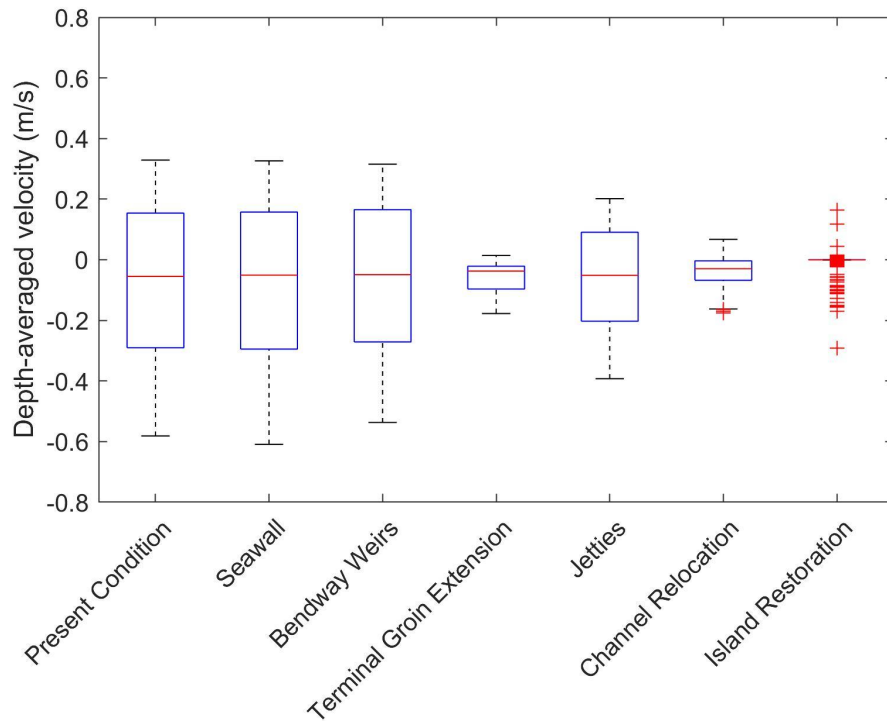


**Figure 18.** Box-and-whisker plots of depth-averaged along-channel velocity versus present condition and alternative at the south flood channel. Negative velocities indicate ebb flows, while positive velocities indicate flood flows. The horizontal red line indicates the median velocity. The vertical length of the blue boxes indicates the 25th and 75th percentiles of velocity. The black whiskers extend to the maximum and minimum velocities, excluding outliers, which are represented with red plus symbols.

Table 9 presents the relative difference in along-channel velocity, the percentage of time that the along-channel velocity was below the erosion threshold, and the resulting effectiveness rating (Table 8) based on the time below the erosion threshold. Relative difference is calculated as the median of the absolute value of the difference between the present condition and alternative along-channel velocity divided by the present condition along-channel velocity. The positive sign on the relative differences presented in Table 9 represents a percent reduction in median velocity relative to the present condition.

**Table 9.** Depth-averaged along-channel comparison

Alternative	Relative Difference (%)	Percent time below Erosion Threshold (%)	Effectiveness
Seawall	7	47	Least Effective
Bendway Weirs	8	49	Least Effective
Terminal Groin Extension	73	100	Highly Effective
Jetties	34	74	Moderately Effective
Channel Relocation	92	100	Highly Effective
Island Restoration	100	100	Highly Effective

The two alternatives with the largest impact on velocities (>92% reduction in along-channel velocity and below the erosion threshold 100% of the time), were channel relocation and island restoration (Table 9). The channel relocation alternative still allowed flows through the south flood channel, but with consistently smaller velocities, particularly on flood compared to ebb. The island restoration alternative was only intermittently wet and so, although velocities exceeded the erosion threshold a few times, these “erosion events” were brief.

The terminal groin extension also had a significant impact on reducing velocities in the south flood channel (73% reduction in along-channel velocity and below the erosion threshold 100% of the time). The flood velocities, in particular, were reduced from a maximum of 0.33 m/s to a maximum of 0.01 m/s, potentially owing to blocking and redirecting of flows by the groin at the flood channel entrance. Ebb flows were also significantly reduced from a maximum of -0.58 m/s to -0.18 m/s.

The jetties were moderately effective, decreasing the along-channel velocities in the south flood channel by 34%, with consistent impacts across tidal cycles that led to an increase in time below the erosion threshold (74%). The seawall and bendway weirs were the least effective, with almost no change in the time below the erosion threshold and only a 7% and 8% reduction in along-channel velocity, respectively. It should be noted that of all the alternatives, the seawall is the only one that is not directly blocking or redirecting flows, thus, its relatively low effect on flow reduction was expected.

### *Spatial Changes in Velocities Across the Inlet During Peak Tidal Flows*

Instantaneous difference maps of velocity vector subtraction between the present condition simulation and each alternative simulation were created during maximum ebb (August 23rd at 0:00 in Figure 17) and maximum flood (August 23rd at 06:00 in Figure 17) to determine other large-scale impacts that the coastal protection alternatives may have on circulation patterns along shoals and channels (Figures 19 and 20). Positive differences (red contours) indicate a reduction in velocity and negative differences (blue contours) indicate an increase in velocity in the alternative simulation, compared with the present condition (Figures 19 and 20).

The seawall and bendway weirs had only small local effects in their vicinities and negligible impact on flows outside of the south flood channel (not shown). The largest impact on flows by the seawall was a small area adjacent to its southern end where velocity reduction was ~0.2 m/s. The bendway weirs also reduced flows inside the south flood channel, with less than 0.1 m/s flow reduction along the shoreline and less than 0.1 m/s flow increase away from the shoreline, with slightly larger impacts on maximum ebb compared to maximum flood, owing to the angling of the weirs into the ebb currents.

The terminal groin extension and jetties drove changes in flow patterns across the entire inlet system during maximum flood and ebb (Figures 19A and 19B). The terminal groin extension resulted in similar changes in circulation patterns for both maximum flood and ebb, with significant (> 0.40 m/s) flow reduction within and to the south of the south flood channel and minor flow reduction on the ebb delta. The results indicate significant flow increase (> 0.50 m/s) on the tip of the groin extension and increase of up to 0.1 m/s on the rest of the flood delta. The main difference between flood and ebb is a larger change in flow velocities (both reduction and increase) in the vicinity of the groin, during maximum ebb flows. The jetties simulation showed tidal asymmetry in changes to the circulation patterns (Figures 19C and

19D). During the maximum ebb, the flows between the jetties on the ebb delta were significantly increased, while flows on the flood delta and on the external side of the jetties on the ebb delta were mainly reduced. During the maximum flood, patterns of change in velocities are complex; flow reduction is simulated in the vicinity of each flood channel and adjacent to the jetties, while flow velocities increase mainly between the jetties, in shallow regions on the flood delta, and further alongshore on the ocean side. Flow increase at the weir location is more noticeable during maximum ebb but also present during maximum flood (circular blue region in the center of red shades along the north jetty), while flow reduction is predominant in the area of the sediment basin.

Flows throughout the inlet system also were altered by the channel relocation and island restoration alternatives (Figure 20), although the magnitude of the differences was small compared to those simulated for the jetties and the terminal groin extension alternatives (Figure 19). The channel relocation alternative increased flows through the center flood channel, reducing flows through the south flood channel and northern part of the flood delta. There is some tidal asymmetry to this alternative, mainly in the region between the center and south flood channel and the inlet mouth. The channel relocation alternative also increases velocities inside the main inlet channel.

The island restoration alternative had the largest impact near the eroding shoreline, with significant flow reduction inside the south flood channel and significant flow increase just to the west of the entrance to the south flood channel (Figure 20). The flow is also increased on the center and northern part of the flood delta, potentially to compensate for the closed-off south flood channel. The strong gradient between the regions of velocity reduction and increase implies that the erosional flows are displaced, rather than fully reduced near the eroding region.

Further analysis of the mitigation alternatives can be found in the submitted manuscript in Appendix E.

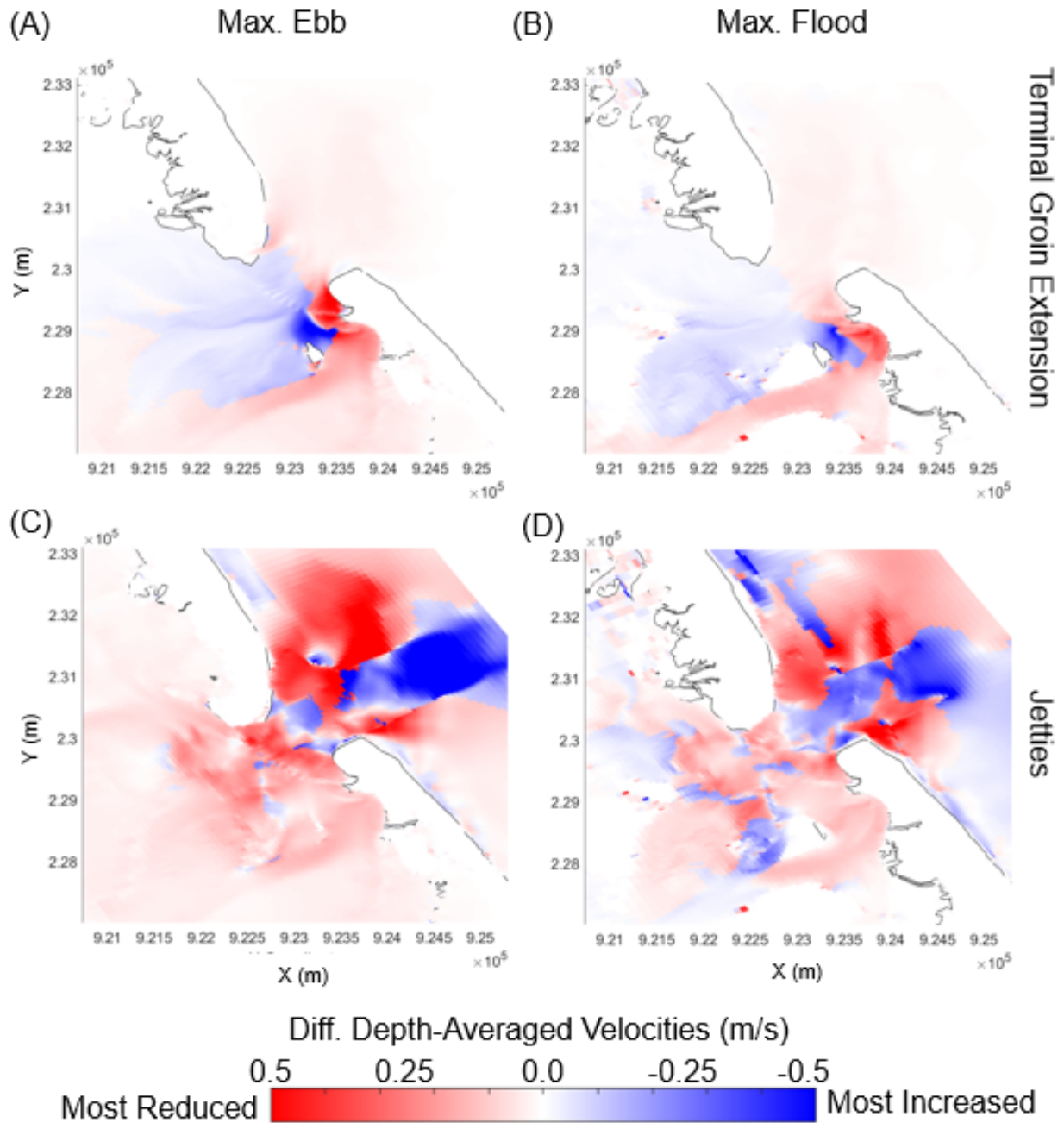


**Figure 19.** Difference in depth-averaged velocity for the present conditions and for the (A, B) terminal groin extension and (C, D) jetties during (A, C) maximum ebb and (B, D) maximum flood. Red and blue colors indicate reduced and increased velocity, respectively, relative to present conditions.

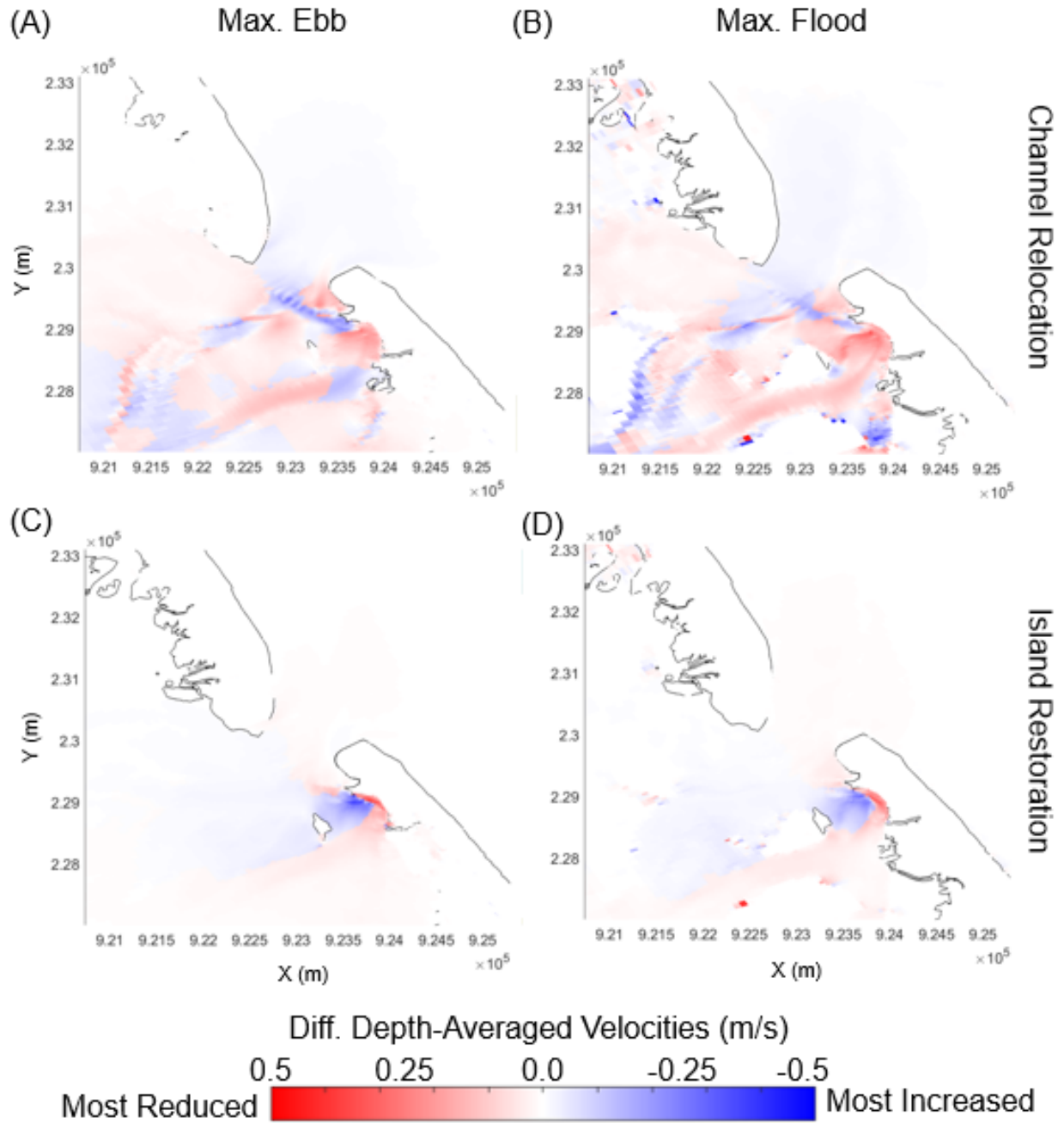


**Figure 20.** Difference in depth-averaged velocity for the present conditions and for the (A, B) channel relocation and (C, D) island restoration during (A, C) maximum ebb and (B, D) maximum flood. Red and blue colors indicate reduced and increased velocity, respectively, relative to present conditions.

## *Assessment of Alternatives*

A thorough assessment of mitigation options requires the consideration of the engineering, environmental, and regulatory issues associated with each option. Table 10 integrates the modeling results with the initial mitigation review summary to provide the advantages and disadvantages of each assessed option from an engineering, environmental, and regulatory perspective.

The jetties, terminal groin extension, and channel relocation alternatives had the largest impacts on velocity across the flood delta, with the jetties also significantly impacting the ebb delta. Large velocity changes could lead to significant morphological evolution of the channels and shoals along new pathways, leading to disruptions of navigation routes and changes to the dredging needs of the inlet. Increased velocities near the tip of the structures (i.e., jetties, terminal groin extension) indicate the potential for scour hole development as reported in other inlets by Lillycrop and Hughes (1993), Ferrarin et al. (2018) and Toso et al. (2019). In addition, the jetties, terminal groin extension, and channel relocation alternatives all show varying degrees of velocity increase inside the main channel of the inlet, which could scour existing structures like the bridge piles and the existing terminal groin.

The island restoration alternative has the most significant velocity impact in the south flood channel, where flows were reduced to near-zero by the creation of new land that remained dry through most of the modeled period. However, the strong increase of flows ( $>1.5$  m/s) at the entrance to the south flood channel may lead to a new channel cutting across the restored island. This option may temporarily “turn back the clock” on erosion without solving the problem in the long term. Similarly, relocating the south flood channel would rely on dredging maintenance, as active channel rotation, shoal movement and morphological changes due to storms and day-to-day processes have been reported at Oregon Inlet (Humberston et al., 2019; Velasquez-Montoya et al., 2020).

Although the seawall was not effective in reducing along-channel velocities, the scoring metric used here may not fairly account for the erosion control provided by this alternative. Hardening of the bank does not reduce flows, but stops erosion by creating a barrier between the shoreline and the estuarine currents. In addition, this alternative has the advantage that its overall impact on velocities is localized and minimal, suggesting that any morphological evolution would mainly occur in the south flood channel, and not impact the rest of the flood delta. It should be noted however, that hardened structures on a shoreline can interfere with sediment sources and longshore transport (Dean and Dalrymple, 2002) causing erosion downstream on unprotected shorelines.

**Table 10.** Coastal protection alternatives with their effects on velocities within the inlet system and their respective advantages and disadvantages. (The colors of the first column represent the effectiveness rating defined in Table 8.)

Alternative	Advantages	Disadvantages
<b>Seawall</b>	<p>Minimum effects to overall inlet hydrodynamics.  Hardened structure stops shoreline erosion and channel encroachment into the adjacent beach/marsh habitat, minimizing the effects of wave action to the shoreline.  Little maintenance is required unless damaged during storm events.</p>	<p>Ineffective at reducing depth-averaged velocity in the southernmost channel.  Beach/marsh material located seaward of the seawall expected to erode due to lack of protection and concentration of wave energy.  Similar to terminal groins and jetties, seawalls generally have a higher order of magnitude initial construction cost than other options.  Does not facilitate creation of additional habitat (replacing previously eroded areas). Reduces the intertidal zone required for marsh habitat.  Extensive federal/state permitting and environmental analysis required.  Current N.C. statutes generally prohibit oceanfront seawalls except on a limited basis. Federal permitting will require analysis of refuge, park, and protected species impacts; post-construction monitoring likely required.</p>
<b>Bendway Weirs</b>	<p>Minimum effects to overall inlet hydrodynamics.  Suitable for deep channel sites; reduces flow velocities against the eroding bank.  Controls excessive channel deepening.  Reduces adjacent bank erosion on the outside bendway. Because excessive river depths are controlled, the opposite side of the riverbank is naturally widened.</p>	<p>Ineffective at reducing depth-averaged velocity in the southernmost channel.  Option is mostly used in river environments and has not been tested in tidal inlets.  Federal and state permitting is required due to potential navigation impacts; because impacts to tidal inlet and adjacent marsh are untested, post-construction monitoring will likely be required.</p>
<b>Terminal Groin Extension</b>	<p>Third most effective at reducing depth-averaged velocity in the southernmost channel.  Hardened structure to block erosive flows.  Little maintenance is required unless damaged during storm events.</p>	<p>Enhances depth-averaged velocity in the northern half of the flood delta; reduces depth-averaged velocity in the ebb delta. Enhances the ebb depth-averaged velocity near the Basnight Bridge piles.  Potential impact to adjacent beaches and shorelines due to interruption in alongshore transport.  Similar to seawalls and jetties, terminal groins generally have a higher order of magnitude initial construction cost than other options.  Does not facilitate creation of additional habitat (replacing previously eroded areas) and reduces the intertidal zone required for marsh habitat.  Extensive federal/state permitting and environmental analysis required.  Current N.C. statutes generally prohibit terminal groins except on a limited basis. Federal permitting will require analysis of refuge, park, and protected species impacts; post-construction monitoring likely required.</p>

\*Table 10 is continued on the next page.

**Table 10 (continued).** Coastal protection alternatives with their effects on velocities within the inlet system and their respective advantages and disadvantages. (The colors of the first column represent the effectiveness rating defined in Table 8.)

Alternative	Advantages	Disadvantages
<b>Jetties</b>	<p>Moderately effective at reducing depth-averaged velocity in the southernmost channel.</p> <p>Stabilizes the inlet channel and ensures navigation within the inlet.</p>	<p>Has the most significant effects on overall inlet hydrodynamics. Interrupts longshore transport, requiring the design and implementation of a sediment bypassing mechanism.</p> <p>May require channel maintenance dredging.</p> <p>Similar to seawalls and terminal groins, jetties generally have a higher order of magnitude initial construction cost than other options.</p> <p>Does not enhance or provide opportunities for habitat restoration; only stops marsh erosion if the structure extends into the Sound.</p> <p>Extensive federal and state permitting is required due to the potential impacts to coastal tidal habitat and navigation. Current N.C. statutes generally prohibit jetties except on a limited basis. Federal permitting will require analysis of refuge, park, and protected species impacts; post-construction monitoring likely required.</p>
<b>Channel Relocation</b>	<p>Second most effective at reducing depth-averaged velocity in the southernmost channel.</p> <p>Represents a beneficial use of dredged materials and opportunity for habitat restoration.</p> <p>Uses a combination of dredging and natural inlet processes to redirect strong currents away from an eroding shoreline.</p>	<p>Enhances depth-averaged velocity in the ebb delta and creates different depth-averaged velocity patterns in the flood delta. Enhances both the ebb and flood depth-averaged velocity near the Basnight Bridge piles.</p> <p>Will require regular maintenance for the new/relocated channel, representing a higher order of magnitude maintenance cost than other alternatives.</p> <p>Modifies morphology and hydrodynamics in the bay.</p> <p>Potential impacts to existing shoal islands and associated habitat, requiring federal and state permits for dredging and dredging material placement. Post-construction monitoring will likely be required.</p> <p>May require stabilization and enhancement structures as part of design.</p>
<b>Island Restoration</b>	<p>Most effective at reducing depth-averaged velocity in the southernmost channel.</p> <p>Represents a beneficial use of dredged materials from navigation channels and an opportunity for habitat enhancement and creation.</p>	<p>Enhances the currents at the edge of the restoration site, which may indicate shorter project life.</p> <p>Could require constant maintenance (deposition of dredged material) due to inlet dynamics and high energy environment, increasing the ongoing maintenance cost.</p> <p>Federal and state permitting required due to potential impacts to navigation routes, tidal habitat, and refuge and park resources.</p> <p>Post-construction monitoring will likely be required.</p>

## B. Online vulnerability indicator/notification system

For a first indication that the roadway may be vulnerable to flood impacts, univariate analysis based on the fragility modeling was conducted to identify water levels at the Marina and wave heights at the Waverider buoy (Figure 3B) corresponding to threshold flooding probabilities. These values were used to assign initial threshold values to an email warning system, which sends an automated email to a list of recipients if threshold values are exceeded. A sample email is shown in Figure 21.



**Figure 21.** Email alert notifying recipients of wave and water level conditions that may lead to roadway flooding.

The code for the present implementation for the email alert system is provided in Appendix C. The present implementation of the code considers a wave height of 6.8 ft, a wave period of 10 seconds, and a water level of 2.6 ft the threshold values. These values reflect minimum values of times when the roadway was reported flooded in TIMS anywhere along the stretch from Pea Island to Rodanthe. The present implementation is run using Amazon Web Services and a Gmail address set up for testing. The code is provided and may be modified as desired for implementation by NCDOT.

Table 11 and Table 12 may be used to assign alternative threshold values of significant wave height (measured at the Waverider buoy) or water level (measured at the Marina tide gauge), considering allowable probabilities of roadway flooding. Failure probabilities are based on roadway closure due to flooding in the TIMS data.

Table 11. Wave Height at the Waverider Buoy,  $H_s$

$H_s$ (m)	$H_s$ (ft)	$P(f)$ (%)
0	0	0
3.68	12.07	10
4.39	14.40	20
4.90	16.08	30
5.34	17.52	40
5.75	18.86	50
6.16	20.21	60
6.60	21.65	70
7.11	23.33	80
7.62	25.00	88

Table 12. Water Level at the Marina Tidal Gauge,  $WL$  (from TIMS model)

$WL$ (m)	$WL$ (ft)	$P(f)$ (%)
0	0	0
0.62	2.03	10
0.77	2.53	20
0.88	2.89	30
0.97	3.18	40
1.06	3.48	50
1.15	3.77	60
1.24	4.06	70
1.35	4.42	80
1.50	4.92	90

Alternatively, Table 13 presents flooding probabilities based on Marina water levels causing roadway transect flooding of the estuarine shoreline in the Pea Island National Wildlife Refuge during bay-side storm events. These water levels are larger than those observed in Table 12 owing to the higher roadway elevations along this specific section of N.C. 12. These tables may be used to investigate roadway flooding vulnerability and identify threshold values for the online vulnerability indicator.

Table 13. Water Level at the Marina Tidal Gauge, *WL* (from numerical model)

<i>WL</i> (m)	<i>WL</i> (ft)	<i>P(f)</i> (%)
0	0	0
1.87	6.14	10
2.03	6.66	20
2.15	7.05	30
2.24	7.35	40
2.34	7.68	50
2.43	7.97	60
2.53	8.30	70
2.65	8.69	80
2.81	9.22	90

### C. Field Database Description

All field data collected as part of this project is provided in a series of GIS files (shapefiles and raster files), spreadsheets (.xlsx), and plain text files (.txt). Appendix F provides a summary of all of the files and associated basic information including data type and collection method, data format, start and end date, datums and units (where applicable), and organization collecting the data.

The files are organized by date and data type. The file structure is illustrated in Figure 22.

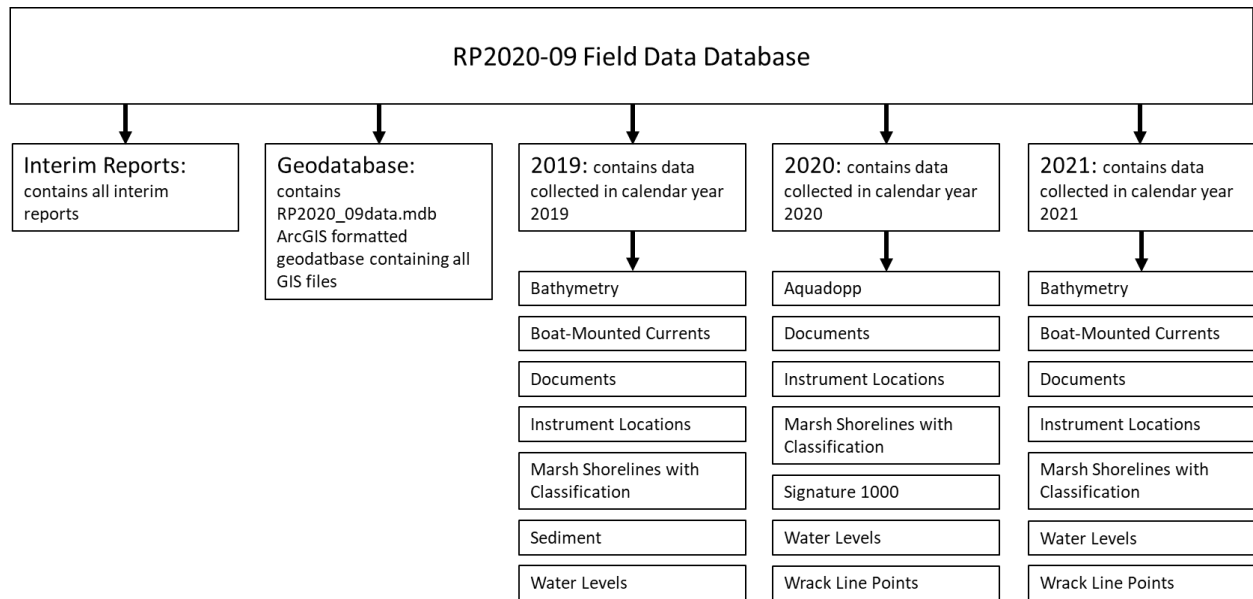


Figure 22. File organization for the field data database provided.

## VI. Recommendations and Next Steps

### *Considerations for future assessments*

The analysis conducted in this project is intended to provide a feasibility-level review of potential engineering alternatives to address erosion conditions within the project study area. It is not intended as a replacement for a site-specific engineering design or in-depth environmental analysis as required by the National Environmental Policy Act. However, this analysis provides insight on the engineering, environmental, and regulatory constraints associated with each potential mitigation alternative.

The field measurements conducted during the research period confirmed the continued evolution of the marsh shoreline throughout the study area, with long-term erosion rates exceeding 2 m/yr (and localized erosion rates exceeding 4 m/yr) observed within the northern portion of the study area near the tidal inlet. As the migration of the channel and the erosion of the marsh shoreline is expected to continue, it is anticipated that the estuarine shoreline conditions could pose a threat to transportation infrastructure within the next decade, if not sooner.

The initial synthesis of mitigation options yielded a variety of structural, natural or nature-based, and hybrid options to address marsh shoreline erosion in the north end of Hatteras Island. Structural solutions such as jetties, seawalls, and bendway weirs can stabilize inlet conditions to reduce shoreline erosion without significantly decreasing flow velocities, but can impact adjacent shorelines and ecosystems by disrupting natural coastal processes. Natural or nature-based solutions offer opportunities to enhance existing ecosystem functions but may require continued maintenance to remain effective and have generally been applied to lower energy environments. Hybrid options offer the benefits of both structural and natural solutions, but these options may require further assessment for use in a high energy environment found at a tidal inlet. Historically, the use of natural or nature-based solutions has generally been preferred from a regulatory standpoint, as these options may minimize the impact to jurisdictional resources, including the wildlife refuge and the surrounding national seashore. Jurisdictional requirements at both the federal and state levels can impact the ability to implement structural and even some of the hybrid mitigation options assessed in this analysis. Nonetheless, it will be important to consider a range of options in order to determine what provides the most benefit (from an engineering perspective) with the least extent of hydrodynamic impact.

The modeling effort conducted under this study indicated that the Terminal Groin Extension, Channel Relocation, and Island Restoration options (Figure 16, Table 10) provide the highest effectiveness in terms of reducing velocities near the marsh shoreline and, therefore, overall shoreline erosion. However, each of these options can be expected to have measurable, if not significant, hydrodynamic impact both within and beyond the project study area, and the regulatory concerns associated with these impacts would need to be addressed. Options such as living shorelines and thin layer placement, while more attractive from an environmental perspective, are not typically utilized near tidal inlets because of the steep channel slopes and high flow velocities in these areas. Thus, living shorelines are not expected to provide the same extent of mitigation benefits as the options assessed in the modeling analysis.

While each alternative was explored separately, future work could look into combinations of alternatives as they could lead to further reductions of flow velocities. Combining the benefits of “gray” and “green” coastal protection alternatives, these hybrid options could result in a solution that is effective in

high-velocity environments while also providing ecological benefits, including habitat creation (Gittman et al., 2014; Sutton-Grier et al., 2015). For example, implementing temporary hard structures to mitigate extreme events until a nature-based solution is fully established (Bouma et al., 2014) or combining wetlands with hardened structures to improve flood defenses in an estuary (Smolders et al., 2020) are hybrid methods that have been implemented or proposed that combine benefits from both ends of the gray-to-green coastal protection spectrum.

As the documented marsh erosion trends are expected to continue, it is recommended that marsh shoreline position be taken into consideration as part of the overall assessment of the project area, similar to the continued examination and forecasting of the ocean shoreline position included in NCDOT's current N.C. 12 monitoring efforts. The data provided under this effort provides a useful opportunity to consider development of an erosion threshold criteria similar to that developed for ocean shoreline vulnerability; the marsh characterization system and the vulnerability indicator system could be considered as parameters for this threshold criteria. With further (site-specific) analysis, the assessment of mitigation options and vulnerability indicator recommendations could also be translated to other sections of N.C. 12 on Hatteras and Ocracoke Islands where marsh shoreline erosion represents a potential threat to the transportation infrastructure. At minimum, continued collection and review of data in the project area vicinity will be critical to the identification, development, and implementation of erosion mitigation as well as transportation infrastructure options.

### *Research implications*

The development of the marsh shoreline characterization system provides an opportunity to build a technique or standardized methodology for the evaluation of marsh shoreline condition, both specific to North Carolina and beyond. The characterization system developed in this study attempts to consolidate both the physical and biological parameters that could be refined in further analysis.

The research approach applied to this project was intended to identify and model the primary drivers of marsh shoreline erosion, rather than to focus simply on the extent and consequences of the erosion. The fragility curves allow for the identification of water levels at which transportation infrastructure could be flooded or otherwise vulnerable to damage; this analysis provides an opportunity for the implementation of a warning system that allows for damage mitigation in advance of actual impact. The numerical model provided a site-specific assessment of potential options and the relationship to infrastructure vulnerability, providing a feasibility review of mitigation alternatives. This approach could be tested, calibrated, and validated for other locations along the Outer Banks or the North Carolina estuarine coastline to inform future planning and flood-risk management efforts.

# Acknowledgements

The authors thank Pablo Hernandez, Adam Venckauskas with NCDOT Division 1; NCDOT divers Benjamin Presgrave, William Cox, and William Mueller; and the U.S. Coast Guard Station Oregon Inlet for their assistance with field work and data collection. North Carolina State University students Carter Rucker, Johnathan Woodruff, Kelly Fawcett, Adam Behr, Sophia Rosenberg, and Vega Sproul, and United States Naval Academy Midshipman Brent Schwartz, Joshua Torres, Ryan Fitzgerald, Nicholas Hilaire, and Justin McCabe assisted with marsh shoreline surveys and data collection. Field deployments were conducted as part of the During Nearshore Event Experiment (DUNEX), which was facilitated by the U.S. Coastal Research Program (USCRP). We thank USCRP for their support of this effort through logistics and coordination. Mike Grilliot and the NSF RAPID team provided bathymetric measurements from 2019, and Peter Traykovski and Nico Traykovski of Woods Hole Oceanographic Institution provided bathymetric measurements from 2021.

# References

- Berkowitz, J. F., and Szimanski, D. M. (2020). Documenting Engineering with Nature® Implementation within the US Army Corps of Engineers Baltimore District - Completed Projects and Opportunities for Chronosequence Analysis. ERDC/TN EWN-20-3. Vicksburg, MS: US Army Engineer Research and Development Center. doi: 10.21079/11681/38141
- Berman, J.W.; Wartman, J.; Olsen, M.; Irish, J.L.; Miles, S.B.; Tanner, T.; Gurley, K.; Lowes, L.; Bostrom, A.; Dafni, J.; et al. Natural hazards reconnaissance with the NHERI RAPID facility. *Front. Built Environ.* 2020, 11, 573067. <https://doi.org/10.3389/fbuil.2020.573067> (accessed on 1 April 2022).
- Blanton, B., Madry, S., Galluppi, K., Gamiel, K., Lander, H., Reed, M., et al. (2008). Report for the State of North Carolina Floodplain Mapping Project: Coastal Flood Analysis System. A RENCI Technical Report TR-08-08. Topographic/BathymetricData.
- Booij, N., Ris, R. C., and Holthuijsen, L. H. (1999). A third-generation wave model for coastal regions: 1. Model description and validation. *J. Geophys. Res.* 104, 7649–7666. doi: 10.1029/98JC02622
- Borchert, S.M.; Osland, M.J.; Enwright, N.M.; Griffith, K.T. Coastal wetland adaptation to sea level rise: Quantifying potential for landward migration and coastal squeeze. *J. Appl. Ecol.* 2018, 55, 2876–2887. <https://doi.org/10.1111/1365-2664.13169>.
- Bouma, T. J., van Belzen, J., Balke, T., Zhu, Z., Airoidi, L., Blight, A. J., et al. (2014). Identifying knowledge gaps hampering applications of intertidal habitats in coastal protection: Opportunities & steps to take. *Coastal Engineering.* 87, 147-157. doi: 10.1016/j.coastaleng.2013.11.014
- Bruun, P. (1978). *Stability of Tidal Inlets. Theory and Engineering.* Trondheim, Norway: Elsevier Scientific Publishing Company.
- Cialone, M.; Elko, N.; Lillycrop, J.; Stockton, H.; Raubenheimer, B.; Rosati, J. During Nearshore Event Experiment (DUNEX): A collaborative community field data collection effort. In *Proceedings of the*

9th International Conference Coastal Sediments, Tampa/St. Petersburg, FL, USA, 27–31 May 2019.  
[https://doi.org/10.1142/9789811204487\\_0253](https://doi.org/10.1142/9789811204487_0253).

- Cleary, W. J., and FitzGerald, D. M. (2003). Tidal Inlet Response to Natural Sedimentation Processes and Dredging-Induced Tidal Prism Changes: Mason Inlet, North Carolina. *J. Coast. Res.* 19, 1018-1025.
- Clinch, A. S., Russ, E. R., Oliver, R. C., Mitasova, H., Overton, M., 2012. Hurricane Irene and the Pea Island Breach: Pre-storm site characterization and storm surge estimation using geospatial technologies. *Shore & Beach*, 80(2), 10p.
- Davinroy, R. D. (1990). Bendway Weirs, A New Structural Solution to Navigation Problems Experienced on the Mississippi River, P.I.A.N.C. A.I.P.C.N. Bulletin.
- Dean, R. G., and Dalrymple, R. A. (2002). *Coastal Processes with Engineering Applications*. Cambridge University Press. doi: 10.1017/CBO9780511754500
- Deltares (2022). Delft3D-FLOW. Simulation of multi-dimensional hydrodynamic flows and transport phenomena, including sediments. User Manual Hydro-Morphodynamics. Version: 4.05, SVN Revision: 75129.
- Derrick, D. L., Pokrefke, T. J., Boyd, M. B., Crutchfield, J. P., and Henderson, R. R. (1994). Design and development of bendway weirs for the Dogtooth Bend Reach, Mississippi River. Hydraulic Model Investigation. Technical Report HL-94-10. Vicksburg, MS: U.S. Army Corps of Engineers Engineer Research and Development Center.
- Ellingwood, B.; Rosowsky, D.; Li, Y.; Kim, J. Fragility assessment of light-frame wood construction subjected to wind and earth-quake hazards. *J. Struct. Eng.* 2004, 130, 1921–1930.
- Emery, W. J., and Thomson, R. E. (2001). *Data Analysis in Physical Oceanography*, 2nd ed. Amsterdam: Elsevier Sci.
- Ferrarin, C., Madricardo, F., Rizzetto, F., McKiver, W., Bellafiore, D., Umgiesser, G., et al. (2018). Geomorphology of scour holes at tidal channel confluences. *Journal of Geophysical Research: Earth Surface*. 123, 1386– 1406. doi: 10.1029/2017JF004489
- Gauchi, J.P. and P. Chagnon, 2001. “Comparison of selection methods of explanatory variables in PLS regression with application to manufacturing process data.” *Chemometrics and Intelligent Laboratory Systems*, 58, 2, 171-193. [https://doi.org/10.1016/S0169-7439\(01\)00158-7](https://doi.org/10.1016/S0169-7439(01)00158-7)
- Gittman, R. K., Popowich, A. M., Bruno, J. F., and Peterson, C.H. (2014). Marshes with and without sills protect estuarine shorelines from erosion better than bulkheads during a Category 1 hurricane. *Ocean & Coastal Management*. 102, 94-102. doi: 10.1016/j.ocecoaman.2014.09.016
- Gulliver, A.; Carnell, P.E.; Trevathan-Tackett, S.M.; Duarte de Paula Costa, M.; Masqué, P.; Macreadie, P.I. Estimating the Potential Blue Carbon Gains from Tidal Marsh Rehabilitation: A Case Study from South Eastern Australia. *Front. Mar. Sci.* 2020, 7, 403. <https://doi.org/10.3389/fmars.2020.00403>.
- Hardaway, C. S., Milligan, D. A., Wilcox, C., and Duhring, K. (2017). Living shoreline design guidelines for shore protection in Virginia’s estuarine environments. SRAMSOE #463. Gloucester Point, VA: Virginia Institute of Marine Science. doi: 10.21220/V5CF1N

- Hjulström, F. (1939). Transportation of Detritus by Moving Water: Part 1. Transportation. SP 10: Recent Marine Sediments, Special Volume. 5-31.
- Humberston, J., Lippmann, T., and McNinch, J. (2019). Observations of wave influence on alongshore ebb-tidal delta morphodynamics at Oregon Inlet, NC. *Marine Geology*. 418, 106040. doi: 10.1016/j.margeo.2019.106040
- Johnston, J.; Cassalho, F.; Miesse, T.; Ferreira, C.M. Projecting the effects of land subsidence and sea level rise on storm surge flooding in Coastal North Carolina. *Sci. Rep.* 2021, 11, 21679. <https://doi.org/10.1038/s41598-021-01096-7>.
- Khandel, O.; Soliman, M. Integrated framework for assessment of time-variant flood fragility of bridges using deep learning neural networks. *J. Infrastruct. Syst.* 2021, 27, 04020045.
- Kraus, N. C. (2008). Engineering of Tidal Inlets and Morphologic Consequences. *Handbook of Coastal and Ocean Engineering*. 867-900. doi: 10.1142/9789812819307\_0031
- Lesser, G.R., Roelvink, J.A., van Kester, J.A.T.M., Stelling, G.S., 2004. Development and validation of a three-dimensional morphological model. *Coast. Eng.* 51, 883–915. <https://doi.org/10.1016/j.coastaleng.2004.07.014>
- Li, Y.; Dong, Y.; Frangopol, D.M.; Gautam, D. Long-term resilience and loss assessment of highway bridges under multiple natural hazards. *Struct. Infrastruct. Eng.* 2020, 16, 626–641.
- Lillycrop W. J., and Hughes S. A. (1993). Scour Hole Problems Experienced by the Corps of Engineers; Data Presentation and Summary. Miscellaneous Paper CERC-93-2. Vicksburg, MS: U.S. Army Corps of Engineers Engineer Research and Development Center.
- Luetlich, R. A., and Westerink, J. J. (2004). Formulation and numerical implementation of the 2D/3D ADCIRC Finite Element Model Version 44.XX.
- Mississippi Watershed Management Organization. (2010). A Guide to Bank Restoration Options for Large River Systems: Part II Bioengineering Installation Manual MWMO Watershed Bulletin 2010-3. 95 pp.
- Over, J.R.; Sherwood, C.R.; Traykovski, P.A.; Olson, A.; Randall, N.; Bales, R.; Brosnahan, S. Bathymetric data in Pea Island National Wildlife Refuge, North Carolina in November 2020 and April, September, and October 2021 in DUNEX topographic, bathymetric, and supporting GPS data collected in Pea Island National Wildlife Refuge, North Carolina 2020–2021. U.S. Geol. Surv. Coast. Mar. Hazards Program 2022, in press. <https://doi.org/10.5066/P9DPZZG2>.
- Padgett, J.E., Spiller, A., and Arnold, C. 2012. Statistical analysis of coastal bridge vulnerability based on empirical evidence from Hurricane Katrina, *Structure and Infrastructure Engineering*, 8(6), 595-605, doi: 10.1080/15732470902855343
- Raposa, K., Wasson, K., Nelson, J., Fountain, M., West J., Endris, C., et al. (2020). Guidance for thin-layer sediment placement as a strategy to enhance tidal marsh resilience to sea-level rise. Published in collaboration with the National Estuarine Research Reserve System Science Collaborative.

- Rosgen, D. L. (2011). Natural Channel Design: Fundamental Concepts, Assumptions, and Methods. In A. Simon, S.J. Bennett, & J.M. Castro (Eds.), *Stream Restoration in Dynamic Fluvial Systems: Scientific Approaches, Analyses, and Tools*, Geophysical Monograph Series 194, pp. 69–93. Washington, D.C.: American Geophysical Union.
- Scurlock, S. M., Baird, D. C., Cox, A. L., and Thornton, C. I. (2012). Bendway weir design – Rio Grande physical model. Colorado State University, Engineering Research Center, Bureau of Reclamation Technical Service Center.
- Smolders, S., João Teles, M., Leroy, A., Maximova, T., Meire, P., and Temmerman, S. (2020). Modeling Storm Surge Attenuation by an Integrated Nature-Based and Engineered Flood Defense System in the Scheldt Estuary (Belgium). *J. Mar. Sci. Eng.* 8, 27. doi: 10.3390/jmse8010027
- Sutton-Grier, A. E., Wowk, K., and Bamford, H. (2015). Future of our coasts: The potential for natural and hybrid infrastructure to enhance the resilience of our coastal communities, economies, and ecosystems. *Environmental Science & Policy.* 51, 137-148. doi: 10.1016/j.envsci.2015.04.006
- Tomiczek, T., Kennedy, A., and S. Rogers, 2014. “Collapse limit state fragilities of wood-framed residences from storm surge and waves during Hurricane Ike.” *J. Waterway, Port, Coastal, and Ocean Engineering*, 140(1), 43-55. [https://doi.org/10.1061/\(ASCE\)WW.1943-5460.0000212](https://doi.org/10.1061/(ASCE)WW.1943-5460.0000212)
- Tomiczek, T.; O’Donnell, K.; Furman, K.; Webbmartin, B.; Scyphers, S. Rapid Damage Assessments of Shorelines and Structures in the Florida Keys after Hurricane Irma. *Nat. Hazards Rev.* 2020, 21, 05019006. [https://doi.org/10.1061/\(ASCE\)NH.1527-6996.0000349](https://doi.org/10.1061/(ASCE)NH.1527-6996.0000349).
- Tomiczek, T., Sciaudone, E. J., Velasquez-Montoya, L., Smyre, E. J., Wargula, A., Fawcett, K., et al. (2022). Investigation of Barrier Island Highway and Marsh Vulnerability to Bay-Side Flooding and Erosion. *Journal of Marine Science and Engineering.* 10, 734. doi: 10.3390/jmse10060734
- Torio, D.D.; Chmura, G.L. Assessing Coastal Squeeze of Tidal Wetlands. *J. Coast. Res.* 2013, 29, 1049–1061.
- Toso, C., Madricardo, F., Molinaroli, E., Fogarin, S., Kruss, A., Petrizzo, A., et al. (2019). Tidal inlet seafloor changes induced by recently built hard structures. *PloS one*, 14(10), e0223240. doi: 10.1371/journal.pone.0223240
- Traykovski, P.; Francis, H. Development of a highly portable unmanned surface vehicle for surf zone bathymetric surveying. *J. Coast. Res.* 2021, 37, 933–945. <https://doi.org/10.2112/JCOASTRES-D-20-00143.1>.
- USACE (U.S. Army Corps of Engineers). (1995). *Design of Coastal Revetments, seawalls and bulkheads.* EM-1110-2-1614. Vicksburg, MS: U.S. Army Corps of Engineers Engineer Research and Development Center.
- USACE (U.S. Army Corps of Engineers). (2001). *Manteo (Shallowbag) Bay North Carolina. Supplement No. 2 Final supplement No. III. Environmental Impacts Statement.* USACE Wilmington District.
- USACE (U.S. Army Corps of Engineers). (2002). *Coastal Engineering Manual.* Washington, DC: USACE.

- U.S. Department of Agriculture, Forest Service, National Technology and Development Program. (2003). A Soil Bioengineering Guide for Streambank and Lakeshore Stabilization. FS-683P. San Dimas, CA.
- U.S. Fish and Wildlife Service. Pea Island National Wildlife Refuge. 2013. Available online: <https://www.fws.gov/refuge/pea-island> (accessed on 5 May 2022).
- van de Lindt, J. W., Peacock, W.G., Mitrani-Reiser, J., Rosenheim, N., Deniz, D., Dillard, M., Tomiczek, T., Koliou, M., Graettinger, A., Crawford, P.S., Harrison, K., Barbosa, A., Tobin, J., Helgeson, J., Peek, L., Memari, M., Sutley, E.J., Hamideh, S., Gu, D., Cauffman, S., and Fung, J. 2020. “Community resilience-focused technical investigation of the 2016 Lumberton, North Carolina, flood: An interdisciplinary approach.” *Nat. Hazards Rev.* 21 (3): 04020029. [https://doi.org/10.1061/\(ASCE\)NH.1527-6996.0000387](https://doi.org/10.1061/(ASCE)NH.1527-6996.0000387).
- Velasquez-Montoya, L., Overton, M. F., Sciaudone, E. J., 2020. Natural and anthropogenic-induced changes in a tidal inlet: Morphological evolution of Oregon Inlet. *Geomorphology* 350 (2020), 106871 1-8. <https://doi.org/10.1016/j.geomorph.2019.106871>
- Velasquez-Montoya, L., Sciaudone, E.J., Smyre, E., and Overton, M.F., 2021. Vulnerability indicators for coastal roadways based on barrier island morphology and shoreline change predictions. *Natural Hazards Review*, 22(2): 04021003.
- Wargula, A., Sciaudone, E., Velásquez-Montoya, L., Fawcett, K., Amodeo, M., Smyre, E., and T. Tomiczek, 2021. “Marsh erosion processes near a coastal highway on the Outer Banks, NC.” *Geo-Extreme 2021: Case Histories and Best Practices*, November 7–10, 2021, Savannah, Georgia.
- Webb, B.; Dix, B.; Douglass, S.; Asam, S.; Cherry, C.; Buhring, B. *Nature-Based Solutions for Coastal Highway Resilience: An Implementation Guide*; Federal Highway Administration: Washington, DC, USA, 2019.
- Wentworth, C. K. (1922). A scale of grade and class terms for clastic sediments. *The Journal of Geology*. 20, 377-392.
- Westerink, J. J., Luettich, R. A., Feyen, J. C., Atkinson, J. H., Dawson, C., Roberts, H. J., et al. (2008). A basin to channel scale unstructured grid hurricane storm surge model applied to southern Louisiana. *Monthly Weather Review*. 136, 833–864. doi: 10.1175/2007MWR1946.1
- Winkler, M. F. (2003). *Defining Angle and Spacing of Bendway Weirs*. Technical Report, CHETN-IX-12. Vicksburg, MS: U.S. Army Corps of Engineers Engineer Research and Development Center.

# APPENDIX A

**Report:**

**Pilot Field Deployment at the Oregon Inlet flood channel and  
along the sound side of Pea Island**



Pea Island, NC, October 08, 2019

Anna Wargula<sup>1</sup>, Ph.D.  
Liliana Velásquez-Montoya<sup>1</sup>, Ph.D.  
Elizabeth Sciaudone<sup>2</sup>, Ph.D., P.E.  
Elizabeth Smyre<sup>3</sup>, P.E.  
Tori Tomiczek<sup>1</sup>, Ph.D.

<sup>1</sup>Department of Naval Architecture and Ocean Engineering, U.S. Naval Academy (USNA)

<sup>2</sup>Department of Civil, Construction and Environmental Engineering, North Carolina State University  
(NCSU)

<sup>3</sup>Dewberry

Interim Report 2: NC DOT RP 2020-09

Monitoring and modeling sound-side erosion near Oregon Inlet to support feasibility level  
transportation planning

December 12, 2019  
Annapolis, MD

## Summary:

This report summarizes a field campaign completed by researchers at the United States Naval Academy (USNA), North Carolina State University (NCSU), and Dewberry as part of the North Carolina Department of Transportation (NCDOT) funded research project RP 2020-09 “Monitoring and modeling sound-side erosion near Oregon Inlet to support feasibility level transportation planning.”

In early October 2019, the research team traveled to Oregon Inlet, NC, to conduct Field Campaign #1 (Task 1a, Appendix A). This pilot field deployment had multiple goals, including (1) to collect measurements of hydrodynamic and sediment characteristics to understand the spatial variability in currents and soil properties in the study area, (2) to coincide with the Pilot DUNEX<sup>1</sup>, a multi-agency, collaborative field campaign on sites spanning the Outer Banks from Duck to Hatteras, NC, in order to develop new collaborations in support of this study, and (3) to test methods for upcoming field deployments in year 2020. The field campaign was a success: the team collected nearly all of the data initially planned, in addition to other datasets that will help broaden understanding of the hydrodynamics and soil characteristics of Pea Island and the flood channel. Data post-processing is currently underway; preliminary field notes suggest alongshore variability in soil and vegetation on land and cross-shore variability in sediment type in the flood channel.

## Site Conditions:

The study area corresponds to the flood channel of Oregon Inlet on the sound-side of the Pea Island National Wildlife Refuge (Figure 1).

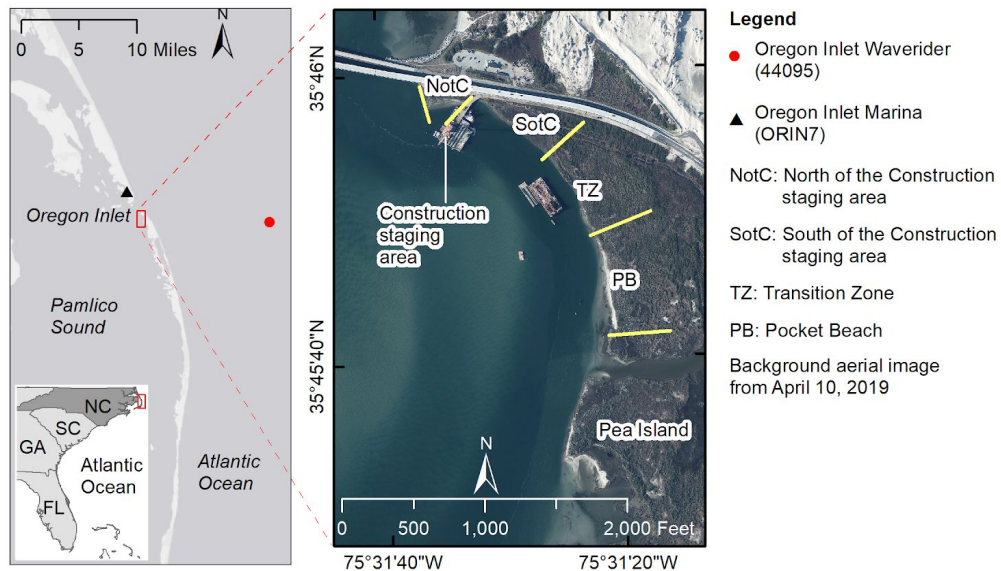


Figure 1: The left hand map shows the study area and nearby tidal gage (black triangle) and waverider buoy (red circle) The right hand map shows the study area divided into roughly 4 regions, each with distinct soil and vegetation characteristics.

<sup>1</sup> News Release: “Multi-stakeholder, During Nearshore Event Experiment begins pilot study”

<https://www.erd.usace.army.mil/Media/News-Releases/Article/1977465/multi-stakeholder-during-nearshore-event-experiment-begins-pilot-study/>

Measurements were collected between October 07 and 11, 2019, during spring tides and an approaching offshore storm (Subtropical Storm Melissa). Sustained winds at the closest NOAA weather station (black triangle, Figure 1) ranged from 3 to 20 knots during much of the week (Figure 2), making boat work challenging. Owing to large offshore wave heights 5 to 14 ft (Figure 2), the inlet mouth was inaccessible for boat-mounted measurements.

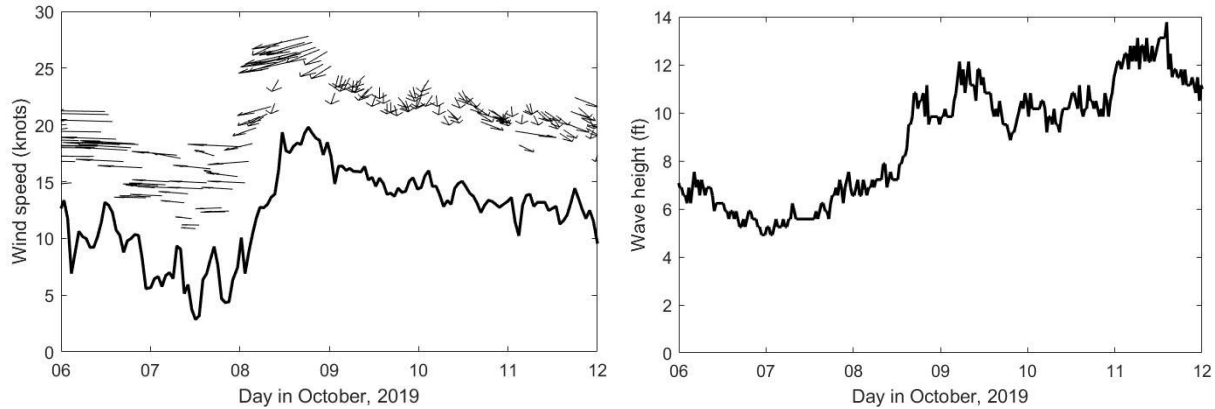


Figure 2. On the left: wind speeds and directions versus time measured at the Oregon Inlet Marina (black triangle in left hand map in Figure 1). On the right: wave heights versus time measured offshore and to the south of Oregon Inlet at NDBC Station 44095 Oregon Inlet Waverider (red circle in left hand map in Figure 1).

Measurements at the NOAA tide gage at the Oregon Inlet Marina (black triangle in left hand map in Figure 1) suggest that water levels were higher than the astronomical spring tides during much of the week, growing to nearly 2 ft above astronomical tides by 11 October (Figure 3). Water levels at Pea Island appeared to be similar to these measured water levels at the marina. The marsh became inaccessible owing to high water even at low tide during the end of the week.

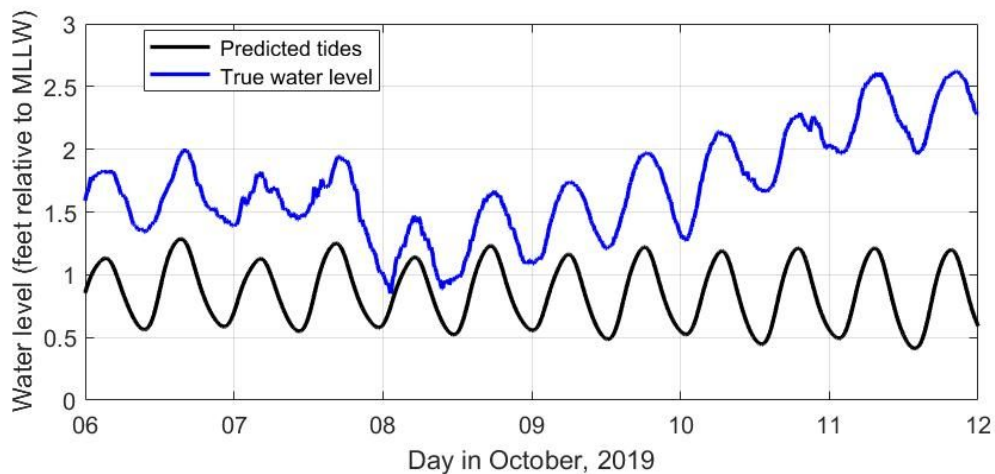


Figure 3. Predicted tidal water levels (black curve) and true water levels (blue curve) relative to Mean Lower Low Water (MLLW) versus time measured at the Oregon Inlet Marina (black triangle, Figure 1).

**Deployment:**

The proposed and completed measurements are shown in Table 1. Marsh edge topography (Item 3, Table 1) was not surveyed, owing to high water levels limiting access to the marsh at the end of the week, during the planned measurement. However, aerial images can continue to be used to identify the location of the shoreline and pre-storm surveys will be conducted in the event of a rapid response field campaign. Water level measurements (Item 7, Table 1) at the four locations shown in triangles in Figure 4, were recovered 12 November 2019. As a result of scheduling the work with the Pilot DUNEX, the team established new collaborations with Dr. Nina Stark and Ms. Reem Jaber [Virginia Tech (VATech)] and Dr. Navid Jafari and Mr. Brian Harris [Louisiana State University (LSU)]. The VATech and LSU teams, using their own funding and working in conjunction with our team, collected soil strength measurements (Item 2, Table 1) in the flood channel and marsh, which they are sharing with our team in support of this project.

Table 1. Field Campaign #1 Measurements

Item	Description	Planned	Completed
1	Sediment samples in the channel and marsh	✓	✓
2	Soil strength in the channel and marsh		✓
3	Marsh edge topography, latitude, and longitude	✓	
4	Marsh vegetation identification		✓
5	Bathymetry of the channel	✓	✓
6	Currents in the channel	✓	✓
7	Water levels in the channel and marsh		✓

Land-based measurements included sediment samples, soil strength, and marsh vegetation identification (Items 1, 2, and 4, Table 1). Locations of the sediment samples and vegetation identification are shown as yellow circles in Figure 4. Surface sediment samples were collected with a trowel and were analyzed at NCSU for sediment grain size distribution. Soil strength in the marsh were collected by Dr. Jafari and Mr. Harris (LSU) using a custom-made penetrometer<sup>2</sup> and are being processed at LSU. Marsh vegetation was identified using identification cards developed by Ms. Kelly Fawcett (NCSU).

<sup>2</sup> Jafari, N.H., Harris, B.D., Cadigan, J.A., and Chen, Q., 2019, Piezocone penetrometer measurements in coastal Louisiana wetlands, *Ecological Engineering*, 127, 338-347, doi:10.1016/j.ecoleng.2018.12.012.

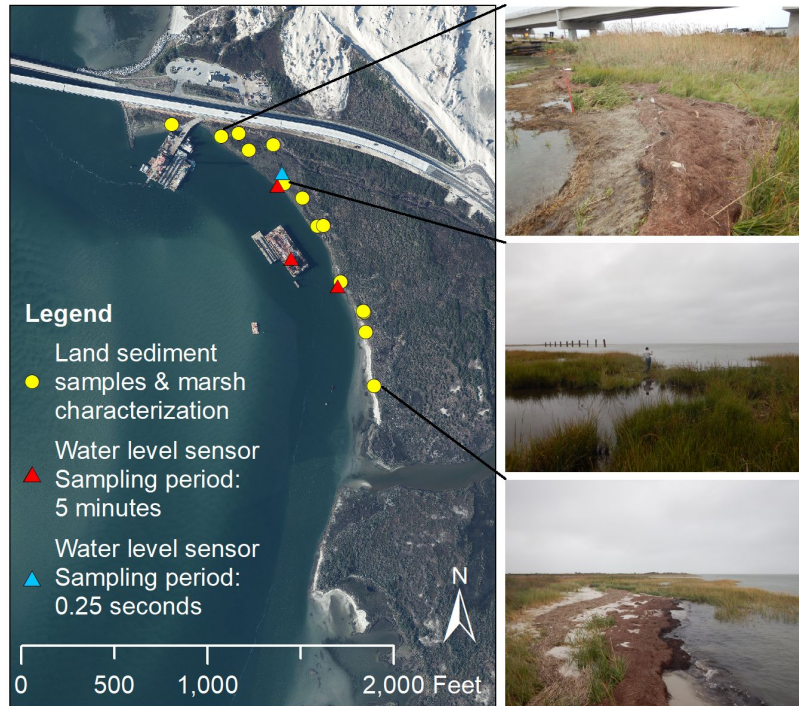


Figure 4. Location of land sediment sampling, marsh characterization, and water level stations.

Measurements in the flood channel included bathymetry, currents, sediment samples, and soil strength (Items 1, 2, 5, and 6, Table 1). Locations of bathymetry measurements and channel bed sediment samples are shown in Figure 5. Locations of current transects and soil strength measurements are shown in Figure 6. Current profiles were measured using a Nortek Signature1000 and RTK-GPS during flood and ebb to capture spatial and tidal variability. Bathymetry measurements were collected using a single beam echosounder in a z-boat operated by the NSF RAPID facility<sup>3</sup> personnel from the University of Washington (UW). Sediment samples were collected with a sediment grabber and were processed at NCSU for sediment grain size distribution. Soil strength measurements were collected by Dr. Stark and Ms. Jaber (VATech) using a custom-made penetrometer<sup>4</sup> and are being processed at VATech.

<sup>3</sup> <https://rapid.designsafe-ci.org/>

<sup>4</sup> Stark, N., and Kopf, A., 2011, Detection and quantification of sediment remobilization processes using a dynamic penetrometer, *OCEANS'11 MTS/IEEE KONA*, Waikoloa, HI, 1-9, doi:10.23919/OCEANS.2011.6106914.

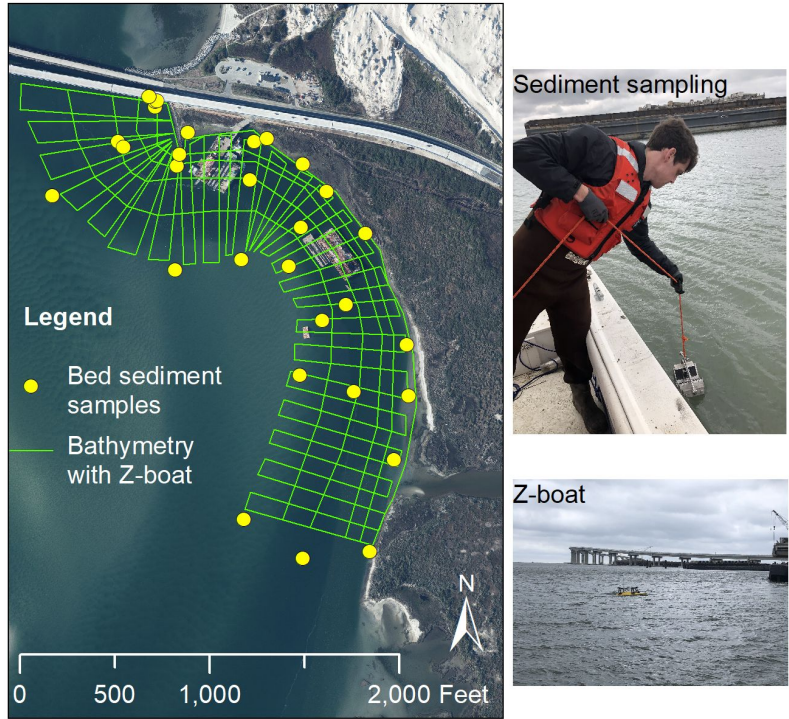


Figure 5. Location of bathymetry measurements and channel bed sediment samples.

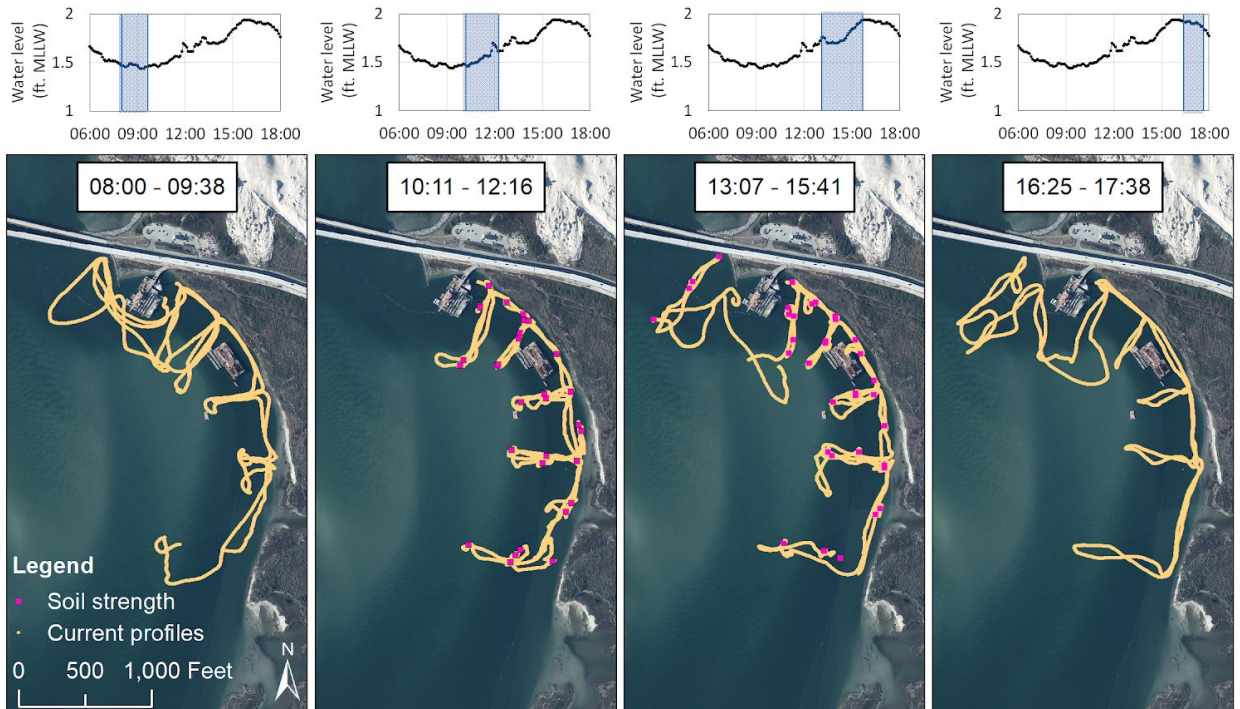


Figure 6. Locations of boat-mounted current measurements (orange transects) and soil strength measurements (pink points) at four different stages of the tidal cycle (shown in the figures on top).

Water levels were measured with pressure gages at 4 locations (red and blue triangles in Figure 4). Three gages were placed in the flood channel on 10 and 26 October, 2019: one on a piling on the sound-side (western) edge of the flood channel and two on the Pea Island shoreline (eastern) side of the flood channel. These three gages measured water levels every 5 minutes and will be used to determine the local variability in water surface elevation owing to tidal and subtidal processes (e.g., wind and storm surge). In addition, a fourth water level gage was deployed on the marsh on 11 October, 2019, measuring water levels four times a second (4 Hz) and will be used to determine the overland flooding and the magnitude of boat wake and wind waves on the marsh. The gages were recovered on 12 November, 2019, after measuring a roughly month of trends in water levels and waves affecting the marsh.

**Preliminary Field Notes:**

Field notes from data collection on the marsh and shoreline suggest alongshore variability in sediment type, soil strength, and vegetation. The area surveyed is roughly divided into four regions (Figure 1): North of the Construction staging area (NotC), South of the Construction staging area (SotC), Transition Zone (TZ), and Pocket Beach (PB). All results shared are preliminary, and data processing is ongoing at this time.

The median sediment grain size ( $D_{50}$ ) are shown in Figure 8. At NotC, the small beach contained mainly fine sand. Going south along the shoreline from SotC to PB, the sediment increased in grain size from coarse silt (SotC) to medium sand (PB). In the flood channel, sediment grain size was larger (medium sand) on the western side of the flood channel and south of the pocket beach. However, finer grain size (fine sand and very fine sand) were found on the eastern and middle of the flood channel in the NotC and SotC regions. This variability may reinforce the alongshore variability in erosion processes along the shore. These results will be compared to the soil strength measurements (gathered by LSU and VATEch researchers) to gain a better understanding of further erodibility in the region.

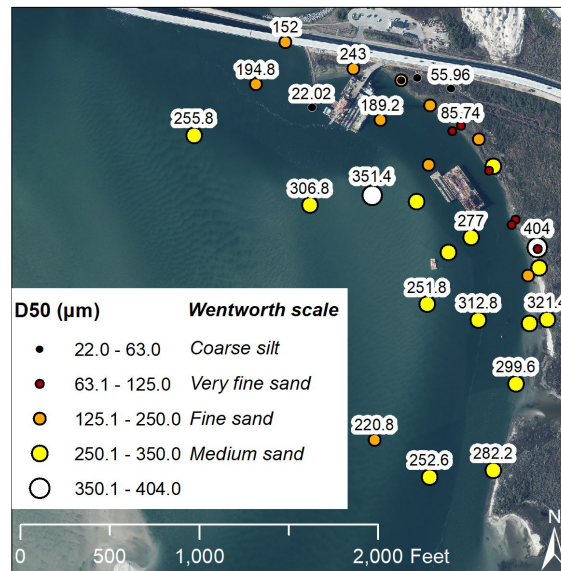


Figure 8. Median sediment grain size (d50) in the flood channel and on land.

The majority of plant species observed on land were various types of grasses and sedges. At NotC, where the ground was solid and sandy, the most abundant plant was the *Phragmites australis*. At SotC, where the water level was higher and the mud was softer, *Spartina patens* (salt meadowgrass), *Spartina alterniflora* (smooth cordgrass), *Salicornia depressa* (Virginia Glasswort), and *Distichlis spicata* (saltgrass) were observed (Figure 9).



Figure 9: From left to right, *Spartina alterniflora* (smooth cordgrass), *Salicornia depressa* (Virginia Glasswort), and *Distichlis spicata* (saltgrass), three of the four vegetation species observed at SotC.

The salt meadowgrass was more prevalent farther down the area surveyed, in the Transition Zone. It was also more common at the water's edge. Smooth cordgrass was the most dense plant between the *Phragmites* and the waterline. Sparsely throughout the cordgrass was Virginia Glasswort (Figure 10).



Figure 10: From left to right, *Spartina patens\** (salt meadowgrass), *Salicornia depressa* (Virginia Glasswort), *Juncus roemerianus* (black needlerush), and *Solidago sempervirens* (seaside goldenrod), some of the species observed at TZ. \*Note that the white on the left hand image is larvae not seeds.

Closer to the sandy beach areas (between TZ and PB, Figure 11) *Borrchia frutens* (seaside oxeye) and *Juncus roemerianus* (black needlerush) were observed. Where the ground became more solid, there were

more established plants such as the seaside oxeye and seaside goldenrod (*Solidago sempervirens*). The mats of dead plant washed up on the shore making up the wrack line were primarily black needlerush and smooth cordgrass.



Figure 11: From left to right, *Borrchia frutens* (seaside oxeye) and *Juncus romerianus* (black needlerush), two common species observed at the PB.

Measurements of bathymetry are still being processed at UW. Most of the planned z-boat track was covered, particularly on the shoreline side, providing a detailed map of the flood channel and sloping bathymetry to shore. In addition, UW surveyed NotC and near the bridge pilings closest to shore.

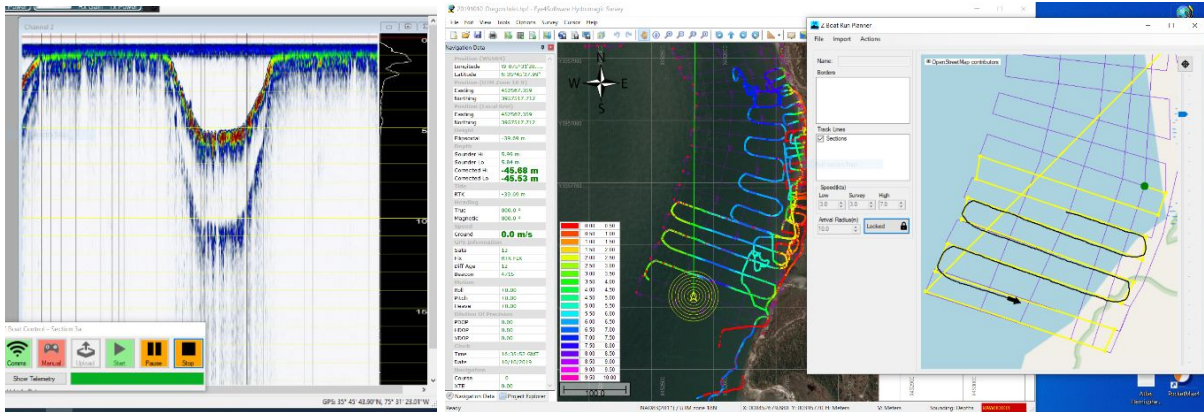


Figure 12. Screenshots from z-boat bathymetry collection showing raw data of the flood channel bathymetry, z-boat actual track (during the first hours of collection), and z-boat planned track .

Currents are also still being processed at USNA. However, our field notes suggest, as in previous preliminary field surveys, the surface currents were stronger between the Basnight Bridge and the transition zone than further south. A vertical flow towards the surface was visually depicted northwest of

the construction staging area at 16:37 on October 08. This upwelling-like flow was previously reported in the preliminary site visit completed in May 2019.

Water level data was downloaded on 15 November from all gages except for the gage located to the North on the shoreline edge (northern red triangle in Figure 4), which will be sent to UW for trouble-shooting and data recovery. Preliminary water level data are shown in Figures 13 and 14. Note that these water levels have not been corrected for fluctuations in atmospheric pressure or quality controlled for bad data. Nor have these data been corrected to the same vertical datum, meaning that the total water level is unknown at this time and the figures should be read as *relative* water levels.

However, several potential patterns may be highlighted. Figure 13 shows nearly 2 weeks of data before the inland marsh gage stopped recording. This figure suggests that non-tidal high water level events at the Oregon Inlet Marina (e.g., elevated black curve on Oct 16 - 17 in Figure 13) do not always lead to flooding of the marsh (e.g., yellow curve on Oct 16 - 17 remains low in Figure 13). In addition, the tidal fluctuations (difference between high and low tide) are higher at the marsh shoreline than at the Oregon Inlet Marina.

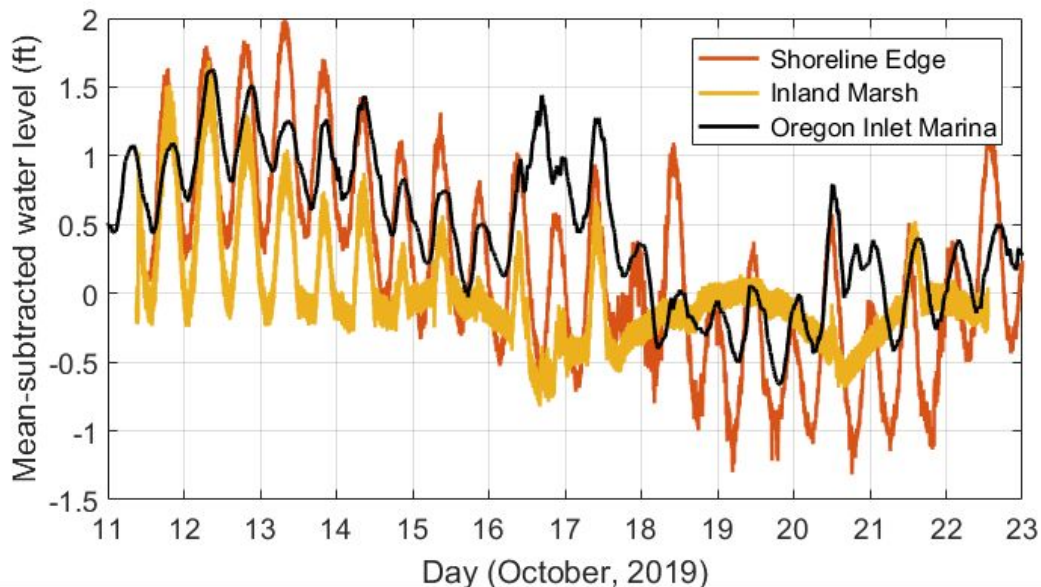


Figure 13: Mean-subtracted (relative) water levels at the shoreline edge (red curve, southern red triangle in Figure 4), inland marsh (yellow curve, blue triangle in Figure 4), and Oregon Inlet Marina (black curve, black triangle in Figure 1) versus time.

Figure 14 shows a little over 2 weeks of data including the water level gage on the piling. Similar to Figure 13, higher tidal fluctuations (larger differences in high and low tide) are evident at the marsh, compared to the Oregon Inlet Marina tidal fluctuations. The piling water levels also deviate from the shoreline edge water levels (compare blue and red curves, Figure 14), suggesting that pressure gradients are set up across the flood channel. These pressure gradients appear to be larger on the ebb, compared to the flood, suggesting tidal variability in the currents in the flood channel.

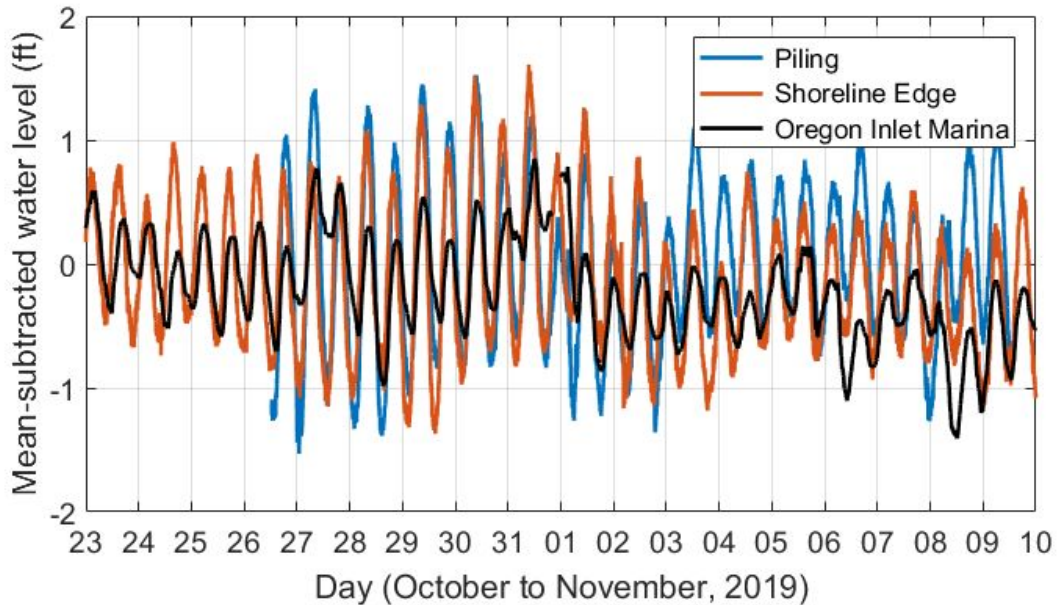


Figure 14: Mean-subtracted (relative) water levels at the piling (blue curve, western red triangle in Figure 4), shoreline edge (red curve, southern red triangle in Figure 4), and Oregon Inlet Marina (black curve, black triangle in Figure 1) versus time.

**Next steps:**

These datasets will be used to update and calibrate the numerical model (Task 2, Appendix A), to plan the long-term deployment of a current meter (Task 1b, Appendix A), to plan a more extensive field campaign in 2020 (Task 1c, Appendix A), and to begin analysis for fragility curve modeling (Task 3, Appendix A). Water level measurements, will be compared with NOAA gage analysis (Task 1e, Appendix A) to determine how existing long term datasets can be used to predict shoreline failure (Task 3h, Appendix A). Once the bathymetric data from NSF RAPID become available, it will be included in the numerical model and compared with previous hydrographic surveys in the area.

**Acknowledgements:**

We thank Pablo Hernandez (NCDOT) for all of his time, logistical support, boat operation, and creative ideas for the pilot field campaign. We thank Becky Harrison (FWS) and Sabrina Henry (NPS) for their guidance on permitting. Dr. Nina Stark (VA Tech), Reem Jaber (VA Tech), Dr. Navid Jafar (LSU), and Brian Harris (LSU) are thanked for their collaborations measuring soil strength in the channel and on the marsh. Dr. Mike Grilliot (UW) and the NSF RAPID team are thanked for their support with making bathymetric measurements and for the use of water level gages and the grab sampler. We also acknowledge the US Army Corps of Engineers Field Research Facility and the DUNEX logistics team for their organizational work to plan and execute a successful field campaign.

**APPENDIX A - Tasks and subtasks**

Table A1. Definition of subtasks

Main Task	Specific Tasks
1. Field Work	a. Field Campaign #1: Pilot study and post-processing data
	b. Long-term deployment of ADV
	c. Field Campaign #2: Winter and post-processing data
	d. Rapid-response pre- and post-storm measurements
	e. Analysis of pre-existing NOAA gauges
	f. Develop database to deliver field data to NCDOT
2. Numerical Modeling	a. Improve sed. Sizes and bathymetry in the model
	b. Enhance spatial resolution of the model
	c. Extend wave grid and implement wind
	d. Model evaluation
	e. Short- and long-term simulations to support development of fragility curves
	f. Simulation to support testing of erosion mitigation alternatives
3. Fragility Curves	a. Standardize failure definition
	b. Analysis of historical shoreline changes
	c. Analysis of field data to identify expected environmental variables
	d. Synthesis of numerical modeling results
	e. Development of empirical fragility curves
	f. Rapid response data analysis
	g. Derive empirical fragility curves for extreme events
	h. Investigate relationships of permanent gauge data with shoreline failure
	i. Development of online vulnerability indicator
4. Feasibility Erosion Mitigation Options	a. Review of demonstration sites for estuarine shoreline erosion mitigation
	b. Literature review on erosion mitigation options for deep channels
	c. Generate a list of site-specific potential mitigation options
	d. Determine feasibility criteria and define alternatives for testing and modeling
	e. Analyze modeling outputs and create recommendations
5. Other Research products and commitments	Final report
	Key milestone progress updates to NCDOT and USFWS
	Workshop with NCDOT
	Broader communication of research

**Report:**  
**Rapid Response Marsh Edge Shoreline Surveys, November 2019**

Elizabeth Sciaudone<sup>1</sup>, Ph.D., P.E.

Liliana Velásquez-Montoya<sup>2</sup>, Ph.D.

Anna Wargula<sup>2</sup>, Ph.D.

Tori Tomiczek<sup>2</sup>, Ph.D.

Elizabeth Smyre<sup>3</sup>, P.E.

<sup>1</sup>Department of Civil, Construction and Environmental Engineering, North Carolina State University

<sup>2</sup>Department of Naval Architecture and Ocean Engineering, U.S. Naval Academy

<sup>3</sup>Dewberry

Interim Report 2: NC DOT RP 2020-09

Monitoring and modeling sound-side erosion near Oregon Inlet to support feasibility level transportation planning

December 16, 2019

Raleigh, NC

## **Summary:**

This report describes two marsh edge shoreline surveys conducted on November 13, 2019 and November 25, 2019, before and after a nor'easter that impacted the study area and caused road closures from the ocean side with water and sand on the road. This fieldwork was conducted as part of Task 1d: Rapid Response Field Campaign for the North Carolina Department of Transportation (NCDOT) funded research project RP 2020-09 "Monitoring and modeling sound-side erosion near Oregon Inlet to support feasibility level transportation planning." NC 12 was closed from the Marc Basnight Bridge to Rodanthe from 5 pm November 16, 2019 to approximately 10 am on November 20, 2019<sup>1</sup>. Sound-side water levels were lower during the beginning of the storm due to the northeasterly winds but rebounded with higher than predicted water levels observed from the afternoon of November 17 to the post-storm survey on November 25. An average recession of the marsh edge of 2.5 m (8.2 ft) was observed between the two surveys. The primary mechanism of erosion observed appeared to be undercutting and slumping of the marsh platform leading to a "chunk" of marsh breaking away from the shoreline. It is noted that the pre-storm condition of the shoreline showed signs of ongoing erosion, which may be related to prior events and/or longer-term processes such as tidal currents.

## **Field Measurement Methods and Site Conditions:**

The objective of the rapid response marsh edge surveys was to document the pre- and post-storm condition of the marsh shoreline and identify mechanisms of erosion. A Trimble R10 GNSS GPS system with mobile connection to continuously operating reference stations (CORS) was used to conduct the surveys. This system has a reported horizontal accuracy of 3 mm + 0.5 ppm RMS and vertical accuracy of 5 mm + 0.5 ppm RMS. At the marsh edge, the "scarp" edge of the marsh or the location of dense vegetation was surveyed (Fig. 1). In some locations, where a small sandy beach was located, the pre-storm survey captured a high water line while the post-storm survey captured the marsh edge. These sections were omitted from assessment of marsh edge erosion, due to differences in measurement location that were not related to erosion. It is estimated that there is up to 30 cm of uncertainty in visual identification/interpretation of the marsh edge.

Personnel for the two surveys included the same GPS operator for both surveys (NCSU graduate student Carter Rucker). On November 13, NCSU undergraduate researcher Kelly Fawcett was part of the field team, and on November 25, NCSU graduate student Johnathan Woodruff accompanied Mr. Rucker to the field. Photos were also taken by Ms. Fawcett and Mr. Woodruff via mobile phone with location services enabled, and notes were taken describing observations of the marsh shoreline and erosion mechanisms.

On November 13, 2019, the survey began at 13:50 EST and concluded at 14:35 EST. On November 25, the survey began at 13:09 EST and concluded at 14:17 EST. Both surveys were

---

<sup>1</sup> source: NCDOT NC 12 Twitter

conducted as close to low tide as practicable (Fig. 2). As shown in Fig. 2, water levels were close to predicted at the time of the pre-storm survey, then slightly elevated (0.1 to 0.2 m above predicted) on November 14-15. During November 16-17, water levels dipped below predicted as winds came from the northeast (Fig. 3), but rebounded as the wind direction shifted by November 18, peaking at approximately 0.6 m above predicted at 18:24 EST that day. Water levels remained above those predicted through the date of the post-storm survey, driven by westerly winds.



Figure 1. Marsh edge survey in progress, November 25, 2019. Points were surveyed via GPS at approximately 2 m to 25 m spacing, depending on marsh edge morphology.

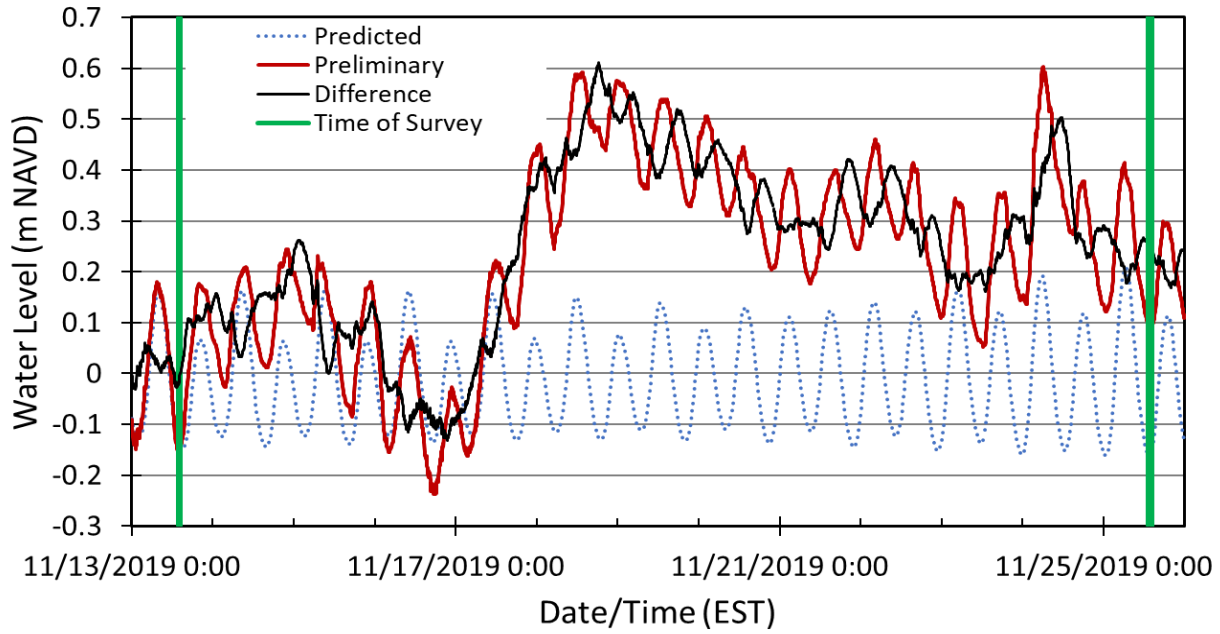


Figure 2. Predicted and preliminary water levels measured at the Oregon Inlet Marina (NOAA/NOS/CO-OPS 8652587), November 13-25, 2019. Time of survey is shown by the green bands.

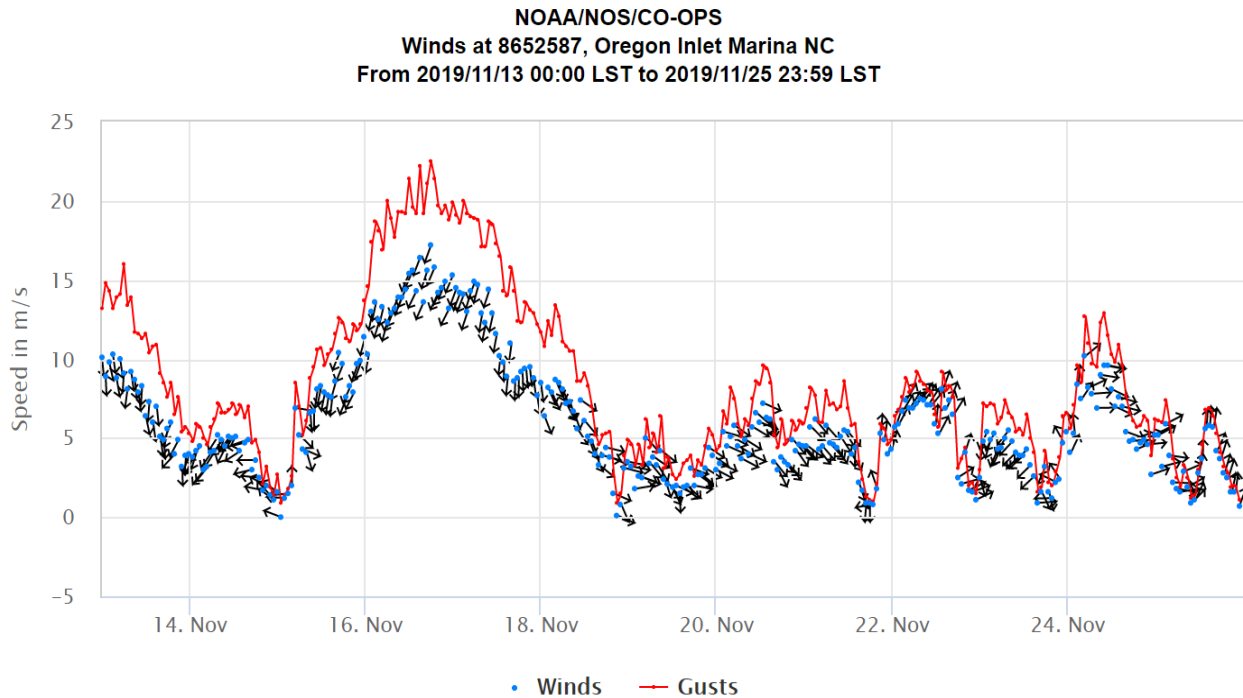


Figure 3. Wind speed, direction, and gust speed measured 2.6 ft. above Mean Sea Level at the Oregon Inlet Marina (NOAA/NOS/CO-OPS 8652587), November 13-25, 2019.

### **Data Analysis Methods:**

The data points surveyed with the R10 system were imported into ArcGIS and connected by lines using GIS tools. The Digital Shoreline Analysis System (DSAS) developed by the USGS<sup>2</sup> was used to create a series of transects at 5 m spacing along the November 25 shoreline extending to the November 13 shoreline. Transects in the sandy beach area as well as transects that were generated across indentations in the shoreline causing exaggerated measurement of change were not considered in the analysis. The length of each transect was calculated, reflecting the marsh edge shoreline change.

Additionally, photos taken in the field via mobile phone were geolocated with the phones' location services data and imported into ArcGIS.

### **Observed Shoreline Change:**

The data collected during the two marsh edge surveys is shown in Fig. 4. This figure also shows the sandy beach area which was excluded from change analysis due to inconsistent identification of the shoreline. The average marsh edge erosion was approximately 2.5 m along the surveyed area. The recession was generally between 1 and 3 m, with a maximum of 5.3 m measured just north of the sandy beach area. The minimum difference was 0.1 m (within the estimated uncertainty in the measurements) toward the southern portion of the site. Fig. 4 also shows comparison images from selected locations along the shoreline.

---

<sup>2</sup> <https://www.usgs.gov/centers/whcmssc/science/digital-shoreline-analysis-system-dsas>



Figure 4. Edge of marsh shoreline survey data (points), November 13 and 25, 2019, shown with background image from August 29, 2019 (NCDOT photo). Lines connecting the surveyed points are also shown. The red circled area was excluded from change analysis due to inconsistent identification of the shoreline in the sandy beach area (in this area on Nov. 13, a wet/dry line in the sand was surveyed, and on Nov. 25, the edge of the marsh vegetation was surveyed). Photos at the indicated areas (a), (b), and (c) are shown at right.

### **November 13, 2019 Observations:**

The shoreline condition as of November 13, 2019 showed signs of ongoing erosion, including exposed root mat and undercutting of the marsh platform as well as sections of marsh that had slumped and detached from the shoreline. Fig. 5 shows an example of this undercutting and slumping at location (b) in Fig. 4. It is noted that this location is near the maximum curvature of the tidal inlet channel.



Figure 5. Ongoing marsh erosion observed on November 13, 2019 at location (b) in Fig. 4. Marsh failure is occurring via undercutting and cracking of the marsh platform which then breaks off and falls into the water.

### **November 25, 2019 Observations:**

On November 25, 2019, many of the areas that exhibited signs of ongoing undercutting had eroded further, with escarpments observed throughout most of the shoreline except within the excluded sandy beach area. Additional detached portions of marsh were evident within the sound. Fig. 6 illustrates this retreat, showing the area indicated in Fig. 4 (b) and in Fig 5 as of the survey on November 24.



Figure 6. Series of escarpments observed on November 23, 2019 near the location shown in Figure 5. In this location the marsh edge retreated nearly 3 m between the two surveys.

### **Implications for Research Project and Future Field Surveys:**

This rapid response survey provided two significant insights into erosion of the marsh edge shoreline at Pea Island:

- Marsh erosion is ongoing, as signs of an eroding shoreline were apparent during the pre-storm survey. This may be due to previous storm impacts and/or influence of the tidal channel.
- Rapid erosion of 2 to 3 m of marsh shoreline is possible over a 12-day time period of elevated water levels.

It was also noted that consistency in identification of the marsh edge location is somewhat difficult to ensure. One improvement in survey methodology to ensure consistent identification of the marsh edge would be to place markers at the marsh shoreline (i.e., stakes, pipes) from which erosion can be measured. Future rapid response surveys may also include deployment of water level sensors to detect both water level fluctuations, and where possible, wind-driven wave heights, to enable quantification of the drivers of the erosion.

**Acknowledgements:**

We thank Pablo Hernandez (NCDOT) for facilitating site access for these surveys and Rebecca Harrison (USFWS) for collaboration and assistance with permitting. We thank Carter Rucker, Kelly Fawcett, and Johnathan Woodruff (NCSU) for their efforts in documenting the marsh shoreline condition.

**Report:**

**Full Field Deployment at the Oregon Inlet flood channel and  
along the sound side of Pea Island**



*Erosion following Hurricane Isaias (August 2020)*

Elizabeth Sciaudone<sup>1</sup>, Ph.D., P.E.

Anna Wargula<sup>2</sup>, Ph.D.

Liliana Velásquez-Montoya<sup>2</sup>, Ph.D.

Tori Tomiczek<sup>2</sup>, Ph.D.

Elizabeth Smyre<sup>3</sup>, P.E.

<sup>1</sup>Department of Civil, Construction and Environmental Engineering, North Carolina State University  
(NCSU)

<sup>2</sup>Department of Naval Architecture and Ocean Engineering, U.S. Naval Academy (USNA)

<sup>3</sup>Dewberry

Interim Report 6: NC DOT RP 2020-09

Monitoring and modeling sound-side erosion near Oregon Inlet to support feasibility level  
transportation planning

December 18, 2020

## **Summary:**

This report summarizes three field campaigns conducted in 2020 by researchers at North Carolina State University (NCSU), the United States Naval Academy (USNA), and Dewberry as part of the North Carolina Department of Transportation (NCDOT) funded research project RP 2020-09 “Monitoring and modeling sound-side erosion near Oregon Inlet to support feasibility level transportation planning.” The goals of the first field campaign on June 22, 2020, were to deploy pressure gages and a tilt current meter and conduct a shoreline survey. The second part of the first field campaign was an additional post-storm survey conducted on August 12, 2020, following Hurricane Isaias (this storm impacted the study site on August 04, 2020). The goals of the second field campaign on August 26, 2020, were to check on the equipment deployed on June 22 and deploy new pressure gages, a tilt current meter, and two current profilers. The goal of the third field campaign on October 01, 2020, was to recover all instrumentation at the site. These field campaigns were led by Dr. Sciaudone and completed with the invaluable support from Mr. Pablo Hernandez, Mr. Adam Venckauskas, the NCDOT Dive Team, and the U.S. Coast Guard Station Oregon Inlet. The field campaign was a success: the team was able to collect most of the planned data except from two instruments that failed. Data post-processing is currently underway and preliminary results are presented here.

## **1. Background:**

The field campaigns described here were conducted to partially meet proposed project goals in Task 1b (Long-term 3-4 week deployment), Task 1c (Full scale ~4 week field campaign), and Task 2d (rapid response field campaign) of the proposed NCDOT project. Task 1b had been scheduled for Fall-Winter 2019-2020, but was delayed due to delays in fund transfer to USNA and COVID-19 restrictions. Task 1c was scheduled for Summer-Fall 2020 and occurred as scheduled, combined with a modified long term deployment. Task 1d is ongoing, as it depends on the occurrence of an extreme weather event. The data collected in these field deployments will be used for model validation and to identify the magnitude of flow velocities, water levels, and waves occurring in the flood channel in the back of Pea Island and near the eroding shoreline. The rapid response data provides information about the shorter-term shoreline response to elevated water levels and waves associated with storms.

## **2. Deployment:**

The goal of the field deployments was to measure the cross-channel (cross-shore) and along-channel (alongshore) variability in currents, water levels, and flooding. Two cross-channel transects, a “southern transect” and “northern transect” were defined at two different regions of the shoreline that have different elevations and historic erosion rates<sup>1</sup> (white dashed lines in Figure 1). The northern transect was perpendicular to the low-lying marsh with largest shoreline loss over the last couple of decades; the southern transect was perpendicular to a higher elevation shoreline with lower rates of historic erosion. The safety of personnel, accessibility and ease of recovery, and ability to tether instruments securely were all considered in the selection of deployment sites.

Field work was conducted in four stages: (1) a marsh shoreline survey and deployment of the southern transect (all except the current profiler) on June 22, 2020, (2) post-hurricane Isaias marsh shoreline and

---

<sup>1</sup> Dunn, M., Sciaudone, E., and Velasquez-Montoya, L. (2019). “Estuarine shoreline erosion driven by flood channel proximity at Pea Island, NC.” *ASBPA National Coastal Conference*, Myrtle Beach, SC, Oct. 22-25, 2019.

wrack line surveys on August 12, 2020, (3) deployment of the northern transect and current profilers on August 26, 2020, and (4) recovery of instruments on October 01, 2020. Figure 1 shows the location of the study site in panel A; positions of the Oregon Inlet marina tidal gage and meteorological station (black triangle) and offshore wave buoy (red circle) in panel B; and the positions of the deployed instruments (red and green symbols), the definition of the northern and southern transects (dashed white lines), and the location of the piling used in the deployment in panel C.

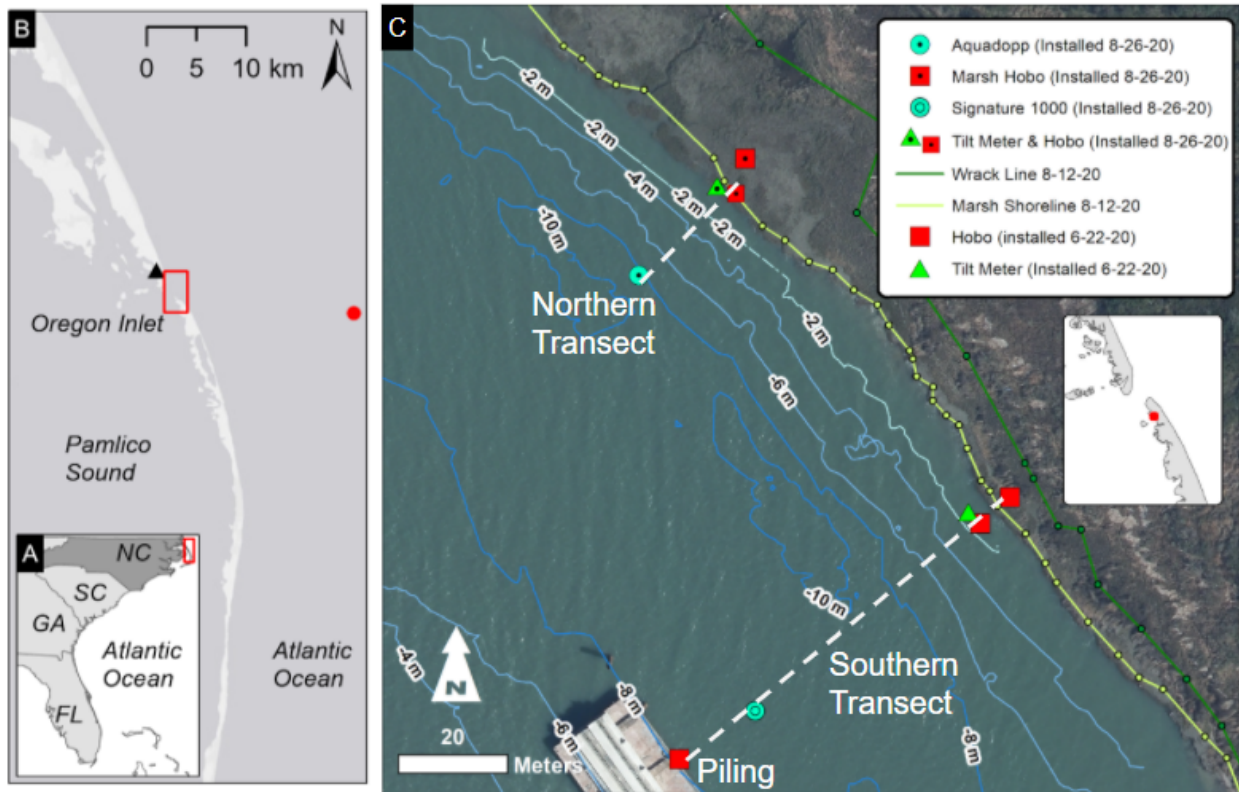


Figure 1. A: USA Southeast coast. B: Northern Outer Banks of North Carolina and nearby tidal gage and meteorological station (black triangle) and waverider buoy (red circle); C: Study site with deployed gages in red and green symbols.

All instruments were successfully deployed and recovered according to plan. All datasets except currents from the two tilt meters have been downloaded and post-processing is underway. Table 1 shows the date of deployment and recovery, elevation relative to NAVD88 (positive up) or local water levels (positive up), and local water depth at deployment (where applicable). All measurements were taken at 10 min intervals, except for sea surface elevation fluctuations, which were measured at 4 Hz for 17 minutes every 30 minutes in order to estimate wave heights every 30 min. The remaining sections of the report display plots of the data with preliminary analyses of our findings.

Table 1. Instrumentation deployed in summer 2020

<b>Instrument (Measured variable)</b>	<b>Deployment (2020)</b>	<b>Elevation (Datum, positive up)</b>	<b>Local Water Depth at Deployment</b>
Hobo (atmospheric pressure)	06/22 - 10/01	office trailer on site	--
Southern transect Hobo on the piling (pressure and temperature)	06/22 - 10/01	-1.3 m (local water level)	8.1 m
Southern transect Hobo near the shoreline (pressure and temperature)	06/22 - 10/01	-3.2 m (local water level)	3.4 m
Southern transect Hobo on marsh (pressure and temperature)	06/22 - 10/01	0.32 m (NAVD88)	--
Southern transect Signature 1000 (current profiles, water levels, and waves)	08/26 - 10/01	-7.5 m local water level)	7.9 m
Northern transect Hobo near the shoreline (pressure and temperature)	08/26 - 10/01	-1.7 m (local water level)	1.8 m
Northern transect Hobo on marsh (pressure and temperature)	08/26 - 10/01	0.03 m (NAVD88)	--
Northern transect Aquadopp (current profiles and water levels)	08/26 - 10/01	-9.95 m (local water level)	10.0 m

The two tilt meters (green triangles in Figure 1C; not shown in Table 1) were sent back to the manufacturer for inspection, following an unsuccessful data recovery on October 06, 2020. The tilt meter on the southern transect was determined to have a software user error that resulted in no data collection during the time of deployment. The tilt meter on the northern transect was determined to have had a slow water leak through the rigid end cap (which is secured at the manufacturer's) and so was destroyed. The latter tilt meter was replaced at no additional cost to the project. Although this loss of data means that currents directly against the shoreline were not measured, the nearby current profiles as well as the numerical model should help fill in some of these gaps with a reasonable estimate of the currents.

### **3. Conditions during Deployment at pre-existing NOAA gauges (Marina and Offshore Data)**

Two major events (Hurricane Isaias on August 04, 2020, and Remnants of Hurricanes Sally and Teddy on September 17-22, 2020) as well as several minor events impacted the Outer Banks during the deployment. Figure 2 shows the wind speed (y-axis) and wind direction (symbol color) obtained from the NOAA's Oregon Inlet Marina meteorological station (Figure 1B, black triangle) and Figure 3 shows the wave height (y-axis) and wave direction (symbol color) from the offshore wave buoy (Figure 1B, red circle).

During Hurricane Isaias, wind speeds reached up to 20.1 m/s (39.1 knots) from the southwest and offshore wave heights reached 4.38 m (14.37 ft). During Hurricanes Sally and Teddy, winds were northerly and 10 m/s (20 knots) and offshore wave heights reached 5.10 m (16.73 ft).

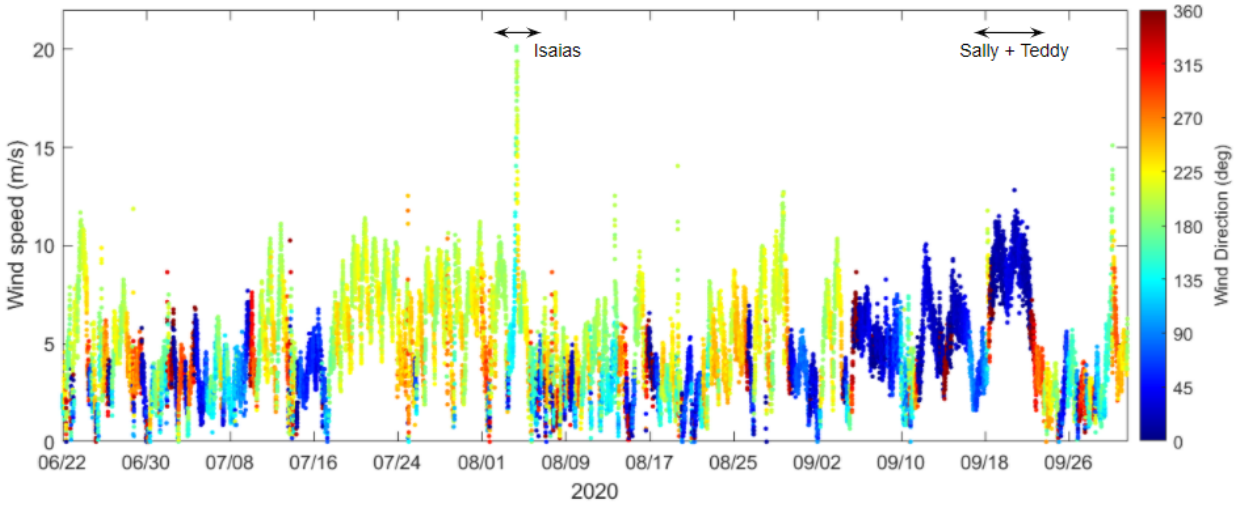


Figure 2. Wind speed corrected to 10 m above sea level (y-axis) and wind direction (symbol color) versus time. Hurricanes Isaias, Sally, and Teddy are noted with the black arrows.

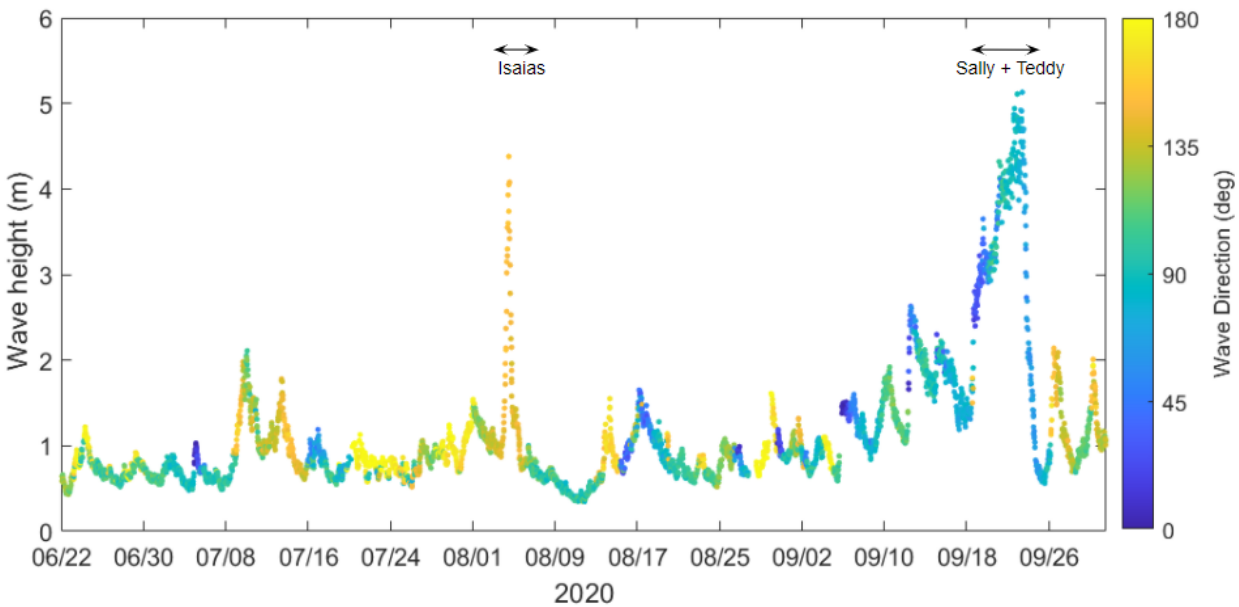


Figure 3. Ocean wave heights (y-axis) and wave direction (symbol color) versus time. Hurricanes Isaias, Sally, and Teddy are noted with the black arrows.

Figure 4 shows the water levels relative to NAVD88 at the marina tidal station (Figure 1, black triangle). Water levels were, on average, 0.22 m (0.72 ft) above NAVD88, just above the MHHW datum (defined at 0.15 m (0.49 ft) above NAVD88). During Hurricane Isaias, water levels at the marina reached a maximum of 0.88 m (2.89 ft) above NAVD88. During Hurricanes Sally/Teddy, the tidal station did not record data between September 18 12:06 ET to September 19 17:30 ET and so the maximum water levels are uncertain. Before the tidal station stopped recording, a maximum water level of 0.63 m (2.07 ft) above NAVD88 was observed.

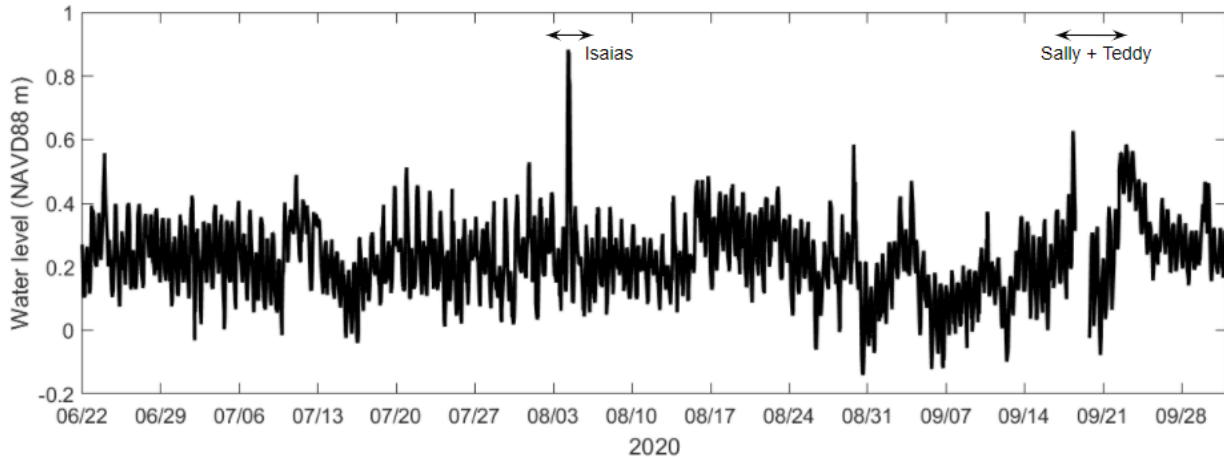


Figure 4. Water levels relative to NAVD88 at the Oregon Inlet Marina station vs. time.

#### 4. Preliminary Results:

This section summarizes preliminary results from the collected datasets. Once data post-processing is complete, these datasets will be used to support the following tasks outlined in the project proposal: to create a field observations database (Task 1f), to validate the numerical model (Task 2d), and to develop fragility curves (Task 3e, 3g).

##### 4.1 Water Levels

Pressure measurements from the Hobo data loggers were corrected for fluctuations in atmospheric pressure measured by the meteorological station at the Marina (Figure 1, black triangle) and a Hobo data logger left on site in an office trailer. The corrected pressure measurements were then converted to water level, assuming a constant salinity of 23 psu and using the fluctuations in temperature simultaneously measured by the data loggers. These water levels have up to 0.1 m of uncertainty owing to uncertainties in the salinity.

##### 4.1.1 Alongshore Variability in Marsh Flooding due to Elevation Differences

The two marsh Hobo data loggers provide information on flooding at the site. The water levels from the marsh Hobo data loggers were adjusted to be relative to NAVD88, using the elevation of the deployment locations by adding 0.32 m and 0.03 m to the southern and northern water levels, respectively (Table 1). The GPS has a reported vertical accuracy of 5 mm.

Figure 5 shows the water elevations at the two marsh locations relative to NAVD88. The low-elevation northern marsh (red curve) experienced constant flooding during the 4-week deployment, while flooding in the southern marsh (blue curve) was episodic, depending on the tides and extreme events during the 3-month deployment. The maximum flooding observed during the deployment at Pea Island was 0.82 m (2.69 ft) NAVD88, during Hurricanes Sally/Teddy.

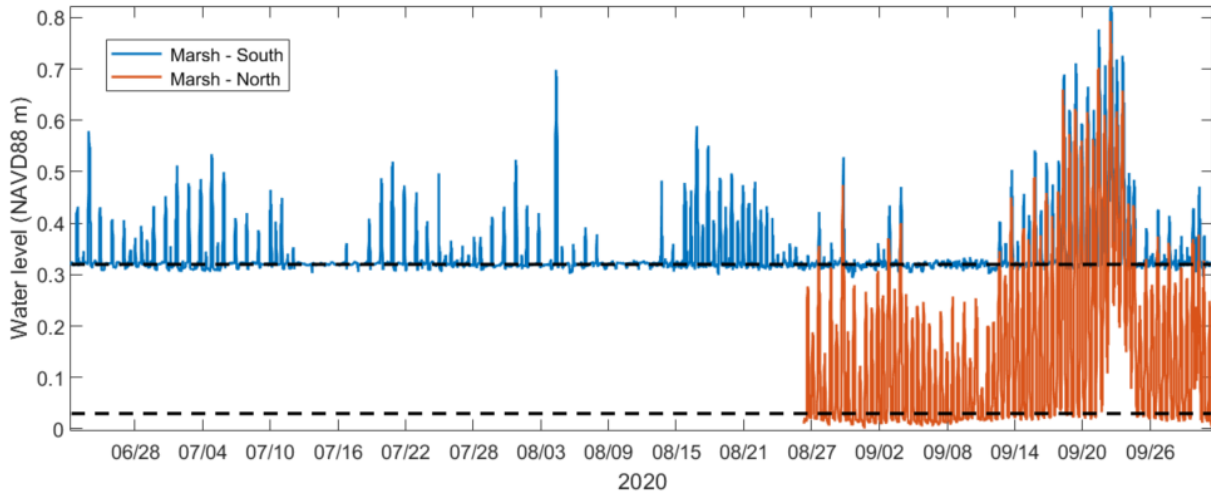


Figure 5. Time series of water level in the southern marsh (blue curve) and northern marsh (red curve) relative to NAVD88. Dashed black lines indicate the topographic elevations of the gages relative to NAVD88.

#### ***4.1.2 Local Water Level Fluctuations Reinforce Significance of Tides***

The three Hobo data loggers deployed at the piling and on the shoreline at the northern and southern transects provide information on the local water level conditions (e.g., tides and surge) at the site.

Figure 6 shows the mean-subtracted water levels at the piling (blue curve). The mean-subtracted water levels at the marina tidal station are also shown for reference (black curve). At recovery on 01 October, it was found that the structure connecting the data logger to the piling had failed. The data suggests that this failure happened abruptly on the morning of September 22 (not shown in Figure 6), near the end of Hurricane Teddy.

A preliminary harmonic analysis of the piling and tidal station water levels confirmed our results from the pilot field study in 2019. The tidal amplitude is larger and tidal constituents account for more of the variance of the water levels at Pea Island than at the Oregon Inlet Marina (the blue curve in Figure 6 has a larger amplitude than black curve). At the piling, the semidiurnal (M2) tide has an amplitude of 0.22 m and tidal constituents account for 72% of the variance in the signal. At the Oregon Inlet Marina, the semidiurnal (M2) tide has an amplitude of 0.10 m and tidal constituents account for 38% of the variance in the signal.

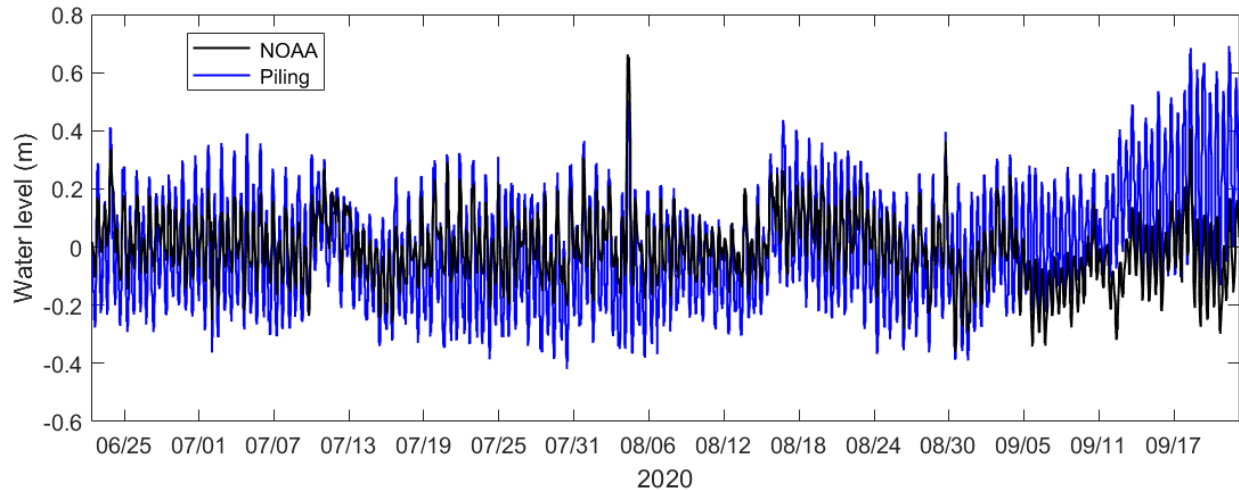


Figure 6. Mean-subtracted water level at the marina (black curve) and the piling (blue curve) vs. time.

Figure 7 shows water levels at the southern and northern shoreline transects in the red and yellow curves, respectively. The mean water level was subtracted from each dataset and a constant 0.22 m was added to the northern shoreline water levels (yellow curve) in order to roughly align the vertical position of the two shoreline water level curves in Figure 7. The mean-subtracted water levels at the marina tidal station are also shown for reference (black curve).

The southern shoreline water levels (red curve) may contain both real and artificial low frequency shifts. For example, there is an upward trend in the data from June to October that is most likely due to a slow sinking of the vertical position of the instrument, potentially with a change in tetherline angle and tension as well as erosion of the shoreline (the instrument was tethered to shore on a stake and essentially hung off the steep shoreline). The data logger was found under 3 ft of mud at recovery, which may have impacted the pressure signal as well. A direct comparison with the stationary water level measurements on the marsh nearby may allow for corrections in these artificial changes in the water level.

A comparison of northern and southern shoreline gages suggest that some low frequency shifts in the signal are real events. Hurricanes Sally and Teddy between September 17 and 22 may have enhanced volumetric flow into the inlet, leading to a steady increase in water levels at the shoreline, which decreased again rapidly as the storm traveled out of the area. This subtidal surge event appears to have been larger at Pea Island than at the Oregon Inlet Marina, confirming our 2019 pilot study observation that not all subtidal events are similar in scale at the two locations. More analysis is needed to understand the wind, wave, and surge conditions that lead to differences between the water levels at these two locations.

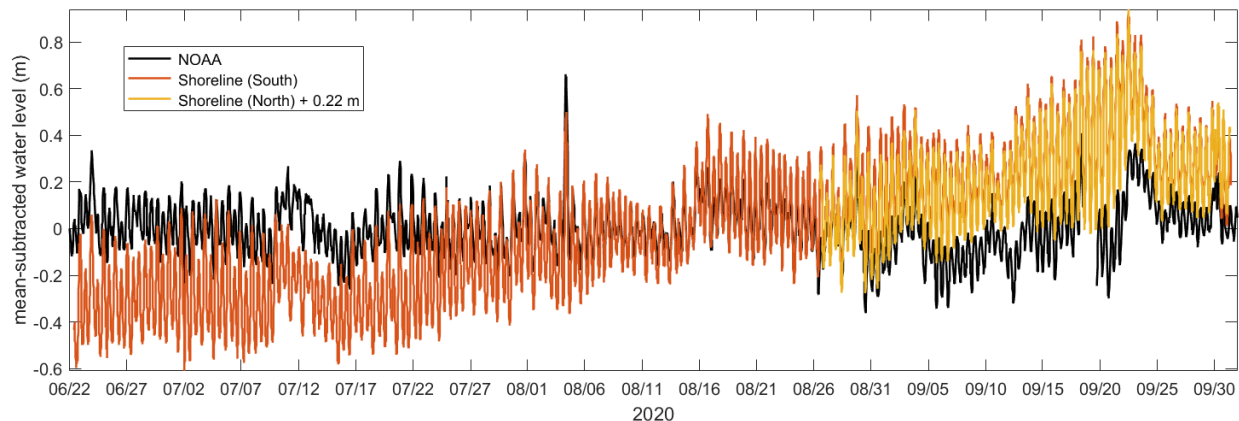


Figure 7. Mean-subtracted water levels at the Oregon Inlet marina (black curve), the southern shoreline transect (red curve), and the northern shoreline transect (yellow curve) vs. time. A constant value of 0.22 m was also added to the northern shoreline transect (yellow curve) in order to roughly align the water levels with those at the southern transect.

#### ***4.2 Temperature Signals Show Abrupt Shifts on Tidal Scales***

The Hobo data loggers simultaneously recorded point measurements of water temperature, which are displayed in Figure 8. Water temperature at 2.7 ft below MLLW at the Oregon Inlet Marina (Figure 1, black triangle) and at 1.5 ft below the waterline at the offshore buoy (Figure 1, red circle) are also shown for reference with black and gray curves (Figure 8).

Temperature did not vary significantly between gages at Pea Island - the blue, red, and yellow curves on Figure 8 overlap with less than 0.5 degrees Celsius differences. However, during a few time periods, all gages experienced a  $\sim 10$  degrees Celsius drop in temperature (e.g., July 17 to August 06, 2020 in Figure 8). These steep drops in temperature often occurred just after a high tide and lasted a few hours before the temperatures climbed steeply back up to warmer pre-high-tide temperatures. This could imply stratification effects or the transit of a cold water mass from the ocean as it enters and leaves the region with the changing of the tide. These cold water mass “events” often coincide with winds that are favorable to upwelling on the Outer Banks, suggesting that their source may be deep ocean water. Steep changes in temperature may have implications for the local hydrodynamics in the flood channel that could have secondary impacts on the currents and water levels near the shoreline. More work is needed to investigate this phenomena.

The Marina temperatures (black curve) are similar to those at Pea Island, except that they do not exhibit abrupt changes in temperature on tidal scales. The offshore wave buoy water temperature measurements are frequently colder than those at the Marina and Pea Island, except during July 7 - 10 and September 18 - 27. The dip in temperature on September 18 coincides with Hurricanes Sally and Teddy. More work is needed to understand the phenomena driving these changes in temperature.

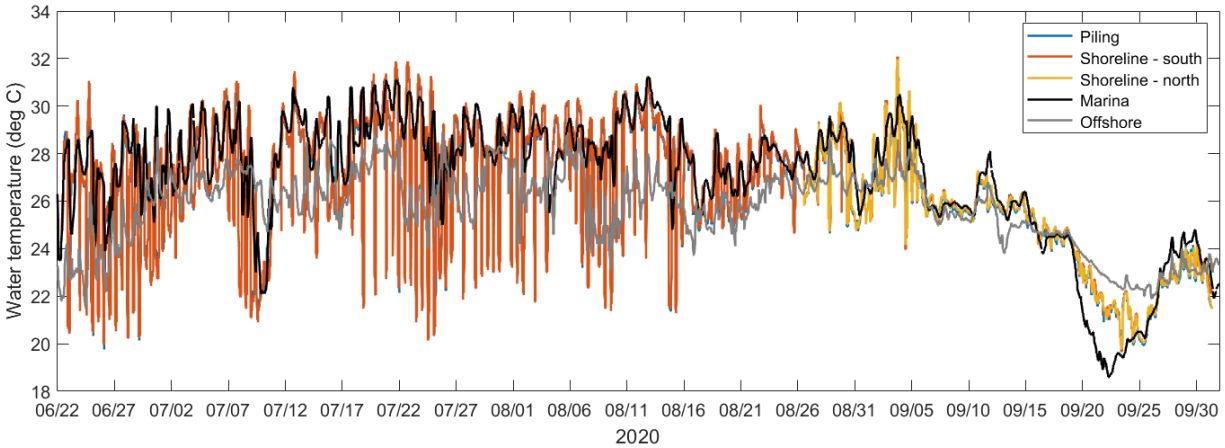


Figure 8. Temperature versus time at the piling (blue curve), southern shoreline (red curve), northern shoreline (yellow curve), marina (black curve), and offshore buoy (gray curve). The blue curve is not visible because it is overlapped by the red curve. The red curve is not visible after 26 August because the yellow curve (deployed at that time) overlaps the red and blue curves. Temperatures were similar to within less than 0.5 degrees Celsius at Pea Island.

### 4.3 Velocity

Velocity profiles in the water column were measured near the northern transect shoreline and near the piling on the southern transect (Figure 1C) using acoustic Doppler current profilers (ADCPs). Velocity data with poor signal to noise ratio were removed and the velocity components were rotated into along-channel (streamwise) and cross-channel (stream-normal) coordinates, where positive along-channel velocities occur during the flood tide (flows into the inlet and to the southeast along Pea Island) and positive cross-channel flows are towards the Pea Island shoreline.

#### 4.3.1 Vertical Variation of Velocity at Maximum Flood and Ebb Exhibit Curvature-Driven Circulation

Figure 9 shows the vertical variation over depth of the along-channel (Figure 9a and 9c) and cross-channel (Figure 9b and 9d) velocity profiles during maximum flood (Figure 9a and 9b) and during maximum ebb (Figure 9c and 9d) at the ADCP near the northern transect. Similar flow structures were seen at the southern transect ADCP.

Cross-channel flows during maximum ebb (Figure 9d) exhibit a structure consistent with channel-curvature-driven helical flow, where the surface flows veer towards the outside of the bend (towards the shoreline) and bottom flows veer towards the inside of the bend (away from the shoreline). Cross-channel flows during maximum flood (Figure 9b) have a similar structure as on the ebb, sometimes with near-surface flows reversing direction again, such that flow is veered away from the shoreline, suggesting another mechanism in addition to curvature may be important near the water surface during the flood. These circulation patterns redistribute the flow momentum in the channel, typically leading to a sub-surface maxima in the along-channel velocities, as seen in the velocity profiles in Figure 9a and 9c.

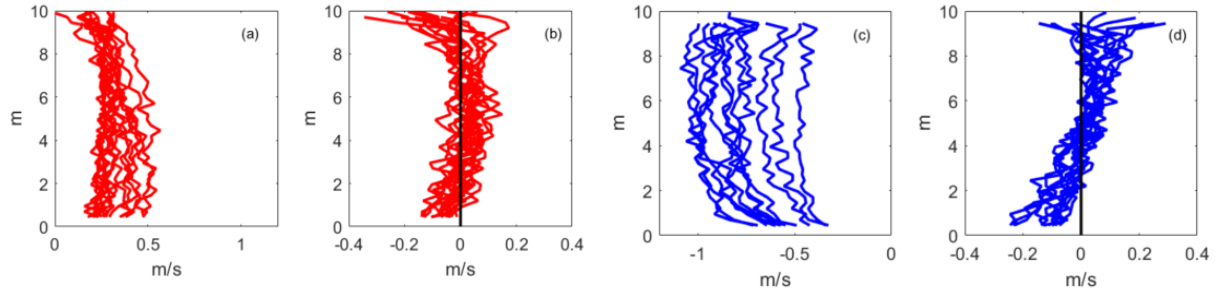


Figure 9. Distance above bottom versus (a-b) maximum flood flows and (c-d) maximum ebb flows, where (a) and (c) are along-channel (streamwise) velocities and (b) and (d) are cross-channel (stream-normal) velocities.

#### 4.3.2 Strongest Depth-Averaged Velocities Occur at the Ebb and During Low Water Levels

Depth averaged along-channel velocity near the northern transect shoreline (purple curve) and near the piling on the southern transect (green curve) are shown in Figure 10. The flows are ebb-dominated in this flood channel with typical flood flows between 0.2 to 0.5 m/s towards the southeast and typical ebb flows between -1.1 to -0.5 m/s towards the northwest. During storm events (e.g., Hurricanes Sally and Teddy on September 17 to 22), the velocities become nearly-unidirectional as ebb flows are reduced or stopped, leading to near-constant southeast flood flows. Occasionally, the flows are ebb-dominated (e.g., August 29) and ebbing northwest flows do not change direction for a tidal cycle. Both flood and ebb flows decrease in magnitude as water levels increase, potentially owing to the increased drag on flows from flooding onto the marsh. More work is needed to understand these phenomena and how they may drive or exacerbate the flooding and erosion at Pea Island.

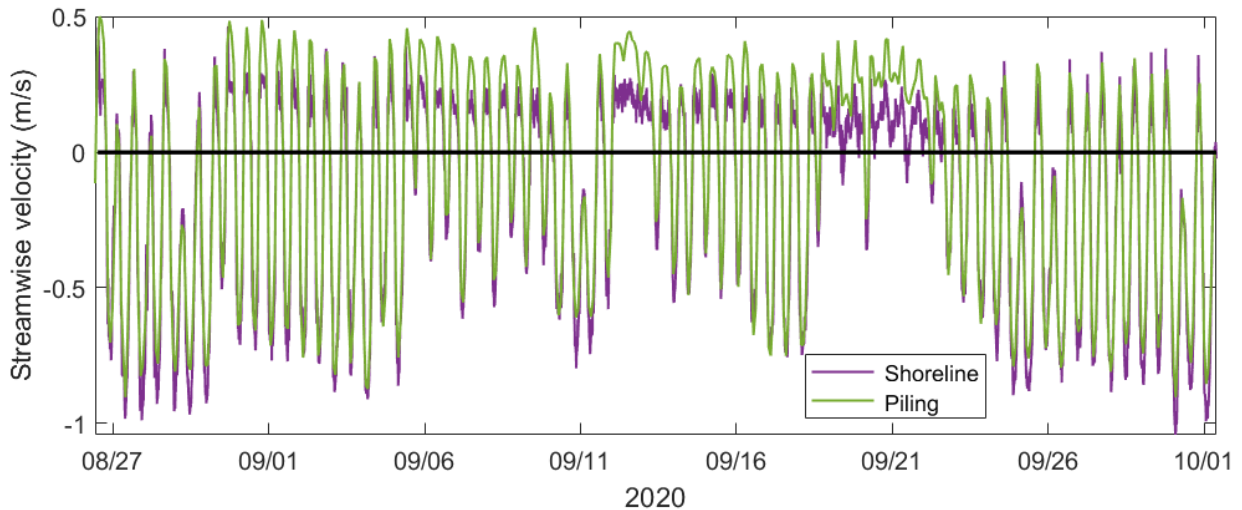


Figure 10. Depth-averaged velocity at the shoreline (measured by the Aquadopp, purple curve) and near the piling (measured by the Sig1000, green curve) versus time. Negative values indicate ebb currents to the northwest and positive values indicate flood currents to the southeast.

#### 4.4 Waves in the Channel

Sea surface elevation fluctuations were measured at 4 Hz for 17 minutes every 30 minutes using Acoustic Surface Tracking on the Sig1000 deployed in the channel of the southern transect near the piling (Figure 1C). Significant wave heights were calculated as four times the standard deviation of the sea surface elevation fluctuations in two separate frequency bands: 0.05 to 0.2 Hz (5 to 20 seconds, blue curve in Figure 11) and 0.2 to 1 Hz (1 to 5 seconds, red curve in Figure 11). The lower frequency band is mainly made up of wind waves across the sound. The higher frequency band includes a combination of locally generated waves and, potentially, boat wakes.

Preliminary analysis suggests that these waves are locally generated and proportional to wind speed and direction. Strong winds from the southwest (perpendicular to the coast orientation) correspond to many of the largest wave heights, potentially owing to a long fetch in this direction. More analysis is needed to investigate the processes driving these waves and what role they may play in shoreline erosion. If the wave energy reaches the shoreline during low water levels, the wave energy may break against the bank of the shoreline, resulting in scarping.

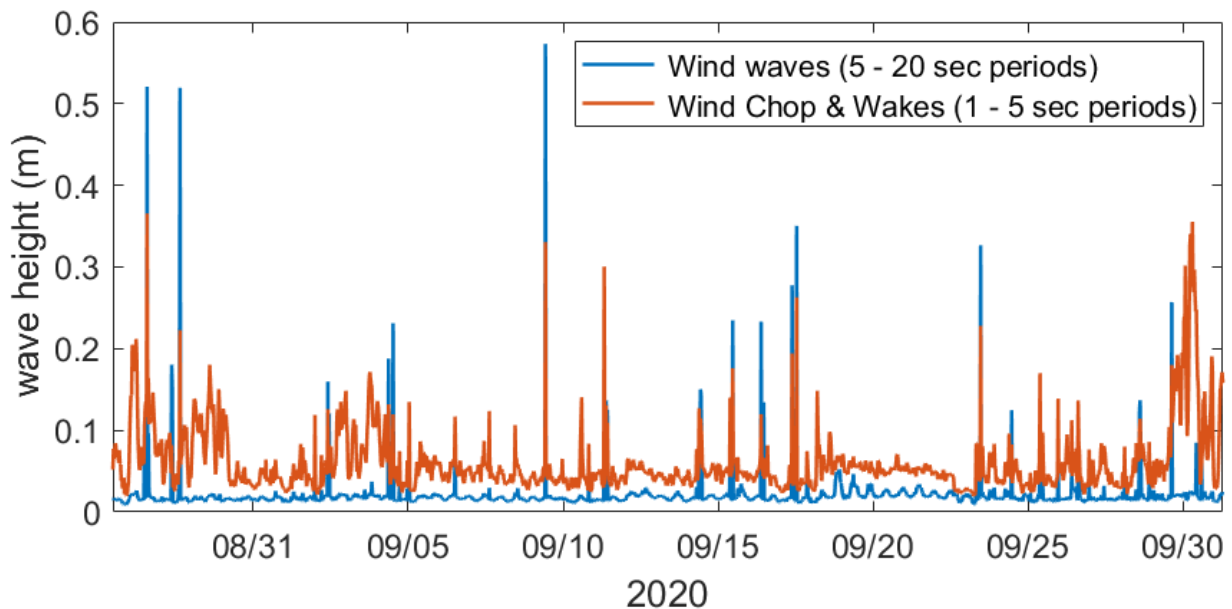


Figure 11. Significant wave heights for periods of 5 - 20 seconds (blue curve) and for periods of 1 - 5 seconds (red curve) versus time from the ADCP on the southern transect, near the piling.

## 5. Rapid Response Marsh Shoreline Surveys:

To date, rapid response shoreline surveys have been conducted before and after two storms, a nor'easter in November 2019, and Hurricane Isaias, which impacted the study area in August 2020. Table 2 shows the survey dates as well as notes on the storm characteristics. It is also noted that the June 22, 2020 shoreline survey took place after the field deployment of instruments and due to time constraints, the survey was limited to the northern portion of the study area.

Table 2. Marsh shoreline survey dates and associated events.

Survey Dates	Storm	Max Water Level at Oregon Inlet Marina (m NAVD)	Max Wave Height at Oregon Inlet Waverider (m)
November 13, 2019 (pre-storm) November 25, 2019 (post-storm)	Nor'easter November 16-20, 2019	0.59	7.6
June 22, 2020 (pre-storm) August 12, 2020 (post-storm)	Hurricane Isaias, August 4, 2020	0.88	4.4

The initial results of the first rapid response survey were reported in a December 2019 interim report titled “Rapid Response Marsh Edge Shoreline Surveys, November 2019.” That report also described the methodology used to survey the shorelines, which will not be repeated here. The average recession of the marsh edge measured during the November 2019 surveys was 2.5 m, with the primary mechanism of erosion observed being undercutting and slumping of the marsh platform, leading to a “chunk” of marsh breaking away from the shoreline.

In order to compare the shoreline changes in November 2019 due to the nor'easter with the shoreline changes observed due to Hurricane Isaias in August 2020, a new offshore baseline and set of approximately shore-perpendicular transects at 5 m spacing were established using the DSAS extension for ArcGIS developed by the US Geological Survey. Figure 12 shows the layout of the baseline and transects as well as the magnitude of the linear regression erosion rate over all four surveys. The areas shown in teal were excluded from analysis due to inconsistent identification of the marsh shoreline feature among surveys. The northern excluded section included a span that was not accessible due to extremely soft ground during at least one survey and the southern areas had different features identified as the shoreline by different operators. This figure illustrates that the highest rates of ongoing erosion are in the northern to middle sections of the study area, consistent with historical analyses.

Figure 13 shows the spatial distribution of shoreline position change from each storm. In general, there was more erosion during the November 2019 nor'easter than Hurricane Isaias. The average shoreline recession observed during Isaias was approximately 0.8 m, less than half that observed during the nor'easter. It is theorized that this could be because of the longer duration of the nor'easter (~5 days as opposed to one day for the hurricane to pass). Additionally, it may also be due to the difference in water levels during each storm. Hurricane Isaias' maximum water level was approximately 0.3 m higher than that of the 2019 nor'easter. This may have reduced the erosion by inundating the marsh and decreasing

the impact of waves on the marsh edge. It is likely that a combination of these factors led to the reduced shoreline recession during Isaias.

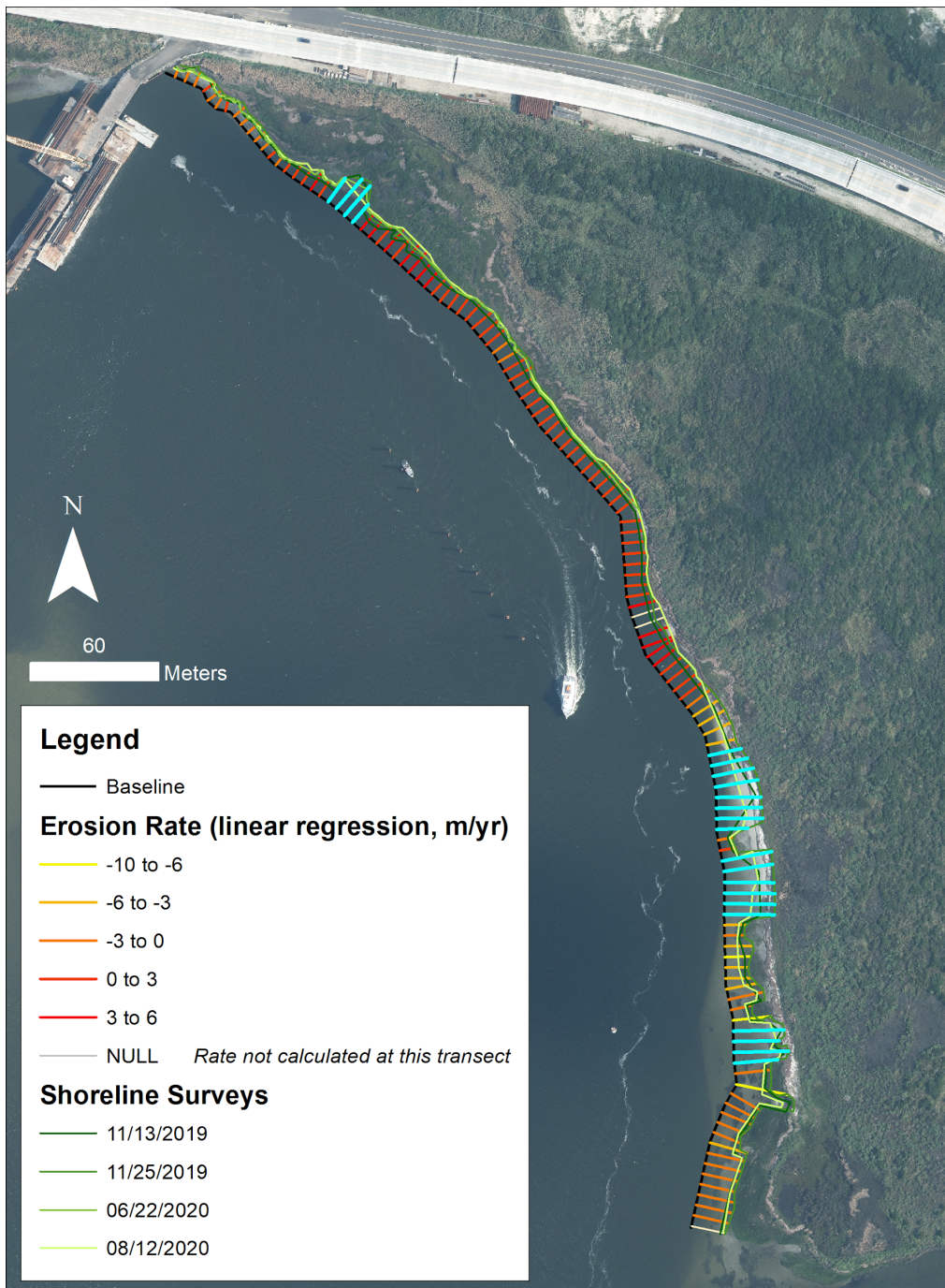


Figure 12. Baseline and transects used to compare all marsh shoreline surveys to date. The areas shown in teal were excluded from analysis due to inconsistent identification of the marsh shoreline feature among surveys.

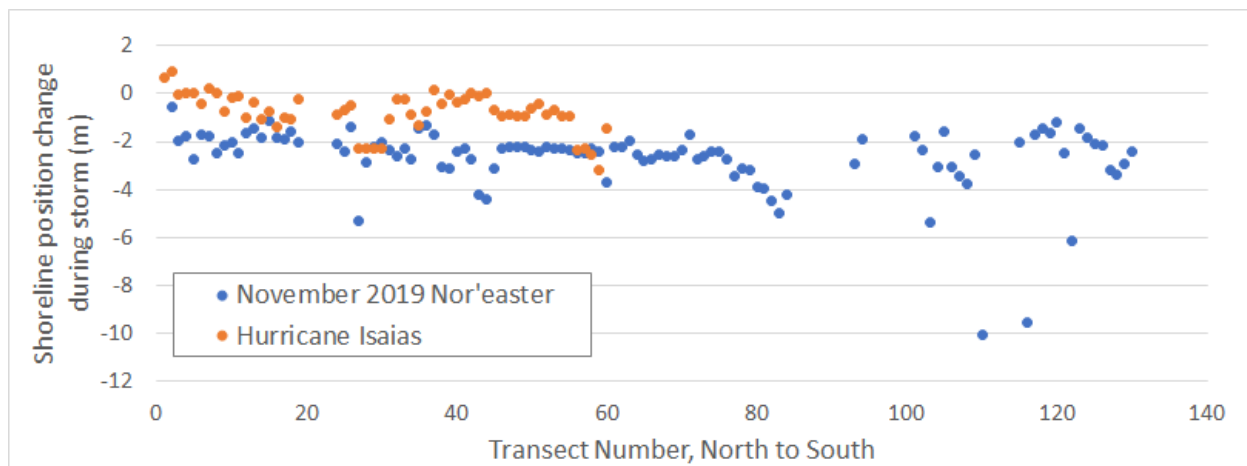


Figure 13. Shoreline position change by transect during the November 2019 nor'easter and Hurricane Isaias.

It is clear that the marsh shoreline erosion is an ongoing process in the northern and central part of the study area. Figure 14 shows the shoreline position relative to the offshore baseline for each survey date. The most landward shorelines in the northern and central areas are the post-storm shorelines (November 25, 2019 and August 12, 2020). In the southern area, the pre-Isaias shoreline was not surveyed as described previously, but the post-storm shoreline was positioned similar to the pre-storm 2019 shoreline (November 13, 2019). This is an area where there is healthy and active marsh growth at the shoreline observed in August 2020.

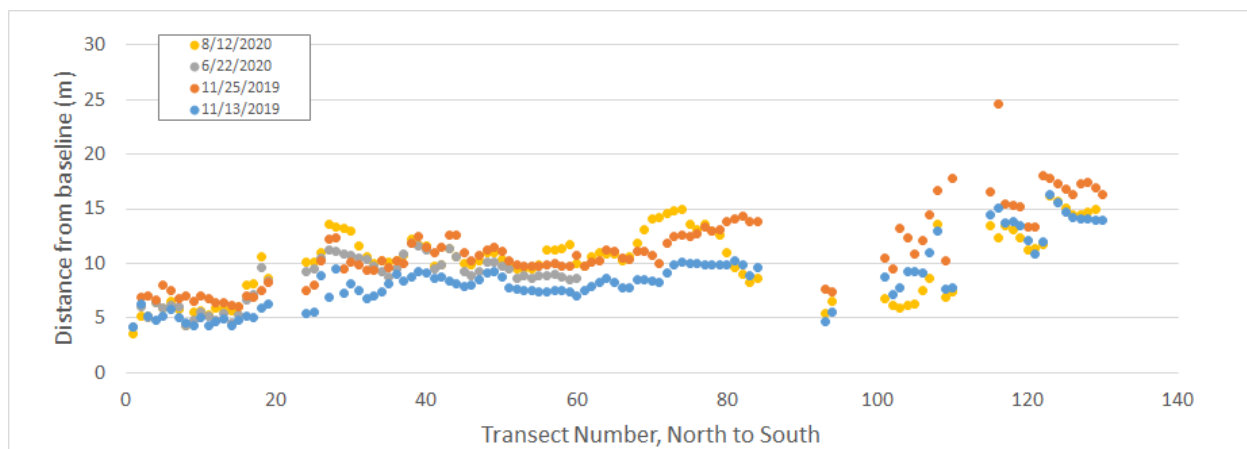


Figure 14. Shoreline position relative to the offshore baseline by date. The larger the distance is from baseline, the more landward the shoreline position.

**Next Steps:**

Analysis of the data collected during the summer/fall 2020 field campaign will continue into 2021. As opportunities arise, additional rapid response shoreline surveys will be conducted. If conditions allow,

water level gages will be deployed in conjunction with the shoreline surveys. It is noted that future deployment strategies will be altered where possible to avoid the instrumentation issues experienced in 2020.

**Acknowledgements:**

We thank Pablo Hernandez and Adam Venckauskas (NCDOT) for all of his time, logistical support, boat operation, and creative ideas for the full deployment. We thank the NCDOT dive team for their dedication and hard work, and the US Coast Guard Station Oregon Inlet for their support ensuring the safety of the dive team. We thank the awesome NCSU students who conducted shoreline surveys during a global pandemic. We also thank Becky Harrison (FWS) and Sabrina Henry (NPS) for their guidance on permitting.

**Report:**

**2021 Field Deployment at the Oregon Inlet flood channel and  
along the sound side of Pea Island**

Elizabeth Sciaudone<sup>1</sup>, Ph.D., P.E.  
Anna Wargula<sup>2</sup>, Ph.D.  
Liliana Velásquez-Montoya<sup>2</sup>, Ph.D.  
Tori Tomiczek<sup>2</sup>, Ph.D.  
Elizabeth Smyre<sup>3</sup>, P.E.



<sup>1</sup>Department of Civil, Construction and Environmental Engineering, North Carolina State University  
(NCSU)

<sup>2</sup>Department of Naval Architecture and Ocean Engineering, U.S. Naval Academy (USNA)

<sup>3</sup>Dewberry

Interim Report 7: NC DOT RP 2020-09  
Monitoring and modeling sound-side erosion near Oregon Inlet to support feasibility level  
transportation planning

January 18, 2022

## Summary

This report summarizes the 2021 field campaigns conducted by researchers at North Carolina State University (NCSU), the United States Naval Academy (USNA), and Dewberry as part of the North Carolina Department of Transportation (NCDOT) funded research project RP 2020-09 “Monitoring and modeling sound-side erosion near Oregon Inlet to support feasibility level transportation planning.” The field campaigns described here were conducted to partially meet proposed project goals in Task 1b (Long-term 3-4 week deployment), Task 1c (Full scale ~4 week field campaign), and Task 2d (rapid response field campaign) of the proposed NCDOT project. Seven field campaigns in total were conducted in 2021, with missions in Table 1.

**Table 1. 2021 Field Campaigns and Data Collection Goals**

<b>Date (2021)</b>	<b>Shoreline and Wrackline Survey</b>	<b>Instruments deployed or recovered</b>	<b>Other goals</b>
March 03	✓	Pressure gauges deployed	
April 20			Bathymetry survey
May 03	✓		
September 08	✓		
September 23		Pressure gauges & tilt meters deployed	
October 25-29	✓	All gauges recovered	Boat mounted current survey (simultaneous bathymetry)
November 23	✓		

In the report to follow, section 1 describes the publicly available datasets from existing metocean stations to show the meteorological and oceanographic conditions during the deployment period; section 2 describes the data from the pressure gauges deployed at Pea Island; section 3 describes the rapid response shoreline and wrackline surveys from 2021; and section 4 describes the change in bathymetry from 2019 to 2021 as well as the cross-channel currents during flood and ebb.

### 1. Atmospheric and Ocean Conditions during 2021 Deployments

The wind and water level conditions measured at the NOAA Oregon Inlet Marina gauges and waves measured at the offshore National Data Buoy Center (NDBC) buoy during the 2021 field campaigns are shown in Figures 1 to 4. Winds were typically out of the north-northeast (NNE) and south-southwest (SSW), with stronger winds out of the SSW (Figure 1). Wind speeds ranged from 0 to 18.1 m/s (0 to 40.5 mph, Figure 2). Wave heights ranged from 0.36 to 5.16 m (1.18 to 16.93 ft, Figure 3). Water levels at the Oregon Inlet Marina ranged from -0.37 to 0.88 m NAVD88 (1.21 to 2.89 ft NAVD88, Figure 4).

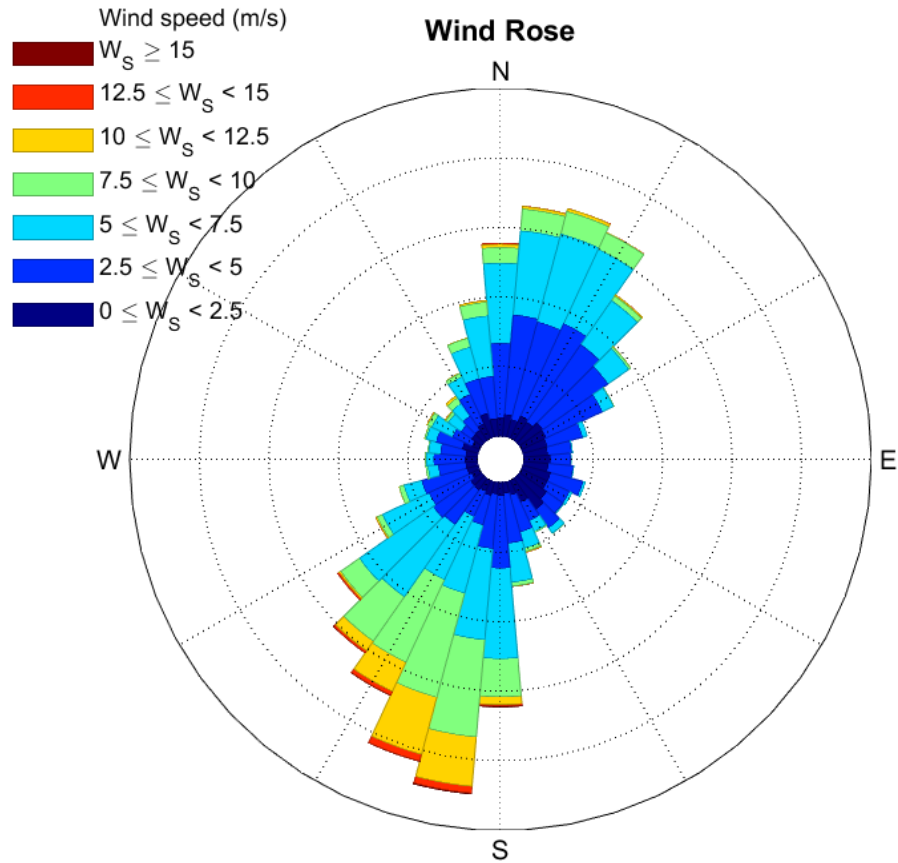


Figure 1. Histogram of wind speeds binned by speed (color contours) and direction (radial position of bin) during the time of the 2021 Pea Island deployments. Wind directions were dominantly out of the NNE and SSW.

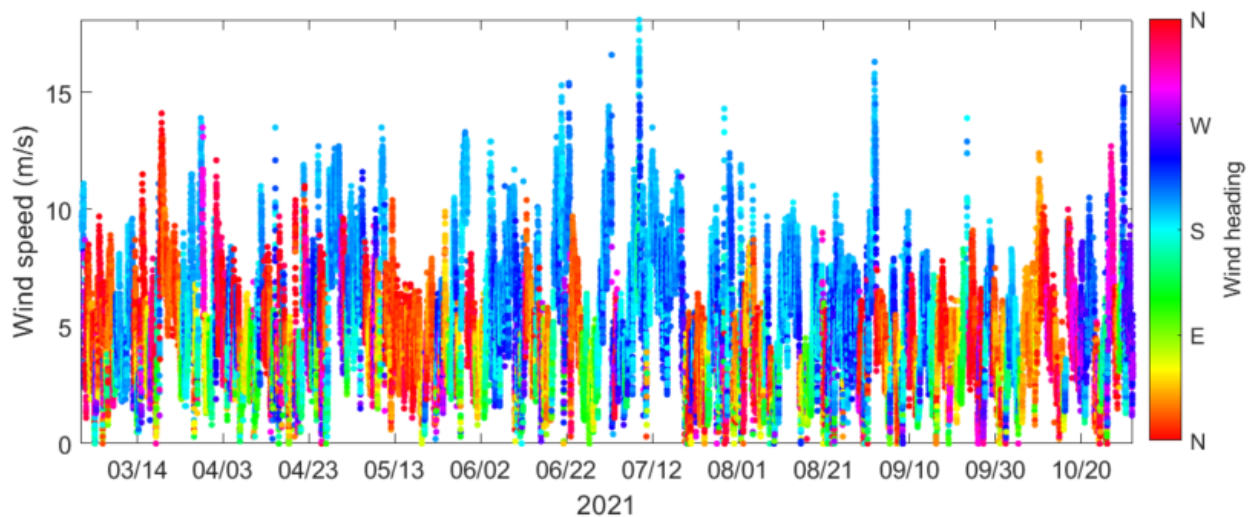
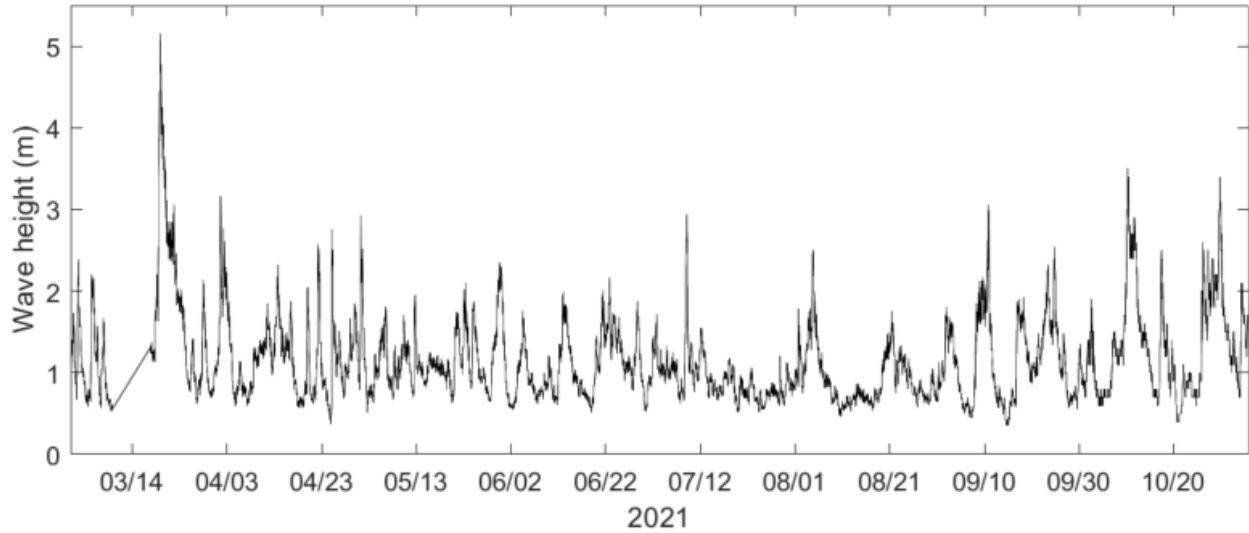
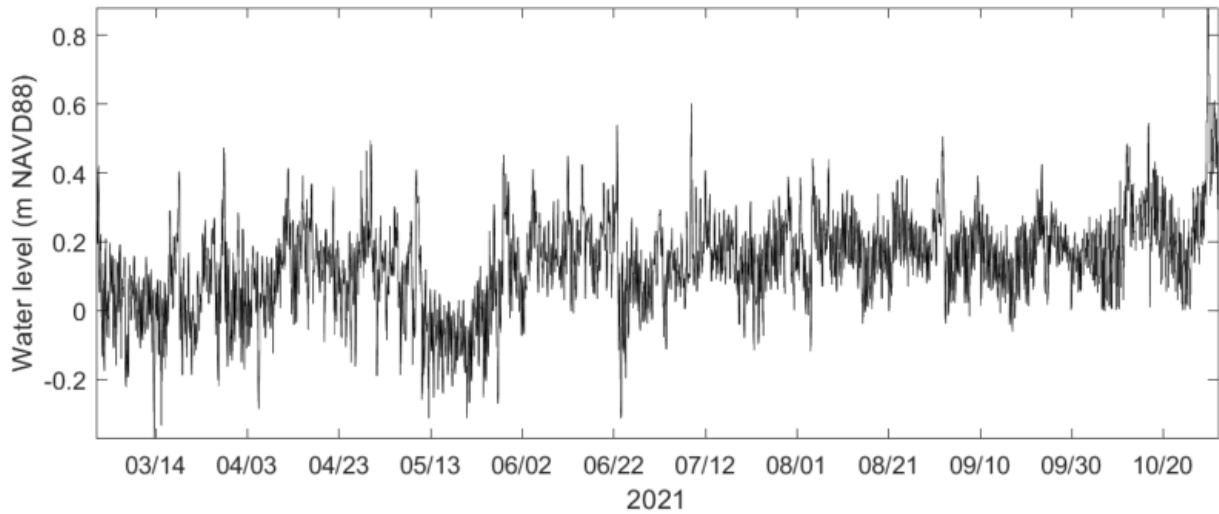


Figure 2. Wind speed versus time where color indicates the heading of the wind during the deployment period.



**Figure 3. Offshore wave height versus time during the Pea Island deployment period.**



**Figure 4. Water levels (m NAVD88) at the Oregon Inlet Marina versus time during the Pea Island deployment period.**

## **2. Stationary gauges on the Marsh and in the Channel**

The goal for deploying stationary pressure gauges was to measure incidents and magnitudes of marsh flooding. The deployments during 2021 were conducted in four stages: (1) deployment of three HOBO pressure gauges on the marsh edge and near the northern wrack line on March 08, (2) data download and redeployment of the gauges on September 08, (3) deployment of two additional HOBO pressure gauges with corresponding tilt current meters in the flood channel near the shoreline on September 23, and (4) recovery of all instruments on October 29. Figure 5 shows the location of the study site on the east coast of the USA (panel A), the locations of the Oregon Inlet Marina tidal gauge and meteorological station (red triangle in panel B), the NDBC wave buoy (red circle in panel B), and the positions of the deployed stationary gauges at Pea Island (orange and yellow symbols, panel C), along with the bathymetry contours measured in April 2021 (blue contour lines, panel C) and the shoreline positions (blue-green toned

contour lines, panel C) and wrack line positions (yellow-brown toned contour lines, panel C) measured in 2021.

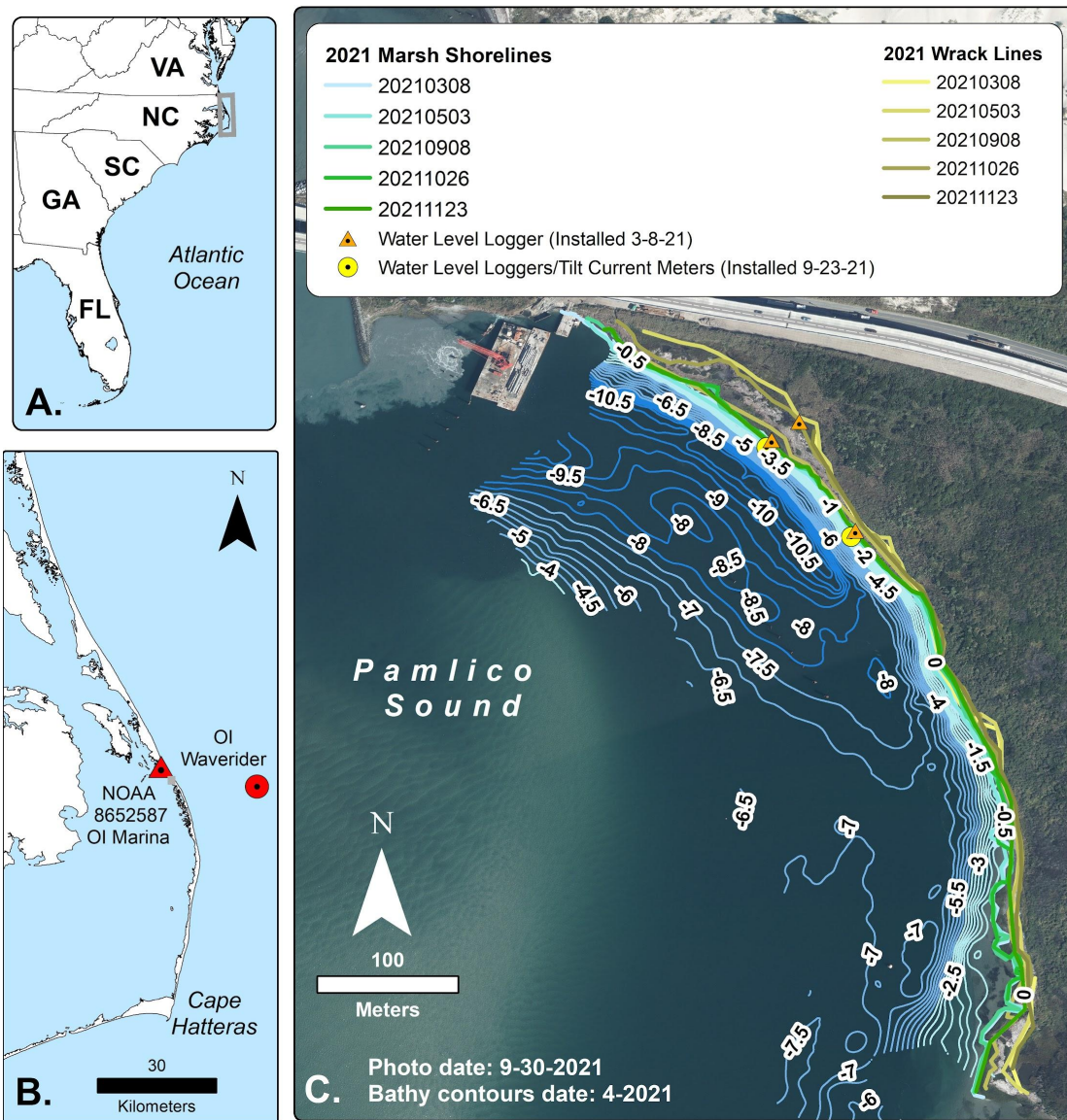


**Figure 5. Map showing locations of permanent and deployed stationary gauges along with 2021 marsh shoreline, wrack line, and bathymetry survey data.**

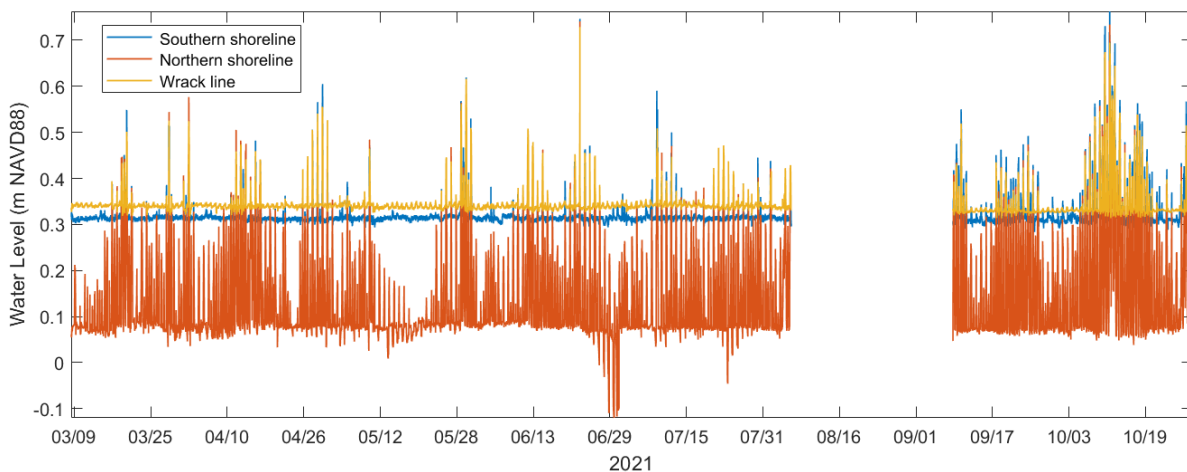
All instruments were successfully deployed and recovered according to plan. All datasets except currents from the two tilt meters have been downloaded and post-processing is underway. Table 2 shows the date of deployment and recovery, elevation relative to NAVD88 (positive up) or local water levels (positive up), and local water depth at deployment (where applicable). All measurements were taken at 10 min intervals.

**Table 2. Instrumentation deployed in 2021**

<b>Instrument (Measured variable)</b>	<b>Deployment (2021)</b>	<b>Elevation (Datum, positive up)</b>	<b>Local Water Depth at Deployment</b>
Hobo (atmospheric pressure)	03/08 - 08/05	office trailer on site, moved to office in Skyco 05/04	--
Southern transect Hobo on marsh (pressure and temperature)	03/08 - 08/05 09/08 - 10/29	0.32 m (NAVD88)	--
Northern transect Hobo on marsh (pressure and temperature)	03/08 - 08/05 09/08 - 10/29	0.08 m (NAVD88)	--
Northern transect Hobo on marsh wrack (pressure and temperature)	03/08 - 08/05 09/08 - 10/29	0.34 m (NAVD88)	--
Northern transect Hobo near shoreline (pressure and temperature)	09/23 - 10/29	--	2.4 m
Southern transect Hobo near shoreline (pressure and temperature)	09/23 - 10/29	--	2.0 m

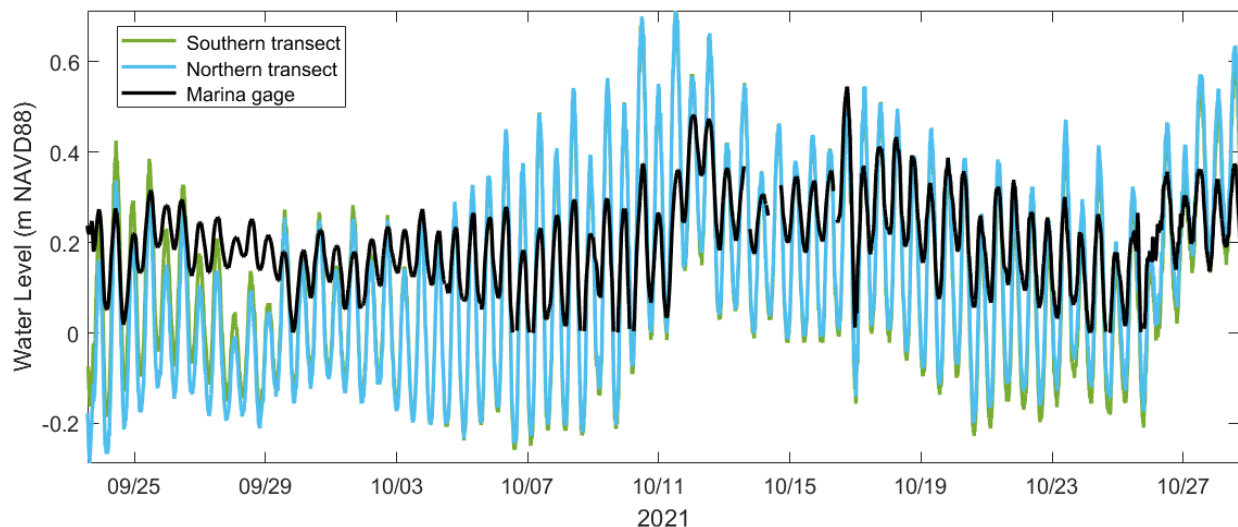
The two tilt meters (yellow circles in Figure 5; not shown in Table 2) are not shown in this report due to concerns with the data quality. In particular, the current headings suggest that the tethering method of the instruments may have biased their movement, leading to erroneous heading readings. More testing is needed of this novel velocity measurement method to determine if the magnitudes may still provide useful information for this study.

Figure 6 shows the water levels (meters, NAVD88) on the marsh from March 09 to October 29. The instruments ran out of memory on August 05, and were re-deployed September 08. The maximum flooding event occurred on 22 June with a water level of 0.74 m NAVD88 (2.42 ft NAVD88). The gauge deployed near the northern shoreline (red curve, Figure 6) has some negative measurements on June 29, which may be owing to the movement of the gauge or issues with assumptions in the data conversion.



**Figure 6. Water level (meters, NAVD88) corrected for atmospheric fluctuations versus time at the southern shoreline gauge (blue curve), northern shoreline gauge (red curve), and the wrack line curve (yellow curve). To convert pressure to time, a time-varying density assuming a salinity of 23 psu was calculated. This density varied between 1007.2 to 1018.4 kg/m<sup>3</sup>.**

Figure 7 shows the water levels (meters, NAVD88) observed at the two submerged water level gauges deployed September 23 to October 29, compared with those observed at the Oregon Inlet Marina gauge. The correction to a NAVD88 datum for the submerged gauges at Pea Island may have  $O(1\text{ cm})$  of error; the correction was approximated by comparing with the water levels measured by the submerged gauges with that measured by the gauges deployed on the marsh at a known elevation relative to NAVD88. The amplitude of the water level changes adjacent to Pea Island are significantly larger than those observed at the marina, similar to observations in prior years.



**Figure 7. Water level (meters, NAVD88) at the southern (green curve) and northern transect (blue curve) and at the NOAA tidal gauge (black curve) versus time.**

### 3. Rapid Response Marsh Shoreline Surveys

Ongoing periodic marsh shoreline and wrack line surveys were conducted five times in 2021. In addition to the survey, a characterization of the shoreline as “severely eroded”, “eroded”, “healthy” or “sandy” was performed at each of the survey points. The March 08, September 08, October 26, and November 23 surveys were conducted using a Trimble R12 real-time kinematic (RTK) GPS system (maximum precision 8 mm horizontal / 15 mm vertical). The May 03, 2021 survey was conducted using a Trimble R1 (maximum precision 50 cm). Because of this difference in accuracy, there is greater uncertainty associated with the May survey. In addition to the shoreline position, the shoreline was classified as either eroded, severely eroded, healthy, or sandy (for the pocket beach sections in the southern portion of the study area). Figure 8 shows the shoreline classifications at each of the survey dates. The majority of the northern half of the study area was classified as eroded or severely eroded in all of the surveys. The only portion classified as healthy was the southernmost section, which was observed to have a gentle slope with marsh plants extending into the sound. In the May 03 and September 08 surveys, some parts of this area were observed to be eroding with a small scarp observed.

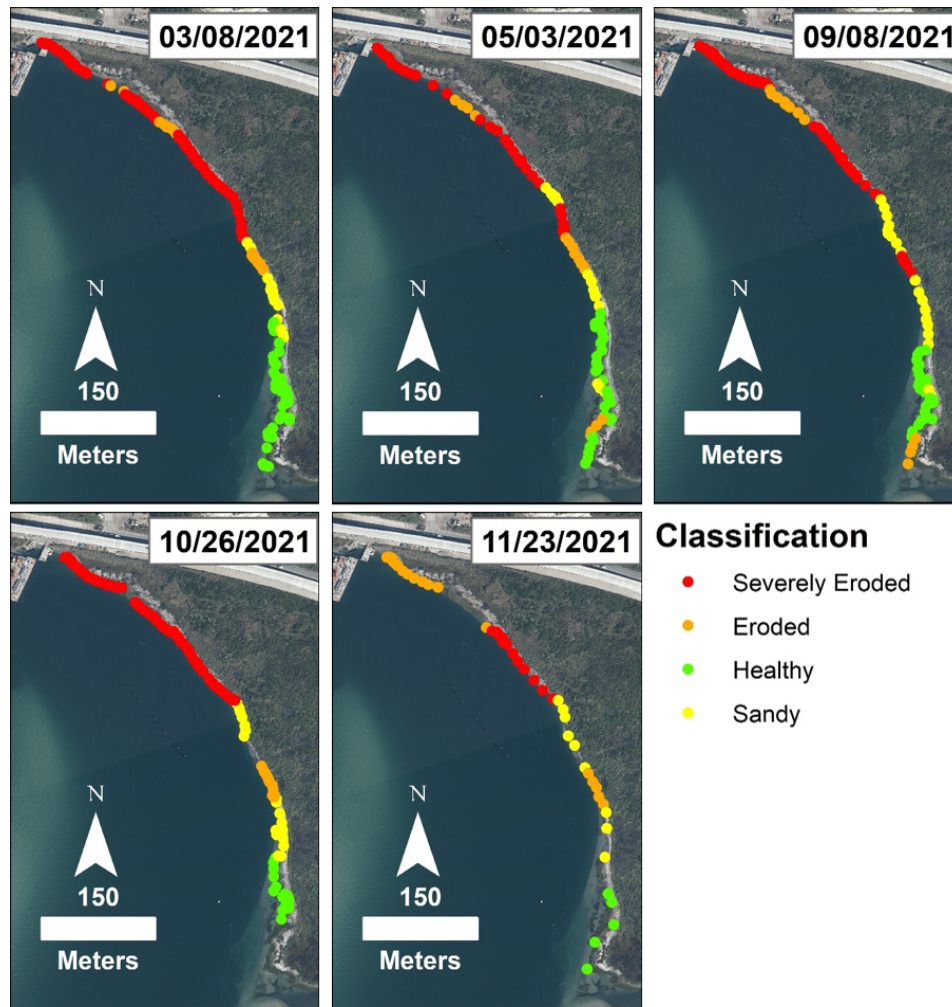


**Figure 8. Shoreline classifications for each of the 2021 marsh shoreline surveys. Due to high water levels some areas were not accessible during the November 23, 2021 survey date, reflected by data gaps. The majority of the northern half of the study area was classified as either eroded or severely eroded for all survey dates. The background image is from September 30, 2021, provided by NCDOT.**

Table 3 lists the highest wave heights and water levels occurring between each of the surveys. For these surveys the maximum wave heights and water levels did not occur on the same dates. The highest observed water level during the survey period was 0.88 m NAVD during an eastern storm on October 29, 2021. The highest wave heights exceeded 5 m during a nor'easter on March 19, 2021, and again during a nor'easter on November 07, 2021. Overwash was observed at Mirlo Beach just north of Rodanthe during both of those wave height events, and roadway closure occurred November 07 to November 09, 2021 according to the NCDOT NC12 social media accounts.

**Table 3. Marsh shoreline survey dates and associated maximum water level and wave height events.**

Survey Date	Dates of Max Water Level (WL) and Wave Height (WH) Between Surveys	Max Water Level at Oregon Inlet Marina (m NAVD)	Max Wave Height at Oregon Inlet Waverider (m)
March 08, 2021	04/29/2021 (WL) 03/19/2021 (WH), nor'easter	0.50	5.16
May 03, 2021	07/29/2021 (WL) 07/09/2021 (WH), TS Elsa	0.60	2.94
September 08, 2021	10/16/2021 (WL) 10/10/2021 (WH)	0.55	3.53
October 26, 2021	10/29/2021 (WL), eastern storm 11/07/2021 (WH), nor'easter	0.88	5.06
November 23, 2021	Last survey	Last survey	Last survey

The observed wrack lines are presented in Figure 9. The furthest landward wrack lines overall were observed in March and October. Because of the different instrument that was used for the survey on May 03, 2021, no elevation data were collected. For all of the other surveys, the average elevations of the wrack line are presented in Table 4. Generally the wrack line elevations were on the order of 0.4 m for all but the September survey. That wrack line was generally closer to the shoreline reflecting a more recent, lower water level event.

**Table 4. Marsh wrack line survey dates and associated average elevations.**

Survey Date	Average Wrack Line Elevation (m)
March 08, 2021	0.44
September 08, 2021	0.22
October 26, 2021	0.40
November 23, 2021	0.47

Overall marsh shoreline change as observed from the 2021 surveys is shown in Figure 10. In this figure, the overall change between March and November 2021 and March and October 2021 are shown. The October data are shown because some areas were inaccessible during the November survey due to high water conditions. Erosion ranging from 2 m to 6 m was common across the study area, with the only accretion observed in the southern area (corresponding to the “healthy” classifications in Figure 8.)

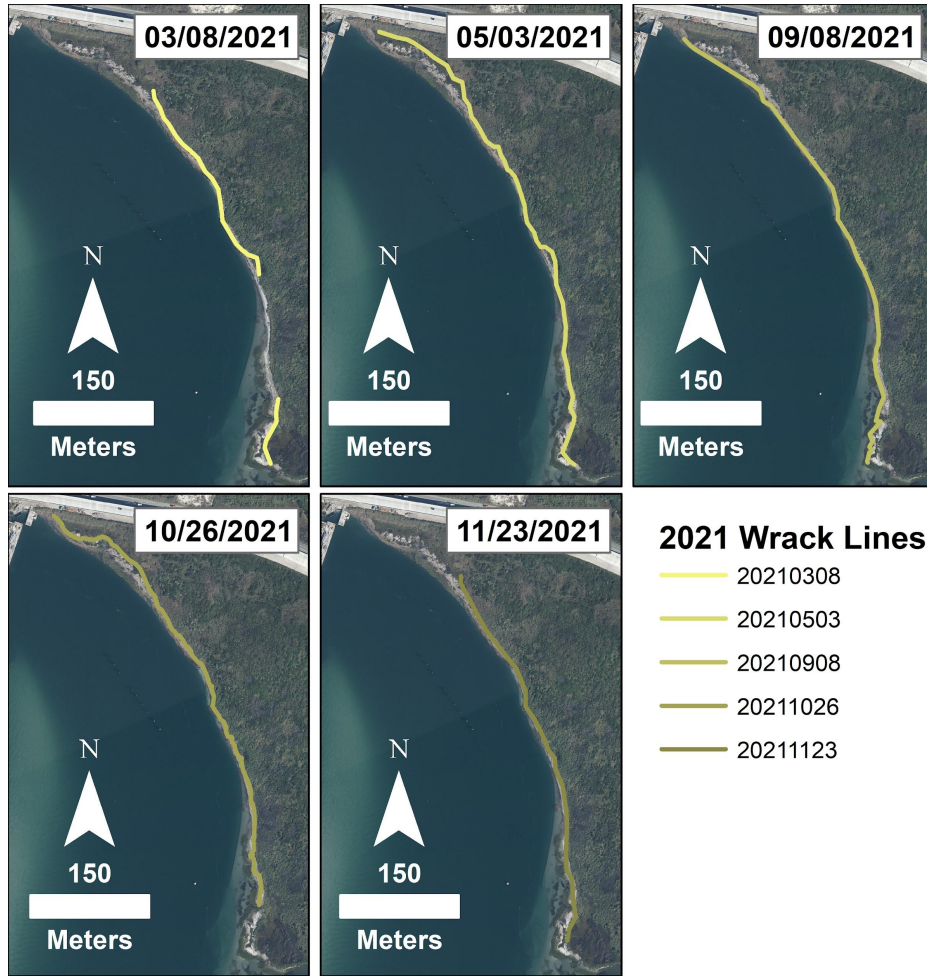


Figure 9. Wrack lines surveyed during 2021. The furthest landward wrack lines were observed in May and October 2021.

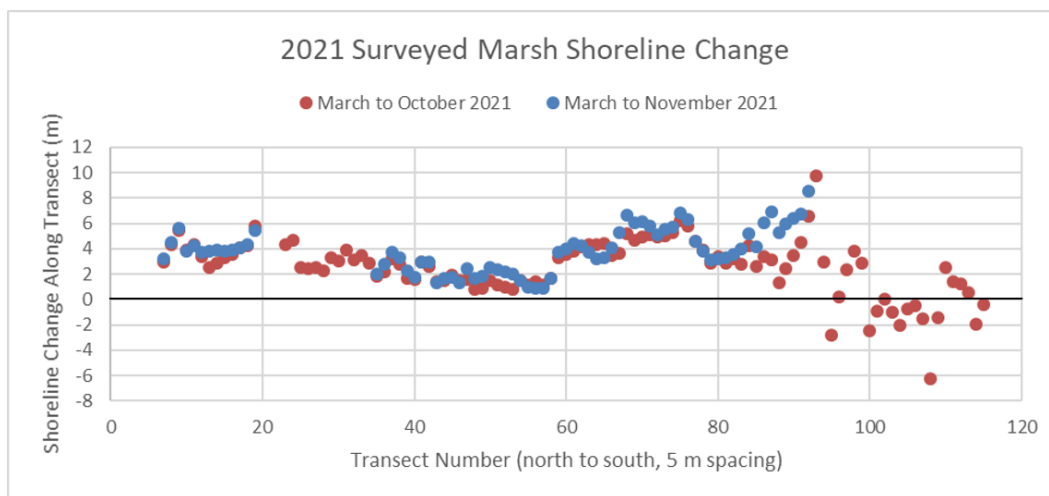


Figure 10. Overall surveyed marsh shoreline changes in 2021. Positive values indicate erosion, and negative values indicate accretion.

#### 4. Boat-mounted Current Surveys and Bathymetry

A bathymetric survey was conducted on April 20, 2021 by Dr. Peter Traykovski of Woods Hole Oceanographic Institution (WHOI) as part of a collaboration made possible via DuNEX (During Nearshore Event eXperiment, a multi-institutional research program organized by the US Coastal Research Program). The survey was completed using a single beam echo sounder with onboard GPS locator mounted on a remotely-driven kayak. This survey was compared with a previous survey conducted October 10, 2019 by staff from the National Science Foundation's (NSF) NHERI RAPID (Natural Hazards Engineering Research Infrastructure Rapid Response Research) program. The survey was performed using the NHERI RAPID program's Z-Boat 1800 with single beam echo sounder. The Z-Boat was also remotely controlled by NHERI staff and performed soundings which were located using an onboard GPS. Both surveys were adjusted to NAVD88 by the respective researchers and shared with the authors in raster format for comparison in GIS.

Figure 11 shows a raster created by subtracting the 2021 survey from the 2019 survey to show the spatial patterns of erosion and accretion. The channel adjacent to the shoreline has deepened over the majority of the surveyed area. Of note, the area closest to the shoreline has significantly deepened (more than 3 m) along the areas that are observing substantial erosion (black arrows). There was accretion observed farther from the shoreline along the northern portion of the study area. These data sets support the hypothesis that channel deepening close to the marsh shoreline is closely linked to the ongoing erosion.

Three transects were defined to undertake boat-mounted current measurements in October 2021. The locations of these transects are shown in Figure 12, along with the location of the -5 m (NAVD88) contour and the shoreline in October 2019 and April 2021. Considering the -5 m contour as the edge of the deepest part of the channel, it is clear that the channel has moved closer to the shoreline which has demonstrated erosion over most of the study area. Even in the southern portion of the study area where the shoreline has not significantly eroded, the channel has moved closer to the shoreline.

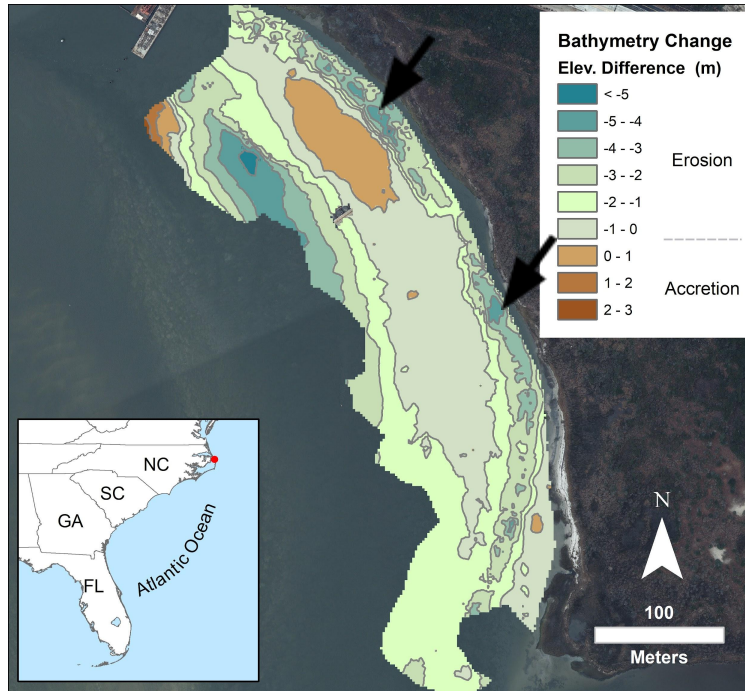


Figure 11. Bathymetry change from October 10, 2019 to April 20, 2021 in meters. Warmer colors indicate accretion and cooler colors indicate deepening. NCDOT image February 6, 2021.

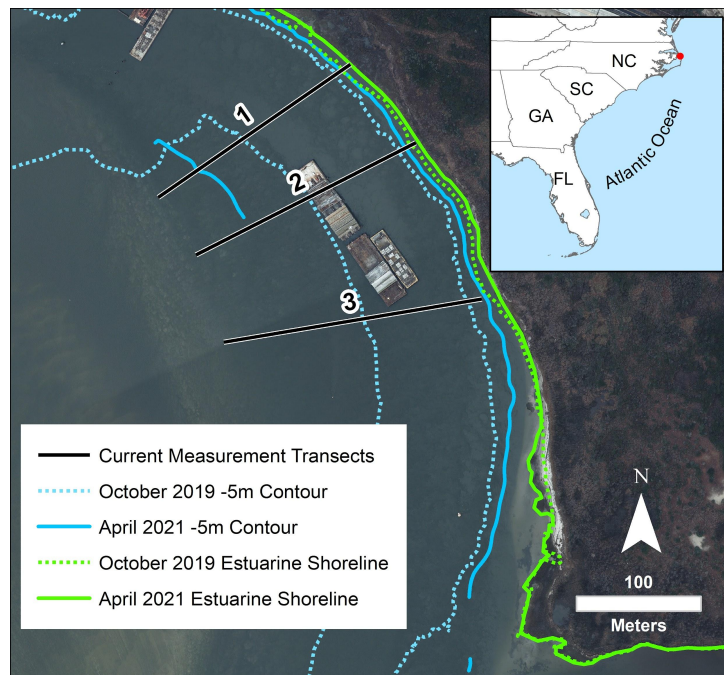
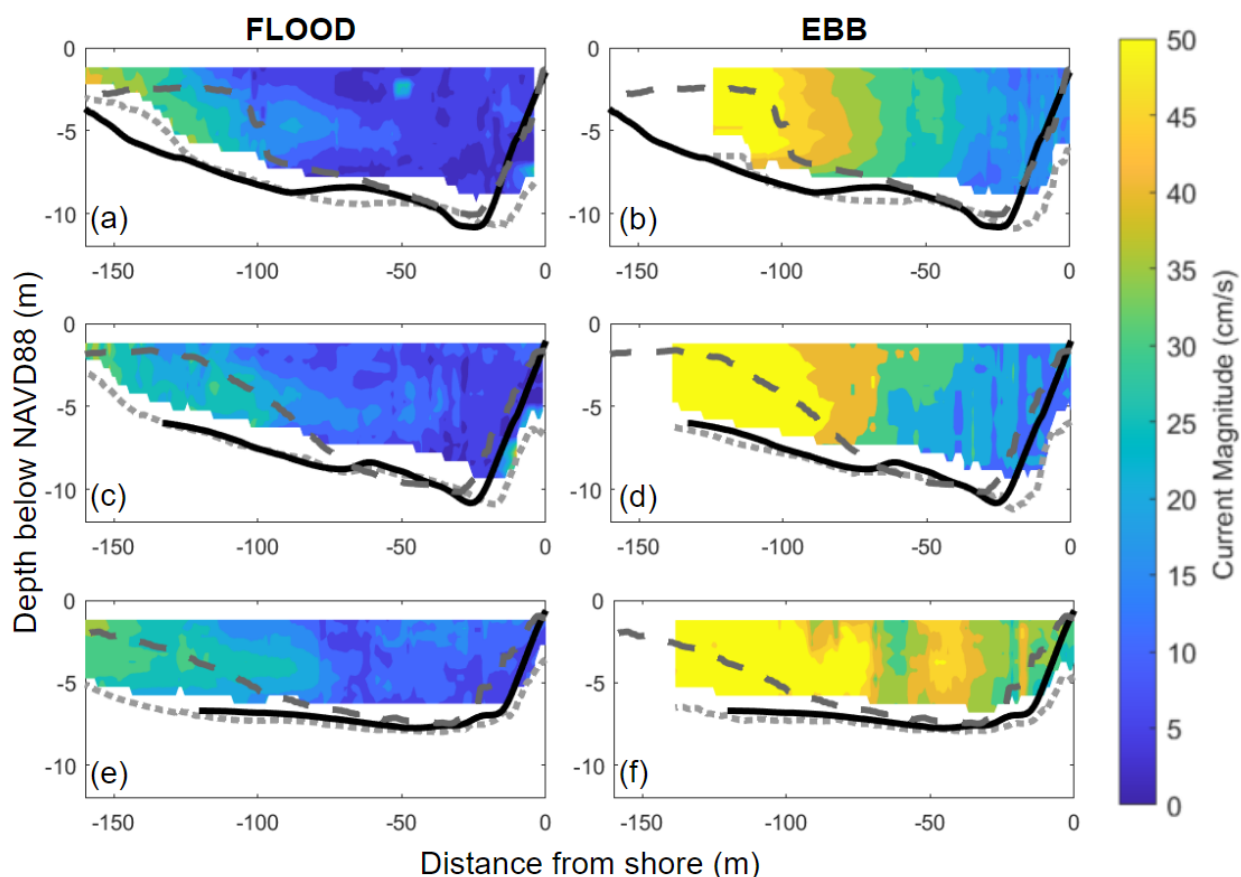


Figure 12. Transects used for boat-mounted current measurements, as well as a comparison of -5 m contour (relative to NAVD88) and estuarine shoreline positions from October 2019 to April 2021. NCDOT image February 6, 2021.

Figure 13 compares the bathymetry measured during October 2019 (dashed dark gray line), April 2021 (solid black line), and October 2021 (dotted light gray line) at the three transects outlined in Figure 12.

Although the October 2019 and April 2021 bathymetry have been corrected to NAVD88, the bathymetry measured in October 2021 has  $O(10\text{ cm})$  of uncertainty in vertical position due to uncertainty in the local water level and thus can only be qualitatively compared to other measurements.

Consistent with Figure 11, Figure 13 shows deepening of the channel near the shoreline edge (right hand side of the panels) between October 2019 (dashed dark gray line) and April 2021 (solid black line), particularly at Transect 2 (c, d) and Transect 3 (e, f). All three transects also show widening of the flood channel, with the deepening of the western edge (left hand side of the panels) between October 2019 (dashed dark gray line) and April 2021 (solid black line). Although there is uncertainty in the vertical position of the October 2021 measurements (dotted light gray line), they suggest further deepening at the shoreline edge for all three transects.



**Figure 13. Current magnitude (color contours) during flood (a, c, e) and ebb (b, d, f) as a function of depth below NAVD88 versus distance from shore at Transect 1 (a, b), Transect 2 (c, d), and Transect 3 (e, f). The solid black line and dashed dark gray line are the transect bathymetry relative to NAVD88 on April 2021 and October 2019, respectively. The dotted light gray line is the approximate bathymetry relative to NAVD88 during the current transects in October 2021.**

Flood currents were measured on October 26, 2021 from 10:01 to 10:18 EDT. Water levels measured on the marsh during the flood transects were 0.30 - 0.37 m NAVD88 and increased to a max water level of 0.43 m NAVD88 at high tide two hours later (October 26 at 12:00 EDT). Ebb currents were measured on

October 28, 2021 from 15:31 to 15:55 EDT. Water levels measured on the marsh during the ebb transects were 0.50 - 0.54 m NAVD88 and had just started decreasing from a max water level of 0.59 m NAVD88 at high tide one hour earlier (October 28 at 14:20 EDT). Due to the proximity (<2 hour) of high tide to the measurement period, measurements may have been conducted just after maximum flood and just before maximum ebb rather than during the peak tidal flows. Both the flood and ebb transects show higher velocities on the western side of the flood channel (left hand side of each panel in Figure 13), furthest from the shoreline. Ebb currents are stronger than flood currents, as has been observed in previous years.

### **Acknowledgements**

We thank Pablo Hernandez (NCDOT) for all of his time, logistical support, boat operation, and creative ideas for the full deployment. We thank the awesome NCSU students and USNA students (Karsten Francis, Ryan Fitzgerald, Justin McCabe, Nicholas Hilaire) who conducted shoreline surveys and collected data. We also thank Becky Harrison (FWS) and Sabrina Henry (NPS) for their guidance on permitting.

# APPENDIX B

## APPENDIX B

### Erosion Mitigation Options Demonstration Site Assessment and Literature Review December 17, 2020

In order to develop recommendations of appropriate site-specific erosion mitigation options, a review of existing demonstration sites as well as relevant scientific and technical review was conducted. Both the demonstration sites and literature review accounted for a variety of mitigation strategies, including structural features, natural and nature-based solutions, and hybrid options.

Demonstration sites selected for review were considered based on their similarity to the project study area. Sites adjacent to existing tidal inlets, adjacent to deep channels, and located along either the Atlantic or Gulf coasts in the southeastern United States were prioritized based on the conditions of the study area. Additional consideration was given to sites completed within national parks or wildlife refuges, to provide insight options that would meet the regulatory requirements associated with these federal lands. The demonstration sites are at varying stages of development, ranging from completion within the most recent calendar year (2020) to up to 20 years post-construction. The information compiled on each site includes a summary of the mitigation strategy, the project location and cost, the year constructed, and available site photographs. Each site has been assigned a project type based on the primary mitigation technique utilized in construction.

The literature review provides insight on the positive and negative aspects of a range of erosion mitigation options, noting potential concerns from engineering, environmental, and permitting perspectives. The literature review included coastal engineering texts, planning and construction manuals, and academic papers pertaining to erosion mitigation.

**Literature review on erosion mitigation options for deep channels and tidal inlets.**

Nature based features **Structural Features** Hybrid Approaches

Erosion mitigation solution for deep channels	Description	Advantages	Disadvantages	References and links	Examples
Channel relocation	<p>Dredging intended to redirect tidal currents away from eroding shoreline by:</p> <ul style="list-style-type: none"> <li>Restoring historical channel alignment</li> <li>Deepening other existing channels</li> <li>Dredging a new channel/fill old channel</li> </ul> <p>Typically combined with sediment placement and island restoration.</p>	<ul style="list-style-type: none"> <li>Beneficial use of dredged materials</li> <li>Provides opportunity for habitat restoration</li> <li>Uses a combination of dredging and natural inlet processes to redirect strong currents away from eroding shoreline</li> </ul>	<ul style="list-style-type: none"> <li>Not a definite solution and will require maintenance</li> <li>Modifies morphology and hydrodynamics in the bay</li> <li>Impacts to existing shoal islands and associated habitat; impacts would require federal/state permits</li> <li>May require stabilization and enhancement structures as part of design</li> </ul>	<p>Tidal Inlet Response to Natural Sedimentation Processes and Dredging-Induced Tidal Prism Changes: <a href="https://www.jstor.org/stable/4299245?seq=1">https://www.jstor.org/stable/4299245?seq=1</a></p> <p>Lessons from inlet relocation: examples from Southern Portugal: <a href="https://www.sciencedirect.com/science/article/abs/pii/S0378383904000894?via%3Dihub">https://www.sciencedirect.com/science/article/abs/pii/S0378383904000894?via%3Dihub</a></p> <p>Rosgen, D.L. (2011). Natural Channel Design: Fundamental Concepts, Assumptions, and Methods. In A. Simon, S.J. Bennett, &amp; J.M. Castro (Eds.), Stream Restoration in Dynamic Fluvial Systems: Scientific Approaches, Analyses, and Tools, Geophysical Monograph Series 194, pp. 69–93. Washington, D.C.: American Geophysical Union. <a href="https://wildlandhydrology.com/resources/docs/River%20Restoration%20and%20Natural%20Channel%20Design/Rosgen_2011_Natural_Channel_Design.pdf">https://wildlandhydrology.com/resources/docs/River%20Restoration%20and%20Natural%20Channel%20Design/Rosgen_2011_Natural_Channel_Design.pdf</a></p> <p>Natural Channel Design Review Checklist, USFWS <a href="https://www.epa.gov/sites/production/files/2015-07/documents/ncd_review_checklist.pdf">https://www.epa.gov/sites/production/files/2015-07/documents/ncd_review_checklist.pdf</a></p>	<ol style="list-style-type: none"> <li>Mason’s Inlet (NC)</li> <li>Bogue Inlet (NC)</li> </ol>
Living Shoreline Type I (Vegetation Only, Biodegradable Edging)	<p>Use of constructed wetlands/ vegetation to provide shoreline stabilization, possibly in combination with biolog/edging.</p>	<ul style="list-style-type: none"> <li>Some wave attenuation through emergent vegetation</li> <li>Least impact to existing conditions</li> <li>Though federal/state permits required, living shorelines consistent with current state coastal restoration goals</li> </ul>	<ul style="list-style-type: none"> <li>Only feasible for low energy sites and not recommended as stabilization for areas with large fetch or high flow velocities</li> <li>In highly erosive environments vegetation/habitat restoration alone would allow continued erosion</li> </ul>	<p>Living Shoreline Design Guidelines (VA): <a href="https://scholarworks.wm.edu/cgi/viewcontent.cgi?article=1833&amp;context=reports">https://scholarworks.wm.edu/cgi/viewcontent.cgi?article=1833&amp;context=reports</a></p> <p>Info from North Carolina Department of Environmental Quality with Links to Permitting Requirements: <a href="https://deq.nc.gov/about/divisions/coastal-management/coastal-management-estuarine-shorelines/stabilization/stabilization-options">https://deq.nc.gov/about/divisions/coastal-management/coastal-management-estuarine-shorelines/stabilization/stabilization-options</a></p>	<ol style="list-style-type: none"> <li>College Creek, Annapolis (MD)</li> <li>Big Bay Creek, Edisto Island, (SC)</li> <li>Orangetown Creek, Charleston (SC)</li> </ol>
Island or shoal creation and restoration	<p>Use of dredged materials to create or enhance islands or shoals in order to enhance habitat and reduce wave and current energy at a shoreline inland of the island or shoal.</p>	<ul style="list-style-type: none"> <li>Beneficial use of dredged materials from navigation channels</li> <li>Potential habitat enhancement and creation. Lots of documentation on how waterbirds and</li> </ul>	<ul style="list-style-type: none"> <li>Potential permitting challenges</li> <li>Impact on benthic communities or SAV</li> <li>Potential impacts on existing navigation routes</li> <li>Can require constant</li> </ul>	<p>Documenting Engineering With Nature Implementation within the US Army Corps of Engineers Baltimore District - Completed Projects and Opportunities for Chronosequence Analysis (Berkowitz and Szimanski, 2020)</p> <p>USACE rules for placement of dredged material:</p>	<ol style="list-style-type: none"> <li>Swan Island (MD)</li> <li>Queen Bess Island (LA)</li> <li>Sabine NWR (LA)</li> </ol>

		shorebirds have benefited from dredged material islands.	maintenance due to inlet dynamics and high energy environment	<a href="https://www.saw.usace.army.mil/Missions/Navigation/Easements/Disposal-Areas/">https://www.saw.usace.army.mil/Missions/Navigation/Easements/Disposal-Areas/</a>	
Thin layer placement	The term “thin-layer placement” (TLP) has been used to describe sediment additions from approximately 1 cm in depth to 50 cm or more. Typical depths in existing project-scale applications are primarily in the 10-20 cm range. This placement is designed to mimic natural sediment accretion in tidal marshes and mitigate sea level rise effects.	<ul style="list-style-type: none"> <li>- Provides opportunity for beneficial use of dredged sediments (as from channel relocation)</li> <li>- Counteracts sea level rise by enabling the marsh to grow in place vertically as sediment is added</li> <li>- Can work well as part of long-term resilience planning with multiple agencies</li> </ul>	<ul style="list-style-type: none"> <li>- Not used to stop bank erosion however can be used in conjunction with another bank erosion prevention method to improve resilience of the marsh</li> <li>- May be a trade-off between long-term sustainability and short-term decrease in vegetative cover</li> <li>- Multiple placement operations may be required/desirable</li> <li>- Relatively new technique which will require coordination and Federal/state permitting</li> </ul>	Guidance for Thin-Layer Sediment Placement as a Strategy to Enhance Tidal Marsh Resilience to Sea-Level Rise <a href="https://www.nerra.org/01/wp-content/uploads/2020/02/TLP-Guidance-for-Thin-Layer-Placement-20200217-HRes.pdf">https://www.nerra.org/01/wp-content/uploads/2020/02/TLP-Guidance-for-Thin-Layer-Placement-20200217-HRes.pdf</a>	<ul style="list-style-type: none"> <li>9. Prime Hook NWR (DE)</li> <li>10. Blackwater NWR (MD)</li> <li>11. John H. Chafee NWR (RI)</li> </ul>
Living shoreline Type 2 (vegetation with breakwater (reef maker) or sill)	Use of vegetation (marsh plantings), structural components (headland breakwater, sill), and possibly fill to diffract waves and reduce wave energy.	<ul style="list-style-type: none"> <li>- Mimics naturally stable pocket beaches using diffraction around breakwaters, with vegetation to stabilize shoreline</li> <li>- Provides erosion protection with co-benefits including carbon storage, habitat creation</li> <li>- Suitable for higher energy environments depending on armor stone weight</li> <li>- May allow for creative use of reef balls and/or oyster reefs in tandem with breakwater armor stone</li> </ul>	<ul style="list-style-type: none"> <li>- Deep offshore depths may be cost-prohibitive, uncertain performance</li> <li>- May encroach on channel</li> <li>- May cause impacts on adjacent shoreline</li> <li>- Federal/state permits will be required for hardened structure and impacts to any existing wetlands; however, living shoreline component consistent with current state coastal restoration goals</li> </ul>	<p>Shoreline Management in the Chesapeake Bay:(Hardaway and Bryne, 1999) <a href="https://scholarworks.wm.edu/cgi/viewcontent.cgi?article=1581&amp;context=reports">https://scholarworks.wm.edu/cgi/viewcontent.cgi?article=1581&amp;context=reports</a></p> <p>Hardaway et al. (2000)- case study for shoreline restoration in Saxis, VA <a href="https://www.vims.edu/research/departments/physical/programs/ssp/_docs/An%20intergrated%20habitat%20enhancement_Saxis.pdf">https://www.vims.edu/research/departments/physical/programs/ssp/_docs/An%20intergrated%20habitat%20enhancement_Saxis.pdf</a></p> <p>Living Shoreline Effectiveness as Erosion Control based on Survey of NC Sites: Polk and Eulie (2018)- focus on shorelines with sills. <a href="https://link.springer.com/article/10.1007/s12237-018-0439-y?shared-article-renderer">https://link.springer.com/article/10.1007/s12237-018-0439-y?shared-article-renderer</a></p> <p>Reefmaker: Bonner Bridge Project Wave Dissipator in Manteo, NC: <a href="https://www.atlanticreefmaker.com/project/bonner-bridge-project-jacksonville-nc/">https://www.atlanticreefmaker.com/project/bonner-bridge-project-jacksonville-nc/</a></p>	<ul style="list-style-type: none"> <li>12. Durant Point (NC)</li> <li>13. Fort Anderson (NC)</li> <li>14. Elizabeth River (VA)</li> <li>15. Rockefeller Wildlife Refuge (LA)</li> <li>16. Moor Shore Rd. (NC)</li> <li>17. Franklin Point State Park (MD)</li> <li>7. Queen Bess Island (LA)</li> <li>8. Sabine National NWR (LA)</li> </ul>
Soil bioengineering - Vegetated geogrids/ Soft armor walls	Soft armor walls are a soft, permanent structural system engineered to be vegetated for bank &	<ul style="list-style-type: none"> <li>- Provides immediate erosion control and slope stabilization even before vegetation exists.</li> </ul>	<ul style="list-style-type: none"> <li>- Needs to be reinforced for walls over 3 ft.</li> <li>- Depend on geotextile strength for material retention</li> </ul>	A Guide to Bank Restoration Options for Large River Systems: Part II Bioengineering Installation Manual. Technical sheets 7, 14: <a href="https://www.mwmo.org/monitoring-and-reports/watersh">https://www.mwmo.org/monitoring-and-reports/watersh</a>	<ul style="list-style-type: none"> <li>18. River Street Cut (NH)</li> <li>19. Riverview Road (WA)</li> </ul>

	shoreline stabilization, retaining wall and erosion control applications using interlocking plates and geotextile bags	<ul style="list-style-type: none"> <li>- Can accommodate steep slopes with no limitation on height.</li> <li>- Site materials (soil/fill) can be reutilized to fill geotextile bags.</li> <li>- Cost effective</li> </ul>	<ul style="list-style-type: none"> <li>- under strong current</li> <li>- Federal/state permits required for construction; geotextile bags may require variance if not consistent with existing state rules</li> </ul>	<a href="https://www.fs.fed.us/t-d/pubs/pdf/fs683/ch_05.pdf">ed-assessment/a-guide-to-bank-restoration-options-for-large-river-systems/</a>	
Flow speed reduction - Root wad with footer	Root wads armor a bank by keeping the current off the bank.	<ul style="list-style-type: none"> <li>- Slows currents</li> <li>- Creates and improves fish-rearing and spawning habitat.</li> <li>- Tolerates high boundary shear stress when logs and root wads are well anchored.</li> </ul>	<ul style="list-style-type: none"> <li>- Should be used in combination with other soil bioengineering techniques or revetment.</li> <li>- Requires durable wood to maximize lifespan</li> <li>- Has a limited lifespan and may require periodic maintenance or replacement.</li> <li>- Mostly used in rivers, not tested in tidal inlets.</li> </ul>	USDA. Soil Bioengineering Techniques: <a href="https://www.fs.fed.us/t-d/pubs/pdf/fs683/ch_05.pdf">https://www.fs.fed.us/t-d/pubs/pdf/fs683/ch_05.pdf</a>	20. Upper Truckee River (CA)
Flow speed reduction - Bendway weirs	A low level, totally submerged rock structure that is positioned from the outside bankline of a riverbend, angled upstream toward the flow.	<ul style="list-style-type: none"> <li>- Suitable for deep channels</li> <li>- Reduces flow velocities against eroding bank</li> <li>- Controls excessive channel deepening</li> <li>- Reduces adjacent bank erosion on the outside bendway. Because excessive river depths are controlled, the opposite side of the riverbank is widened naturally</li> </ul>	<ul style="list-style-type: none"> <li>- Mostly used in rivers, not tested in tidal inlets.</li> <li>- Federal/state permitting required due to potential habitat impacts and navigation</li> <li>- Could affect or kill SAV</li> </ul>	USACE: <a href="https://www.mvs-wc.usace.army.mil/arec/Basics_Weirs.html">https://www.mvs-wc.usace.army.mil/arec/Basics_Weirs.html</a>  Davinroy, 1990. A new structural solution to navigation problems experienced in the Mississippi River. P.IAN.C. - A.I.P.C.N. - BULLETIN No. 69: <a href="https://www.mvs-wc.usace.army.mil/arec/Documents/Bendway_Weirs/A_New_Structure_Solution_To_Navigation_Problems.pdf">https://www.mvs-wc.usace.army.mil/arec/Documents/Bendway_Weirs/A_New_Structure_Solution_To_Navigation_Problems.pdf</a>	21. Mississippi River at Barfield
Jetties	Rocky shore-perpendicular structure adjacent to tidal inlet to confine tidal flow and control migration and sediment deposition in the inlet. Jetties may be single or double.	<ul style="list-style-type: none"> <li>- Stabilizes the inlet channel</li> <li>- Ensures navigation in the inlet</li> </ul>	<ul style="list-style-type: none"> <li>- Interrupt longshore transport</li> <li>- Requires design and implementation of sediment bypassing mechanism</li> <li>- May require dredging for channel maintenance</li> <li>- Do not enhance nor provide opportunity for habitat restoration</li> <li>- Only stops marsh erosion if structure extends into the Sound</li> <li>- Extensive federal and state permitting process due to</li> </ul>	Kraus, 2008. Engineering of tidal inlets and morphologic consequences: <a href="https://pdfs.semanticscholar.org/fbc5/247371eb80404c77d767caee0e98a10dc037.pdf">https://pdfs.semanticscholar.org/fbc5/247371eb80404c77d767caee0e98a10dc037.pdf</a>  Brunn, 1978. Stability of Tidal Inlets. Theory and Engineering. Developments in Geotechnical Engineering, Vol 23. Elsevier Scientific Publishing Company.	22. Masonboro Inlet, NC

			potential impacts to coastal habitats and navigation		
Seawalls/bulkhead / Revetments and Terminal groin extension	Vertical hardened structure constructed along the shoreline of rock, concrete, metal, or other non-native material. May be held in place by tie-back rods or other anchoring devices. Typically build to protect slopes from wave action.	<ul style="list-style-type: none"> <li>- Stops shoreline erosion and channel encroachment into the adjacent beach/marsh habitat.</li> <li>- Long-term solution for shoreline impact; little maintenance unless damaged by storm events</li> <li>- Minimizes the effects of wave action on the shoreline</li> </ul>	<ul style="list-style-type: none"> <li>- Beach/marsh material located seaward of the wall/bulkhead will erode away due to lack of protection and concentration of wave energy.</li> <li>- Potential impact to adjacent beaches and shorelines due to interruption in alongshore transport.</li> <li>- Higher initial construction cost than other options</li> <li>- Does not facilitate creation of additional habitat (replacing previously eroded areas)</li> <li>- Reduces the intertidal zone required for marsh habitat</li> <li>- Extensive federal/state permitting required; current NC law prohibits oceanfront seawalls except on limited basis</li> </ul>	<p>Dean, R.G. and R. A. Dalrymple. 2002. Coastal Processes with Engineering Applications. Cambridge University Press.</p> <p>USACE, 2002. Coastal Engineering Manual</p> <p>USACE, 1995. Design of Coastal Revetments, seawalls and bulkheads:  <a href="https://www.delmar.ca.us/DocumentCenter/View/1899/Design-of-Coastal-Revetments-Seawalls-and-Bulkheads_Army-Corps-of-Engineers-1995">https://www.delmar.ca.us/DocumentCenter/View/1899/Design-of-Coastal-Revetments-Seawalls-and-Bulkheads_Army-Corps-of-Engineers-1995</a></p>	

Maybe future phases could include permitting issues  
 Cost (million, tens of millions, hundreds of millions?)

## REVIEW OF DEMONSTRATION SITES FOR ESTUARINE SHORELINE EROSION MITIGATION

### Channel Relocation

#### **Project #1**

**Name:** Mason Inlet Relocation

**Location:** Mason Inlet, NC. New Hanover County

**Project Type:** Inlet channel relocation

**Year built:** 2002

**Cost:** \$ 8 Million

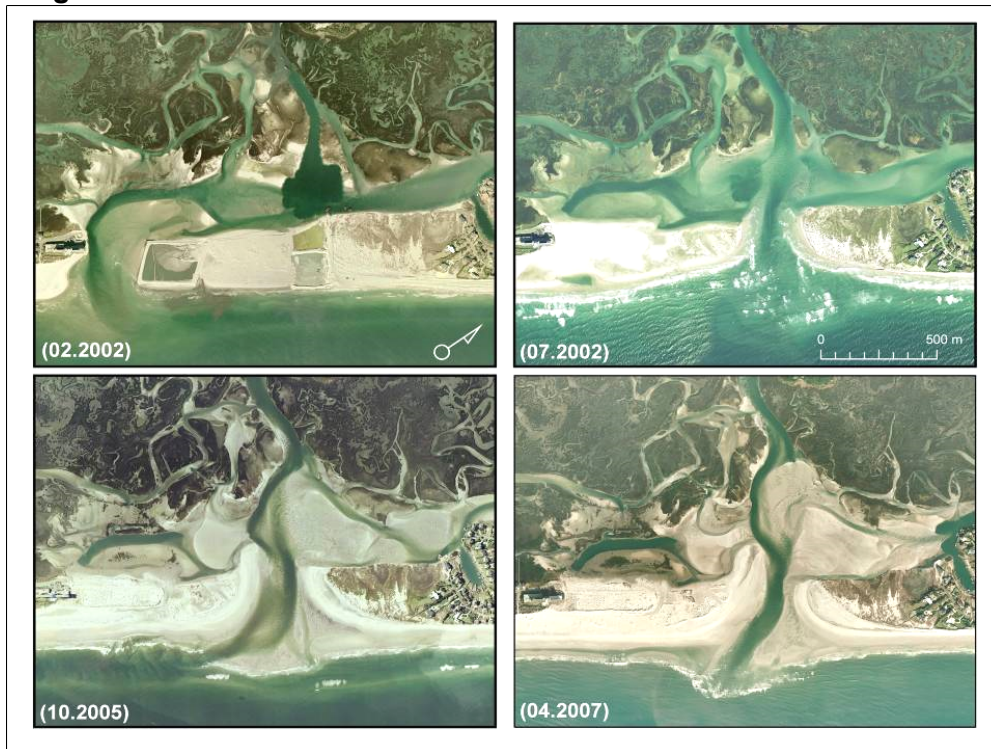
**Description:** Channel had migrated adjacent to structures on Wrightsville Beach (Shell Island Resort). Operations dredged the channel through the accreted spit and created a more direct route to the Intracoastal Waterway. Monitoring and maintenance is ongoing via Mason Inlet Preservation Group and New Hanover County. Dredging every 2-4 years.

#### **Links and references:**

[http://people.uncw.edu/hillj/classes/EVS360/VERP/Mason\\_Inlet\\_Project\\_Summary.pdf](http://people.uncw.edu/hillj/classes/EVS360/VERP/Mason_Inlet_Project_Summary.pdf)

<https://www.jstor.org/stable/4299245?seq=1>

**Image 1:**



## Project #2

**Name:** Bogue Inlet Relocation

**Location:** Bogue Inlet, NC. Town of Emerald Isle, Carteret County.

**Project Type:** Inlet channel relocation

**Year built:** 2005

**Cost:** \$ 11.4 Million

**Description:** Main ebb channel had migrated adjacent to structures on The Point. The Town of Emerald Isle relocated the channel to a more central location between Emerald Isle and Bear Island in 2005. The project included the completion of channel realignment with concurrent dike construction. The final length of the dike was 2,200 linear feet. The sand removed was used for beach nourishment along 4 miles of ocean beach in western Emerald Isle. Town monitors channel position and tentatively plans to relocate again in 2022 (17 years later).

### Links and references:

<http://www.carteretcountync.gov/659/Phase-III---Bogue-Inlet-2005>

Image 1:



**Living Shoreline Type I (Vegetation Only/Biodegradable Edging)**

**Project #3**

**Name:** St. John's College Living Shoreline at College Creek

**Location:** Annapolis, Maryland

**Project Type:** Living Shoreline Type I (Vegetation with Coir Log)

**Year built:** 2006

**Cost:** \$70,000

**Description:** Replaced 800 ft of deteriorating timber bulkhead with sediment placement, marsh plantings, and coir log-stabilization. The timber bulkhead was deteriorating and the shoreline behind the bulkhead slumping due to sediment loss associated with tidal intrusions

**Links and references:**

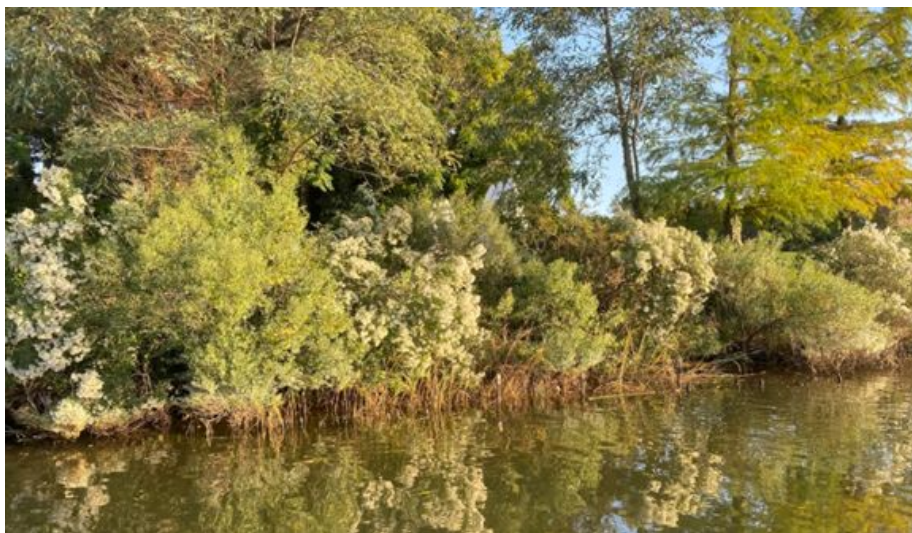
<https://www.habitatblueprint.noaa.gov/storymap/lis/index.html>

[https://dnr.maryland.gov/ccs/Documents/training/lisrles\\_rs.pdf](https://dnr.maryland.gov/ccs/Documents/training/lisrles_rs.pdf)

**Image 1:**



Shortly after construction



Present-day (2020) photograph

#### **Project #4**

**Name:** Big Bay Creek,

**Location:** Edisto Island, South Carolina

**Project Type:** Living Shoreline Type I (Vegetation with Coir Log)

**Year built:** 2016

**Cost:** Unknown

#### **Description:**

Experimental treatment installed in 2016 along an intertidal bank on the inside bend of Big Bay Creek, SC. The creek width was small and located in a no wake zone, resulting in a low-energy environment suitable for a vegetation-only treatment. Coir logs were placed to stabilize slopes of 20%, comprising mainly silt, clay, and sand. Sediment accumulation was measured during the first two years following installation, and marsh grass began to colonize the bank behind the coir log as of May, 2019.

#### **Links and references:**

<http://floridalivingshorelines.com/wp-content/uploads/2019/10/SumLivingShoreSCDNR.pdf>

#### **Image 1:**



**Figure 3.16.** A single-row coir log treatment at Big Bay Creek (Figure 3.4) in July 2016 (upper left), October 2017 (upper right), September 2018 (lower left), and May 2019 (lower right).

**Project #5**

**Name:** Orangegrove Creek

**Location:** Charleston, South Carolina

**Project Type:** Living Shoreline Type I (Vegetation with Coir Log)

**Year built:** 2017

**Cost:** unknown

**Description:** Double-row coir log experimental treatment installed in 2017 along an intertidal bank on an inside bend of Orangegrove Creek. The site was considered to be low energy owing to the limited boat traffic and narrow creek width (203 ft) at the site. The bank had a slope of 24% and comprised mainly silt and clay. Sediment accumulated in the first 20 months following installation. One coir log broke away from its stakes and went missing between August 2018 and April 2019. No marsh expansion was observed.

**Links and references:**

<http://floridalivingshorelines.com/wp-content/uploads/2019/10/SumLivingShoreSCDNR.pdf>

**Image 1:**



**Figure 3.17.** Double-row coir log treatment at Orangegrove Creek in August 2017 (upper left), May 2018 (upper right), and April 2019 (lower). The upper left coir log went missing at some point between August 2018 and April 2019.

## **Island/Shoal Creation/Restoration**

### **Project #6**

**Name:** Swan Island Restoration

**Location:** Swan Island part of the Glenn Martin National Wildlife Refuge, Chesapeake Bay, MD

**Project Type:** Island restoration using dredged material

**Year built:** 2019

**Cost:** ?

**Description:** 70,000 cubic yards of sediments dredged from the Big Thorofare and Twitch Cove federal channels by the U.S. Army Corps of Engineers, Baltimore District, were reused to restore habitat at Swan Island, which is part of the Martin National Wildlife Refuge on Smith Island. The material is used to restore dune habitat and to create high and low marsh habitats; act as a buffer for restored habitat from wind and waves; and provide a natural breakwater for the Town of Ewell. Monitoring of habitat and land cover is underway.

### **Links and references:**

<https://storymaps.arcgis.com/stories/0c801897e5e24396bd44dfe0732f18ec>

<https://www.nab.usace.army.mil/Media/Images/igphoto/2001856524/>

<https://coastalscience.noaa.gov/news/swan-island-restoration-begins/>

### **Image 1:**



Swan Island before dredge application and planting, 2017. Credit: U.S. Army Corps of Engineers.



Swan Island after dredge application and planting, 2019. Credit: NOAA's National Centers for Coastal Ocean Science.

**Project #7****Name:** Queen Bess Island, LA**Location:** Barataria Bay, LA**Project Type:** Barrier Island Restoration with Dredged Material**Year built:** 2019-2020**Cost:** Funded by NRDA (National Resource Damage Assessment) Restoration Program. \$18.7 million**Description:**

This project was a partnership between Coastal Protection and Restoration Authority and the Louisiana Department of Wildlife and Fisheries. It was designed to restore suitable colonial waterbird nesting habitat through the beneficial use of dredged material, vegetation planting, and riprap/aggregate placement. 36 acres were restored and/or benefited from this project.

**Links and references:**

<https://coastal.la.gov/news/queen-bess/>

**Images:**

Pre-construction (2019) <https://coastal.la.gov/news/queen-bess/>



Post-construction (2020) <https://coastal.la.gov/news/queen-bess/>

**Project #8****Name:** Marsh Creation, Restoration, and Mitigation**Location:** Sabine National Wildlife Refuge, Louisiana**Project Type:** Marsh restoration using material dredged from the Calcasieu Ship Channel and linear terrace construction**Year built:** Ongoing since 1993**Cost:** ?**Description:** This project has multiple aspects.

Essentially material dredged from the Calcasieu Ship Channel is used to restore habitat lost when areas have converted from emergent marsh to open water. USACE conducts analysis on the dredged sediments to ensure that they do not contain contaminants. Through partnering with U.S. Corps of Engineers (COE), National Oceanic and Atmospheric Administration (NOAA), Louisiana Department of Natural Resources (LA DNR), Coastal Protection Restoration Authority (CPRA), and our Ecological Services office, the U.S. Fish and Wildlife Service Refuge staff has restored 3,200 acres of marsh on Sabine National Wildlife Refuge since 1993. An additional 600 acres is being planned. In addition to the marsh creation via dredge material, earthen terraces were constructed in 1990 and 2001 to reduce wind-related wave intensity and slow water movement allowing fine sediments to settle, provide favorable conditions for SAVs and improve habitat for fish/other aquatic species. There is another aspect called "Living Reef Shoreline Protection Barrier" which states that the USFWS is partnering with the Nature Conservancy, LA Coastal Protection Restoration Authority, Shell, Chevron, Citgo, and the NFWF to create a reef from live propagating oysters to protect an eroding shoreline. This will protect adjacent marshes as well as a hurricane evacuation route, Highway 27.

**Links and references:**

[https://www.fws.gov/refuge/sabine/wildlife\\_and\\_habitat/restoration\\_and\\_mitigation\\_sites.html](https://www.fws.gov/refuge/sabine/wildlife_and_habitat/restoration_and_mitigation_sites.html)

**Image 1:**

## **Thin Layer Placement**

### **Project #9**

**Name:** Prime Hook NWR Recovery and Resiliency Project

**Location:** Prime Hook National Wildlife Refuge, Delaware

**Project Type:** Dredging historical tidal channels and using dredged material to build up shoreline and marsh

**Year built:** Sept. 2015 - Sept. 2016

**Cost:** \$20 million to repair beach and dune breaches; \$19.8 million to restore a robust marsh environment (funding from Hurricane Sandy Disaster Relief Appropriations) [other published estimates say "\$38 million"]

**Description:** Converted managed impoundments back to area with circulating tidal channels by dredging, and restore beach and dune using the dredged material. Has been successful attracting plovers and other endangered birds. Water quality and fisheries have improved. During the Fowler Beach replenishment project, 1.4 million cubic yards of Delaware Bay sand were used to rebuild 2 miles of the beach. The dune was restored to a height of 9 feet with a 100- to 600-foot-wide back barrier platform between the dune line and marsh. More than 500,000 plugs of beach grass and 10,000 feet of fencing have been added to stabilize the dune and back barrier.

Early on, officials decided to restore most of the destroyed area to a saltwater marsh and end more than 30 years of maintaining a freshwater habitat, originally created to attract freshwater waterfowl. Twenty-five miles of restored channels have allowed more freshwater to flow into the refuge to sustain about 1,200 acres of freshwater marsh. Mud pumped out of the channels formed flats to allow marsh grass to grow. All of the water-control structures used to prevent saltwater intrusion were dismantled to allow for water flow. In addition, smaller ditches not only help with water flow, but also allow for natural control of mosquitoes as fish larvae swim in the channels and feed on mosquitoes.

### **Links and references:**

[https://www.fws.gov/refuge/Prime\\_Hook/what\\_we\\_do/marshrestoration.html](https://www.fws.gov/refuge/Prime_Hook/what_we_do/marshrestoration.html)

<https://www.capegazette.com/article/rebirth-occurring-prime-hook-refuge-marshes/162767>

<https://www.capegazette.com/article/piping-plover-among-prime-hook-success-stories/164538>

Video: <https://www.youtube.com/watch?v=YiQLWO0bpbk&feature=youtu.be>

*(Project mentioned by Becky Harrison of PINWR)*

**Image 1:**



**Project #10**

**Name:** Planning for Marsh Migration at the Blackwater National Wildlife Refuge (Blackwater 2100)

**Location:** Blackwater National Wildlife Refuge, Cambridge, Maryland

**Project Type:** Thin layer placement

**Year built:** 2016

**Cost:** \$1.1 million (post-Sandy grants)

**Description:** Dredge America helped restore the natural salt marsh using a thin layer deposition method of dredging. By spraying “dredge material” over the existing marsh surface, we raised the existing marsh platform to provide plant resiliency, combating rising sea levels at the site. Our goal for the project was to remove and place approximately 26,000 cubic yards of sediment to restore up to 30 acres of the fragile marsh habitat. Completing the first large-scale wetland restoration project ever attempted at Blackwater, and the first thin-layer project in the Chesapeake watershed, the restoration was a resounding success, having been completed on time and under budget.

**Links and references:**

<https://dredgeamerica.com/news/blackwater-national-wildlife-refuge-marsh-restoration/>

<https://climatechange.lta.org/wp-content/uploads/cct/2015/04/Blackwater-2100-report.pdf>

<https://usfwsnortheast.wordpress.com/2017/10/19/taking-marsh-restoration-to-a-new-level/>

*(Project mentioned by Becky Harrison of PINWR)*

**Image 1:**

## Project #11

**Name:** Thin Layer Placement at Chafee Refuge to Rebuild Marsh Habitat

**Location:** John H. Chafee National Wildlife Refuge, Narragansett, RI

**Project Type:** Marsh restoration using dredged material and recycled clam shells

**Year built:** 2016-17, 2018

**Cost:** for 2016-17 effort: \$1.4 million cooperative agreement between The Nature Conservancy and the U.S. Fish and Wildlife Service, supported by federal funding for Hurricane Sandy recovery

**Description:** Thin layer placement of dredged material on 30 acres of existing salt marsh, adding up to six inches of elevation to the marsh. Larger project following testing on 11 acres at Sachuset Point NWR using trucked in sand. Also incorporating plantings. 24,000 cy of reclaimed material, 3,000 bags of clam and oyster shells to protect against marsh edge erosion/hold sediment and water on the marsh platform. No more than 6" placement thickness.

### Links and references:

[https://www.fws.gov/uploadedFiles/Region\\_5/NWRS/North\\_Zone/Rhode\\_Island\\_Complex/John\\_H\\_Chafee/Release\\_JHCNWR\\_TLD\\_announcement.pdf](https://www.fws.gov/uploadedFiles/Region_5/NWRS/North_Zone/Rhode_Island_Complex/John_H_Chafee/Release_JHCNWR_TLD_announcement.pdf)

<https://www.ecori.org/natural-resources/2018/12/6/dredging-at-chafee-refuge-to-rebuild-marsh-habitat>

<https://www.northeastoceancouncil.org/wp-content/uploads/2017/05/Nonstructural-Management-Practices-that-Build-Resiliency.pdf>

Note: There are many other similar projects linked to this one at other RI Refuges:

<https://www.fws.gov/hurricane/sandy/projects/KeyHabitats.html>

<https://storymaps.arcgis.com/stories/308db7dec4d34d788705294da0f441f6>

Reference: "Guidance for thin-layer sediment placement as a strategy to enhance tidal marsh resilience to sea-level rise" includes information on design, examples/lit review, permitting information, and monitoring recommendations:

<https://www.nerra.org/01/wp-content/uploads/2020/02/TLP-Guidance-for-Thin-Layer-Placement-20200217-HRes.pdf>

Image 1:



Image 2:



**Living Shoreline Type 2 (Vegetation with breakwater or sill)**

**Project #12**

**Name:** Durant Point, NC Coastal Federation

**Location:** Hatteras Village, NC. Privately owned property facing the Pamlico Sound

**Project Type:** Living Shoreline Type 2

**Year built:** 2009

**Cost:** \$350/linear foot

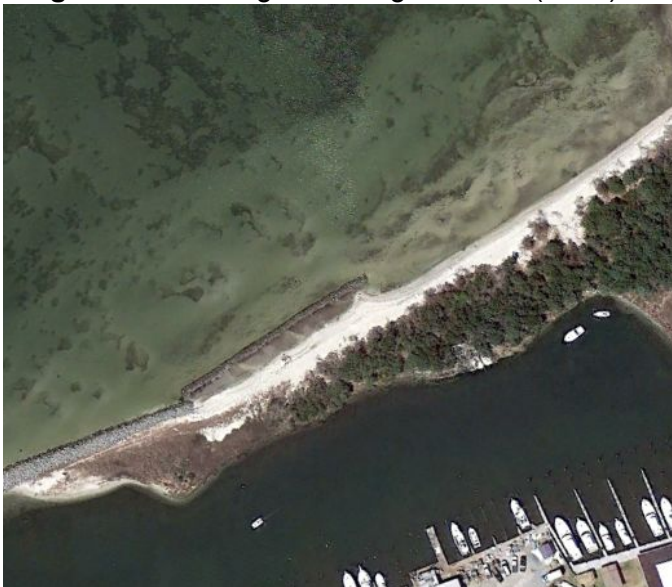
**Description:** shoreline stabilization with a low-profile granite sill 30 feet offshore. The shoreline was re-graded for marsh grass planting. The project protects nearly 330 linear feet of shoreline and creates and protects nearly 1.2 acres of coastal marsh. Volunteers helped plant marsh grasses behind the sill.

**Links and references:** <https://www.nccoast.org/project/durants-point-living-shoreline/>

**Image 1:** Living shoreline state in 2013



**Image 2:** Aerial image of Living shoreline(2013) from google earth



## Project #13

**Name:** Fort Anderson

**Location:** Brunswick Town, NC. Land owned by the North Carolina Department of Natural and Cultural Resources.

**Project Type:** Reef maker Living Shoreline

**Year built:** 2019

**Cost:** \$ 10 million

**Description:** This project includes use of a proprietary technology called the “Reefmaker” which consists of a fiberglass piling driven down into the bottom of the river with concrete disks stacked on top and clamped in place. This not only resists boat wake within the channel leading to the harbor at Wilmington but also creates habitat for fish, crabs and oysters. It is of particular interest because it has been deployed next to a deep navigation channel. The same technology is being used in Oregon Inlet flood channel for SAV mitigation (chevron formation).

### Links and references:

<http://www.ncbiwa.org/files/Boyd-Brunswick%20Town-Living%20Shoreline-compressed.pdf>

<https://www.atlanticreefmaker.com/brunswick-town-introductory-video/>

Image 1:



Image2:



**Project #14****Name:** Elizabeth River Living Shoreline at Lambert's Point**Location:** Norfolk Southern Lamberts Point Coal Terminal, Norfolk, VA**Project Type:** Living Shoreline Type 2**Year built:** 2020**Cost:** \$ 206 K**Description:** The project spans approximately 1,400 ft of shoreline. The upland embankment was protected by 1) regrading, placing geotextile for slope stabilization, and plantings, and 2) construction of a segmented sill nearshore in approximately three feet of water. Field inspection and monitoring to propose corrective action recommendations are scheduled from 2021 to 2025.**Links and references:** Dewberry Archives.**Image 1:**

**Project #15**

**Name:** Rockefeller Wildlife Refuge Gulf Shoreline Stabilization Project

**Location:** Rockefeller Wildlife Refuge, Cameron Parish, LA

**Project Type:** Breakwater

**Year built:** June 2020

**Cost:** funding secured \$ 34 million from the Coastal Wetlands Planning, Protection and Restoration Act (CWPPRA)

**Description:** A 3-mile long breakwater protects more than 250 acres of coastal marsh. Due to the soft soil found in the area, a lightweight material was used to construct the breakwater and reduce sinking. The design also incorporates gaps at regular intervals that allow water and fish to pass through.

**Links and references:**

<https://www.fisheries.noaa.gov/feature-story/rockefeller-refuge-project-protects-vulnerable-louisiana-shoreline>

<https://www.hdrinc.com/portfolio/rockefeller-wildlife-refuge-gulf-shoreline-stabilization-project>

[https://www.lacoast.gov/reports/project/2014-10-28%20RR%20Shore%20Stabilization%20\(ME18\)%20Design%20Report%20Final.pdf](https://www.lacoast.gov/reports/project/2014-10-28%20RR%20Shore%20Stabilization%20(ME18)%20Design%20Report%20Final.pdf)

**Image 1:**



**Project #16****Name:** Moor Shore Road Living Shoreline**Location:** Kitty Hawk, NC

<https://www.google.com/maps/place/36°03'35.7%22N+75°41'55.5%22W/@36.059921,-75.7009387,639m/data=!3m2!1e3!4b1!4m14!1m7!3m6!1s0x89a4e03a9281b38d:0x8e05b312711bfa07!2sMoor+Shore+Rd.+Atlantic,+NC+27949!3b1!8m2!3d36.0610313!4d-75.7004001!3m5!1s0x0:0x0!7e2!8m2!3d36.0599209!4d-75.6987517?hl=en>

**Project Type:** Living shoreline Type 2 - Vertical sill construction, native species planting**Year built:** Completed 2019**Cost:**

**Description:** Project included construction of seven vertical sills along 600 feet of estuarine shoreline. The sill used is 18 inches wide, raised between 6 and 12 inches above the water line, with breaks every 75 to 100 feet to allow for fish passage. Marsh grasses were then planted for shoreline protection and stabilization as well as the creation of additional habitat.

The project was constructed to address shoreline erosion and to protect the adjacent roadway, which is used as an emergency route with US 158 is closed due to flooding. Project funding came from four agencies, including the Town of Kitty Hawk, NOAA, Dare County Soil and Water, and NCDOT. This is NCDOT's first documented living shoreline project in the state.

**Links and references:**

<https://www.nccoast.org/2019/01/moor-shore-road-living-shoreline-construction-begins-in-kitty-hawk/>

<https://www.nccoast.org/2019/07/volunteers-help-complete-moor-shore-road-living-shoreline-project/>

**Image 1:**

**Project #17**

**Name:** Franklin Point State Park Living Shoreline

**Location:** Shady Side, MD

**Project Type:** Living Shoreline Type 2

**Year built:** planned 2020

**Cost:** \$70k for design, \$1.3mil for construction

**Description:** Plan to restore 1,100 ft of peninsula exposed to >100 mi fetch south-southeast down Chesapeake Bay and eroding at a rate of 4 ft/yr. Contract awarded to Coastal Design, a firm from Gloucester, VA. Possible pilot site for beneficial use of dredge material.

**Links and references:**

<https://www.eyeonannapolis.net/2019/10/public-meeting-slated-to-review-plans-for-living-shoreline-to-protect-franklin-point-state-park/>

<https://www.capitalgazette.com/environment/ac-cn-shoreline-grants-20180823-story.html>

<https://www.arundelrivers.org/restoration/living-shorelines/>

Riverkeeper Jeff Holland at 443-758-7797, email [jeff@arundelrivers.org](mailto:jeff@arundelrivers.org)

**Image 1:**



**Image 2:** *Photo taken October 2019, after planting.*



## **Soil Bioengineering (Geogrids)**

### **Project #18**

**Name:** Toe protection at River Street Cut

**Location:** Seabrook, NH

**Project Type:** Soil bioengineering - Geogrid & seawall

**Year built:** 2004 - 2005

**Cost:** N/A

**Description:** 12-in.-thick marine mattresses measuring approximately 5 ft wide and 30 ft long were installed for protection against scour by waves and currents at the Blackwater River. The project was a collaborative effort between the U.S. Army Engineer District, New England, and the state of New Hampshire. The erosion channel along River Street was filled with dredged material. The placed material was contained on both sides by fiberglass-reinforced polymer (FRP) composite vertical sheetpile walls.

### **Links and references:**

<https://apps.dtic.mil/dtic/tr/fulltext/u2/a444644.pdf>

### **Image 1:**



**Project #19****Name:** Riverview Road**Location:** Snohomish County, WA**Project Type:** Soil bioengineering - Geogrid**Year built:** N/A**Cost:** N/A

**Description:** Bank stabilization project to protect Riverview Road. A structural earth wall made of multiple soil wraps, was built in a step-like geometry starting from the river waterline until the top of the embankment. Each layer is created by a 13-foot wide roll of polypropylene or polyethylene geo-grid fabric filled with compacted gravel. The outer face of the wall was covered with coir fabric and topsoil and all the embankment was planted with vegetation.

**Links and references:**

[https://www.fema.gov/pdf/about/regions/regionx/Engineering\\_With\\_Nature\\_Web.pdf](https://www.fema.gov/pdf/about/regions/regionx/Engineering_With_Nature_Web.pdf)

**Image 1:**

**Flow Speed Reduction (Root Wad with Footer)**

**Project #20**

**Name:** Upper Truckee River

**Location:** Near Lake Tahoe, CA

**Project Type:** Root wad

**Year built:** early 90s

**Cost:** N/A

**Description:** Root wads were installed along the outer edge of the eroding bank of the river. The root wads were reported to reduce flow velocities in the river, which can reach 4 ft/s. The root wads allow vegetation establishment along the river bank.

**Links and references:**

[https://www.engr.colostate.edu/~bbledsoe/CIVE413/Bioengineering\\_for\\_Streambank\\_Erosion\\_Control\\_report1.pdf](https://www.engr.colostate.edu/~bbledsoe/CIVE413/Bioengineering_for_Streambank_Erosion_Control_report1.pdf)

**Image 1:**





## **Jetties**

### **Project # 22**

**Name:** Masonboro Inlet, NC

**Location:** Masonboro Inlet, NC

**Project Type:** Jetty

**Year built:** North Jetty: 1965. South Jetty: 1980

**Cost:** N/A

**Description:** The Jetties of Masonboro Inlet were built to maintain navigation through the inlet. The north jetty was the first weir jetty built in the United States. The south jetty was constructed 14 years later. The northern shoulder of the inlet formed after construction of the south jetty. Previously, sediment would enter the interior channel and settle there to be dredged for beach nourishment of the neighboring island. This sand eventually formed a spit and required vessels entering the inlet to make sharp turns in strong cross currents to remain in the navigation channel. However, by using the sand spit as an extended deposition basin area, the U.S. Army Engineer District, Wilmington, has only had to dredge the deposition area every 3 to 4 years, and the dredging also keeps the spit from further encroaching into the navigation channel

### **Links and references:**

<https://apps.dtic.mil/dtic/tr/fulltext/u2/1038027.pdf>

<https://apps.dtic.mil/sti/pdfs/ADA588871.pdf>

### **Image 1:**



Numerous inlets have been stabilized using jetties, some examples include:

Ft. Pierce Inlet, FL

South Lake Worth Inlet, FL

Jupiter Inlet, FL

Sebastian Inlet, FL

Ocean City Inlet, MD

Masonboro Inlet, NC

Rudee, Inlet VA

# APPENDIX C

```
#!/usr/bin/env python3
```

```
# -*- coding: utf-8 -*-
```

```
"""
```

```
Created on Mon Oct 25 18:39:32 2021
```

```
@author: vegasproul
```

```
"""
```

```
import netCDF4
```

```
import numpy as np
```

```
import time
```

```
import calendar
```

```
import requests
```

```
import pandas as pd
```

```
import json
```

```
from datetime import datetime, timedelta
```

```
import openpyxl
```

```
from openpyxl import load_workbook
```

```
from openpyxl.styles import Font
```

```
import smtplib
```

```
from email.message import EmailMessage
```

```
import gspread
```

```
from oauth2client.service_account import ServiceAccountCredentials
```

```
v = 1 # number of hours between each check
```

```
# Initialization
```

```
stn = '192'
```

```
startdate = (datetime.now() - timedelta((1*v)/24)).strftime('%m/%d/%Y')
```

```
enddate = (datetime.now()).strftime('%m/%d/%Y')
```

```
## Import the data from CDIP Server
```

```
# CDIP Realtime Dataset URL
```

```
try:
```

```
    data_url = 'http://thredds.cdip.ucsd.edu/thredds/dodsC/cdip/realtime/' + stn + 'p1_rt.nc'
```

```
    nc = netCDF4.Dataset(data_url)
```

```
except: # if it fails for ANY error type
```

```
    EMAIL_ADDRESS = "PealslandFloodAlert@gmail.com"
```

```
    EMAIL_PASSWORD = "kiawcxdtgcfmykoe" # gmail app password
```

```
msg = EmailMessage()
```

```
msg['Subject'] = 'CDIP Wave Data Retrieval Failure'
```

```

msg['From'] = EMAIL_ADDRESS
msg['To'] = 'PealslandFloodAlert@gmail.com'
message="The email alert script is not functioning properly because it could not access CDIP
wave data."
print(message)
msg.set_content(message)
with smtplib.SMTP_SSL('smtp.gmail.com', 465) as smtp:
    smtp.login(EMAIL_ADDRESS, EMAIL_PASSWORD)
    smtp.send_message(msg)

```

```

# Read Buoy Variables

```

```

ncTime = nc.variables['sstTime'][:]
timeall = [datetime.fromtimestamp(t) for t in ncTime] # Convert ncTime variable to datetime
stamps
Hs = nc.variables['waveHs']
Tp = nc.variables['waveTp']
Dp = nc.variables['waveDp']

```

```

Hs = np.array(Hs)
Tp = np.array(Tp)

```

```

month_name = calendar.month_name[int(startdate[0:2])]
year_num = (startdate[6:10])

```

```

# Find nearest value in numpy array
def find_nearest(array,value):
    idx = (np.abs(array-value)).argmin()
    return array[idx]

```

```

# Convert from human-format to UNIX timestamp
def getUnixTimestamp(humanTime,dateFormat):
    unixTimestamp = int(time.mktime(datetime.strptime(humanTime, dateFormat).timetuple()))
    return unixTimestamp

```

```

# Time index values
unixstart = getUnixTimestamp(startdate,"%m/%d/%Y")
neareststart = find_nearest(ncTime, unixstart) # Find the closest unix timestamp
nearIndex = np.where(ncTime==neareststart)[0][0] # Grab the index number of found date

```

```

unixend = getUnixTimestamp(enddate,"%m/%d/%Y")
future = find_nearest(ncTime, unixend) # Find the closest unix timestamp
futureIndex = np.where(ncTime==future)[0][0] # Grab the index number of found date

```

```

HsObserved = max(Hs[-2*v:])*3.28084 # convert from m to ft
HsObserved = round(HsObserved,2)
TpObserved = round(max(Tp[-2*v:]),2)
TpObserved = round(TpObserved,2)

WaterLevelendDate = (datetime.now()).strftime('%Y%m%d %H:%M')

r =
requests.get('https://api.tidesandcurrents.noaa.gov/api/prod/datagetter?end_date='+WaterLevel
endDate+'&range=6&station=8652587&product=water_level&datum=navd&units=english&time_
zone=lst_ldt&application=web_services&format=json').text
d = json.loads(r)

try:
    r =
requests.get('https://api.tidesandcurrents.noaa.gov/api/prod/datagetter?end_date='+WaterLevel
endDate+'&range=6&station=8652587&product=water_level&datum=navd&units=english&time_
zone=lst_ldt&application=web_services&format=json').text
except requests.exceptions.RequestException as e: # if it fails for ANY error type
    EMAIL_ADDRESS = "PealslandFloodAlert@gmail.com"
    EMAIL_PASSWORD = "kiawcxdtgcfmykoe" # gmail app password

    msg = EmailMessage()

    msg['Subject'] = 'NOAA Data Retrieval Failure'
    msg['From'] = EMAIL_ADDRESS
    msg['To'] = 'PealslandFloodAlert@gmail.com'
    message="The email alert script is not functioning properly because it could not access
NOAA water level data."
    print(message)
    msg.set_content(message)
    with smtplib.SMTP_SSL('smtp.gmail.com', 465) as smtp:
        smtp.login(EMAIL_ADDRESS, EMAIL_PASSWORD)
        smtp.send_message(msg)

#print(d)
#print(d['data'])

waterLevel_data = []
for i in d['data']:
    waterLevel_data.append([i['t'],i['v']])

```

```

#print(waterLevel_data)
water_df = pd.DataFrame(data=waterLevel_data, columns=['Time', 'Water Level'])
#print(water_df)
maxWaterLevel = round(float(max(water_df.iloc[-10*v:,1])),2)

HsTarget = float(6.8) #to change wave height threshold change this number
TpTarget = float(10) #to change wave period threshold change this number
WaterLevelTarget = float(2.6) #to change water level threshold change this number

EMAIL_ADDRESS = "PealIslandFloodAlert@gmail.com"
EMAIL_PASSWORD = "kiawcxdtgcfmykoe" # gmail app password

msg = EmailMessage()

msg['Subject'] = 'Flood Alert in effect for Hatteras Island'
msg['From'] = EMAIL_ADDRESS
msg['To'] = 'vegasproul0817@gmail.com', 'ejsciaud@ncsu.edu', 'wargula@usna.edu',
'vjohnson@usna.edu', 'lilyve30@gmail.com', 'esmyre@dewberry.com'

condition=(HsObserved>=HsTarget and TpObserved>=TpTarget) or
maxWaterLevel>=WaterLevelTarget

if(condition):

    message="A coastal flood alert has been issued for Hatteras Island. A flood alert means
current wave conditions and water levels may bring flash floods and tidal surges. \n\nCurrent
Wave Height: "+str(HsObserved)+"ft \nCurrent Peak Wave Period: "+ str(TpObserved)+"s
\nCurrent Water Level: "+str(maxWaterLevel)+"ft \n\nPlease monitor https://drivenc.gov for
updates."

    print(message)
    msg.set_content(message)

# scope =
["https://spreadsheets.google.com/feeds",'https://www.googleapis.com/auth/spreadsheets',"https
://www.googleapis.com/auth/drive.file","https://www.googleapis.com/auth/drive"]
#
# creds = ServiceAccountCredentials.from_json_keyfile_name("creds.json", scope)
#
# client = gspread.authorize(creds)
#
# sheet = client.open("emailalertAWS").sheet1 # Open the spreadhseet
#

```

```

# data = sheet.get_all_records()
# no_rows = str(len(data)+2)
#
# sheet.format("A"+no_rows+":D"+no_rows, {
#     "horizontalAlignment": "LEFT",
#     "textFormat": {
#         "foregroundColor": {
#             "red": 1.0,
#             "green": 0,
#             "blue": 0
#         },
#         "fontSize": 10,
#         "bold": True
#     }
# })
#
# insertRow = [(datetime.now()).strftime('%Y/%m/%d %H:%M'), str(HsObserved),
str(TpObserved), str(maxWaterLevel)]
# sheet.append_row(insertRow)

with smtplib.SMTP_SSL('smtp.gmail.com', 465) as smtp:
    smtp.login(EMAIL_ADDRESS, EMAIL_PASSWORD)
    smtp.send_message(msg)

print("completed")
else:
    print("No new alerts")
# scope =
["https://spreadsheets.google.com/feeds", "https://www.googleapis.com/auth/spreadsheets", "https
://www.googleapis.com/auth/drive.file", "https://www.googleapis.com/auth/drive"]
#
# creds = ServiceAccountCredentials.from_json_keyfile_name("creds.json", scope)
#
# client = gspread.authorize(creds)
#
# sheet = client.open("emailalertAWS").sheet1 # Open the spreadhseet
#
# data = sheet.get_all_records()
# no_rows = str(len(data)+2)
#
# insertRow = [(datetime.now()).strftime('%Y/%m/%d %H:%M'), str(HsObserved),
str(TpObserved), str(maxWaterLevel)]

```

```
# sheet.append_row(insertRow)
```

```
print(HsObserved)
```

```
print(TpObserved)
```

```
print(maxWaterLevel)
```

# APPENDIX D

# Modeling the hydrodynamics of a tidal inlet during bay-side storms

Liliana Velasquez-Montoya<sup>1</sup>, Anna Wargula<sup>1</sup>, Tori Tomiczek<sup>1</sup>, Elizabeth J. Sciaudone<sup>2</sup>,  
Elizabeth Smyre<sup>3</sup>.

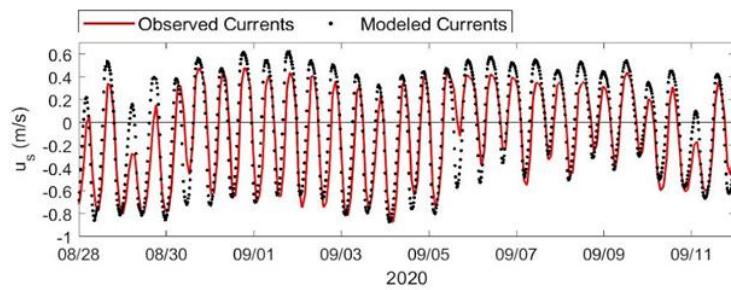
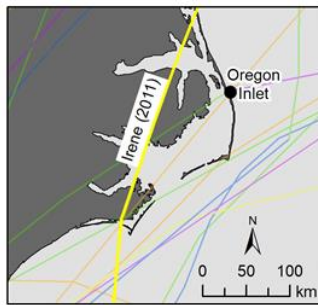
<sup>1</sup>United States Naval Academy, 590 Holloway Road, 11D, Annapolis, MD 21402, USA

<sup>2</sup>North Carolina State University, 915 Partners Way, Raleigh, NC 27695-7908, USA

<sup>3</sup>Dewberry, 2610 Wycliff Road, Suite 410, Raleigh, NC 27607-3073, USA

\*Corresponding author: velasque@usna.edu

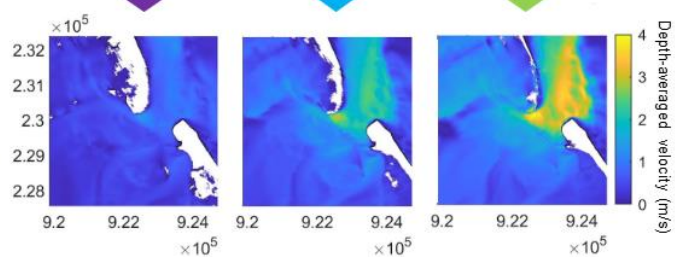
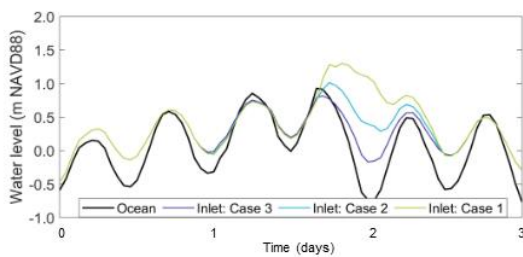
## Graphical Abstract



**Storm Category (2010-2020)**

1	Tropical Storm
2	Tropical Depression
3	Extratropical Storm

Bay-side storms summary	Case 3	Case 2	Case 1
Max. water level north bay (m)	0.50	2.00	3.50
Max. Water level south bay (m)	0.25	1.00	1.75
Max wave height (m)	7	7	7



10

11       **Abstract**

12  
13 Bay-side storms, defined here as storms with tracks on the landward side of barrier islands, may  
14 disturb the hydrodynamics of inner bays to a larger extent than on the ocean side. These storms  
15 are common in large-scale  $O(> 100,000 \text{ m})$  estuarine systems and have the potential to modify  
16 the circulation in bays and within tidal inlets. Here, we provide an overview of the hydrodynamic  
17 response of a tidal inlet under forcings caused by bay-side storms and explore the role of waves  
18 in modulating the release of storm surge from the back-barrier regions into the ocean. A two-  
19 dimensional horizontal numerical model including wave-current interactions is calibrated and  
20 validated against field observations of water levels and depth-averaged velocities at Oregon Inlet,  
21 NC. The model is then used to investigate the effect of synthetic bay-side storms with varying  
22 wave conditions and water levels based on those generated by Hurricane Irene (2011), which is  
23 the strongest bay-side storm to hit the Outer Banks of North Carolina in the last two decades.  
24 Effect of timing of the peak storm surge during the ebb and flood phases of the tide is also  
25 explored.

26  
27 Results from synthetic storms indicate that, during bay-side storms, the water level gradient along  
28 the inlet favors ebbing flows regardless of the timing of the storms relative to tidal phase. These  
29 results suggest that waves might be responsible for any influx of volume to the bay during high  
30 bay-side surge events. Wave blocking effects were found to be stronger along the ebb shoal and  
31 only reached the flood delta when bay water levels were nearly the same as the ocean water  
32 levels. Reduction of currents by waves in the inlet have the potential to extend the duration of the  
33 inundation period in the back barrier region. Bay-side storms also caused flux enhancement over  
34 inlet shoals and channels in the flood delta, which could have implications for the  
35 morphodynamics of the system.

36  
37 **Keywords:** Numerical modeling, Storm surge, Albemarle-Pamlico Sound, Estuarine circulation,  
38 Bay-side storms, Hurricane Irene

## 1. Introduction

Tidal inlets are the main connecting channels between oceans and bays where oceanic processes like currents and waves converge with estuarine waters. This connecting function makes tidal inlets strategic for navigation (Kraus, 2008) and the life cycle of marine life (Pietrafesa and Janowitz, 1985; Chanta et al., 2000). Navigation allows for socioeconomic activities such as commerce, tourism, fisheries, and military operations. From the ecosystemic perspective, tidal inlets facilitate fish larvae transport onshore into nursery regions within estuaries (Flores-Coto and Warlen, 1992; Joyeux, 1999; Forward, 1999).

Tidal inlets on barrier islands typically open during storms, and they tend to remain open if the tidal currents are strong compared to the infilling process caused by wind and waves (Escoffier, 1940; O'Brien, 1969; Jarrett, 1976; van de Kreeke, 1992; Friedrichs et al., 1993). Once open, tidal inlets can reach stability and remain open for centuries as long as they continue to capture a sufficiently large tidal prism (Hayes and Fitzgerald, 2013). The circulation of tidal inlets has been studied in length during non-storm conditions (Brown, 1928; Keulegan, 1967; Aubrey and Weishar, 1988; DiLorenzo, 1988; Geyer and Signell, 1992), and in the past two decades interest has been growing to understand how tidal inlet hydrodynamics may change during storms (Reffitt et al., 2020; Melito et al., 2020).

Throughout their lifetime, tidal inlets can experience the passing of numerous extreme storms that encompass the neighboring ocean and estuarine waters. While some studies have found that tidal inlets have a negligible effect on open coast storm surge hydrographs (Salisbury and Hagen, 2007), their effects on storm surge hydrographs in bays, lagoons, and riverine systems can be more important. Tidal inlets can funnel storm surges and ocean wave setup from the ocean into bays (Bertin et al., 2009; Malhadas et al., 2009; Irish and Cañizares, 2009; Olabarrieta et al., 2011; Orescanin et al., 2014; Wargula et al., 2014) and direct infragravity waves to the back-barrier lagoons (Bertin and Olabarrieta, 2016; Bertin et al., 2018) and upstream of rivers (Melito et al., 2020).

Most of the studies that have investigated the hydrodynamics of tidal inlets during storms have focused on storms traveling on the ocean-side of the inlet that create a shore-directed pressure gradient. However, storms passing along the back-barrier bays and inland are also possible in large-scale estuaries ( $O(100,000\text{ m})$ ), like the Albemarle-Pamlico Sound in North Carolina, USA,

73 the Chesapeake Bay along the U.S. Mid-Atlantic Coast, the Chandeleur Sound in Louisiana, USA,  
74 the Wadden Sea north of Germany and the Netherlands, the Saloum Delta in Senegal, and the  
75 Kurisches Haff on the Baltic coast, among others. Herein we refer to “bay-side storms” as those  
76 with tracks on the landward side of barrier islands. These storms tend to disturb bays’  
77 hydrodynamics more significantly than the ocean. Their ocean-side effects are restricted to  
78 increased wave energy due to the portion of the storm winds that reaches the ocean.

79  
80 Numerical modeling has been used to study the effects of bay-side storms in large estuaries. Li  
81 et al. (2006) and Shen et al. (2006) found that a land-side storm can cause high-salinity shelf  
82 water to intrude into the Chesapeake Bay, and landward-directed winds may cause significant  
83 inundation in the upper branches of the estuary. In a study specific to Hurricane Irene, which  
84 moved along the Albemarle-Pamlico Sound, Mulligan et al. (2015) found that both locally-  
85 generated waves and storm surge contribute to flooding along estuarine shorelines and reported  
86 that total water levels exceeded 2 m in some parts of the system. In the same estuarine system,  
87 Cyriac et al. (2018) suggest a non-linear response of shallow coastal waters to meteorological  
88 forcing. The importance of bay-side storms on morphological changes in barrier islands have  
89 been presented by Smallegan and Irish (2017) for the New Jersey coast. These studies have  
90 been valuable to understanding the large-scale estuarine hydrodynamics and inundation  
91 predictions during bay-side storms; however, the response of tidal inlets to bay-side storms  
92 remains less understood.

93  
94 This study uses numerical simulations based on the coastal modeling platform Delft3D (Lesser et  
95 al., 2004) coupled with the third generation wave model Simulating WAVes Nearshore (SWAN)  
96 (Booij et al., 1999) to explore the hydrodynamic response of a tidal inlet to storm surge and waves  
97 during bay-side storms. We investigate these processes by calibrating and validating a two-  
98 dimensional horizontal (2DH) hydrodynamic model of Oregon Inlet and the Albemarle-Pamlico  
99 Sound system in North Carolina, USA and applying it to study the response of the inlet to a set of  
100 synthetic bay-side storms with varying surge and wave conditions. The storms’ hydrographs are  
101 developed based on Hurricane Irene (2011), which was the hurricane with the largest bay-side  
102 storm surge measured since 1979 in the region (Clinch et al., 2012). Time series of simulated  
103 water levels at the inlet and the ocean are analyzed and used to describe temporal changes in  
104 discharge through the inlet. The competing impacts of bay-side surge and ocean-side waves on  
105 inlet discharge are examined through evaluating the integrated cross-shore momentum balance  
106 (Orescanin et al., 2014). The role of waves at modulating the release of storm surge from the

107 back-barrier regions into the ocean and causing circulation changes in the flood and ebb deltas  
108 is also explored via geospatial analysis of simulations and by calculating the contribution of the  
109 wave radiation stress gradient to the one-dimensional momentum balance. Results from this  
110 study highlight the importance of tidal inlets as “relief valves” when bay-side water levels exceed  
111 those on the ocean side. Flushing time variability during flood and ebb, as well as back-barrier  
112 flooding near the tidal inlet, are discussed.

113

## 114 **2. Study Site**

115

116 Oregon Inlet is located on the Outer Banks of North Carolina, connecting the Atlantic Ocean and  
117 the Albemarle-Pamlico Sound (Figure 1). The inlet opened between Bodie Island and Hatteras  
118 Island during a storm in 1846 and has since become a fundamental channel for the economic  
119 development of the communities around it (Moffatt & Nichol and Coastal Economics & Business  
120 Services, 2014). The inlet, with maximum depths of 16 m, has a dynamic main ebb channel  
121 heading towards the northeast into the Atlantic Ocean. This main channel is surrounded by an  
122 ebb delta with bedforms that migrate seasonally as a response of incident waves (Humberston et  
123 al., 2019). On the flood delta, the inlet has three main, divergent, sinuous channels that mix ocean  
124 and estuarine waters.

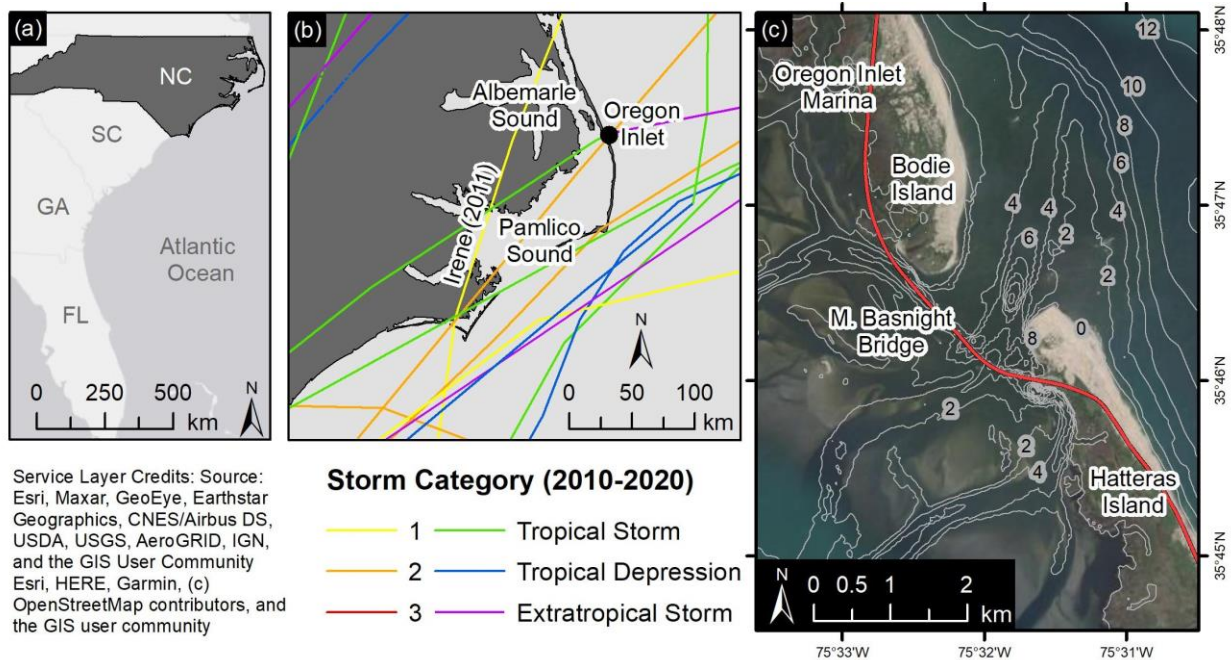
125

126 The Albemarle-Pamlico Sound is the second largest estuarine system in the US after the  
127 Chesapeake Bay. The estuarine waters in this bay are well-mixed with average depths on the  
128 order of 5 m. Near Oregon Inlet, the width of the bay from the back-barrier shoreline of the Outer  
129 Banks to mainland North Carolina is 20 km. The daily water level fluctuations in the bay range  
130 from a maximum of 1 m near the inlet (Wargula et al., 2021) to less than 0.3 m in more interior  
131 locations ~2 km away from the inlet. The hydrodynamics and waves in the estuary largely depend  
132 on wind speed and direction (Luettich et al., 2002; Mulligan et al., 2015; Clunies et al., 2017).

133

134 The Outer Banks of North Carolina have a seasonal wave climate. During the winter, extratropical  
135 storms known as nor’easters are common. Wave conditions during these storms typically exceed  
136 2 m at 17 m depth, with durations lasting from a couple of days to weeks. Effects of nor’easters  
137 are more noticeable on the ocean side of the barrier island chain, but these storms can also  
138 increase water levels in the bay. During the summer, calm conditions prevail, but tropical storms  
139 can reach the area by traveling along the ocean, bay, and mainland, particularly during the June-

140 through-November hurricane season (Figure 1b). Depending on the strength and the track of the  
 141 storms, the barrier island chain can be inundated from the bay or ocean sides.  
 142



143  
 144 Figure 1. Study Area. (a) Location of North Carolina (NC) relative to the Southeast United States. (b) The  
 145 Outer Banks and storm tracks from 2010 to 2020. (c) Oregon Inlet. Contour lines indicate depths in  
 146 meters relative to NAVD88.

147  
 148 Storm surge rebound, where water is pushed towards the mainland (west) and later into the back  
 149 barrier (east), is common for storms traveling from south to north along the Albemarle-Pamlico  
 150 Sound. Some examples of hurricanes with major bay-side effects include Hurricane Emily (1993),  
 151 which created a bay-side wrackline reaching 2.9 m in elevation in some portions of the Outer  
 152 Banks (Bush et al., 1996), Hurricane Floyd (1999), which triggered 500-year floods in the rivers  
 153 draining into the Pamlico Sound (Bales, 2003) and caused water levels to reach 1.5 m near  
 154 Oregon Inlet, and Hurricane Irene (2011), which drove total water levels (surge + tide) to reach  
 155 2.1 m near Oregon Inlet (Clinch et al., 2012; Kurum et al. 2012). In addition to bay-side storms,  
 156 hurricanes with tracks over the nearby ocean and winds circulating over the sound can create a  
 157 similar water level rebound effect. Rey and Mulligan (2021) reported water level gradients of 2 m  
 158 along the Pamlico Sound during Hurricane Dorian in 2019, with low water levels (-0.5 m) in the  
 159 back barrier region as wind was blowing to the west and high water levels (1.5 m) as the wind  
 160 was blowing to the southeast. These examples provide evidence of the significant water level  
 161 gradients that can develop in large bays as storms travel along them.

162  
163  
164  
165  
166  
167  
168  
169  
170  
171  
172  
173  
174  
175  
176  
177  
178  
179  
180  
181  
182  
183  
184  
185  
186  
187  
188  
189  
190  
191  
192  
193  
194  
195

### **3. Methods**

A 2DH hydrodynamic model forced by water levels and waves was calibrated and validated using field data collected in Fall 2019 and Summer 2020. The model was used to simulate synthetic bay-side storms with varying surge and wave conditions. Model outputs were analyzed using geospatial approaches to assess the effects of sound-side storms on the hydrodynamics of the inlet. This section describes the field data collection campaigns, the numerical model set up and validation.

#### **3.1 Field Observations**

The observations used in the model calibration and validation involved a combination of data from a permanent monitoring station and field surveys completed in 2019 and 2020 as part of a study that is investigating inlet-driven estuarine shoreline erosion in the north end of Hatteras Island. The NOAA Station 8652587 at the Oregon Inlet Marina (green diamond in Figure 2), hereafter referred to as the “Marina,” is located on the estuarine side of Bodie Island, 3 km north of Oregon Inlet. Marina water levels and atmospheric pressure, both measured in 6-minute intervals, were interpolated to a 10-min interval time step before use in field survey data processing and model skill score calculations.

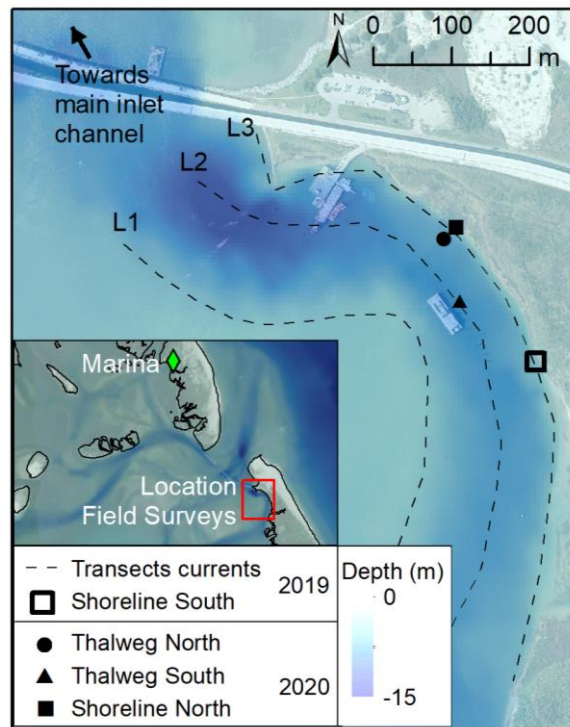
In 2019, field observations of water levels and flow velocity were collected on the estuarine side of Hatteras Island as part of the pilot DURING Nearshore Event eXperiment (DUNEX), a multi-agency, -academic and -stakeholder collaborative community experiment to study nearshore processes during coastal storms (Cialone et al., 2019). Absolute pressure was measured from October 11 to November 10, 2019 at 10-minute intervals using a TruBlue 255 Water Level Gauge. This sensor was deployed 1 km south the southern shoulder of the inlet in the flood channel near the estuarine shoreline (black unfilled square, Figure 2), herein referred to as the “Shoreline South”. Pressure data were adjusted for atmospheric fluctuations measured at the Marina and converted to water levels assuming a salinity of 23 psu and using the fluctuations in temperature simultaneously measured by the data logger. Further information on data collection and processing can be found in Wargula et al. (2021).

On October 07, 2019, during the maximum flood tide, current profiles were measured using a downward facing acoustic Doppler current profiler (ADCP) on a boatmount at 5 to 7 points along

196 three along-channel transects, L1, L2, and L3, which trace the outer shoals, thalweg, and inner  
197 shoulder of the southernmost channel, respectively (Figure 2). Further information on data  
198 collection and processing can be found in Jaber et al. (2021). The current magnitudes were depth-  
199 averaged over the measured water column and horizontally-averaged over a 15-m radius (less  
200 than 1 minute of measurements) around each point in the transect.

201  
202 In a return field survey in 2020, measurements of pressures (water levels) and flow velocities  
203 were collected from August 28 to September 12 at fixed locations on the estuarine side of Hatteras  
204 Island, shown with black-filled symbols in Figure 2. An Onset U20 HOB0 Titanium data logger  
205 was deployed in the flood channel near the shoreline, referred to herein as the “Shoreline North”  
206 gauge (Figure 2). Pressure measurements, which were collected in 10-minute intervals, were  
207 corrected for fluctuations in atmospheric pressure measured at the Marina. The corrected  
208 pressure measurements were converted to water level, assuming a constant salinity of 23 psu  
209 and using the fluctuations in temperature simultaneously measured by the data logger.

210



211  
212 Figure 2. Measurement locations during the 2019 and 2020 field deployments on a background aerial  
213 image from August 2019 and bathymetry shaded in blue. The dashed curves indicate the boat-mounted  
214 current measurement transects L1, L2, and L3. The symbols indicate mooring locations of instruments  
215 measuring water level (squares) and currents (circle and triangle).

216

217 Two ADCPs, a Nortek Aquadopp and a Nortek Signature1000, were deployed in the summer of  
218 2020 near the deepest point of the flood channel that meanders between the estuarine shoreline  
219 and a shoal in the flood delta; the ADCP locations are herein referred to as the “Thalweg North”  
220 and “Thalweg South,” respectively. The “Thalweg South” deployment was located exactly in the  
221 deepest part (thalweg) of the flood channel. The “Thalweg North” deployment was located at a  
222 depth 1 m shallower than the deepest part of the channel at a horizontal distance of 30 m from  
223 the thalweg. The Thalweg North and Thalweg South ADCPs were deployed upward-looking on  
224 bottom mounts in 10.0 m and 7.9 m water depths, respectively, sampling velocity at 1 Hz and 4  
225 Hz, respectively, for 2 minutes every 10 minutes, starting at the top of the hour. The raw  
226 measurements were ensemble-averaged over each 2-minute interval to represent 10-min interval  
227 currents. Each ADCP measured vertical profiles in 0.25 m bins with a blanking distance of 0.20  
228 m. Roughly 0.5 m of the water column near the bottom was unresolved due to the blanking  
229 distance and distance of the sensor above the bottom. Roughly 1 m of the water column near the  
230 surface was unresolved due to acoustic reflections. Each ADCP’s flow measurements were  
231 depth-averaged over the measured water column.

232

### 233 **3.2 Numerical Model**

234 A 2DH numerical model based on Delft3D (Lesser et al., 2004) coupled with SWAN (Booij et al.,  
235 1999) was set up for Oregon Inlet (Velasquez-Montoya and Overton, 2017; Velasquez-Montoya  
236 et al., 2020) and further refined to study the hydrodynamics of the inlet during bay-side extreme  
237 storm events. Delft3D solves the two-dimensional unsteady shallow-water equations in  
238 orthogonal curvilinear grids, where the flow is forced by user-defined boundary conditions. SWAN  
239 is a third-generation phased-averaged spectral wave model that solves the wave action equation  
240 including, among other processes, wave-current interaction. Model formulations are explained in  
241 detail in Deltares (2022).

242

243 The hydrodynamic model of Oregon Inlet is composed of two internally coupled curvilinear grids  
244 that extend nearly 33 km alongshore. Computational cells range in size from 470 m offshore to  
245 15 m and 20 m in the inlet. The computational grid includes 570 km<sup>2</sup> of the Albemarle-Pamlico  
246 Sound and extends to the edge of mainland North Carolina (Figure 3). The wave model includes  
247 the hydrodynamic domain but expands 70 km alongshore in the ocean and bay sides to prevent  
248 lateral boundary artifacts from propagating into the area of interest. The hydrodynamic model has  
249 a 30 s time step and communication with SWAN is set to 30 minutes. The 30 s time step was

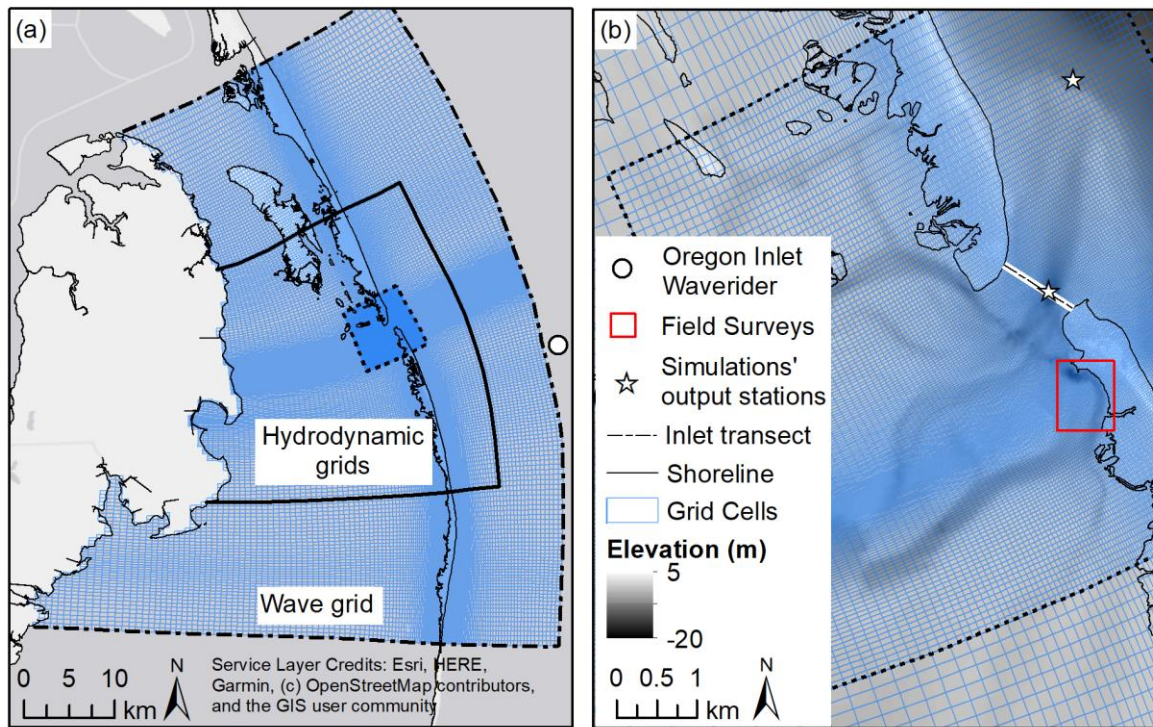
250 selected based on a sensitivity analysis that indicated that model results do not significantly  
251 change when using time steps of 1.2 s, 12 s and 30 s. Given these results, the larger time step  
252 was selected to ensure numerical stability and accuracy while gaining computational efficiency.  
253 With the selected time step, Courant numbers were generally below 10 as recommended by  
254 Deltares (2022).

255  
256 The bathymetry of the model is a composite of a 2019 US Army Corps of Engineers (USACE)  
257 Wilmington District survey of the inlet with point spacing ranging from 0.5 m to 30 m, a 2019 digital  
258 elevation model from the North Carolina Department of Transportation (NCDOT) of Hatteras  
259 Island with 5-m resolution, and the 10-m resolution NC Floodplain Mapping Project Digital  
260 Elevation Model created from historical surveys from the National Oceanographic and  
261 Atmospheric Administration (NOAA) of the ocean and bay (Blanton et al., 2008). All topo-  
262 bathymetric datasets were converted to m relative to NAVD88. The piles of the recently-built Marc  
263 Basnight Bridge across the inlet are schematized as porous plates with spatially-varying loss  
264 coefficients ranging from 0.03 to 0.375 as defined by Farraday and Charlton (1983). The terminal  
265 groin, located in the south shoulder of the inlet, is schematized as a thin dam preventing flow  
266 between adjacent cells (Deltares, 2022).

267  
268 The model has two open boundaries in the bay and three on the ocean side. The open-ocean  
269 boundary and the bay-side lateral boundaries are forced with temporally varying water levels  
270 extracted from large-scale Advanced Circulation (ADCIRC) model simulations completed as part  
271 of the Coastal Emergency Risks Assessment (CERA) (CERA, 2019). In Oregon Inlet, this large-  
272 scale mesh has element sizes varying from 30 m to 50 m. The ADCIRC mesh has an average  
273 resolution of 500 m along the bay-side region where boundary conditions are extracted for Delft3D  
274 and 1,500 m along the Delft3D ocean boundary. The lateral boundaries of the Delft3D model on  
275 the ocean side are Neumann boundaries with zero water level gradient. The boundary along  
276 mainland NC is closed. Because the Delft3D domain for Oregon Inlet only accounts for a relatively  
277 small portion of the Albemarle-Pamlico Sound, it was assumed that wind effects, known to be a  
278 main driver of hydrodynamics in the sound (Luettich et al., 2002; Mulligan et al., 2015; Clunies et  
279 al., 2017), were accounted for in the imposed boundary conditions from the large-scale ADCIRC  
280 model. This assumption was confirmed to be adequate by running simulations with and without  
281 wind effects in Delft3D and observing no significant changes in simulations' results. Thus, wind  
282 stress was not directly included in the simulations, but wind effects are indirectly accounted for  
283 with the surge forcing from the large-scale model.

284  
285  
286  
287  
288  
289  
290  
291  
292  
293  
294  
295  
296

The wave model is forced with spatially constant and time-varying wave conditions. Wave boundary conditions are extracted from the 44095 Oregon Inlet Waverider Buoy located at the oceanward edge of the model domain (Figure 3a). This gauge is located at a depth of 18.3 m offshore of the inlet (circle in Figure 3a). This gauge is owned and maintained by the University of North Carolina Coastal Studies Institute. Default parameters for SWAN are used in the simulations. The wave forcing at the open boundary is prescribed by a JONSWAP spectrum with a 3.3 peak enhancement factor. Energy dissipation due to bottom friction follows the empirical model of JONSWAP(Hasselmann et al., 1973) with a bottom friction coefficient of  $0.067 \text{ m}^2/\text{s}^3$ . Whitecapping is controlled by wave steepness and is represented using the formulation of Komen et al. (1984). Depth-induced breaking follows the Battjes and Janssen (1978) model with constant dissipation coefficient ( $\alpha$ ) of 1 and the breaker parameter ( $\gamma$ ) of 0.73.



297  
298  
299  
300

Figure 3. (a) Flow and wave model domain. (b) Locations of simulation outputs and field surveys completed in 2019 and 2020 with respect to the model domain.

301 **3.3 Model Evaluation**

302 The model calibration was completed using time-varying water levels and spatially-varying  
303 currents from the 2019 field survey. The model validation was completed using time-varying water  
304 levels and currents from the 2020 field survey. Skill metrics include those typically used to  
305 evaluate hydrodynamic model performance (Sutherland et al., 2004; Bosboom, et al., 2014; Mao  
306 and Xia, 2018;) and are defined in Equations 1 to 5, where the < > notation indicates temporal or  
307 spatial averaging.

308  
309 The Pearson Correlation Coefficient (CC) defined in Equation 1 varies between 1 and -1 as it  
310 measures the linear correlation between the Model Outputs (Mod) and Observations (Obs), and  
311 their corresponding standard deviations ( $\sigma_{Mod_n}, \sigma_{Obs_n}$ ):

312  
313 
$$CC = \frac{\frac{1}{N} \sum_{n=1}^N (Mod_n - \langle Mod \rangle)(Obs_n - \langle Obs \rangle)}{\sigma_{Mod_n} \sigma_{Obs_n}} \quad (\text{Equation 1})$$

314  
315 Where  $N$  is the total number of data points, and  $n$  is the indexed variable representing each data  
316 point.

317  
318 The Root-Mean-Square Deviation (RMSD) defined in Equation 2 has the same units of the  
319 variable and computes the square root of the averaged squared difference between Mod and Obs  
320 values:

321  
322 
$$RMSD = \left[ \frac{1}{N} \sum_{n=1}^N (Mod_n - Obs_n)^2 \right]^{1/2} \quad (\text{Equation 2})$$

323  
324 Relative Bias (RB) defined in Equation 3 measures the relative difference between Mod and Obs  
325 values as a decimal:

326  
327 
$$RB = \frac{\sum_{n=1}^N (Mod_n - Obs_n)}{\sum_{n=1}^N |Obs_n|} \quad (\text{Equation 3})$$

328  
329 Brier Skill Score (BSS) defined in Equation 4 is less than 1. In coastal modeling, it is interpreted  
330 as the model-added accuracy relative to a situation in which no modeling is done (Bosboom, et  
331 al., 2014). A positive value indicates that the simulation is better than a no modeling scenario  
332 (Brier, 1950);

333

334 
$$BSS = 1 - \frac{\frac{1}{N} \sum_{n=1}^N (Mod_n - Obs_n)^2}{\frac{1}{N} \sum_{n=1}^N (Obs_n - \langle Obs_n \rangle)^2} \quad (\text{Equation 4})$$

335

336 The Willmott Skill (*WS*) is calculated via Equation 5 and determines the level of model skill,  
337 defined as poor (0 - 0.3), good (0.3 - 0.6), very good (0.6 - 0.8), and excellent (0.8 - 1) (Willmott,  
338 1981).

339

340 
$$WS = 1 - \frac{\frac{1}{N} \sum_{n=1}^N (Mod_n - Obs_n)^2}{\frac{1}{N} \sum_{n=1}^N (|Mod_n - \langle Obs_n \rangle| + |Obs_n - \langle Obs_n \rangle|)^2} \quad (\text{Equation 5})$$

341

## 342 **4. Results**

343

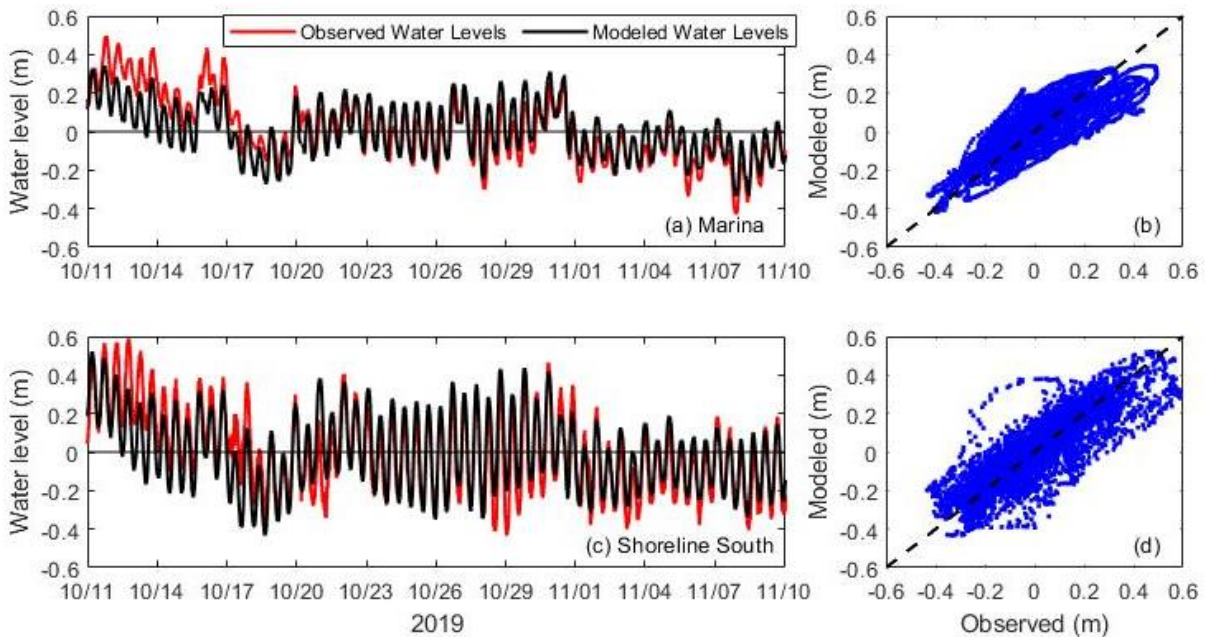
### 344 **4.1 Model Calibration**

345 Calibration of the model parameters was attained by simulating 30 days (October 11 to November  
346 10, 2019) of hydrodynamic conditions at the inlet. After a 10 day-spin up period, model outputs  
347 were compared with observed water levels and currents from the 2019 field survey. The best  
348 comparison of model results and observations was obtained with a Chezy coefficient of 55 using  
349 the Fredsøe (1984) formulation for stress due to wave forces and a horizontal eddy viscosity of 1  
350 m<sup>2</sup>/s; default values were used for all other parameters. Decreasing the Chezy coefficient from  
351 65 m<sup>1/2</sup>/s (default) to 55 m<sup>1/2</sup>/s (i.e. increasing the bottom drag coefficient) during the calibration  
352 period decreased simulated velocities and resulted in a 10% decrease in the RMSE, leading to a  
353 better agreement between observed and simulated depth-averaged velocities, with no effect on  
354 water levels or waves.

355

356 Observed and modeled temporal fluctuations of water levels were compared at the Marina and  
357 Shoreline South locations for 30 days during the 2019 field survey (Figure 4). The tidal amplitude  
358 near Hatteras Island is roughly twice as large as that at the Marina, potentially owing to its  
359 proximity to the inlet. The water levels were mean-subtracted owing to uncertainty in the vertical  
360 datum of the instruments in the field at Hatteras Island. Model skill metrics (Equations 1-2 and 4-  
361 5) are shown in Table 1, along with the root-mean-square (*RMS*) magnitudes of the observed and  
362 modeled mean-subtracted water levels. *RB* results (Equation 3) are not presented in Table 1  
363 because they are near-zero due to the mean-subtraction. Observed and modeled water levels  
364 have good agreement (high *CC*, low *RMSE*, positive *BSS*, *WS* score over 0.9) at both locations,

365 although the modeled *RMS* water levels are somewhat smaller than observed *RMS* water levels  
 366 at both locations. It should be noted that although the general statistics for water levels are  
 367 considered good, there is a period between October 11 and 16, 2019 when some of the water  
 368 level discrepancies are higher than the tidal range at the Marina. These discrepancies can be  
 369 explained by the complex and shallow bathymetry surrounding this station. Nevertheless, these  
 370 differences account for 0.2% (8/4321 data points) of the calibration period; for the remaining  
 371 99.8% of the data points, the differences are smaller than 0.3 m and simulated water levels closely  
 372 followed observed ones at the Marina. At the Shoreline South location, where the tidal range is 1  
 373 m, 1.6% of the data points resulted in differences larger than 0.3 m. Overall, the calibration  
 374 statistics and the ability of the model to simulate the general patterns of water levels at a protected  
 375 location in the bay (Marina) and near the inlet (Shoreline South) indicate that the model is capable  
 376 of representing the water levels at the study site.  
 377



378  
 379 Figure 4. (a, c) Mean-subtracted observed (red curves) and modeled (black curves) water levels versus  
 380 time and (b, d) modeled versus observed mean-subtracted water levels at the (a, b) Marina and at the (b,  
 381 d) Shoreline South. The black dashed line in (b, d) indicates the 1:1 line.

382

383 Table 1. Skill scores of time-varying water levels during the 2019 field survey

Location (2019)	<i>RMS</i> Observed (m)	<i>RMS</i> Modeled (m)	<i>CC</i>	<i>RMSD</i> (m)	<i>BSS</i>	<i>WS</i>
Marina	0.17	0.14	0.82	0.10	0.68	0.90
Shoreline South	0.21	0.20	0.85	0.11	0.71	0.92

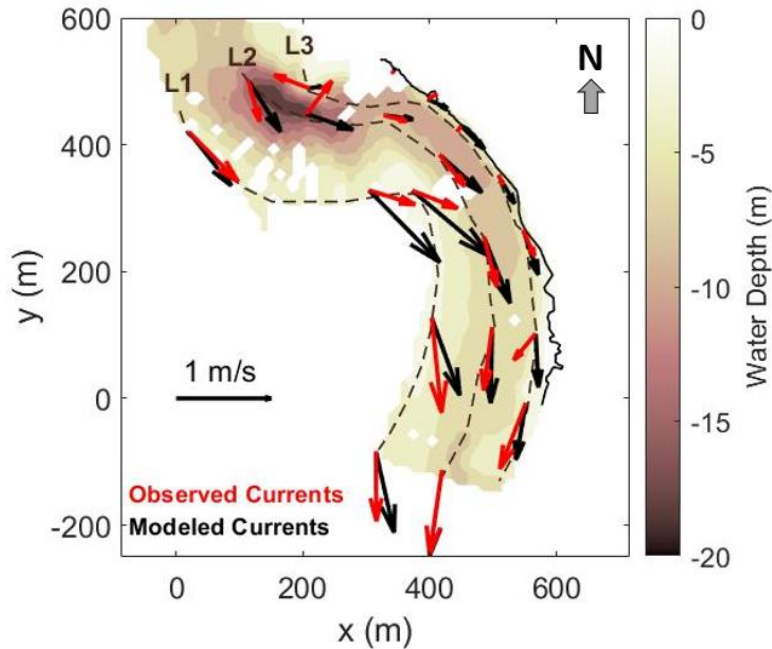
384

385 Current magnitudes (length of red arrows in Figure 5) measured at maximum flood during the  
 386 2019 field survey were compared at each along-channel line to modeled current magnitudes  
 387 (length of black arrows in Figure 5) to determine the model’s ability to capture spatial variability in  
 388 flows. Modeled currents were interpolated to the same point in time as the observations. Current  
 389 magnitudes were typically stronger in the thalweg (L2) and outer edge of the channel (L1) than  
 390 close to shore (L3). The model skill in reproducing the spatial variability in current magnitude at  
 391 maximum flood along each line was evaluated by comparing the observed currents with modeled  
 392 currents at the same times and locations (Table 2). Table 2 also presents the mean and standard  
 393 deviation in the current magnitudes in each along-channel line.

394

395 Good agreement between observed and modeled flood velocities was found in the channel (L2)  
 396 and at the shoreline (L3), with an excellent and very good *WS* score, respectively. Although  
 397 modeled velocities were higher (positive *RB*), the *RMSD* was less than the standard deviation in  
 398 velocities along these lines. Along the outer shoals (L1), however, the *WS* score was poor, *BSS*  
 399 and *CC* were negative, and *RB* was large, owing to the significantly higher modeled velocities.  
 400 Model discrepancies along L1 can be attributed to the dynamic and temporally varying  
 401 bathymetry of the flood delta shoals that is not considered in the fixed-bathymetry simulations.

402



403  
 404 Figure 5. Observed depth-averaged and horizontally-averaged currents (red arrows) and modeled depth-  
 405 averaged currents (black arrows) overlaid on measured water depth (color contours) during the 2019 field  
 406 survey. The reference point (0,0) for the x-y coordinate system is 35°45'41.20"N and 75°31'44.98" W. The  
 407 black arrow at (0,0) is a 1 m/s reference. The black curve on the right hand side of the color contours  
 408 indicates the location of the shoreline edge in November 2019. The dashed brown curves indicate transects  
 409 L1, L2 and L3 (as shown in Figure 2).

410  
 411 Table 2. Skill scores of spatially-varying depth-averaged velocity during the 2019 field survey

Line (2019)	Observed Mean [st. dev.] (m/s)	Modeled Mean [st. dev.] (m/s)	CC	RMSD (m/s)	RB	BSS	WS
L1	0.71 [0.20]	0.92 [0.15]	-0.54	0.35	0.30	-2.97	0.25
L2	0.55 [0.20]	0.65 [0.20]	0.81	0.11	0.17	0.63	0.91
L3	0.30 [0.22]	0.35 [0.21]	0.55	0.18	0.15	0.25	0.79

412  
 413 **4.2 Model Validation**  
 414 The overall validation period was 15 days from August 28 to September 12, 2020. Similar to the  
 415 calibration period, during the validation, the model reproduced water level magnitudes and  
 416 temporal fluctuations in mean-subtracted water levels with reasonable accuracy, exhibiting similar  
 417 patterns as the model-data comparison for the 2019 field survey water levels (Table 3).

419 Table 3. Skill scores of time-varying water levels and depth-averaged velocity during the 2020 field survey

Location (2020)	<i>RMS</i> Observed (m or m/s)	<i>RMS</i> Modeled (m or m/s)	<i>CC</i>	<i>RMSD</i> (m or m/s)	<i>RB</i>	<i>BSS</i>	<i>WS</i>
Marina*	0.12	0.12	0.76	0.08	0	0.48	0.87
Shoreline North*	0.16	0.17	0.89	0.08	0	0.76	0.94
Thalweg North†	0.41	0.34	0.86	0.22	-0.34	0.64	0.90
Thalweg South†	0.40	0.44	0.89	0.22	-0.22	0.69	0.93

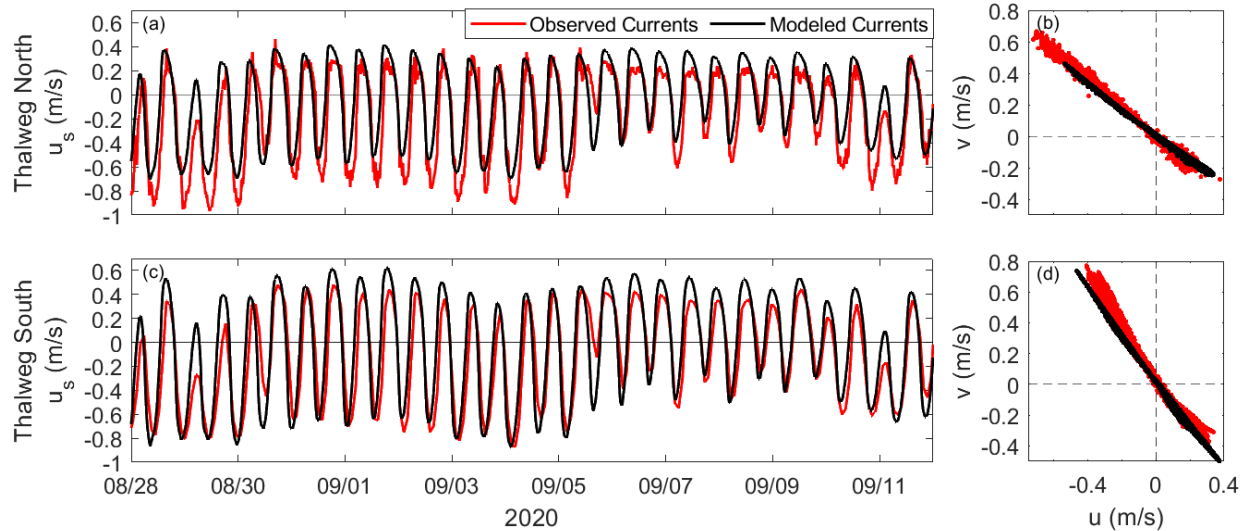
420 \*Mean-subtracted water level (m), †Major-axis velocity (m/s)

421  
 422 Observed and simulated depth-averaged velocity components at the Thalweg North and Thalweg  
 423 South locations were rotated into principal flow axes (Emery and Thomson, 2001) in order to  
 424 compare the major-axis flows (Table 3 and Figure 6a and 6c). The principal axes for the observed  
 425 and modeled velocities at the Thalweg North location were -47.7 degrees and -51.3 degrees,  
 426 respectively (positive is clockwise relative to north, Figure 6b). The principal axes for the observed  
 427 and modeled velocities at the Thalweg South location were -32.1 degrees and -34.1 degrees,  
 428 respectively (Figure 6d). Ebb flows are typically twice the magnitude of flood flows at both  
 429 locations (Figure 6a and 6c).

430  
 431 The model shows excellent agreement with observed major-axis flows (*WS* score over 0.90) and  
 432 a high correlation and *BSS* (Table 3). The *RMSD* and *RB* results and time series shown in Figure  
 433 6a and 6c suggest a consistent, although small, overestimation in flood flows at both locations  
 434 and a consistent and small underestimation in ebb currents at the Thalweg North location.  
 435 Occasional “events” with large shifts in the velocity (e.g., the lack of flood flows on August 29 and  
 436 September 11, Figure 6a and 6c) are reproduced in the model, although not to the same degree,  
 437 potentially owing to differences in the subtidal processes and comparisons of velocities averaged  
 438 every 10 minutes vs. instantaneous model outputs generated every 10 minutes.

439  
 440 It should be noted that the model was evaluated against spatially-varying depth-averaged currents  
 441 for the calibration period, while the model’s ability to reproduce temporal variation in currents at  
 442 two locations was tested during the validation phase. Results from the calibration and validation  
 443 demonstrate that the model can accurately reproduce spatiotemporal variation of water levels and  
 444 depth-averaged currents within the inlet.

445



446  
 447 Figure 6. (a, c) Observed (red curves) and modeled (black curves) depth-averaged major axis velocities  
 448 (positive is flooding, to the southeast) versus time and (b, d) depth-averaged velocity components in the  
 449 north-south direction ( $v$ , positive is north) versus that in the east-west direction ( $u$ , positive is east) from the  
 450 observations (red points) and model (black points).

451  
 452 **4.3 Synthetic bay-side storms**

453 After the model was successfully calibrated and validated, it was applied to study the  
 454 hydrodynamics of the inlet during bay-side storms. Boundary conditions to simulate bay-side  
 455 storms are based on the water levels observed in the bay and the ocean during Hurricane Irene  
 456 (2011), which was the hurricane with the largest bay-side storm surge measured since 1979  
 457 (Clinch et al., 2012). This hurricane disturbed the water surface for nearly 24 hours, causing a  
 458 larger change in water levels in the bay compared to the ocean, with peak surge occurring at the  
 459 inlet during the start of the ebb tide. In the north region of the bay, NOAA's Oregon Inlet Marina  
 460 recorded a peak surge (i.e., measured water level minus tidal prediction) of 2.1 m. In the south  
 461 region of the bay at station 8654467 USCG Station Hatteras, the surge reached 1.1 m. On the  
 462 other hand, station 8651370 Duck, NC on the ocean side only reached a maximum total water  
 463 level of 0.9 m, which was only 0.3 m higher than the expected tidal level. Significant wave height  
 464 on the ocean side at station 44056 Duck FRF, NC located at 17.8 m water depth reached 7.0 m  
 465 during the peak of the storm.

466  
 467 A set of synthetic storms were designed to have the same duration as Hurricane Irene; however  
 468 the maximum water levels inside the bay, wave conditions in the ocean, and timing of the peak  
 469 storm surge at the inlet were varied to account for potentially stronger and weaker storms and

470 difference in tidal phase. Given the small surge levels displayed on the ocean side during  
 471 Hurricane Irene, the open ocean boundary is forced with tidal water levels only. Table 4 shows  
 472 the range of maximum water levels forced at the lateral model boundaries in the Albemarle-  
 473 Pamlico Sound. Each one of the water level cases shown in Table 4 is forced with six different  
 474 maximum significant wave height conditions ranging in 1 m intervals from 2 m to 7 m during the  
 475 peak of the storm. These values were selected based on historical wave records from the US  
 476 Army Corps of Engineers Field Research Facility at Duck, NC and the analysis of the wave climate  
 477 near Oregon Inlet by Velásquez-Montoya et al. (2020). These simulation settings resulted in  
 478 seven water level cases, each forced with six wave conditions, for a total of 42 synthetic bay-side  
 479 storm simulations. To test the effects of the timing of the storm relative to the tidal phase, the peak  
 480 surge was simulated to occur at the start of ebb (similar to Hurricane Irene) and flood tides.

481

482 Table 4. Maximum water levels at the bay boundaries

Storm	Max. water level at North Bay Boundary (m NAVD88)	Max. water level at South Bay Boundary (m NAVD88)	Sig. wave heights at Ocean Boundary (m)
Case 0 (No Storm)	0.20	0.10	0
Case 1	3.50	1.75	2, 3, 4, 5, 6, 7
Case 2*	2.00	1.00	2, 3, 4, 5, 6, 7
Case 3	0.50	0.25	2, 3, 4, 5, 6, 7

483 \*Closest case to Hurricane Irene when wave heights = 7 m

484

#### 485 **4.4 Water levels and volumetric discharge resulting from bay-side storms**

486 Time series of discharge and water levels in the ocean and at the center of the inlet from the  
 487 simulations shown in Table 4 are analyzed herein. Simulations' output stations are shown as stars  
 488 for point outputs and a dashed-line for integrated output across the inlet transect in Figure 3b.  
 489 Figure 7 shows the time series of water levels at the ocean and the center of the inlet and  
 490 discharge before, during and after the storm's arrival when the storm surge occurs during ebb and  
 491 flood. For all cases, before the storm arrives and around day 1.0 for ebb (panel a and b) and day  
 492 0.7 for flood (panel c and d), ocean-side water levels increase 0.70 m relative to Case 0 (no  
 493 storm). This surge forces volume into the inlet mouth until day 1.7 for ebb (panel a and b) and day  
 494 1.4 for flood (panel c and d) when the bay-side surge abruptly increases bay-side water levels,  
 495 driving flows out of the inlet mouth.

496

497 Simulated water levels at the inlet were higher than those on the ocean side after the arrival of  
498 the bay-side surge (day 1.7 for ebb and day 1.4 for flood), and peak water levels were higher  
499 when the storm arrived during flood than during ebb. However, the differences in water level  
500 between the ocean and the inlet are twice as large for the storms approaching during ebb than  
501 those approaching during flood (Figure 7a and c). For all cases, the water level gradient along  
502 the inlet remains positive (pushing water out) throughout the flood tidal phase, suggesting that  
503 waves might be responsible for any influx (ocean to bay transport) of volume during the high bay-  
504 side surge events.

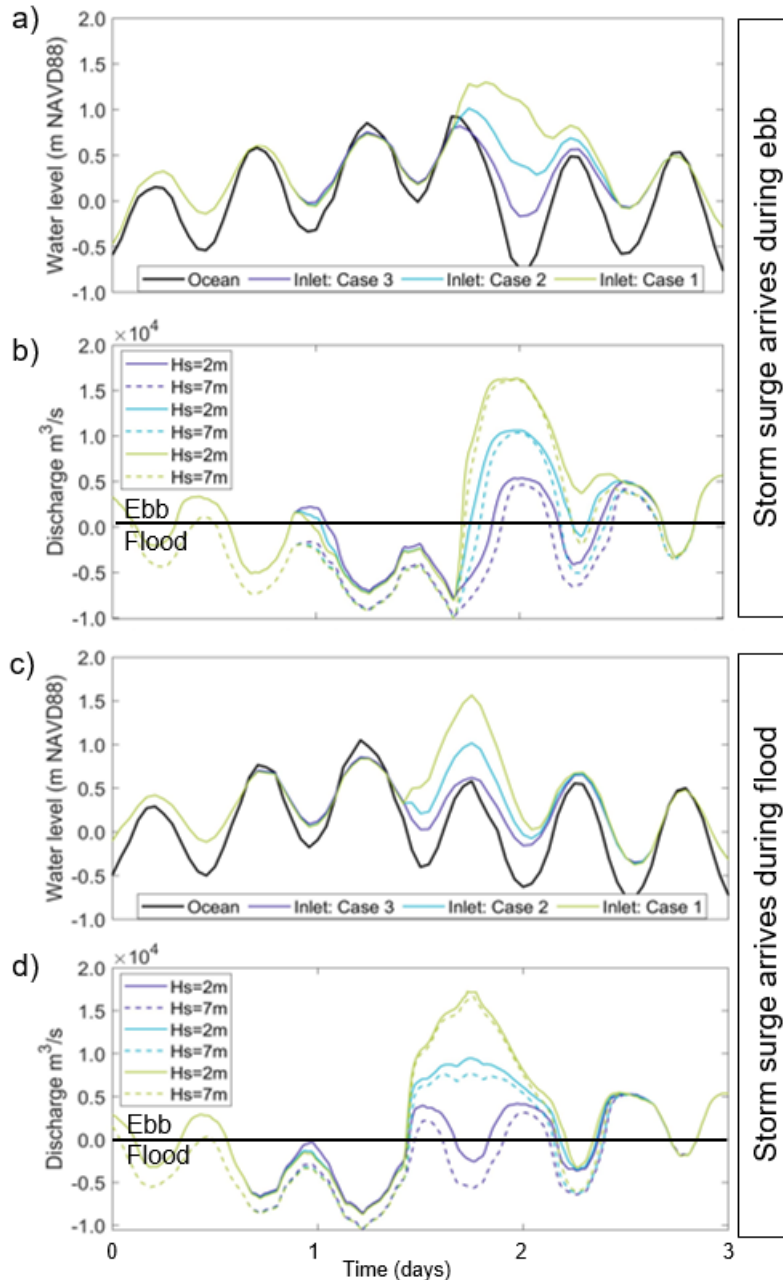
505

506 Regardless of whether a bay-side storm arrives during ebb or flood, the ebbing discharge towards  
507 the ocean is predominant, with peak discharges ranging from 5,000 to 16,000 m<sup>3</sup>/s. The role of  
508 waves in modulating the discharge through the inlet is shown in Figure 7b and d, with the  
509 differences between the solid and dashed lines indicating that as the storm approaches, 7 m  
510 waves can increase flood discharge by 1,500 m<sup>3</sup>/s relative to 2 m waves (until day 1.5 in Figure  
511 7). During the peak of the storm, when the water is predominantly ebbing, 7 m wave heights tend  
512 to decrease the discharge through the inlet by nearly 700 m<sup>3</sup>/s. This effect appears more  
513 pronounced for less severe storms (e.g., storm Cases 2 and 3 in Table 4), suggesting that high  
514 waves could block the release of the bay-surge to the ocean when it generates a discharge of  
515 less than about 10,000 m<sup>3</sup>/s. This result indicates the potential of waves in enhancing inundation  
516 in the back-barrier regions.

517

518 The Case 1 storms arriving during ebb tide lead to a total duration of ebb discharge of 23.8 hrs,  
519 which is equivalent to 99% of the forced storm conditions in the simulation. This percentage is  
520 76% for an equivalent storm arriving during flood tide. A similar pattern is followed by the Case 2  
521 and 3 storms as well. These results indicate that bay-side storms arriving during the ebbing phase  
522 of the tide could create a prolonged ebb as the bay water drains through the inlet. On the other  
523 hand, bay-side storms arriving during flood tide, despite potentially generating higher total water  
524 level peaks, tend to drain faster.

525



526

527 Figure 7. Time series of water levels at the ocean and the center of the inlet and discharge when the  
 528 storm arrives during ebb (a and b) and flood (c and d).

529

### 530 **4.5 Cross-Shore Momentum Balances**

531 The relative importance of bay-side surge and ocean-side waves to driving inlet discharge are  
 532 examined by calculating the cross-shore momentum balance terms at the inlet. The governing  
 533 equation for the cross-shore momentum balance at the inlet is simplified by assuming Coriolis  
 534 and nonlinear advection terms are negligible at first order (Jay, 1991; Olabarrieta et al., 2011;

535 Wargula et al., 2018). Each term is integrated across the inlet width such that the momentum  
 536 terms are a function of volume discharge through the inlet,  $Q$ , following Orescanin et al. (2014):  
 537

$$538 \quad \frac{\partial Q}{\partial t} = gA \frac{\eta_o - \eta_b}{L} - C_D \frac{Q|Q|}{A^2} b + R_s b \quad \text{(Equation 6)}$$

539  
 540 where  $t$  is time,  $g$  is the gravitational acceleration,  $A$  is the cross-sectional area,  $\eta_o$  and  $\eta_b$  are the  
 541 water levels at ocean- and bay-side points, respectively,  $L$  is the cross-shore distance between  
 542 the ocean- and bay-side points,  $b$  is the inlet width,  $C_D$  is the bottom friction coefficient, and  $R_s$  is  
 543 the radiation stress gradient in the cross-shore direction. Because wind effects are only captured  
 544 indirectly in the model through the pressure gradient imposed on the model boundaries, wind  
 545 stress was not included in Equation 6.

546  
 547 Volume discharge  $Q$  (Figures 7(b) and 7(d)) and time-varying area  $A$  were calculated by  
 548 integrating across the inlet transect (dashed-dot line in Figure 3(b)). Inlet width  $b$  is calculated to  
 549 be 1.43 km (dashed-dot line in Figure 3(b)). Pressure gradient was estimated as the water level  
 550 gradient between points offshore of the ebb shoal and inside the bay, which were separated by a  
 551 distance  $L$  of 5.49 km along an axis aligned with the inlet's main channel. The gradient in radiation  
 552 stress  $R_s$  is estimated following Apotsos et al., (2008) as:

$$554 \quad R_s = \frac{1}{16} g H_b^2 \frac{(\cos^2(\theta) + 0.5)}{\Delta x} \quad \text{(Equation 7)}$$

555  
 556 where  $H_b$  is the significant wave height at breaking,  $\theta$  is the wave direction relative to the inlet  
 557 channel axis, and  $\Delta x$  is the distance from the location of breaking to the inlet mouth. Equation 7  
 558 neglects the radiation stress inside the inlet; the potential consequences of neglecting inland  
 559 radiation stress are explored in Section 4.6. The breaking wave height was identified as that at  
 560 the position of maximum dissipation in a cross-shore transect aligned with the inlet's main  
 561 channel. The distance  $\Delta x$  ranged from 2.65 km to 2.93 km from the position of maximum  
 562 dissipation to the center of the inlet. The maximum breaking wave height  $H_b$  was 3.41 m for all  
 563 7.00 m boundary significant wave height cases and ranged from 1.71 m to 1.91 m for the 2.00 m  
 564 boundary significant wave height cases, depending on the surge levels on the bay side. Waves  
 565 approach the inlet channel axis from an oblique angle, with wave direction relative to the inlet  
 566 channel axis ranging from 43 degrees to 63 degrees clockwise of the inlet channel axis (i.e., out  
 567 of the northeast).

568

569 Bottom stress (the 2nd term on the right hand side of Equation 6) is estimated using the quadratic  
570 drag relationship, where the bottom friction coefficient  $C_D$  is estimated using the Case 0 model  
571 simulation. A linear regression was calculated between the time-varying discharge and pressure  
572 gradient (first two terms in Equation 6) and the bottom stress term, neglecting the drag coefficient.  
573 The slope of a linear fit was 0.0068, with 95% confidence intervals of +/- 0.0002. A  $C_D$  of 0.0068  
574 was applied to bottom stress calculations for all model runs. This drag coefficient value is within  
575 the range of those reported by other studies that have used momentum balances to estimate drag  
576 coefficients at inlets (Orescanin et al., 2014; Wargula et al., 2014).

577

578 Figure 8 shows the pressure gradient, wave forcing (or wave radiation stress gradient), and  
579 bottom stress as a function of time for each Case with 7-m waves when the storm arrives during  
580 ebb (panel a) and during flood (panel b). The time-varying discharge, which is important at slack  
581 tide and at the start and end of the pulse of bay-side surge, is not included in Figure 8 because it  
582 is less than  $4 \text{ m}^3/\text{s}^2$  in magnitude in all cases.

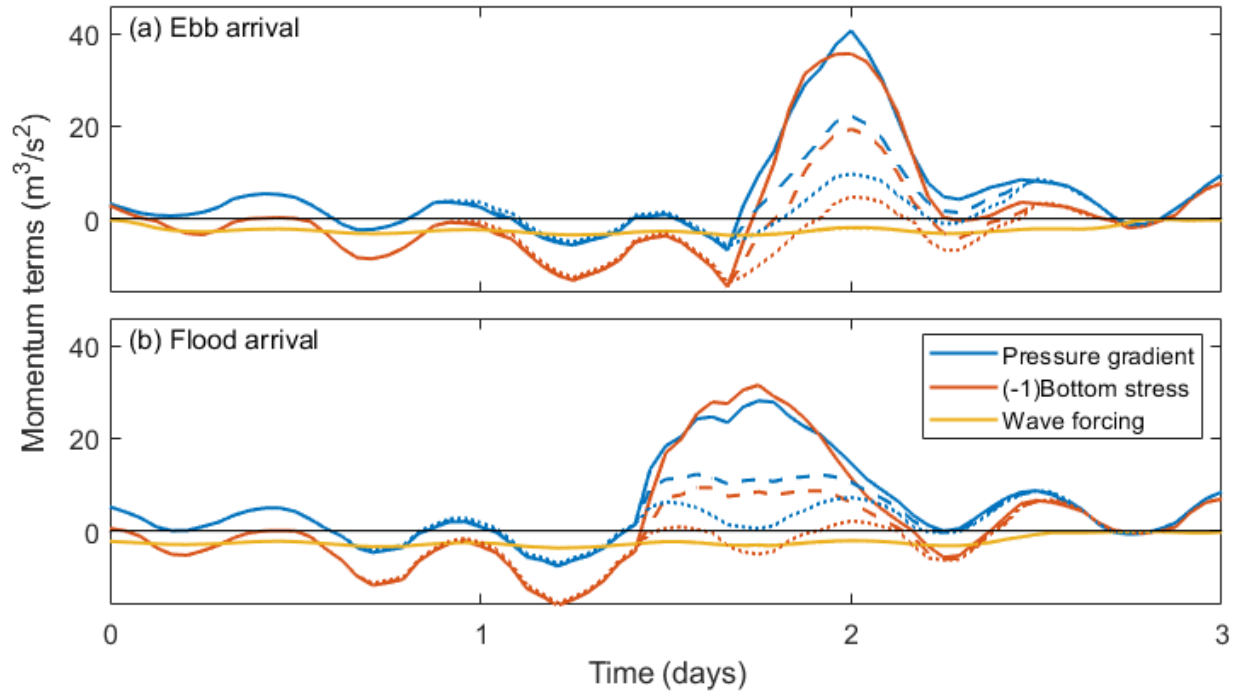
583

584 Momentum balance residuals are small (not shown), with a median magnitude of less than 12%  
585 of the corresponding magnitude of the bottom stress term. Bottom stress is correlated with the  
586 sum of pressure gradient, time-varying discharge, and wave radiation stress gradient with an  $R^2$   
587 of 0.96 to 0.99 for all storm Cases. This suggests that the residuals account for less than 4% of  
588 variability in the momentum balances. The largest peaks in the residuals occur just before and  
589 after the peak of the bay-side surge and may be owing to the neglected advection terms as well  
590 as spatial variability in the momentum terms, which are not captured using a one-dimensional,  
591 linear momentum balance (Equation 6). In particular, the residual of the momentum balance  
592 before the arrival of the bay-side surge is correlated with wave radiation stress gradients with an  
593  $R^2$  of 0.61 for Cases with 7-m waves ( $R^2 < 0.05$  for Cases with 2-m waves). This  $R^2$  value suggests  
594 that the wave radiation stress gradients may be somewhat underestimated.

595

596 The wave radiation stress gradient for storm Cases with 2-m waves is negligible (less than  $1$   
597  $\text{m}^3/\text{s}^2$ ) compared to the pressure gradient and bottom stress terms (not shown) and does not  
598 change the correlation of the terms with bottom stress ( $R^2 = 0.97$  to  $0.98$  with or without wave  
599 forcing for Cases 1 to 3 and 2-m waves). Thus, although 2-m waves may have important impacts  
600 on the hydrodynamics of the edge of the ebb shoal (see section 4.6), they do not play a significant  
601 role in driving discharge through the inlet mouth.

602



603

604 Figure 8. Pressure gradient (blue curves), bottom stress (red curves), and wave radiation stress gradient  
605 (yellow curves) versus time during 7-m wave cases when the bay-side storm arrives (a) during ebb and (b)  
606 during flood. The solid, dashed, and dotted line styles correspond to Cases 1, 2, and 3, respectively (note  
607 that wave forcing appears to have only a solid line style because of overlap). Positive (negative) values for  
608 pressure gradient and wave forcing correspond to forcing of discharge towards the ocean (bay). Positive  
609 (negative) values for bottom stress correspond to the inlet discharging in the ebb direction (flood direction),  
610 i.e., from bay to ocean (from ocean to bay).

611

612 The wave radiation stress gradient for storm Cases with 7-m waves is of similar order of  
613 magnitude as bottom stress and pressure gradient before the arrival of surge, and is always  
614 negative, meaning that it forces water mass from the ocean to the bay. Although a change in  
615 water level and currents can modulate the breaking wave height and breaking location (important  
616 for  $\Delta x$  in Equation 7), the differences in breaking wave height between Cases with 7-m waves are  
617 small ( $O(10 \text{ cm})$ ) and the breaking location remains the same throughout the storm, potentially  
618 owing to  $O(100 \text{ m})$  model grid sizes on the edge of the ebb shoal. As a result, the magnitude and  
619 variability of the wave radiation stress gradient is similar for all Cases with 7-m waves (yellow  
620 curve, Figure 8).

621

622 Although wave forcing is similar in magnitude and variability for each Case, its contribution to  
623 variability in volumetric discharge decreases with increasing bay-side surge levels. During the  
624 storm, the squared correlation between bottom stress and the summation of forcing terms  
625 improves from  $R^2 = 0.85$  to  $0.97$  without wave forcing to  $R^2 = 0.96$  to  $0.99$  with wave forcing  
626 included, with the greatest and least increases in  $R^2$  ( $0.10$  and  $0.01$ ) during Case 3 and Case 1,  
627 respectively.

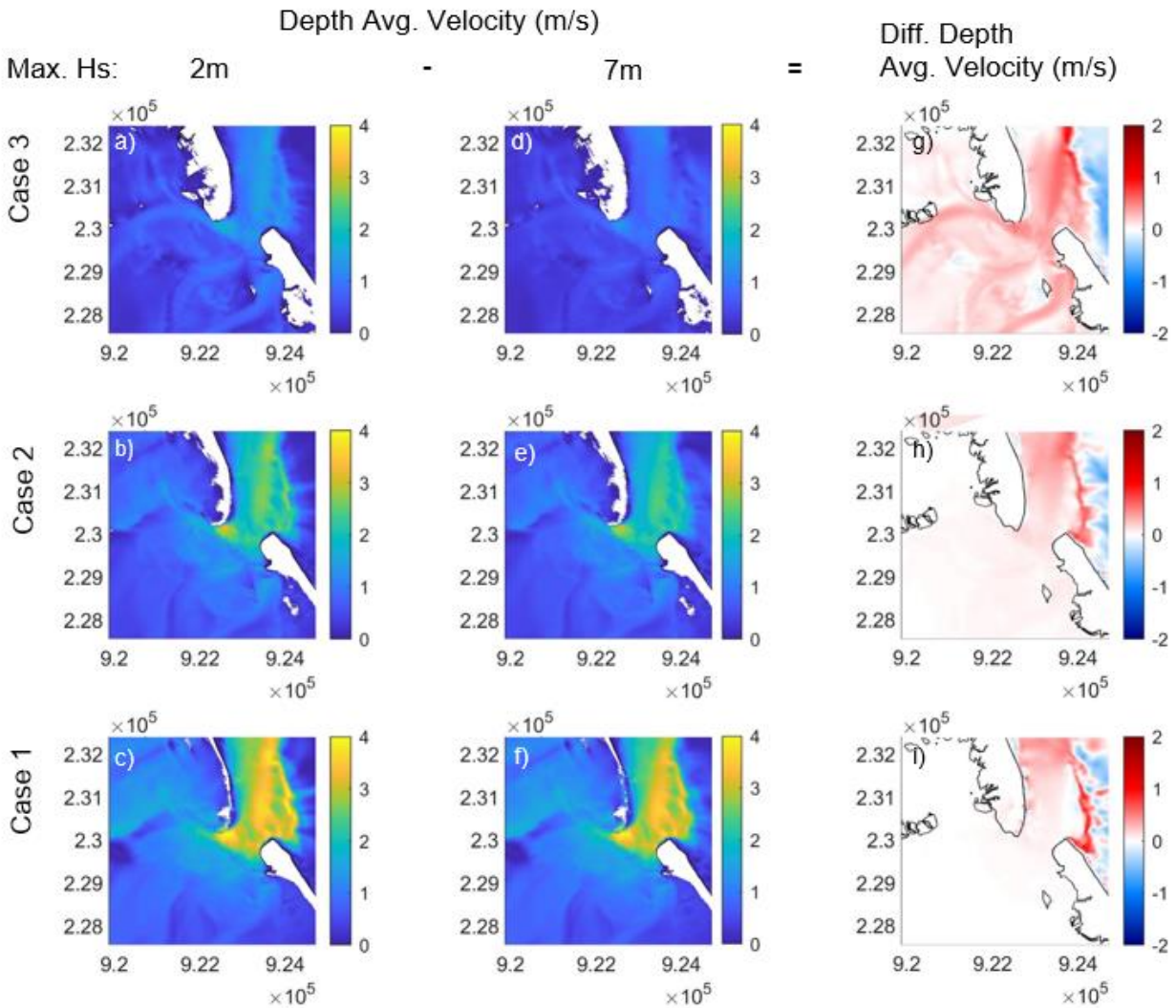
628  
629 Although the bay-side surge drives discharge magnitude and direction to first order, wave forcing  
630 causes a phase lag in the response of the inlet to the bay-ocean water level gradient. The time  
631 difference in the zero-crossing of the pressure gradient and bottom stress terms at the start of the  
632 bay-side surge (day 1.7 during ebb and day 1.4 during flood) decreases from 2.45 hours (3.70  
633 hours) to 1.39 hours (0.98 hours) as surge levels increase from Case 3 to Case 1, respectively,  
634 when the storm arrives during ebb (flood). At the peak of bay-side surge, wave impacts on  
635 discharge decrease as surge levels increase inside the bay. However, as explained in the next  
636 section, waves contribute to the spatial variability of currents on the ebb shoal and other parts of  
637 the inlet.

#### 638 639 **4.6 Spatial distribution of currents, water levels, waves, and fluxes during bay-side storms**

640 Bay-side storms have the potential to inundate long stretches of barrier islands and regions  
641 around tidal inlets. The main difference between these types of storms and those traveling along  
642 the ocean-side is that most of the inundation during bay-side storms impacts the back-barrier  
643 region of the barrier islands (Figure 9). Based on the model outputs, the back-barrier inundation  
644 extent depends mostly on the surge levels and barrier island elevations. For all simulations, There  
645 was a north to south gradient in water level inside the bay, with an  $O(10\text{ cm})$  water level decrease  
646 from north to south across the region shown in Figure 9. As seen in the left and center panels in  
647 Figure 9, back-barrier inundation around Oregon Inlet is more severe along the northern spit than  
648 the southern shoulder of the inlet, which may in part be owing to higher water levels in the north  
649 during the peak of the storm. The inundation extent south of Oregon Inlet is limited by the man-  
650 made elevated sand barriers along the ocean side of the roadway located along the barrier island  
651 system.

652  
653 Simulations indicate that bay-side total water levels exceeding 2 m (NAVD88) have the potential  
654 to completely submerge the northern spit and result in channelized flows through existing  
655 estuarine channels. This pattern appears to be exacerbated if the storm arrives during flood tide,

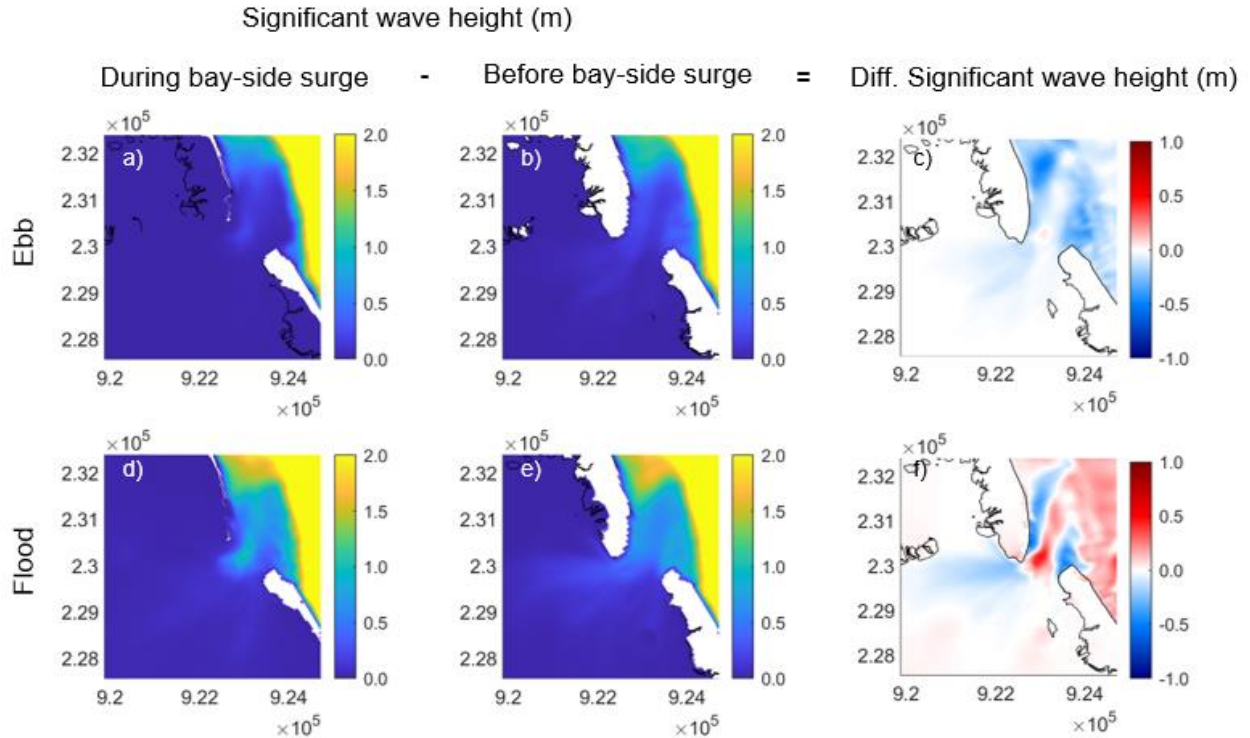
656 as the ocean side is already experiencing rising water levels. It should be noted that flows  
 657 funneled through pre-existing estuarine channels that meander through the barrier island have  
 658 been identified as one of the triggers for barrier island breaching along the Outer Banks  
 659 (Velasquez-Montoya et al., 2021a).  
 660



661  
 662 Figure 9. Spatial distribution of depth-averaged velocities during ebb tide for storm Cases 1, 2, and 3 with  
 663 2-m (left) and 7-m (middle) wave heights. The panels in the right column show the spatial distribution of  
 664 differences in depth-averaged velocities from simulations with 2-m and 7-m wave heights. Warm colors  
 665 (shades of red) indicate the regions where ebbing velocities are larger for a storm with 2-m wave heights  
 666 compared to the same storm with 7-m wave heights, while cool colors (shades of blue) indicate the  
 667 opposite.  
 668

669 While direct wave effects are not as significant as surge levels at driving inundation during bay-  
670 side storms, the waves drive changes in ebbing and flooding velocities through the inlet, altering  
671 volumetric discharge and the resulting inundation duration. The right hand side panels in Figure  
672 9 show the spatial effect of waves on depth-averaged velocities and how those effects can be  
673 diminished by storm surges. Red shadows indicate regions where ebbing velocities are larger for  
674 a storm with 2-m wave heights compared to the same storm with 7-m wave heights, while shades  
675 of blue indicate the opposite trend. The band of dark red colors along the edge of the ebb delta  
676 seen for the three storm cases indicates the blocking effect that waves have on ebbing currents,  
677 potentially owing to the interaction between breaking waves and the ebb jet. Intra-model  
678 comparisons indicate that 7-m waves can reduce ebb velocities by up to 1 and 2 m/s. This wave  
679 blocking effect becomes more localized in the ebb delta as the surge levels increase. For  
680 example, the surf zone width on an axis aligned with the inlet channel was estimated by  
681 calculating the distance between the position of maximum wave dissipation and the position  
682 where wave dissipation first decreases to 1 N/ms. Before the bay-side surge arrives, the surf zone  
683 is roughly 900 m and 700 m wide for the 7-m and 2-m wave heights, respectively. These surf  
684 zone widths narrow to roughly 200 m and 400 m for the Case 1 and Case 3 bay-side surges with  
685 the 7-m and 2-m wave heights, respectively.

686  
687 The smaller spatial extent of the red shadows for the Case 1 storm (Figure 9i) compared to the  
688 other two storm cases indicates the predominance of bay surge levels at driving the inlet  
689 hydrodynamics during bay-side storms, while wave effects tend to become more pronounced  
690 when the surge levels are low or at times when they can propagate through the inlet without being  
691 blocked by surge. Figure 10 shows that when the bay-side surge arrives during ebb, as it did  
692 during Hurricane Irene, waves break at the edge of the ebb delta and less than 1 m-high waves  
693 propagate into the ebb shoals, but barely any wave energy enters the main channel of the inlet  
694 as the surge arrives. On the other hand, when the surge arrives during flood, waves also break  
695 around the edge of the ebb delta, but they continue to propagate into the ebb shoals and main  
696 channel of the inlet. The one-dimensional momentum balance developed in section 4.5 indicated  
697 the predominance of the pressure gradient and the bottom stress terms over the wave forcing on  
698 the scale of the entire inlet system (i.e., taking gradients over 2 km - 5 km length scales). However,  
699 the spatial variability demonstrated in Figure 10 suggests significant wave radiation stress  
700 gradients can develop on smaller scales inside the inlet mouth and alongshore of the ebb shoal,  
701 depending on the timing of surge arrival with the tide, leading to spatially-varying, local wave  
702 impacts on the currents and water levels.



703

704 Figure 10. Spatial distribution of significant wave height for storm Case 1 when the bay-side surge arrives  
 705 during ebb (top row) and flood (bottom row) with 7-m wave heights forced at the boundary. The panels in  
 706 the right column (panels c and f) show the spatial distribution of differences in significant wave height  
 707 between the time when the bay-surge arrived at day 2 during ebb and day 1.75 during flood (panels a and  
 708 d) and before its arrival to the inlet at day 0.44 during ebb and 0.25 during flood (panels b and e). Positive  
 709 differences (shades of red) in panels c and f, indicate the regions where significant wave heights are larger  
 710 during the bay-side surge than before its arrival to the inlet, while negative values (shades of blue) indicate  
 711 the regions where significant wave heights are larger before the bay-side surge arrival to the inlet.

712

713 The spatially-varying impacts of waves and surge on water levels and flows also drive spatially-  
 714 varying impacts on the volume flux across the delta, influencing water mass exchange. The  
 715 difference in flux between the strongest storm (Case 1 with 7-m wave heights) and the no storm  
 716 scenario (Case 0) at the time of maximum discharge (Day 1.96, Figure 6b) are presented in Figure  
 717 9a. The figure shows that the largest increases in flux magnitude occurred in the main inlet  
 718 channel across the ebb delta and in the northern flood channel, particularly as it passes near the  
 719 northern barrier island.

720

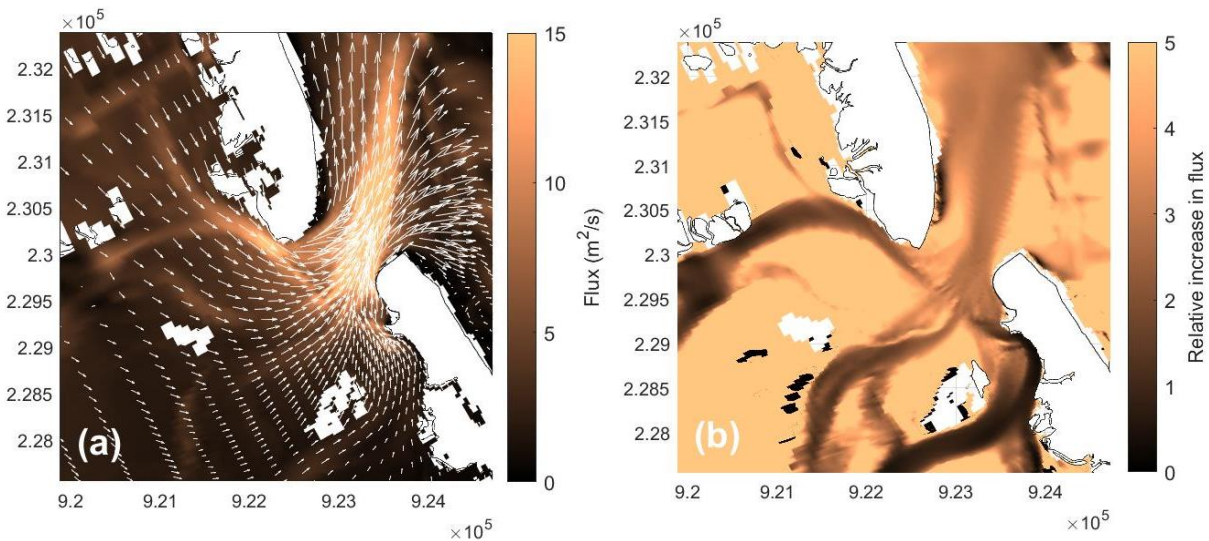
721 The enhanced flux through the northern channel is driven by a combination of the north-to-south  
 722 water level gradient and enhanced flow velocities (Figure 9c, 9f). Between the three flood  
 723 channels, the least enhancement in flux is seen in the deepest southern flood channel, which is

724 typically the channel with the dominant contribution to discharge. This trend suggests that bay-  
725 side storms may lead to a temporary change in the relative dominance of flood channels, which  
726 could lead to channel scouring that shifts the channels' relative contributions to discharge even  
727 after the storm has passed.

728

729 Although the largest change in magnitude of velocity and flux owing to the bay-side storm and  
730 waves are mainly observed inside the channels (Figures 9 and 11a), the relative increases in  
731 velocity (not shown) and flux (Figure 11b) compared to the no storm (Case 0) are much larger on  
732 the shallow shoals compared to deeper channels. This relatively large impact on shallow regions  
733 may be owing to the  $O(1\text{ m})$  increase in water level in the bay, roughly doubling the water depth  
734 on the shallow shoals of the flood delta and inside the inlet mouth. Inside the inlet mouth, the  
735 Case 1 storm flux across the northern shoals is enhanced 500% relative to Case 0, while in the  
736 main channel, the flux enhancement is close to 300%. On the flood delta, flux on the shallow  
737 shoals is more than an order of magnitude ( $>1000\%$ ) larger than that during Case 0, while in the  
738 flood channels, the relative increase can be as small as 50% (e.g., in the southern flood channel  
739 along the Hatteras Island shoreline).

740



741

742 Figure 11. Color contours show (a) the flux during Case 1 (with 7 m wave heights) and (b) the increase in  
743 flux relative to Case 0 at moment of maximum discharge out of the inlet (Day = 1.96, Figure 7b). The  
744 white arrows show the direction of flux.

745

746

747 **5. Discussion**

748

749 ***5.1 Competing bay-side surge and ocean waves at the inlet***

750 Comparisons between simulations with varying levels of surge and incoming ocean waves  
751 provide an overview of the potential implications of bay-side storms on the hydrodynamics and  
752 inundation scenarios around tidal inlets. Our results indicate that, during bay-side storms, tidal  
753 inlets are at the confluence of competing bay-surge and wave forcings. Large bay-surge levels  
754 tend to dominate over wave-driven processes by regulating their effects at the inlet and their  
755 potential to enter the bay. This result indicates a contrasting difference with ocean-side storms,  
756 for which pressure gradients between the ocean and the bay tend to favor the propagation of  
757 waves or wave-induced set up into the lagoons (Irish and Cañizarez, 2009; Malhadas et al., 2009).

758

759 Despite enhanced bay water levels dominating over wave effects in the overall dynamics of the  
760 system, wave effects predominate at the edge of the ebb delta, where wave-current interaction  
761 reduces ebb currents draining the bay. For the most severe storm simulations, the blocking effect  
762 is localized in the ebb delta; only under the least severe storm scenario could waves reduce  
763 ebbing currents throughout the whole extent of the inlet, including the flood delta. These results  
764 support findings on strong wave-current interaction in tidal inlets by Dodet et al. (2013) and  
765 reduction of currents in the ebb shoal due to breaking waves by Olabarrieta et al. (2011). Although  
766 the reduction of ebb currents by waves could potentially lessen morphological changes at the  
767 inlet, slowing the draining of the lagoon can prolong inundation along the back barrier. In this  
768 regard, indirect wave effects during bay-side storms include the spatial and temporal  
769 enhancement of inundation patterns along low lying back-barrier regions.

770

771 ***5.2 Potential for inundation and morphological changes***

772 The combination of prolonged bay inundation and the presence of paleo inlets and meandering  
773 estuarine channels in the back-barrier region creates the hydrodynamic and morphologic setting  
774 for lagoon-side barrier breaching. Near Oregon Inlet, Hurricane Irene (2011) created two  
775 intermittent inlets that connected the lagoon and the ocean. Such breaching events allow for faster  
776 draining of the lagoon and can act as a relief valve even after the storm has passed. However,  
777 they do so at the expense of infrastructure vulnerability along barrier islands (Hansen and  
778 Sallenger, 2007; Velasquez-Montoya et al., 2021a) and long-term (years to decades)  
779 morphological (Velasquez-Montoya et al., 2018) and ecosystemic changes in the surrounding  
780 regions (Velasquez-Montoya et al., 2021b).

781

782 Although the focus of this study is on the vicinity of a tidal inlet, it should also be noted that all  
783 storm scenarios led to inundation on the mainland, confirming that bay-side storms have the  
784 potential to inundate not only the back of barrier islands, but also low-lying regions landward of  
785 the bay, as suggested by Peng et al. (2004). Although analyzing widespread inundation along the  
786 mainland is beyond the scope of this study, our results indicate that storm surges generated by  
787 bay-side storms could significantly inundate the mainland around the Albemarle-Pamlico Sound,  
788 a rural region vulnerable to sea level rise and storms (Johnston et al., 2021; Bhattachan et al.,  
789 2018).

790

791 In addition to inundation and potential breaching of barrier islands, the relative changes in flux  
792 patterns caused by bay-side storms could lead to changes in sediment transport pathways inside  
793 the inlet, which can in turn modify the morphology of the channels and shoals in the ebb and flood  
794 deltas, as well as in the main inlet gorge. This result builds upon the findings by Humberston et  
795 al. (2019), who found seasonal wave patterns can lead to interannual variability of the ebb delta  
796 shoals. The channelization of the ebb flux provides evidence for the potential relevance of bay-  
797 channels to funnel and direct flows within the flood delta. These results indicate that the  
798 directionality of the channels relative to the surge approach can modify the fluxes at different  
799 regions in the inlet. These results agree with the evidence presented by Velasquez-Montoya et  
800 al. (2020), who reported movement of shoals and bathymetric changes at Oregon Inlet on the  
801 order of 5 m caused by Hurricane Irene.

802

### 803 ***5.3 Model considerations and future research opportunities***

804 The numerical model used in this study accounts for wave-current interactions at the inlet, which  
805 have proven to be a major factor driving the hydrodynamics of the system during bay-side storms.  
806 However, the model excludes the contribution of infragravity waves, which have been found to  
807 propagate into inlets and lagoons during ocean-side storms (Bertin and Olabarrieta, 2016; Bertin  
808 et al., 2018; Melito et al., 2020). Future research opportunities include the implementation of the  
809 surfbeat wave model in Delft3D to account for long waves and their effects during bay-side storms.

810

811 Future work could analyze inundation patterns in detail and the influence of existing estuarine  
812 channels at triggering breaching events. For the latter application, higher resolution (less than 5  
813 m cell sizes) are needed to account for the initial stages of ocean- and bay-side connectivity.  
814 Spatially-varying bed roughness or the vegetation module within Delft3D may also need to be

815 implemented to better represent flow conditions within the marshes in the back-barrier region.  
816 Additional work could explore morphological changes caused by bay-side storms. Such work  
817 could provide insights on the migration of shoals and channels that could in turn feed into the  
818 hydrodynamic changes at tidal inlets during these extreme events.

819

#### 820 ***5.4 Broader implications to other inlets***

821 Numerical modeling studies have reported modulation of storm surge by the phase of tides at the  
822 Albemarle-Pamlico Sound in the United States (Thomas et al., 2019), the Ria de Aveiro Lagoon  
823 in Portugal (Pinheiro et al., 2020), and the Yangtze estuary in China (Yin et al., 2021). However,  
824 those interactions have been less explored for bay-side storms and at smaller scales. This study  
825 provides evidence of the relevance of tide-bay surge interaction on the scale of an inlet ( $O(1,000$   
826  $m)$ ). The one-dimensional momentum balance presented in section 4.5 suggests that the wave  
827 radiation stress gradients on the inlet scale (i.e., from ebb shoal to inlet mouth) are similar for the  
828 same offshore wave height and differing surge and tide levels. However, spatial comparisons of  
829 wave heights at the same tidal phase, with and without bay side surge, show a complex breaking  
830 pattern on the ebb shoal and inside the inlet mouth (Figure 10). Those patterns suggest tide and  
831 surge modulate the impacts of waves on currents in the inlet system (Figure 9). Although pressure  
832 gradient and bottom stress were typically dominant over the wave forcing on the inlet scale during  
833 large bay-side surge events (Figure 8), the spatially varying patterns of wave breaking will drive  
834 circulation patterns that impact transport of water masses and morphological evolution on the ebb  
835 shoal.

836

837 Increases in water levels inland of an inlet can be driven by processes not related to storm surge,  
838 such as by wind-driven gradients across a large bay or high discharge events owing to runoff or  
839 extreme rainfall. Results from this study are applicable to not only other inlets along the Albemarle-  
840 Pamlico Sound and in other barrier island systems, such as the Wadden Sea, which also  
841 experiences storm-driven water level gradients (van Weerdenburg et al., 2019), but also other  
842 types of estuarine and inlet systems. For example, at intermittent inlets in smaller estuarine  
843 systems with high river inflows that drive an offshore-directed pressure gradient, ocean-side wave  
844 effects on the lagoon are restricted to periods when tidal water levels exceed lagoonal forcing  
845 (Wainwright and Baldock, 2015; Orescanin and Scooler, 2018). In addition, bay-side surges being  
846 released through tidal inlets are comparable to excess runoff flowing through perched estuarine  
847 mouths, which are typically located above the low tide ocean water level (Cooper, 2001; Williams

848 and Stacey, 2016). The latter systems are common along the coastlines of California and South  
849 Africa.

850

851 Although flooding during hurricanes is typically addressed as an oceanfront issue, bay-side  
852 storms can result in severe flooding in the back-barrier regions (Mulligan et al. 2015). This study  
853 found that flooding patterns around a tidal inlet can vary depending on the directionality of the  
854 surge and the morphological features near the inlet and neighboring barrier islands, suggesting  
855 the potential development of two dimensional (along and across inlet) water level gradients  
856 around the inlet system. Ongoing research is exploring the effects that such gradients may have  
857 on the inlet hydrodynamics under different types of storms.

858

## 859 **6. Conclusions**

860

861 The response of tidal inlets to bay-side storms was analyzed using a numerical model for Oregon  
862 Inlet, NC. Outputs from the coupled hydrodynamic and wave model were evaluated against  
863 observed water levels and depth-averaged velocities for more than 50 days distributed between  
864 2019 and 2020. Several model performance statistics indicate that the model is capable of  
865 simulating spatiotemporal hydrodynamics at the inlet. After successfully calibrating and validating  
866 the model, it was used to simulate bay-side storm conditions in large bays, specifically at the  
867 Albemarle-Pamlico Sound. Synthetic storms based on the wave and water level conditions  
868 generated by Hurricane Irene (2011) were used to explore the competing influence of waves and  
869 bay-side surge at the inlet.

870

871 Simulation outputs indicate that during bay-side storms, the water level gradient along the inlet  
872 remains positive (i.e., pushing water out into the ocean), suggesting that waves might be  
873 responsible for any influx of volume to the bay during high bay-side surge events. Regardless of  
874 whether a bay-side storm arrives during the ebb or flood phases of the tide, the ebbing discharge  
875 towards the ocean is predominant. This dominance of ebb discharge is a significant difference  
876 from ocean-side storms, which tend to generate storm surges that propagate from the ocean  
877 through inlets and into bays. On the other hand, similar to ocean-side events, during bay-side  
878 storms, waves tend to have a larger impact on the hydrodynamics at the ebb delta, where they  
879 block ebbing flow. This blocking results in slowing down the flushing of the surge in the bay, thus  
880 extending the duration of the inundation period in the back-barrier region near the inlet.

881

882 Comparison of bay-side storms against no-storm conditions indicates that the flux distribution  
883 through the channels in the flood delta can change during the peak ebb phase of the storm. Flow  
884 enhancement over shoals and channels on the flood delta could result in changes in sediment  
885 transport pathways and morphological changes at the inlet. The results presented here indicate  
886 that in addition to potential morphological changes along the inlet, bay-side storms can also trigger  
887 major inundation in the back-barrier region surrounding the inlet, while inundation from the ocean  
888 side is not as significant.

889

## 890 **Acknowledgements**

891 The authors are grateful to the North Carolina Department of Transportation for providing the  
892 funds to conduct this study through Grant #2020-09. Special thanks to Mr. Pablo Hernandez for  
893 his support and resourcefulness during field campaigns. The authors would also like to thank  
894 USNA graduates Ms. Marissa Amodeo for her assistance with statistical calculations during the  
895 calibration phase of the model as well as Mr. Joshua Torres and Mr. Brent Schwartz for their  
896 support during field surveys. The authors are also grateful to the anonymous reviewers for their  
897 thoughtful suggestions, which significantly enhanced the content of this manuscript.

## 898 **Disclaimer**

899 The contents of this paper reflect the views of the author(s) and not necessarily the views of the  
900 Universities. The authors are responsible for the facts and the accuracy of the data presented  
901 herein. The contents do not necessarily reflect the official views or policies of either the North  
902 Carolina Department of Transportation or the Federal Highway Administration at the time of  
903 publication. This report does not constitute a standard, specification, or regulation.

## 904 **References**

905

906 Apotsos, A., Raubenheimer, B., Elgar, S., Guza, R. 2008. Wave-driven setup and alongshore  
907 flows observed onshore of a submarine canyon. *Journal of Geophysical Research*. 113,  
908 C07025. <http://dx.doi.org/10.1029/2007JC004514>.

909

910 Aubrey, D. G., Weishar, L. 1988. Hydrodynamics and sediment dynamics of tidal inlets, volume  
911 29. Book Series:Lecture Notes on Coastal and Estuarine Studies. <https://doi.org/10.1029/LN029>

912

913 Battjes, J. and J. Janssen, 1978. Energy loss and set-up due to breaking of random waves. In  
914 Proceedings 16th International Conference Coastal Engineering, ASCE, p. 569–587.  
915

916 Bales, J.D. 2003. Effects of Hurricane Floyd inland flooding, September–October 1999, on  
917 tributaries to Pamlico Sound, North Carolina. *Estuaries* 26, 1319–1328).  
918 <https://doi.org/10.1007/BF02803634>  
919

920 Blanton, B., Madry, S., Galluppi, K., Gamiel, K., Lander, H., Reed, M., Stillwell, L., Blanchard-  
921 Montgomery, M., 2008. Report for the State of North Carolina Flood-plain Mapping Project:  
922 Coastal Flood Analysis System. Topographic/Bathymetric Data.  
923

924 Bertin, X., Fortunato, A. B., Oliveira, A., 2009. A modeling-based analysis of processes driving  
925 wave-dominated inlets. *Continental Shelf Research*, 29(2009), 819–834.  
926 <https://doi.org/10.1016/j.csr.2008.12.019>  
927

928 Bertin, X., Olabarrieta, M., 2016. Relevance of infragravity waves in a wave-dominated inlet.  
929 *Journal of Geophysical Research: Oceans*. 121, 5418–5435,  
930 <https://doi.org/10.1002/2015JC011444>  
931

932 Bertin X., de Bakker, A., van Dongeren, A., Coco, G., André, G., Ardhuin, F., Bonneton, P.  
933 Bouchette, F., Castelle, B., Crawford, W. C., Davidson, M., Deen., M, Dodet, G., Guérin,  
934 T., Inch, K., Leckler, F., McCall, R., Muller, H., Olabarrieta, M., Roelvink, D. Ruessink, G., Sous,  
935 D., Stutzmann, E., Tissier, M., 2018. Infragravity waves: From driving mechanisms to impacts.  
936 *Earth-Science Reviews*, 177, 2018, 774-799. <https://doi.org/10.1016/j.earscirev.2018.01.002>.  
937

938 Booij, N., Ris, R.C., Holthuijsen, L.H., 1999. A third-generation wave model for coastal regions:  
939 1. Model description and validation. *J. Geophys. Res.* 104, 7649–  
940 7666, <http://dx.doi.org/10.1029/98JC02622>.  
941

942 Bhattachan, A., Jurjonas, M. D., Moody, A. C., Morris, P. R., Sanchez, G. M. Smart, L. S.,  
943 Taillie, P. J., Emanuel, R. E., Seekamp, E. L., 2018. Sea level rise impacts on rural coastal  
944 social-ecological systems and the implications for decision making. *Environmental Science &*  
945 *Policy*, 90 (2018), 122-134. <https://doi.org/10.1016/j.envsci.2018.10.006>  
946

947 Bosboom, J., Reniers, A.J.H.M, Luijendijk, A. P., 2014. On the perception of morphodynamic  
948 model skill. Coastal Engineering, 94 (2014), 112 - 125.  
949 <http://dx.doi.org/10.1016/j.coastaleng.2014.08.008>  
950

951 Brier, G. W. 1950. Verification of forecasts expressed in terms of probability. Monthly Weather  
952 Review. 78, 1-3. [https://doi.org/10.1175/1520-0493\(1950\)078<0001:VOFEIT>2.0.CO;2](https://doi.org/10.1175/1520-0493(1950)078<0001:VOFEIT>2.0.CO;2)  
953

954 Brown, E. I. 1928. Inlets on sandy coasts. Proceedings of the American Society of Civil  
955 Engineers, Vol 54, Part I, pp 505-523.  
956

957 Bush, D. M., Young, R. S., Webb, C. A., Thielier, E. R. 1996. Soundside impacts of a northward  
958 tracking tropical cyclone: Hurricane Emily (31Aug93), Cape Hatteras area, North Carolina. J.  
959 Coastal Res., 12(1), 229–239.  
960

961 Coastal Emergency Risks Assessment (CERA). <<https://coastalrisk.live/>> (Accessed August  
962 2019).  
963

964 Chanta R. J., M. C. Curranb,c, K. W. Ableb, Glenna, S. M. 2000. Delivery of Winter Flounder  
965 (*Pseudopleuronectes americanus*) larvae to settlement habitats in coves near tidal inlets.  
966 Estuarine, Coastal and Shelf Science (2000) 51, 529–541  
967 <https://doi.org/10.1006/ecss.2000.0694>  
968

969 Cialone, M., Elko, N., Lillycrop, J., Stockton, H., Raubenheimer, B., Rosati, J. 2019. During  
970 Nearshore Event Experiment (DUNEX): A collaborative community field data collection effort.  
971 Proceedings of the 9th International Conference Coastal Sediments. Tampa/St. Petersburg,  
972 Florida, USA, 27 – 31 May 2019 [https://doi.org/10.1142/9789811204487\\_0253](https://doi.org/10.1142/9789811204487_0253)  
973

974 Clinch, A. S., Russ, E. R., Oliver, R. C., Mitasova, H., Overton, M., 2012. Hurricane Irene and  
975 the Pea Island Breach: Pre-storm site characterization and storm surge estimation using  
976 geospatial technologies. Shore & Beach, 80(2), 10p.  
977

978 Clunies, G. J., Mulligan, R. P., Mallinson, D. J., Walsh, J. P., 2017. Modeling hydrodynamics of  
979 large lagoons: Insights from the Albemarle-Pamlico Estuarine System. Estuarine, Coastal and  
980 Shelf Science. 189(2017), 90-103. <https://doi.org/10.1016/j.ecss.2017.03.012>

981  
982 Cooper, J. A. G., 2001. Geomorphological variability among microtidal estuaries from the wave-  
983 dominated South African coast. *Geomorphology* 40(1-2), 99-122. [https://doi.org/10.1016/S0169-](https://doi.org/10.1016/S0169-555X(01)00039-3)  
984 [555X\(01\)00039-3](https://doi.org/10.1016/S0169-555X(01)00039-3)  
985  
986 Cyriac, R. Dietrich, J. C., Fleming, J. G., Blanton, B. O., Kaiser, C., Dawson, C. N., Luettich, R.  
987 A., 2018. Variability in Coastal Flooding predictions due to forecast errors during Hurricane  
988 Arthur. *Coastal Engineering*, 137, 59-78. <https://doi.org/10.1016/j.coastaleng.2018.02.008>  
989  
990 Deltares, 2022. Delft3D-FLOW. Simulation of multi-dimensional hydrodynamic flows and  
991 transport phenomena, including sediments. User Manual Hydro-Morphodynamics. Version 4.05  
992 SVN Revision 75129. Delft, The Netherlands, 698 p.  
993  
994 DiLorenzo, J. L. 1988. The overtide and filtering response of small inlet/bay systems, Lecture  
995 Notes on Coastal and Estuarine Studies, Vol 29, D. G. Aubrey and L. Weishar, eds., Springer-  
996 Verlag, New York  
997  
998 Dodet, G., Bertin, X., Bruneau, N., Fortunato, A. B., Nahon, A., Roland, A., 2013. Wave-current  
999 interactions in a wave-dominated tidal inlet. *Journal of Geophysical Research Oceans*, 118(3),  
1000 1587 - 1605. <https://doi.org/10.1002/jgrc.20146>  
1001  
1002 Emery, W. J., Thomson, R. E. 2001. *Data Analysis Methods in Physical Oceanography*, 2nd  
1003 ed., Elsevier Sci, Amsterdam.  
1004  
1005 Escoffier, F.F., 1940. The stability of tidal inlets. *Shore & Beach*, Vol. 8., 114–115.  
1006  
1007 Farraday, R.V., Charlton, F.G., 1983. *Hydraulic Factors in Bridge Design*. Wallingford,  
1008 Oxfordshire, England.  
1009  
1010 Flores-Coto, C., Warlen, S.M., 1992. Spawning time, growth and recruitment of larval spot  
1011 *Leiostomus xanthurus* into a North Carolina estuary. *Fish. Bull. U.S.* 91:, 8 22.  
1012

1013 Forward Jr, Reinsel, Peters, Tankersley, Churchill, Crowder, Hettler, Warlen, and Green, 1999.  
 1014 Transport of fish larvae through a tidal inlet. *Fisheries Oceanography*, 8: 153-172.  
 1015 <https://doi.org/10.1046/j.1365-2419.1999.00026.x>  
 1016

1017 Fredsøe, J., 1984. Turbulent boundary layer in wave-current interaction. *Journal of Hydraulic*  
 1018 *Engineering* 110: 1103–1120.  
 1019

1020 Friedrichs, C. T., Aubrey, D. G., Giese, G. S., Speer, P. E., 1993. Hydrodynamical modeling of a  
 1021 multiple-inlet estuary/barrier system: Insight into tidal inlet formation and stability. In: Aubrey G.  
 1022 D. and Giese, G. S.: *Formation and Evolution of Multiple Tidal Inlets Coastal and Estuarine*  
 1023 *Studies*, Volume 44, Pages 95-112, The American Geophysical Union.  
 1024

1025 Geyer, W. R., Signell, R. P. 1992. A Reassessment of the role of tidal dispersion in estuaries  
 1026 and bays,” *Estuaries*, Vol 15, 97-108.  
 1027

1028 Hansen, M., Sallenger, A., 2007. Barrier island vulnerability to breaching: A case study on  
 1029 Dauphin Island, Alabama. Sixth International Symposium on Coastal Engineering and Science  
 1030 of Coastal Sediment Process, May 13-17, 2007 | New Orleans, Louisiana, United States.  
 1031 [https://doi.org/10.1061/40926\(239\)157](https://doi.org/10.1061/40926(239)157)  
 1032

1033 Hasselmann, K., T. P. Barnett, E. Bouws, H. Carlson, D. E. Cartwright, K. Enke, J. Ewing, H.  
 1034 Gienapp, D. E. Hasselmann, P. Kruseman, A. Meerburg, P. Müller, D. J. Olbers, K. Richter, W.  
 1035 Sell and H. Walden, 1973. Measurements of wind wave growth and swell decay during the Joint  
 1036 North Sea Wave Project (JONSWAP). *Deutsche Hydrographische Zeitschrift* 8 (12).  
 1037

1038 Hayes, M.O., FitzGerald, D.M., 2013. Origin, evolution, and classification of tidal inlets. In: Kana,  
 1039 T.; Michel, J., and Voulgaris, G. (eds.), *Proceedings, Symposium in Applied Coastal*  
 1040 *Geomorphology to Honor Miles O. Hayes*, *Journal of Coastal Research*, Special Issue No. 69,  
 1041 14–33. Coconut Creek (Florida), ISSN 0749-0208.  
 1042

1043 Humberson, J., Lippmann, T., McNinch, J., 2019. Observations of wave influence on alongshore  
 1044 ebb-tidal delta morphodynamics at Oregon Inlet, NC. *Marine Geology.*, 418, 106040.  
 1045 <https://doi.org/10.1016/j.margeo.2019.106040>  
 1046

1047 Irish J. L., Cañizares, R., 2009. Storm-wave flow through tidal inlets and its influence on bay  
1048 flooding. Journal of Waterway, Port, Coastal and Ocean Engineering, 135(2), 52-60.  
1049 [https://doi.org/10.1061/\(ASCE\)0733-950X\(2009\)135:2\(52\)](https://doi.org/10.1061/(ASCE)0733-950X(2009)135:2(52))  
1050

1051 Jaber, R., Stark, N., Wargula, A., Velásquez-Montoya, L., Sciaudone, E., 2021. Variations in  
1052 sediment strength along the tidal inlet channel near Pea Island, NC. GEO-EXTREME 2021,  
1053 Savannah, Georgia.  
1054

1055 Jarrett, J.T., 1976. Tidal Prism - Inlet Area Relationships. General Investigation of Tidal Inlets  
1056 (GITI), Report 3, US Army Coastal Engineering Research Center/Waterways Experiment  
1057 Station.  
1058

1059 Jay, D.A., 1991. Green's law revisited: tidal long-wave propagation in channels with strong  
1060 topography. Journal of Geophysical Research. 96, 20,585-20,598.  
1061 <https://dx.doi.org/10.1029/91JC01633>  
1062

1063 Johnston, J., Cassalho, F., Miesse, T., Ferreira, C. M., 2021. Projecting the effects of land  
1064 subsidence and sea level rise on storm surge flooding in Coastal North Carolina. Scientific  
1065 Reports 11, 21679. <https://doi.org/10.1038/s41598-021-01096-7>  
1066

1067 Joyeux, J.C., 1999. The abundance of fish larvae in estuaries: within-tide variability at Inlet and  
1068 immigration. Estuaries.22(4), 889-904  
1069

1070 Keulegan, G. H. 1967. Tidal flow in entrances water-level fluctuations of basins in  
1071 communications with seas, Technical Bulletin No. 14, Committee on Tidal Hydraulics, U.S.  
1072 Army Engineer Waterways Experiment Station, Vicksburg, MS.  
1073

1074 Komen, G., S. Hasselmann and K. Hasselmann, 1984. On the existence of a fully developed  
1075 wind-sea spectrum. Journal of Physical Oceanography 14, 1271–1285.  
1076  
1077

1078 Kraus, 2008. Engineering of Tidal Inlets and Morphologic Consequences. USACE REPORT  
1079

1080 Kurum, O., Overton, M., Mitasova, H. 2012. "Land Cover and Sediment Layers as Controls of  
1081 Inlet Breaching." 33rd International Conference on Coastal Engineering, P. Lynett and J. M.  
1082 Smith, eds., Santander, Spain, 1–9.  
1083

1084 Lesser, G.R., Roelvink, J.A., van Kester, J.A.T.M., Stelling, G.S., 2004. Development and  
1085 validation of a three-dimensional morphological model. *Coast. Eng.* 51, 883–915.  
1086 <https://doi.org/10.1016/j.coastaleng.2004.07.014>  
1087

1088 Li, Ming, Zhong, L., Boicourt, W. C., Zhang, S, Zhang, D. 2006. Hurricane-induced storm  
1089 surges, currents and destratification in a semi-enclosed bay. *Geophysical Research Letters*, vol  
1090 33 L02604. <https://doi.org/10.1029/2005GL024992>  
1091

1092 Luettich, R. A., Carr, S. D., Reynolds-Fleming, J., Fulcher, C. W., McNinch, J. E., 2002. Semi-  
1093 diurnal seiching in a shallow, micro-tidal lagoonal estuary. *Continental Shelf Research*, 22 (11-  
1094 13), 1669-1681. [https://doi.org/10.1016/S0278-4343\(02\)00031-6](https://doi.org/10.1016/S0278-4343(02)00031-6)  
1095

1096 Malhadas, M. S., Leitao, P., Silva, A., Neves, R. 2009. Effect of coastal waves on sea level in  
1097 Obidos Lagoon, Portugal. *Continental Shelf Research* 29, 1240-1250.  
1098 <https://doi.org/10.1016/j.csr.2009.02.007>  
1099

1100 Mao, M., Xia, M. 2018. Wave-current dynamics and interactions near the two inlets of a shallow  
1101 lagoon-inlet-coastal ocean system under hurricane conditions. *Ocean Modelling*, 129, 124-144.  
1102 <https://doi.org/10.1016/j.ocemod.2018.08.002>  
1103

1104 Melito, L. Postacchini, M. Sheremet, A., Calantoni, J., Zitti, G., Darvini, G., Penna, P., Brocchini,  
1105 M., 2020. Hydrodynamics at a microtidal inlet: Analysis of propagation of the main  
1106 wave components. *Estuarine, Coastal and Shelf Science*, 235, 106603.  
1107 <https://doi.org/10.1016/j.ecss.2020.106603>  
1108

1109 Moffatt & Nichol and Coastal Economics & Business Services, 2014. A study of the economic  
1110 impacts of Oregon Inlet navigability to Dare County, the surrounding Region, and the state of  
1111 North Carolina. Final Report prepared for Dare County, Raleigh, NC, 151 p.  
1112

1113 Mulligan, R. P., Walsh, J. P. , Wadman, H. M., 2015. Storm surge and surface waves in a  
1114 shallow lagoonal estuary during the crossing of a hurricane. Journal of Waterway, Ports,  
1115 Coastal and Ocean Engineering, 141(4). [https://doi.org/10.1061/\(ASCE\)WW.1943-  
1116 5460.0000260](https://doi.org/10.1061/(ASCE)WW.1943-5460.0000260)  
1117

1118 O'Brien, M.P., 1969. Equilibrium flow areas of inlets on sandy coasts. J. Waterw. Harbours Div.  
1119 95, 43–52.  
1120

1121 Olabarrieta, M., Warner, J. C., Kumar, N., 2011. Wave-current interaction in Willapa Bay.  
1122 Journal of Geophysical Research: Oceans., 116 (12), 1-27.  
1123

1124 Orescanin, M. M., Raubenheimer, B., Elgar, S., 2014. Observations of wave effects on inlet  
1125 circulation. Continental Shelf Research, 82 (2014), 37-42.  
1126 <https://doi.org/10.1016/j.csr.2014.04.010>  
1127

1128 Orescanin, M. M., Scooler, J., 2018. Observations of episodic breaching and closure at an  
1129 ephemeral river. Continental Shelf Research, 166, 77-82.  
1130 <https://doi.org/10.1016/j.csr.2018.07.003>  
1131

1132 Peng, M., Xie, L., Pietrafesa, 2004. A numerical study of storm surge and inundation in the  
1133 Croatan–Albemarle–Pamlico Estuary System. Estuarine, Coastal and Shelf Science 59(1), 121-  
1134 137. <https://doi.org/10.1016/j.ecss.2003.07.010>  
1135

1136 Pietrafesa, L. J., Janowitz, G. S. 1985. Physical oceanographic processes affecting larval  
1137 transport around and through North Carolina inlets. United States.  
1138

1139 Pinheiro, J. P., Lopes, C. L., Ribeiro, A., Sousa, M., Dias, J. M., 2020. Tide-surge interaction in  
1140 Ria de Aveiro lagoon and its influence in local inundation patterns. Continental Shelf Research  
1141 (200), 104132. <https://doi.org/10.1016/j.csr.2020.104132>  
1142

1143 Reffit, M., Orescanin, M. M., Massey, C., Raubenheimer, B., Jensen, E. J., Elgar, S., 2020.  
1144 Modeling storm surge in a small tidal two-inlet system. Journal of Waterway, Port, Coastal, and  
1145 Ocean Engineering, 146(6). [https://doi.org/10.1061/\(ASCE\)WW.1943-5460.0000606](https://doi.org/10.1061/(ASCE)WW.1943-5460.0000606)  
1146

1147 Rey, A. J. M. and Mulligan, R. P., 2021. Influence of hurricane wind field variability on real-time  
1148 forecast simulations of the coastal environment. *Journal of Geophysical Research: Oceans*,  
1149 126(1), e2020JC016489. <https://doi.org/10.1029/2020JC016489>  
1150

1151 Salisbury, M. B., Hagen S., 2007. The effect of tidal inlets on open coast storm surge  
1152 hydrographs. *Coastal Engineering* 54(5), 377-391.  
1153 <https://doi.org/10.1016/j.coastaleng.2006.10.002>  
1154

1155 Shen, J., Wang, H., Sisson, M., Gong, W., 2006. Storm tide simulation in the Chesapeake Bay  
1156 using an unstructured grid model. *Estuarine, Coastal and Shelf Science*, vol 68, Issues 1–2, p.  
1157 1-16. <https://doi.org/10.1016/j.ecss.2005.12.018>  
1158

1159 Smallegan, S. M., Irish, J. L., 2017. Barrier island morphological change by bay-side storm  
1160 surge. *Journal of Waterway, Port, Coastal, and Ocean Engineering*, 143(5).  
1161 [https://doi.org/10.1061/\(ASCE\)WW.1943-5460.0000413](https://doi.org/10.1061/(ASCE)WW.1943-5460.0000413)  
1162

1163 Sutherland, J., Peet, A. H., Soulsby, R. L., 2004. Evaluating the performance of morphological  
1164 models. *Coastal Engineering*, 51 (2004), 917 - 939.  
1165 <https://doi.org/10.1016/j.coastaleng.2004.07.015>  
1166

1167 van de Kreeke, J., 1992. Stability of tidal inlets; Escoffier's analysis. *Shore & Beach*, 60., 9–12.  
1168

1169 Thomas, A., Dietrich J. C., Asher, T. G., Bell, M., Copeland, J. H., Cox, A. T., Dawson, C. N.,  
1170 Fleming J. G., Luettich, R. A. Influence of storm timing and forward speed on tides and storm  
1171 surge during Hurricane Matthew. *Ocean Modelling*, 137, 1-19.  
1172 <https://doi.org/10.1016/j.ocemod.2019.03.004>  
1173

1174 van Weerdenburg, R. Pearson, S., van Prooijen, B., Laan, S., Elias, E., Tonnon, P. K., Wang, Z.  
1175 B., 2021. Field measurements and numerical modelling of wind-driven exchange flows in a tidal  
1176 inlet system in the Dutch Wadden Sea. *Ocean & Coastal Management*(215), 105941.  
1177 <https://doi.org/10.1016/j.ocecoaman.2021.105941>  
1178

1179 Velásquez-Montoya, L., Overton, M. F. 2017. Impacts of seasonal forcings on the  
1180 hydrodynamics of Oregon Inlet, NC. In: Proceedings of Coastal Dynamics, Helsingor, Denmark.  
1181 June 12-16, 2017.  
1182  
1183 Velasquez-Montoya, L., Sciaudone, E. J., Mitasova, H., Overton, M., 2018. Observation and  
1184 modeling of the evolution of an ephemeral storm-induced inlet: Pea Island Breach, North  
1185 Carolina, USA. *Continental Shelf Research*, 156, 55-69.  
1186 <https://doi.org/10.1016/j.csr.2018.02.002>  
1187  
1188 Velasquez-Montoya, L., Overton, M. F., Sciaudone, E. J., 2020. Natural and anthropogenic-  
1189 induced changes in a tidal inlet: Morphological evolution of Oregon Inlet. *Geomorphology* 350  
1190 (2020), 106871 1-8. <https://doi.org/10.1016/j.geomorph.2019.106871>  
1191  
1192 Velasquez-Montoya, L., Sciaudone, E. J., Smyre, E., Overton, M. F., 2021a. Vulnerability  
1193 indicators for coastal roadways based on barrier island morphology and shoreline change  
1194 predictions. *Natural Hazards Review* 22(2), [https://doi.org/10.1061/\(ASCE\)NH.1527-](https://doi.org/10.1061/(ASCE)NH.1527-6996.0000441)  
1195 [6996.0000441](https://doi.org/10.1061/(ASCE)NH.1527-6996.0000441)  
1196  
1197 Velasquez-Montoya, L., Sciaudone, E. J., Harrison, R., Overton, M., 2021b. Land cover changes  
1198 on a barrier island: Yearly changes, storm effects, and recovery periods. *Applied Geography*  
1199 135 (2021) 102557. <https://doi.org/10.1016/j.apgeog.2021.102557>  
1200  
1201 Wainwright D. J., Baldock, T. E., 2015. Measurement and modelling of an artificial coastal  
1202 lagoon breach. *Coastal Engineering* 101, 1-16.  
1203 <http://dx.doi.org/10.1016/j.coastaleng.2015.04.002>  
1204  
1205 Wargula, A., Raubenheimer B., Elgar, S., 2014. Wave-driven along-channel subtidal flows in a  
1206 well-mixed ocean inlet. *Journal of Geophysical Research: Oceans*. 119, 2987–3001,  
1207 <https://doi.org/10.1002/2014JC009839>  
1208  
1209 Wargula, A., Raubenheimer B., Elgar, S., 2018. Tidal Flow Asymmetry Owing to Inertia and  
1210 Waves on an Unstratified, Shallow Ebb Shoal, *Journal of Geophysical Research: Oceans*. 123(9),  
1211 6779-6799. <https://doi.org/10.1029/2017JC013625>  
1212

1213 Wargula, A., Sciaudone, E., Velásquez-Montoya, L., Fawcett, K., Amodeo, M., Smyre, E.,  
1214 Tomiczek, T. 2021. Marsh erosion processes near a coastal highway on the Outer Banks, NC.”  
1215 GEO-EXTREME 2021, Savannah, Georgia.  
1216  
1217  
1218  
1219  
1220 Williams M. E. and Stacey M. T., 2016. Tidally discontinuous ocean forcing in bar-built  
1221 estuaries: The interaction of tides, infragravity motions, and frictional control. Journal of  
1222 Geophysical Research Oceans, 121(1), 571-585. <https://doi.org/10.1002/2015JC011166>  
1223  
1224 Willmott, C. J. 1981. On the validation of models. Physical Geography 2(2). 184-194,  
1225 <https://doi.org/10.1080/02723646.1981.10642213>  
1226  
1227 Yin, C., Zhang, W., Xiong, M., Wang, J., Zhou, C., Dou, X., Zhang, J., 2021. Storm surge  
1228 responses to the representative tracks and storm timing in the Yangtze Estuary, China. Ocean  
1229 Engineering, 233, 109020. <https://doi.org/10.1016/j.oceaneng.2021.109020>  
1230  
1231

# APPENDIX E

# Hydrodynamics of a tidal inlet under gray to green coastal protection interventions

1 **Liliana Velasquez-Montoya<sup>1\*†</sup>, Anna Wargula<sup>1†</sup>, Jessica Nangle<sup>1</sup>, Elizabeth Sciaudone<sup>2</sup>,**  
2 **Elizabeth Smyre<sup>3</sup>, Tori Tomiczek<sup>1</sup>**

3 <sup>1</sup>United States Naval Academy, Naval Architecture and Ocean Engineering Department, Annapolis,  
4 Maryland, USA

5 <sup>2</sup>North Carolina State University, Department of Civil, Construction and Environmental Engineering,  
6 Raleigh, North Carolina, USA

7 <sup>3</sup>Dewberry, Raleigh, North Carolina, USA

8 **\* Correspondence:**

9 Liliana Velasquez-Montoya

10 [velasque@usna.edu](mailto:velasque@usna.edu)

11

12 <sup>†</sup>These authors have contributed equally to this work and share first authorship

13

14 **Keywords: numerical modeling, tidal inlets, estuarine shoreline, erosion mitigation,**  
15 **engineering with nature, gray to green engineering spectrum**

16 **Abstract**

17 Fast currents flowing through tidal inlets tend to generate dynamic morphological changes, leading to  
18 management challenges in maintaining navigability and protecting infrastructure on adjacent  
19 shorelines. Hardened or “gray” coastal protection interventions have been implemented worldwide to  
20 stabilize channels and shorelines in tidal inlets systems. Although these structural interventions  
21 typically attain their goals, there is an increasing need to consider nature-based or “green”  
22 interventions that also address system resiliency and environmental impacts by creating habitat and  
23 providing ecological services. For a better implementation of gray to green interventions in tidal  
24 inlets, their effectiveness and their effects on the hydrodynamics of these dynamic coastal systems  
25 need to be understood.

26

27 The hydrodynamic effects of gray to green coastal protection interventions for tidal inlets are  
28 assessed here by exploring six interventions intended to protect against erosion on the estuarine-side  
29 shoreline near the inlet. A field-calibrated numerical model for Oregon Inlet located in North  
30 Carolina, USA, is used to simulate tidal currents under both present conditions and after  
31 implementing a seawall, a set of bendway weirs, a terminal groin extension, a dual-jetty system, a  
32 flood channel relocation, and an island restoration project. Comparisons of time series of flow  
33 velocities in the flood channel along the eroding, estuarine shoreline are used to identify the  
34 effectiveness of each coastal protection alternative at reducing erosive velocities. Geospatial  
35 difference maps are used to determine hydrodynamic changes caused by each alternative throughout  
36 the inlet system.

37

38 With no coastal protection interventions, the velocities along the eroding shoreline exceeded an  
39 erosive threshold velocity (defined as 0.2 m/s) during 50% of the simulated period. Based on an  
40 effectiveness categorization developed within this study, alternatives closer to the green side of the  
41 coastal protection intervention spectrum, such as channel relocation and island restoration, tend to  
42 display the most effectiveness at reducing flow velocities at the eroding shoreline while resulting in  
43 minimal inlet-wide hydrodynamic changes. On the other hand, gray alternatives either cause minimal  
44 (seawall and bendway weirs) or extreme (jetties) changes in velocities throughout the inlet system.  
45 These comparisons of gray and green coastal protection interventions in tidal inlets serves as an  
46 example to inform decision making and alternative selection at other inlet systems.

## 47 **1 Introduction**

48 Tidal inlets, which connect the open ocean to an inland body of water (e.g., a sound or bay), are  
49 naturally prone to dynamic changes, as longshore sediment transport elongates and erodes the  
50 upstream and downstream barrier islands, respectively (Bruun, 1978; Hayes, 1980; Hayes and  
51 FitzGerald, 2013). Given the dynamicity of tidal inlets and their economic relevance for navigation,  
52 recreation, and fisheries, neighboring communities face complex management and engineering  
53 challenges related to these coastal features (Beck and Wang, 2019; Elko et al., 2020; Toso et al.,  
54 2019). With the aim to allow for safe navigation through inlets or to protect infrastructure (e.g.,  
55 roads, electrical and utility lines, private property), inlets have historically been stabilized, in this  
56 context meaning that an inlet is kept open in a somewhat fixed location (Bruun, 1978; Dean and  
57 Dalrymple, 2002). This stabilization can be accomplished through traditional, “gray” engineering  
58 solutions (e.g., hardened structures), including jetties and terminal groins (Bruun, 1978; Dean and  
59 Dalrymple, 2002; Kraus, 2008; Seabergh and Kraus, 2003; Seabergh et al., 1997), using “green”  
60 (e.g., nature-based) engineering alternatives, like channel relocation (Cleary and FitzGerald, 2003;  
61 Vila-Concejo et al., 2004; Rosgen, 2011), or through hybrid approaches. Although gray, green, or  
62 hybrid engineering interventions may accomplish their intended stabilization goals, they can also  
63 lead to other consequences, such as changes in circulation patterns and morphological adjustment of  
64 ebb deltas and channels (Wang and Beck, 2012; Garel et al., 2014; Velasquez-Montoya et al., 2020),  
65 development of scour holes (Lillycrop and Hughes, 1993; Ferrarin et al., 2018; Toso et al., 2019),  
66 severe erosion of the downdrift barrier island (Seabergh and Kraus, 2003; Houston and Dean, 2016).  
67 Morphological adjustments may also create the need for permanent or seasonal dredging and  
68 mechanical sand bypassing (Seabergh and Kraus, 2003; Toso et al., 2019).

69  
70 Natural or anthropogenically-induced hydrodynamic changes of tidal inlets tend to lead to rapid  
71 morphological adjustments on the beaches and ebb delta on the ocean side, where breaking waves  
72 and longshore currents drive sediment transport (Hayes and FitzGerald, 2013). If erosive patterns are  
73 present on the ocean side, they may be mitigated through well-documented solutions such as beach  
74 nourishments and dune restoration (Elko et al., 2020) or hardened structures (Dean and Dalrymple,  
75 2002). However, the estuarine side of a tidal inlet is often made up of a complex flood delta of  
76 meandering channels and shallow shoals, surrounded by low-lying marshlands, where the erosive  
77 forces come from channelized currents, fetch- and depth-limited wind waves, and vessel wakes.  
78 Thus, if an eroding estuarine shoreline develops near a tidal inlet, different coastal protection  
79 approaches are needed compared to those employed on the ocean side shorelines.

80  
81 Green engineering methods, such as Natural and Nature-Based Features (NNBF), have been broadly  
82 used along estuarine shorelines and have been shown to mitigate erosion while also enhancing  
83 ecosystem benefits (Bridges et al., 2015; 2021). Large-scale NNBF solutions for mitigating shoreline  
84 erosion in and near a tidal inlet can include channel relocation (Cleary and FitzGerald, 2003; Vila-

85 Concejo et al., 2004; Rosgen, 2011) and island restoration (Berkowitz and Szimanski, 2020), while  
86 localized NNBF solutions can include living shorelines (Hardaway and Byrne, 1999; Hardaway et  
87 al., 2017; Polk and Eulie, 2018) and thin layer placement (Wilber 1992; Berkowitz et al., 2017;  
88 2019). NNBF and hardened solutions may also be combined, such as by including a rock sill on the  
89 offshore edge of a living shoreline to break wave energy or by armoring eroding banks with  
90 stabilizing material that is natural or native (e.g., root wad or vegetated geogrids).

91  
92 Although several engineering interventions on the gray to green spectrum (SAGE, 2017; Webb et al.,  
93 2019; Singhvi et al., 2022) have been applied to estuarine shoreline erosion problems, their  
94 comparative impacts on circulation patterns near tidal inlet systems are less understood. This study  
95 aims to increase understanding of the hydrodynamic consequences and performance of coastal  
96 protection alternatives near tidal inlets. A field-calibrated numerical model is used to investigate the  
97 changes in flow velocities owing to gray and green coastal protection interventions, with a focus on  
98 the estuarine flood delta. A total of six coastal protection alternatives are considered and compared in  
99 their performance at reducing erosive flow velocities near a estuarine shoreline in the back-barrier  
100 region of a barrier island. An effectiveness scale based on the duration of flow velocities below an  
101 erosion threshold is proposed and used to categorize the performance of the six alternatives.  
102 Geospatial analysis of flow velocities at peak tidal flows are also presented to illustrate the  
103 differences between hydrodynamic effects at local scales (i.e., shoreline) and inlet scales created by  
104 each coastal protection alternative.

105  
106 The study is completed for Oregon Inlet, North Carolina (NC), on the east coast of the United States,  
107 and results are discussed in a generalized context for their potential application to other tidal inlet  
108 systems where gray or green coastal protection alternatives need to be considered. Erosion and loss  
109 of marshland along estuarine shorelines have been reported worldwide (Bendoni et al., 2016;  
110 FitzGerald and Hughes, 2019; Murray et al., 2022), and such problems are exacerbated near tidal  
111 inlets where fast currents can undercut shorelines causing marshland collapse. The novelty of this  
112 work resides in the exploration of the hydrodynamic effectiveness of gray to green coastal protection  
113 alternatives around deep and steep shoreline-adjacent channels created by tidal inlets, which are  
114 intrinsically different environments from the typical shallow and gentle sloping estuarine shorelines.

## 115 **2 Study Site**

116 Oregon Inlet, which was formed by a storm in 1846, is the northernmost tidal inlet on the barrier  
117 island system known as the Outer Banks of North Carolina, USA (Figure 1). It is the only stable inlet  
118 within nearly 210 km of shoreline and provides connectivity between the Albemarle-Pamlico Sound,  
119 the Intracoastal Waterway, and the Atlantic Ocean. The inlet is approximately 1 km wide in its most  
120 constricted section and has a complex system of shoals and channels with maximum depths of 15 m  
121 in the deepest channels. The ebb and flood deltas extend approximately 3.5 km offshore and 10 km  
122 inland, respectively. The flood delta on the estuarine side of the inlet is composed of three main  
123 channels, herein referred to as the north, center, and south flood channels (Figure 1).

124 The main transportation and coastal infrastructure surrounding Oregon Inlet are, respectively, the 4.5  
125 km-long Marc Basnight Bridge that crosses the inlet and a terminal groin that was constructed along  
126 the northern edge of the southern barrier island (Hatteras Island) in 1991. The terminal groin was  
127 built to protect the abutment of the original bridge crossing the inlet, the Herbert C. Bonner Bridge,  
128 from potential scouring due to the southern migration of the inlet. Since then, the northern barrier  
129 island (Bodie Island) has extended to the southwest (Joyner et al., 1998) and the main channel of the  
130 inlet has rotated counterclockwise (Velasquez-Montoya et al., 2020). As the inlet's main channel has

131 rotated, the channels and shoals in the flood delta have evolved as well. Aerial imagery from 2003 to  
132 2021 have shown that the south channel has curved and encroached into the estuarine shoreline of  
133 Hatteras Island, causing shoreline erosion rates on the order of 3.4 to 4.5 m/yr (Dunn et al., 2019;  
134 Tomiczek et al., 2022).

135 The south flood channel meanders along the estuarine shoreline on the edge of the Pea Island  
136 National Wildlife Refuge, located on Hatteras Island (Figure 1(C)). The channel's thalweg depths  
137 vary from 6 m to 15 m, relative to the North American Datum of 1988 (NAVD88), creating steep  
138 slopes with the adjacent shoreline that range between 15% (~ 1:7) to 45% (~ 1:2). Flow velocities in  
139 this channel are ebb-dominated and reach up to 1 m/s under typical conditions. The eroding estuarine  
140 shoreline adjacent to the south flood channel is 1-km long, with areas covered by marshes, salt flats,  
141 and small pocket beaches (Velasquez-Montoya et al., 2021). Erosion on the estuarine side of the  
142 barrier island results in loss of habitat for migratory birds and an increased proximity of the estuarine  
143 waters to the only roadway that connects the refuge and the communities along Hatteras Island with  
144 mainland North Carolina.

145 Tides on the Outer Banks of North Carolina are semidiurnal with an ocean-side range of 1 m. Waves  
146 are seasonal; the most energetic period occurs from October to April when extratropical storms  
147 generate significant waves heights above 3 m mostly from the northeast. During the remaining half of  
148 the year, wave energy is low, except when tropical storms and hurricanes reach the area (Inman and  
149 Dolan, 1989; Velasquez-Montoya et al., 2020). On the estuarine side, the Albemarle-Pamlico Sound  
150 is a well-mixed estuary with average depths of 5 m. Flow stratification has only been reported near  
151 the riverine discharges located more than 20 km away from the tidal inlet (Giese et al., 1985).

## 152 **3 Methods**

### 153 **3.1 Numerical model setup**

154 Given that the Albemarle-Pamlico Sound is a well-mixed estuary, a two-dimensional depth-averaged  
155 numerical model based on Delft3D (Lesser et al., 2004) was set up to simulate the hydrodynamic  
156 conditions at Oregon Inlet under present conditions and different coastal protection alternatives. The  
157 hydrodynamic model extends 35 km alongshore and 27 km cross-shore, including Mainland NC to  
158 the west and ocean depths of about 25 m to the east. The hydrodynamic model has two subdomains  
159 that allow for increased resolution near the inlet, where the computational cells reach 15 m in length.  
160 Water level boundary conditions are obtained from large-scale simulations of the Advanced  
161 Circulation Model (ADCIRC) (Westerink et al., 2008; Luettich and Westerink, 2004), part of Coastal  
162 Emergency Risk Assessment (CERA) archives.

163 The hydrodynamic model is coupled with the third-generation wave model Simulating Waves  
164 Nearshore (SWAN) (Booij et al., 1999). The wave model extends 70 km alongshore with Oregon  
165 Inlet located in the middle of the domain to prevent boundary artifacts from reaching the area of  
166 interest. Wave boundary conditions are extracted from the closest wave buoy to the site, Station  
167 44095 - Oregon Inlet, owned by the University of North Carolina System Coastal Studies Institute  
168 (black star in Figure 1(B)). Spatially constant, time-varying wind speed and direction are extracted  
169 from the closest meteorological station to Oregon Inlet, the National Oceanic and Atmospheric  
170 Administration's (NOAA's) Oregon Inlet Marina, NC - Station ID: 8652587 (green triangle in Figure  
171 1(C)), and are used for wind-wave growth in SWAN and wind-driven flows in Delft3D.

172

173 The bathymetry and topography of the model were obtained from different sources, thus interpolation  
174 and smoothing were performed within Delft3D to retain realistic features while preventing  
175 interpolation artifacts from multi-source data merging. The bathymetry of the ocean-side was  
176 obtained from the 10-m resolution digital elevation model of the North Carolina Floodplain Mapping  
177 Project (Blanton et al., 2008). The bathymetry of the Albemarle-Pamlico Sound was extracted from  
178 NOAA’s H11032 hydrographic survey, and the depths of the inlet channels and shoals were obtained  
179 from the 2019 U.S. Army Corps of Engineers (USACE) hydrographic survey (Figure 1(C)). All  
180 depths and elevations were converted to meters and referenced from the NAVD88 vertical datum.  
181 The terminal groin in the south shoulder of Oregon Inlet is schematized as a thin dam, which is an  
182 infinitely thin object that prevents flow between adjacent computational cells (Deltares, 2022). The  
183 piles of the Marc Basnight Bridge are schematized as porous plates using spatially varying energy  
184 loss coefficients ranging from 0.03 to 3.75 dependent on the bridge pile sizes relative to the size of  
185 the computational cells (Deltares, 2022).

186 The numerical model for Oregon Inlet has been calibrated and validated for previous hydrodynamic  
187 and morphological studies for the inlet. The details of the calibration and validation can be found in  
188 Velasquez-Montoya and Overton (2017), Velasquez-Montoya et al. (2020), and Velasquez-Montoya  
189 et al. (submitted). In summary, model calibration and validation has been performed on the ocean and  
190 estuarine side of the inlet by comparing simulated currents, water levels, and waves with field data  
191 from 2014, 2019, and 2020. In the latest model evaluation phase using 15 days measurements from  
192 2020, the model was found to accurately represent the hydrodynamics at the south flood channel of  
193 the inlet with Willmott Skill scores for depth-averaged velocities ranging from 0.90 to 0.93, which  
194 rate as excellent performance in accordance with Willmott (1981).

### 195 **3.2 Simulations**

196 A 30-day period of typical oceanographic and atmospheric conditions in the absence of major storms  
197 in 2020 was selected to simulate the hydrodynamics of Oregon Inlet under six estuarine coastal  
198 protection alternatives (Table 1) and present conditions. A calm period was selected as it better  
199 represents the daily hydrodynamic conditions in the back-barrier region and along the tidal inlet and  
200 because previous studies suggest that daily stresses may dominate over episodic storms in causing  
201 long term marsh erosion (Leonardi et al., 2018). All simulations were forced with tides, waves, and  
202 winds from August 12 to September 11, 2020, with a spin up period of 15 days to ensure  
203 hydrodynamic conditions stabilized from initial conditions. This period also corresponds to the  
204 model validation period, where water levels and depth-averaged velocities were accurately simulated  
205 (Velasquez-Montoya et al., submitted). A summary of the boundary conditions is shown in Figure 2.  
206 Water levels on the ocean boundary included neap and spring conditions, with a maximum total  
207 water level of 1.00 m (NAVD88). Significant wave heights predominantly from the east quadrant  
208 ranged between 0.36 m and 1.86 m and wind speed reached a maximum of 12.50 m/s with varying  
209 directions.

210 The “present condition” simulation includes the existing features as close as possible to 2020 (e.g.,  
211 terminal groin and Basnight Bridge piles) without any potential coastal protection alternative on the  
212 estuarine side of the inlet. The present condition simulation is used as a benchmark for comparison of  
213 depth-averaged velocities with simulations that include one inlet intervention at a time. Comparisons  
214 of time-series of depth-averaged velocities, herein referred to as “velocities,” for the sake of  
215 simplicity, are completed initially at the south flood channel to assess alternative performance, as  
216 explained in section 3.4. Thereafter, additional time-series comparisons are presented at three other  
217 channels that compose the inlet (i.e., main, north, center in Figure 1(C)). Lastly, geospatial difference

218 maps of velocities during peak ebb and peak flood conditions are presented for all alternatives  
219 relative to the present condition simulation to better understand the spatial distribution of  
220 hydrodynamic effects throughout the system.

### 221 **3.3 Coastal protection alternatives**

222 After a review of coastal protection alternatives historically implemented for estuarine shorelines,  
223 tidal inlets, and deep channels, ten alternatives ranging from gray to green to hybrid structures were  
224 identified as the most commonly used in these environments. Those alternatives included channel  
225 relocation, island restoration, thin layer placement, living shorelines, living shorelines with sills, soil  
226 bioengineering (including vegetated geogrids and root wads), bendway weirs, seawalls, terminal  
227 groins, and jetties. Of this initial set of alternatives, six are investigated here (Table 1). The six  
228 alternatives were selected based on their historical use in or near tidal inlets, their potential to reduce  
229 constant high erosive flows near a deep channel, and the possibility to reasonably schematize them in  
230 the numerical model. Their intended purposes, as well as known advantages and disadvantages in  
231 terms of coastal processes are listed in Table 1.

232 The alternatives that were discarded include living shorelines (with and without sills), thin layer  
233 placement, and soil bioengineering. Living shorelines typically require gentle slopes (Hardaway et  
234 al., 2017) that are not necessarily present near flood channels of tidal inlets. Thin layer placement,  
235 which is recommended to enhance vertical marsh resilience to sea level rise (Raposa et al., 2020), is  
236 not expected to enhance resilience to horizontal erosion as it cannot reduce fast, erosive flows along  
237 channel banks. Some soil bioengineering techniques such as live posts and live cribwalls, which are  
238 extensively used in riverine systems to strengthen the soil in exposed banks and slow high flows  
239 (Mississippi Watershed Management Organization, 2010; U.S. Department of Agriculture, Forest  
240 Service, National Technology and Development Program, 2003), are not feasible in a submerged  
241 bank with brackish and cold water. It should be noted that although these alternatives are not  
242 considered here, their use in other environments have proven to be adequate. The remaining six  
243 alternatives considered in this study and their schematization within the numerical model are  
244 described in the following paragraphs.

245 Seawalls are a traditional option to stop erosion along banks and shorelines by hardening the edge  
246 between land and water. Seawalls (also known as bulkheads and revetments) are vertical, hardened  
247 structures made of rock, concrete, metal, or other non-native material and constructed along the  
248 eroding shoreline (Dean and Dalrymple, 2002; USACE, 1995; 2002). The seawall evaluated in this  
249 study extends 900 m along the eroding shoreline (red line in Figure 3(A)). The structure was  
250 schematized in the numerical model as a thin dam, in the same way the existing terminal groin is  
251 included in the model. The line of the thin dam follows the grid cell edges closest to the shoreline.

252 Bendway weirs are submerged rock structures positioned on the outside bankline of a riverbend,  
253 typically in a unidirectional-flow channel, angled upstream towards the flow in order to slow erosive  
254 velocities (Davinroy, 1990; Winkler, 2003). These structures have been built along bends in the  
255 Mississippi River (Derrick et al., 1994), the Rio Grande River (Scurlock et al., 2012), and other rivers  
256 in the US. Although bendway weirs have not been used in coastal channels with bi-directional tidal  
257 flow, this alternative was considered to explore potential flow reduction of the prevalent currents at  
258 the site. Inside the south flood channel of Oregon Inlet, ebb currents are nearly 3 times larger than the  
259 flood currents (Velasquez-Montoya et al., submitted), leading to asymmetric forces along the channel  
260 banks. Bendway weirs angled into these strong ebb flows may help reduce the dominant cause of  
261 erosion. Following Winkler (2003), the dimension and angles of four bendway weirs were calculated,

262 with alongshore spacing of 150 m, cross-channel lengths of 80 m (spanning the deepest part of the  
263 flood channel), and angled 20 degrees from the shoreline towards the ebb currents (red lines in Figure  
264 3(B)). A 2D weir feature was added in Delft3D that results in energy loss due to constriction of the  
265 flow. The energy loss is converted into an effective friction coefficient and added in the momentum  
266 equation (Deltares, 2022). In the model, the weirs are defined by their start and end nodes in the  
267 domain. Weir heights meet local USACE navigation channel depths (4.5 m depth relative to  
268 NAVD88). The default friction coefficient of 1 was used as recommended in the Delft3D manual  
269 (Deltares, 2022).

270 Terminal groins are similar to jetties, but typically shorter and built on the tip of a barrier island to  
271 stabilize its position and interrupt inlet migration (Dean and Dalrymple, 2002). The terminal groin  
272 extension considered here was based on similar examples at Indian River Inlet, DE and Ocean City  
273 Inlet, MD, where shoreline armoring extends along the barrier island into the estuarine shoreline or  
274 the channels in the flood delta to redirect flows. Given the present conditions at Oregon Inlet, a  
275 terminal groin extension was started at the existing revetment and extending perpendicular across the  
276 width of the deepest portion of the entrance to the south flood channel. In Delft3D, this alternative  
277 was schematized as a 240 m long thin dam (Deltares, 2022) (red line in Figure 3(C)), similar to the  
278 seawall, but located across the channel instead of along the shoreline. Different from the bendway  
279 weirs, this alternative completely blocks flow along its length.

280 Jetties are single or double rocky, shore-perpendicular structures built to confine tidal flow through  
281 and control migration of and sediment deposition in tidal inlets (Brunn, 1978; Kraus, 2008). The jetty  
282 system considered in this study was based on a dual jetty design for Oregon Inlet by the USACE  
283 (2001). The jetty system has a 3055-m long northern jetty and a southern jetty, which connects to the  
284 existing terminal groin for a total length of 2004 m (red lines in Figure 3(D)). In the north jetty, a  
285 305-m long weir at mean sea level (- 0.04 m NAVD88) is included to allow sedimentation in a 0.24  
286 km<sup>2</sup> deposition basin with a depth of 6.13 m below NAVD88 (USACE, 2001). Within Delft3D, this  
287 alternative was schematized as a combination of thin dams for the jetties' extensions into the ocean, a  
288 2D weir with a friction coefficient of 1 (default, Deltares, 2022) and a change in the bathymetry of  
289 the inlet based on that proposed by USACE (2001) to align the main channel with the center of the  
290 jetties (dashed red lines in Figure 3(D)).

291 Channel relocation involves changes to the inlet channels' locations through dredging and sediment  
292 placement with the aim to deepen some channels and close others (Rosgen, 2011) while increasing or  
293 maintaining a tidal prism that would keep the inlet open (Cleary and FitzGerald, 2003). This  
294 alternative was implemented in the numerical model by modifying the bathymetry in the domain.  
295 The south flood channel was filled to a depth of 1.80 m NAVD88 (dotted red lines, Figure 3(E)) and  
296 the center channel was deepened from depths ranging from 3.00 - 4.50 m (NAVD88) to a new  
297 maximum depth along the thalweg of 7.50 m NAVD88 (dashed red lines, Figure 3(E)). It should be  
298 noted that the change in bathymetry is instantaneous; in other words, the simulation is spun up with  
299 the bathymetric changes already in place, rather than accounting for dredging and sediment  
300 placement periods.

301 Island restoration (or shoal creation and restoration) is a method involving building back land lost to  
302 erosion (Berkowitz and Szimanski, 2020). Island restoration projects involve sediment placement as  
303 well as planting vegetation for the creation of habitat. The island restoration alternative investigated  
304 in this study entails rebuilding the back-barrier region in the north tip of Hatteras Island (just south of  
305 Oregon Inlet) that has been rapidly eroding. In the model, bathymetric and topographic changes were  
306 completed to account for this alternative; the addition of vegetation on the island is not accounted for.

307 A total of 830 m of shoreline were considered to be restored. The new estuarine shoreline position  
308 was set to that of October 1989, prior to the construction of the terminal groin in Oregon Inlet. The  
309 location of this shoreline was obtained from georectified historical aerial images taken by the North  
310 Carolina Department of Transportation. The restored island has an elevation of 0.60 m NAVD88 (red  
311 area, Figure 3(F)); this elevation corresponds to the average elevation at which well-developed,  
312 healthy marsh vegetation is present at the site (Wargula et al., 2021). The topography of the back-  
313 barrier was leveled up to the 0.60 m contour, for a total restored area of 77,340 m<sup>2</sup>. At the edge of the  
314 restored shoreline, the bathymetry gets deeper up to a depth of 5 m (NAVD88) with a slope into the  
315 flood channel of 12.5% (1:8). Similar to other alternatives, the simulation is spun up with the new  
316 bathymetry and topography already in place.  
317

### 318 **3.4 Evaluation of alternatives performance**

319 The potential for the alternatives to mitigate erosion along the shoreline was quantified by examining  
320 the duration of along-channel velocities below an erosion threshold relative to the median sediment  
321 size as defined by Hjulström (1939). Median sediment grain size diameters  $D_{50}$  in the flood channel,  
322 measured in 2019, range from 22 to 351  $\mu\text{m}$  (medium silt to medium sand on the Wentworth scale)  
323 (Wentworth, 1922), with fines typically close to the shoreline edge and coarser grains in the middle  
324 of the flood channel (Wargula et al., 2021). For this range of sediment grain sizes, the minimum  
325 velocity needed to erode the particles, according to the Hjulström diagram, is approximately 0.20  
326 m/s. This velocity is therefore considered the threshold for comparison with simulations' outputs.

327 Along-channel velocities at the location "South," shown as a green marker in Figure 1, were  
328 extracted for all alternatives and the present condition simulations. This point is located in the more  
329 convex section of the shoreline where the historical erosion rates are the highest (Tomiczek et al.,  
330 2022). Velocities in the south flood channel were rotated into along- and cross-channel velocity  
331 components using principal axes (Emery and Thomson, 2001). In the present condition simulation,  
332 the velocities near the shoreline are ebb-dominated, with a principal axis angle of 132 degrees  
333 (azimuthal) (Emery and Thomson, 2001). The principal axis angles for most alternatives were within  
334 3 degrees of that in the present condition, except for the seawall and channel relocation alternatives,  
335 which had principal axis angles of 140 degrees and 110 degrees (azimuthal), respectively, resulting  
336 from veering of the flows compared to the present condition.

337 In the present condition, along-channel velocities at the south flood channel are below the 0.20 m/s  
338 erosion threshold 49% of the time. Given that historical data indicates that the shoreline suffers  
339 erosion under this condition, it is expected that a reduction in the duration of velocities greater or  
340 equal to 0.20 m/s, would result in a reduction of erosional processes at the shoreline. Based on this  
341 assumption, the main criterion to define the effectiveness of an alternative is the percentage of time  
342 that velocities are below the erosion threshold during typical flow conditions. To facilitate  
343 comparison and categorization between alternatives, three levels of effectiveness at reducing erosion  
344 were defined. The categories are Least Effective, Moderately Effective, and Highly Effective,  
345 corresponding to velocities below the erosion threshold (0.20 m/s) for less than 50% (almost no  
346 change in erosive flows relative to the present condition), 50% to 80%, and more than 80% of the  
347 time, respectively (Table 2).

348 Changes to velocities across the flood delta and inlet mouth were also examined to determine impacts  
349 on inlet circulation caused by each alternative. Along-channel velocities inside the main, north, and  
350 center channels (green circles in Figure 1(C)) are compared between alternatives and the present

351 condition for the duration of the simulation. In addition, instantaneous geospatial difference maps of  
352 velocity magnitude in the present condition simulation and each alternative simulation (i.e., Velocity  
353 Present Condition - Velocity Alternative) were examined during maximum ebb (August 23rd at 0:00)  
354 and maximum flood (August 23rd at 06:00) to determine other large-scale impacts that the set of  
355 alternatives may have on circulation patterns in the inlet system.

## 356 **4 Results**

### 357 **4.1 Changes in along-channel flows at the eroding estuarine shoreline**

358 For the present condition simulation, along-channel (major axis) velocities ranged -0.58 to 0.33 m/s  
359 (positive to the southeast, during the flood), with a median velocity of -0.06 m/s, consistent with ebb-  
360 dominated flows. Cross-channel (minor axis) velocities were small, ranging from -0.03 to 0.02 m/s  
361 (positive to the southwest), suggesting strong channelization. The cross-channel (minor axis) flow  
362 magnitudes were less than 0.03 m/s for all alternatives except for the channel relocation and island  
363 restoration alternatives, which had cross-channel flows ranging -0.07 to 0.06 m/s and -0.12 to 0.05  
364 m/s, respectively, potentially owing to the reduced channelization of flows in these alternatives.

365 Within each model simulation, total velocity magnitude is less than 0.02 m/s greater than the  
366 maximum along-channel velocities at the south flood channel. The percentage of time below the  
367 erosion threshold for the total velocity magnitude and the along-channel velocity component is also  
368 similar for each model configuration. To preserve the flood/ebb asymmetry, the along-channel  
369 component of velocity was used to evaluate the performance of each alternative.

370 Figure 4 summarizes the along-channel velocities in the present condition and for all of the  
371 alternatives. The median flows for all alternatives are negative, consistent with ebb-dominant  
372 velocities in the south flood channel, except for the island restoration case, which has a median of 0  
373 m/s, consistent with no flow (i.e., the island was dry) for the majority of the time series. The  
374 strongest median velocity, -0.06 m/s, is simulated in the present condition; all alternatives reduce the  
375 magnitude of this median velocity, with the seawall causing the least reduction in velocity (median  
376 velocity of -0.05 m/s) and island restoration causing the greatest reduction (median velocity of 0  
377 m/s). Maximum flood and ebb flows are also reduced relative to present conditions for all cases  
378 except for the seawall case, which had maximum ebb flows of -0.61 m/s, slightly larger in magnitude  
379 than the maximum ebb flows of -0.58 m/s in the present condition.

### 380 **4.2 Alternative effectiveness at reducing erosional flows**

381 Figure 5 shows comparisons of the along-channel velocity in the south flood channel during the  
382 present condition (red curves) and alternatives (black points) over the simulated period. The seawall  
383 and bendway weir alternatives resulted in an average change in along-channel velocity of 0.02 m/s.  
384 This change in velocities is small compared to that caused by other alternatives; thus, they are not  
385 shown in Figure 5. The terminal groin extension, channel relocation, and island restoration  
386 alternatives show constant flow reduction through the simulated period. The jetties also show a  
387 consistent reduction of flow velocities, but not as significant as that caused by the other three  
388 alternatives displayed in Figure 5. The near-zero velocities for island restoration correspond to times  
389 when the island is dry (Figure 5(D)).

390 Table 3 presents the relative difference in along-channel velocity, the percentage of time that the  
391 along-channel velocity was below the erosion threshold, and the resulting effectiveness rating (Table  
392 2) based on the time below the erosion threshold (Section 3.3). Relative difference is calculated as

393 the median of the absolute value of the difference between the present condition and alternative  
394 along-channel velocity divided by the present condition along-channel velocity. The positive sign on  
395 the relative differences presented in Table 3 represents a percent reduction in median velocity relative  
396 to the present condition.

397 The two alternatives with the largest impact on velocities (>92% reduction in along-channel velocity  
398 and below the erosion threshold 100% of the time), were channel relocation and island restoration  
399 (Table 3). The channel relocation alternative still allowed flows through the south flood channel  
400 (Figure 5(C)), but with consistently smaller velocities, particularly on flood compared to ebb. The  
401 island restoration alternative was only intermittently wet (Figure 5(D)) and so, although velocities  
402 exceeded the erosion threshold a few times, these “erosion events” were brief.

403 The terminal groin extension also had a significant impact on reducing velocities in the south flood  
404 channel (73% reduction in along-channel velocity and below the erosion threshold 100% of the time,  
405 Table 3). The flood velocities, in particular, were reduced from a maximum of 0.33 m/s to a  
406 maximum of 0.01 m/s (Figure 5(A)), potentially owing to blocking and redirecting of flows by the  
407 groin at the flood channel entrance. Ebb flows were also significantly reduced from a maximum of -  
408 0.58 m/s to -0.18 m/s (Figure 5(A)).

409 The jetties were moderately effective, decreasing the along-channel velocities in the south flood  
410 channel by 34% (Table 3), with consistent impacts across tidal cycles (Figure 5(B)) that led to an  
411 increase in time below the erosion threshold (74%, Table 3). The seawall and bendway weirs were  
412 the least effective, with almost no change in the time below the erosion threshold and only a 7% and  
413 8% reduction in along-channel velocity, respectively (Table 3). It should be noted that of all the  
414 alternatives, the seawall is the only one that is not directly blocking or redirecting flows, thus, its  
415 relatively low effect on flow reduction was expected. The discussion on this topic is expanded in  
416 Section 5.1.

#### 417 **4.3 Changes in along-channel velocity in different channels**

418 The impact that each alternative may have on circulation patterns in the other channels that form the  
419 inlet system were investigated by examining the change in along-channel velocities inside the main,  
420 north, and center channels (locations shown in Figure 1(C)), shown in Figure 6. Negligible change in  
421 along-channel velocities (less than 3% median relative difference and less than 1 degree change in  
422 principal flow axis angle) occurred in the simulations for the seawall, bendway weirs, and island  
423 restoration alternatives in all three locations (Figure 6).

424 The jetties resulted in the largest changes to along-channel velocities in all the channels. In the main,  
425 north, and center channels, the principal flow axes were rotated 20 degrees clockwise, 27 degrees  
426 counterclockwise, and 43 degrees counterclockwise relative to those in the present condition,  
427 respectively. In the main channel, flows were more channelized (cross-channel velocity range  
428 decreased from 0.26 m/s in the present condition to 0.18 m/s in the jetties alternative) and the  
429 magnitudes of maximum flood and ebb flows were reduced relative to the present condition (Figure  
430 6(A)), with a median relative difference of 16%. On flood, along-channel flows were increased in the  
431 north flood channel (Figure 6(B)) and decreased in the south and center flood channels (Figures 4  
432 and 6(C)). On ebb, flows were decreased in the south and north flood channels (Figures 4 and 6(B))  
433 and increased in the center flood channel (Figure 6(C)). Overall the median relative difference in  
434 along-channel velocities were 39% and 18% for the north and center channels, respectively. These  
435 changes in flows through the three flood channels are a consequence of the relocation and rotation of  
436 the main channel under this alternative (Figure 3(D)).

437

438 The largest impacts of the terminal groin extension and channel relocation simulations were located  
439 in the center flood channel (median relative difference of 15% and 22%, respectively), where the  
440 magnitudes of both the maximum flood and ebb were increased (Figure 6(C)), potentially to  
441 compensate for the reduction of flows in the south flood channel through blocking and channel in-  
442 filling (Figure 4). Changes in the along-channel flows in the north and main channels were small,  
443 with a median relative difference of less than 10% and less than 6% in each location for both  
444 alternatives (Figures 6(A) and 6(B)).

#### 445 **4.4 Spatial changes in velocities across the inlet during peak tidal flows**

446 Instantaneous difference maps of velocity vector subtraction between the present condition  
447 simulation and each alternative simulation were created during maximum ebb (August 23rd at 0:00)  
448 and maximum flood (August 23rd at 06:00) to determine other large-scale impacts that the coastal  
449 protection alternatives may have on circulation patterns along shoals and channels (Figures 7 and 8).  
450 Positive differences (red contours) indicate a reduction in velocity and negative differences (blue  
451 contours) indicate an increase in velocity in the alternative simulation, compared with the present  
452 condition (Figures 7 and 8).

453 The seawall and bendway weirs had only small local effects in their vicinities (Figure 4) and  
454 negligible impact on flows outside of the south flood channel (not shown). The largest impact on  
455 flows by the seawall was a small area adjacent to its southern end where velocity reduction was ~0.2  
456 m/s. The bendway weirs also reduced flows inside the south flood channel, with less than 0.1 m/s  
457 flow reduction along the shoreline and less than 0.1 m/s flow increase away from the shoreline, with  
458 slightly larger impacts on maximum ebb compared to maximum flood, owing to the angling of the  
459 weirs into the ebb currents.

460 The terminal groin extension and jetties drove changes in flow patterns across the entire inlet system  
461 during maximum flood and ebb (Figures 7(A) and 7(B)). The terminal groin extension resulted in  
462 similar changes in circulation patterns for both maximum flood and ebb, with significant ( $> 0.40$  m/s)  
463 flow reduction within and to the south of the south flood channel and minor flow reduction on the  
464 ebb delta. The results indicate significant flow increase ( $> 0.50$  m/s) on the tip of the groin extension  
465 and increase of up to 0.1 m/s on the rest of the flood delta. The main difference between flood and  
466 ebb is a larger change in flow velocities (both reduction and increase) in the vicinity of the groin,  
467 during maximum ebb flows.

468 The jetties simulation showed tidal asymmetry in changes to the circulation patterns (Figures 7(C)  
469 and 7(D)). During the maximum ebb, the flows between the jetties on the ebb delta were significantly  
470 increased, while flows on the flood delta and on the external side of the jetties on the ebb delta were  
471 mainly reduced. During the maximum flood, patterns of change in velocities are complex; flow  
472 reduction is simulated in the vicinity of each flood channel (also shown in Figure 6) and adjacent to  
473 the jetties, while flow velocities increase mainly between the jetties, in shallow regions on the flood  
474 delta, and further alongshore on the ocean side. Flow increase at the weir location (Figure 3(D)) is  
475 more noticeable during maximum ebb but also present during maximum flood (circular blue region  
476 in the center of red shades along the north jetty), while flow reduction is predominant in the area of  
477 the sediment basin.

478 Flows throughout the inlet system also were altered by the channel relocation and island restoration  
479 alternatives (Figure 8), although the magnitude of the differences was small compared to those

480 simulated for the jetties and the terminal groin extension alternatives (Figure 7). The channel  
481 relocation alternative increased flows through the center flood channel (also shown in Figure 6(C)),  
482 reducing flows through the south flood channel and northern part of the flood delta. There is some  
483 tidal asymmetry to this alternative, mainly in the region between the center and south flood channel  
484 and the inlet mouth. The channel relocation alternative also increases velocities inside the main inlet  
485 channel.

486 The island restoration alternative had the largest impact near the eroding shoreline, with significant  
487 flow reduction inside the south flood channel and significant flow increase just to the west of the  
488 entrance to the south flood channel (Figure 8). The flow is also increased on the center and northern  
489 part of the flood delta, potentially to compensate for the closed-off south flood channel. The strong  
490 gradient between the regions of velocity reduction and increase implies that the erosional flows are  
491 displaced, rather than fully reduced near the eroding region.

## 492 **5 Discussion**

493 Overall, island restoration, channel relocation, and terminal groin extension alternatives were the  
494 most effective at both reducing velocity magnitudes (73% to 100%) and increasing the time below  
495 the erosion threshold (100%) in the south flood channel (Table 3). However, the wider impact of  
496 these coastal protection interventions on circulation across the delta and inlet must also be  
497 considered, owing to the potential for morphological evolution and hydrodynamic patterns that could  
498 shorten project life durations. For example, despite island restoration being rated as the most  
499 effective alternative at reducing velocities along the shoreline, the increased currents along the “new  
500 shoreline” could lead to fast erosion of the restored land, thus potentially decreasing the durability of  
501 a project of this kind. Table 4 presents a summary of the effects of each alternative along the  
502 shoreline, alongside the effects on velocities in the surrounding areas.

503 Based on the metrics developed here, alternatives closer to the green side of the coastal protection  
504 intervention spectrum (SAGE, 2017; Webb et al., 2019; Singhvi et al., 2022), such as channel  
505 relocation and island restoration, tend to display the most effectiveness at reducing flow velocities at  
506 the eroding shoreline. These alternatives also tend to have a more localized effect on velocities,  
507 without significantly modifying the overall hydrodynamics throughout the inlet system. On the other  
508 hand, the alternatives on the gray side of the coastal protection spectrum, cause two opposite effects  
509 on the hydrodynamics of the inlet; they either cause minimal or extreme changes in velocities. While  
510 the seawall and bendway weirs didn't cause significant changes in currents (Table 3), the terminal  
511 groin extension and the jetties proved to be interventions that would change the flow velocities  
512 throughout the inlet system (Figure 7). Since the seawall cuts off the interaction between the  
513 shoreline and the channel rather than reducing the velocities, its effects become relevant for  
514 morphological impacts downstream and local scour. Such considerations are discussed in Section  
515 5.1.

516 All of the coastal protection alternatives explored here have been implemented to a certain extent in  
517 different inlet systems worldwide, except bendway weirs, which have not been tested in coastal or  
518 tidal environments. Instead, this structural solution to channel bend erosion has been limited to  
519 riverine environments. Thus, the true benefits and drawbacks of bendway weirs need to be explored  
520 further via physical modeling and more detailed studies with varying degrees of vertical flow  
521 blockage, spacing, and directions. Studies of this kind already exist for rivers (Davinroy, 1990;  
522 Winkler, 2003; Lyn and Cunningham, 2010; Siefken et al., 2021), but the effects of this structural  
523 measure under the effects of tides and waves remains to be explored. Other research opportunities

524 include accounting for the effects of vegetation in alternatives like island restoration, as marsh fields  
525 have been shown to protect shorelines in estuarine environments (Gittman et al., 2014; Paquier et al.,  
526 2016).

527 While each alternative was explored separately, future work could look into combinations of  
528 alternatives as they could lead to further reductions of flow velocities. Combining the benefits of gray  
529 and green coastal protection alternatives could result in a solution that is effective in high-velocity  
530 environments while also providing ecological benefits by creating habitat for local species (Gittman  
531 et al., 2014; Sutton-Grier et al., 2015). For example, implementing temporary hard structures to  
532 mitigate extreme events until a nature-based solution is fully established (Bouma et al., 2014) or  
533 combining wetlands with hardened structures to improve flood defenses in an estuary (Smolders et  
534 al., 2020) are hybrid methods that have been implemented or proposed that combine benefits from  
535 both ends of the gray-to-green coastal protection spectrum.

536 The results presented here are intended to illustrate the ability of gray-to-green coastal protection  
537 infrastructure at reducing flows that could erode back-barrier regions surrounded by deep inlet  
538 channels. The coastal interventions studied here and their effects on the hydrodynamics of the inlet  
539 are exploratory in nature, and any project must consider hydrodynamic, morphological, and  
540 environmental parameters unique to the site, as well as economic, social, and policy considerations,  
541 to find an optimal solution or combination of solutions.

## 542 **5.1 Morphological Considerations**

543 Morphological simulations were not conducted in this study; however, the potential impact on  
544 morphology caused by the coastal protection alternatives is examined through the discussion of the  
545 large-scale changes in circulation patterns. It is also noted that morphological evolution may, in turn,  
546 change the hydrodynamics. Such feedback between hydrodynamics and morphology could then  
547 potentially affect the effectiveness of a given alternative in mitigating erosion in the long term.

548 The jetties, terminal groin extension, and channel relocation alternatives had the largest impacts on  
549 velocity across the flood delta, with the jetties also significantly impacting the ebb delta. Large  
550 velocity changes could lead to significant morphological evolution of the channels and shoals along  
551 new pathways, leading to disruptions of navigation routes and changes to the dredging needs of the  
552 inlet. Increased velocities near the tip of the structures (i.e., jetties, terminal groin extension) indicate  
553 the potential for scour hole development as reported in other inlets by Lillycrop and Hughes (1993),  
554 Ferrarin et al. (2018) and Toso et al. (2019). In addition, the jetties, terminal groin extension, and  
555 channel relocation alternatives (Figures 7 and 8) all show varying degrees of velocity increase inside  
556 the main channel of the inlet, which could scour existing structures like the bridge piles and the  
557 existing rubble mound terminal groin.

558 The island restoration alternative has the most significant velocity impact in the south flood channel,  
559 where flows were reduced to near-zero by the creation of new land that remained dry through most of  
560 the modeled period. However, the strong increase of flows (>1.5 m/s) at the entrance to the south  
561 flood channel may lead to a new channel cutting across the restored island. This option may  
562 temporarily “turn back the clock” on erosion without solving the problem in the long term. Similarly,  
563 relocating the south flood channel would rely on dredging maintenance, as active channel rotation,  
564 shoal movement and morphological changes due to storms and day-to-day processes have been  
565 reported at this inlet (Humberston et al., 2019; Velasquez-Montoya et al., 2020).

566 Although the seawall was not effective in reducing along-channel velocities, the scoring metric used  
567 here may not fairly account for the erosion control provided by this alternative. Hardening of the  
568 bank does not reduce flows, but stops erosion by creating a barrier between the shoreline and the  
569 estuarine currents. In addition, this alternative has the advantage that its overall impact on velocities  
570 is localized and minimal, suggesting that any morphological evolution would mainly occur in the  
571 south flood channel, and not impact the rest of the flood delta. It should be noted however, that  
572 hardened structures on a shoreline can interfere with sediment sources and longshore transport (Dean  
573 and Dalrymple, 2002) causing erosion downstream on unprotected shorelines.

## 574 **5.2 Broader implications to other inlets and coastal systems**

575 The results presented for Oregon Inlet help illustrate the varying spatial and temporal effects that  
576 different coastal protection alternatives have on the flow velocities in tidal inlets. Gray to green  
577 coastal protection interventions tend to show varying influence on inlet systems, causing changes in  
578 flow velocities that range in scale from tens of meters around the vicinity of the intervention to  
579 kilometers expanding along ebb and flood deltas. The spatial extent where flow velocities change has  
580 important consequences on inlet stability, navigation, and the inlet ecology. Based on the results  
581 presented here, green interventions like island restoration and channel relocation result in minimal  
582 inlet-wide hydrodynamic changes, compared to gray alternatives like jetties, which have the potential  
583 to completely modify the hydrodynamics at an inlet.

584  
585 A general comparison of gray to green coastal protection interventions near tidal inlets serves as a  
586 first step to differentiating the effectiveness and consequences of using a range of alternatives in  
587 different parts of the engineering spectrum. It should be noted that for each of the alternatives  
588 presented here, further technical analysis including changes in geometry, location, and response to  
589 extreme events should be performed to gain in-depth knowledge of design features needed for  
590 specific locations. For example, in the case of channel relocations, Vila-Concejo et al. (2004) suggest  
591 that the position of the new channel is a key factor for the success of these types of interventions. For  
592 groins and shore-normal structures used for sediment trapping, length, elevation, porosity and  
593 shoreline characteristics should be considered for successful designs (Basco and Pope, 2004).  
594 Estuarine shoreline restoration that typically entails sediment nourishments and planting of  
595 vegetation needs to consider sediment consolidation, restored land elevation, relative sea level rise,  
596 and local vegetation characteristics (Campbell et al., 2005).

597  
598 Whether a gray or a green coastal protection alternative is better suited for erosional processes near a  
599 tidal inlet will depend on the particular morphology and environmental forces (i.e., wave climate,  
600 tidal range, geological setting, existing infrastructure, sediment and vegetation characteristics)  
601 present at the inlet. Nevertheless, assessing the effectiveness of coastal protection alternatives would  
602 benefit from standardized engineering metrics of success during initial project planning phases. In  
603 this regard, the effectiveness categories for coastal protection alternatives based on percent duration  
604 of an erosion threshold (Table 2) developed here can be applied in any other tidal inlet system where  
605 erosion may threaten critical infrastructure, private properties, or valuable habitat and resources.

606  
607 Even with hydrodynamic and morphological modeling, there is always a risk with implementing  
608 coastal protection alternatives in dynamic environments such as tidal inlets. Construction of gray or  
609 green interventions in tidal inlets could result in unintended consequences due to natural and  
610 anthropogenic influences that may occur through decadal and century timescales. In-depth feasibility  
611 studies for the gray to green spectrum of coastal protection measures should include environmental,  
612 economic, and societal impacts. In addition, monitoring efforts of pre- and post-project construction

613 would allow for assessments of project effectiveness and success and provide the required  
614 information for adaptive management in future projects at other dynamic tidal inlet systems.

## 615 **6 Conflict of Interest**

616 The authors declare that the research was conducted in the absence of any commercial or financial  
617 relationships that could be construed as a potential conflict of interest.

## 618 **7 Author Contributions**

619 Conceptualization, L.V.-M., A.W., T.T., E.J.S., and E.S.; Methodology, L.V.-M., A.W., T.T., E.J.S.,  
620 and E.S.; Software, L.V.-M.; Validation, L.V.-M. and A.W.; Formal Analysis, L.V.-M., A.W., and  
621 J.N.; Investigation, L.V.-M., A.W., and J.N.; Writing—Original Draft Preparation, L.V.-M. and  
622 A.W.; Writing—Review and Editing, L.V.-M., A.W., T.T., E.J.S., and E.S.; Visualization, L.V.-M.,  
623 A.W., and J.N.; Supervision, L.V.-M.; Project Administration, L.V.-M., A.W., T.T., E.J.S., and E.S.;  
624 Funding Acquisition, L.V.-M., A.W., T.T., E.J.S., and E.S.; All authors have read and agreed to the  
625 published version of the manuscript.

## 626 **8 Funding**

627 This project was funded by the North Carolina Department of Transportation (NCDOT) Grant  
628 #2020-09 and National Science Foundation (NSF) CBET Grant #2110262. Any opinions, findings,  
629 conclusions, or recommendations expressed in this material are those of the authors and do not  
630 necessarily reflect the views of the NCDOT, the NSF, the United States Naval Academy, North  
631 Carolina State University, or Dewberry. This paper does not constitute a standard, specification, or  
632 regulation.

## 633 **9 Acknowledgments**

634 We acknowledge former United States Naval Academy students Brent Schwartz, Katie Miller, Kyle  
635 Cortez, Austin McWherter, and Benjamin Johnson, who put forth preliminary designs for the channel  
636 relocation and island restoration alternatives as part of their Capstone Senior Design Project in 2020.

## 637 **10 References**

638 Basco, D. R., and Pope, J. (2004). Groin functional design guidance from the coastal engineering  
639 manual. *Journal of Coastal Research* SI(33), 121-130.

640  
641 Beck, T. M., and Wang, P. (2019). Morphodynamics of barrier-inlet systems in the context of  
642 regional sediment management, with case studies from west-central Florida, USA. *Ocean & Coastal*  
643 *Management*. 177, 31-51. doi: 10.1016/j.ocecoaman.2019.04.022

644  
645 Bondoni, M., Mel, R., Solari, L., Lanzoni, S., Francalanci, S., and Oumeraci, H. (2016). Insights into  
646 lateral marsh retreat mechanism through localized field measurements, *Water Resour. Res.* 52, 1446–  
647 1464. doi:10.1002/2015WR017966

648  
649 Berkowitz, J. F., Piercy, C., Welp, T., and VanZomeran, C. (2019). Thin Layer Placement: Technical  
650 definition for the U.S. Army Corps of Engineers Applications. ERDC TN-19-1. Vicksburg, MS: U.S.  
651 Army Corps of Engineers Engineer Research and Development Center.

652

653 Berkowitz, J. F., VanZomeran, C., and Piercy, C. (2017). Marsh restoration using thin layer sediment  
654 addition: initial soil evaluation. *Wetland Science & Practice*. 34, 13-17.  
655

656 Berkowitz, J. F., and Szimanski, D. M. (2020). Documenting Engineering with Nature®  
657 Implementation within the US Army Corps of Engineers Baltimore District - Completed Projects and  
658 Opportunities for Chronosequence Analysis. ERDC/TN EWN-20-3. Vicksburg, MS: US Army  
659 Engineer Research and Development Center. doi: 10.21079/11681/38141  
660

661 Blanton, B., Madry, S., Galluppi, K., Gamiel, K., Lander, H., Reed, M., et al. (2008). Report for the  
662 State of North Carolina Floodplain Mapping Project: Coastal Flood Analysis System. A RENCI  
663 Technical Report TR-08-08. Topographic/BathymetricData.  
664

665 Booij, N., Ris, R. C., and Holthuijsen, L. H. (1999). A third-generation wave model for coastal  
666 regions: 1. Model description and validation. *J. Geophys. Res.* 104, 7649–7666. doi:  
667 10.1029/98JC02622  
668

669 Bouma, T. J., van Belzen, J., Balke, T., Zhu, Z., Airoidi, L., Blight, A. J., et al. (2014). Identifying  
670 knowledge gaps hampering applications of intertidal habitats in coastal protection: Opportunities &  
671 steps to take. *Coastal Engineering*. 87, 147-157. doi: 10.1016/j.coastaleng.2013.11.014  
672

673 Bridges, T. S., Wagner, P. W., Burks-Copes, K. A., Bates, M. E., Collier, Z. A., Fischenich, C. J., et  
674 al. (2015). Use of Natural and Nature-Based Features (NNBF) for Coastal Resilience Final Report.  
675 ERDC SR-15-1. Vicksburg, MS: U.S. Army Corps of Engineers Engineer Research and Development  
676 Center.  
677

678 Bridges, T. S., King, J. K., Simm, J. D., Beck, M. W., Collins, G., Lodder, Q., et al. (2021).  
679 International Guidelines on Natural and Nature-Based Features for Flood Risk Management.  
680 Vicksburg, MS: U.S. Army Engineer Research and Development Center. doi: 10.21079/11681/41946  
681

682 Bruun, P. (1978). *Stability of Tidal Inlets. Theory and Engineering*. Trondheim, Norway: Elsevier  
683 Scientific Publishing Company.  
684

685 Campbell, T., Benedet L., and Thomson G. (2005). Design considerations for barrier island  
686 nourishments and coastal structures for coastal restoration in Louisiana. *Journal of Coastal Research*,  
687 SI(44), 186-202.  
688

689 Cleary, W. J., and FitzGerald, D. M. (2003). Tidal Inlet Response to Natural Sedimentation Processes  
690 and Dredging-Induced Tidal Prism Changes: Mason Inlet, North Carolina. *J. Coast. Res.* 19, 1018-  
691 1025.  
692

693 Davinroy, R. D. (1990). Bendway Weirs, A New Structural Solution to Navigation Problems  
694 Experienced on the Mississippi River, P.I.A.N.C. A.I.P.C.N. Bulletin.  
695

696 Dean, R. G., and Dalrymple, R. A. (2002). *Coastal Processes with Engineering Applications*.  
697 Cambridge University Press. doi: 10.1017/CBO9780511754500  
698

699 Deltares (2022). Delft3D-FLOW. Simulation of multi-dimensional hydrodynamic flows  
700 and transport phenomena, including sediments. User Manual Hydro-Morphodynamics. Version: 4.05,  
701 SVN Revision: 75129.

702  
703 Derrick, D. L., Pokrefke, T. J., Boyd, M. B., Crutchfield, J. P., and Henderson, R. R. (1994). Design  
704 and development of bendway weirs for the Dogtooth Bend Reach, Mississippi River. Hydraulic  
705 Model Investigation. Technical Report HL-94-10. Vicksburg, MS: U.S. Army Corps of Engineers  
706 Engineer Research and Development Center.  
707  
708 Dunn, M., Sciaudone, E., and Velasquez-Montoya, L. (2019). Estuarine shoreline erosion driven by  
709 flood channel proximity at Pea Island, NC. Presented at ASBPA National Coastal Conference,  
710 Myrtle Beach, SC, USA, 22–25 October 2019.  
711  
712 Elko, N., Mckenna, K., Briggs, T. R., Brown, N., Walther, M., and York, D. (2020). Best  
713 management practices for coastal inlets. *Shore & Beach*. 88, 75-83. doi: 10.34237/1008838  
714  
715 Emery, W. J., and Thomson, R. E. (2001). *Data Analysis in Physical Oceanography*, 2nd ed.  
716 Amsterdam: Elsevier Sci.  
717  
718 Ferrarin, C., Madricardo, F., Rizzetto, F., McKiver, W., Bellafiore, D., Umgiesser, G., et al. (2018).  
719 Geomorphology of scour holes at tidal channel confluences. *Journal of Geophysical Research: Earth*  
720 *Surface*. 123, 1386– 1406. doi: 10.1029/2017JF004489  
721  
722 FitzGerald, D. M., and Hughes, Z. (2019). Marsh Processes and Their Response to Climate Change  
723 and Sea-Level Rise. *Annual Review of Earth and Planetary Sciences*. 47(1), 481-517. doi:  
724 10.1146/annurev-earth-082517-010255  
725  
726 Garel E., Sousa, C., Ferreira, O., and Morales, J. A. (2014). Decadal morphological response of an  
727 ebb-tidal delta and down-drift beach to artificial breaching and inlet stabilisation. *Geomorphology*.  
728 216, 13-25. doi: 10.1016/j.geomorph.2014.03.031  
729  
730 Giese, G. L., Wilder, H. B., and Parker, G. G. (1985). Hydrology of major estuaries and sounds of  
731 North Carolina. U.S. Geological Survey Water Supply Paper 2221, 108. doi: 10.3133/wsp2221  
732  
733 Gittman, R. K., Popowich, A. M., Bruno, J. F., and Peterson, C.H. (2014). Marshes with and without  
734 sills protect estuarine shorelines from erosion better than bulkheads during a Category 1 hurricane.  
735 *Ocean & Coastal Management*. 102, 94-102. doi: 10.1016/j.ocecoaman.2014.09.016  
736  
737 Hardaway, C. S., and Byrne, R.J. (1999). *Shoreline Management in Chesapeake Bay*. Report.  
738 College of William and Mary, Virginia Institute of Marine Science, Gloucester Points, VA. doi:  
739 10.21220/V5DB1X  
740  
741 Hardaway, C. S., Milligan, D. A., Wilcox, C., and Duhring, K. (2017). Living shoreline design  
742 guidelines for shore protection in Virginia’s estuarine environments. SRAMSOE #463. Gloucester  
743 Point, VA: Virginia Institute of Marine Science. doi: 10.21220/V5CF1N  
744  
745 Hayes, M. O. (1980). General morphology and sediment patterns in tidal inlets. *Sedimentary*  
746 *Geology*. 16, 139-156. doi: 10.1016/0037-0738(80)90009-3  
747  
748 Hayes, M. O., and FitzGerald, D. M. (2013). Origin, evolution, and classification of tidal inlets. *J.*  
749 *Coast. Res. Sp. Issue* 6, 14–33. doi: 10.2112/SI\_69\_3  
750

751 Houston J. R., and Dean, R. G. (2016). Erosional Impacts of Modified Inlets, Beach Encroachment,  
752 and Beach Nourishment on the East Coast of Florida. *J. Coast. Res.* 32, 227–240. doi:  
753 10.2112/JCOASTRES-D-15-00105.1  
754

755 Hjulström, F. (1939). Transportation of Detritus by Moving Water: Part 1. Transportation. SP 10:  
756 Recent Marine Sediments, Special Volume. 5-31.  
757

758 Humberston, J., Lippmann, T., and McNinch, J. (2019). Observations of wave influence on alongshore  
759 ebb-tidal delta morphodynamics at Oregon Inlet, NC. *Marine Geology.* 418, 106040. doi:  
760 10.1016/j.margeo.2019.106040  
761

762 Inman, D. L., and Dolan, R. (1989). The Outer Banks of North Carolina: budget of sediment and inlet  
763 dynamics along a migrating barrier system. *J. Coast. Res.* 5, 193-237.  
764

765 Joyner, B. P., Overton, M. F., and Fisher, J. S. (1998). Post-stabilization morphology of Oregon Inlet,  
766 NC. International Conference on Coastal Engineering, Copenhagen, Denmark, June 22-26, 1998. doi:  
767 10.1061/9780784404119.237  
768

769 Kinzli, K. D., and Myrick, C. (2009). Bendway weirs: Could they create habitat for endangered Rio  
770 Grande Silvery Minnow. *River Research and Applications.* doi: 10.1002/rra.1277  
771

772 Kraus, N. C. (2008). Engineering of Tidal Inlets and Morphologic Consequences. *Handbook of*  
773 *Coastal and Ocean Engineering.* 867-900. doi: 10.1142/9789812819307\_0031  
774

775 Lesser, G. R., Roelvink, J. A., van Kester, J. A. T. M., and Stelling, G. S. (2004). Development and  
776 validation of a three-dimensional morphological model. *Coast. Eng.* 51, 883–915. doi:  
777 10.1016/j.coastaleng.2004.07.014  
778

779 Leonardi, N., Carnacina, I., Donatelli, C., Ganju, N. K., Plater, A. J., Schuerch, M., et al. (2018).  
780 Dynamic interactions between coastal storms and salt marshes: A review. *Geomorphology.* 301, 92-  
781 107. doi: 10.1016/j.geomorph.2017.11.001  
782

783 Lillycrop W. J., and Hughes S. A. (1993). Scour Hole Problems Experienced by the Corps of  
784 Engineers; Data Presentation and Summary. Miscellaneous Paper CERC-93-2. Vicksburg, MS: U.S.  
785 Army Corps of Engineers Engineer Research and Development Center.  
786

787 Luettich, R. A., and Westerink, J. J. (2004). Formulation and numerical implementation of the 2D/3D  
788 ADCIRC Finite Element Model Version 44.XX.  
789

790 Lyn, D. A., and Cunningham, R. (2010). A laboratory study of bendway weirs as a bank erosion  
791 countermeasure. Joint Transportation Research Program, FHWA/IN/JTRP-2010/24. Final Report.  
792 doi: 10.5703/1288284314249  
793

794 Mississippi Watershed Management Organization. (2010). A Guide to Bank Restoration Options for  
795 Large River Systems: Part II Bioengineering Installation Manual MWMO Watershed Bulletin 2010-  
796 3. 95 pp.  
797

798 Murray, N. J., Worthington, T. A., Bunting, P., Duce, S., Hagger, V., Lovelock, C., et al. (2022).  
799 High-resolution mapping of losses and gains of Earth's tidal wetlands. *Science* 376(6594), 744-749.  
800 doi: 10.1126/science.abm9583.  
801

802 Paquier, A.-E., Haddad, J., Lawler, S., and Ferreira, C. M. (2016). Quantification of the Attenuation  
803 of Storm Surge Components by a Coastal Wetland of the US Mid Atlantic, *Estuaries and Coasts*. 40,  
804 930-946. doi: 10.1007/s12237-016-0190-1  
805

806 Polk, M. A., and Eulie, D. O. (2018). Effectiveness of living shorelines as an erosion control method  
807 in North Carolina. *Estuaries and Coasts*. 41, 2212-2222. doi: 10.1007/s12237-018-0439-y  
808

809 Raposa, K., Wasson, K., Nelson, J., Fountain, M., West J., Endris, C., et al. (2020). Guidance for  
810 thin-layer sediment placement as a strategy to enhance tidal marsh resilience to sea-level rise.  
811 Published in collaboration with the National Estuarine Research Reserve System Science  
812 Collaborative.  
813

814 Rosgen, D. L. (2011). Natural Channel Design: Fundamental Concepts, Assumptions, and Methods.  
815 In A. Simon, S.J. Bennett, & J.M. Castro (Eds.), *Stream Restoration in Dynamic Fluvial Systems:  
816 Scientific Approaches, Analyses, and Tools*, Geophysical Monograph Series 194, pp. 69–93.  
817 Washington, D.C.: American Geophysical Union.  
818

819 SAGE (System Approach to Geomorphic Engineering). (2017). Natural and Structural Measures for  
820 Shoreline Stabilization. *Systems Approach to Geomorphic Engineering*, 7  
821

822 Scurlock, S. M., Baird, D. C., Cox, A. L., and Thornton, C. I. (2012). Bendway weir design – Rio  
823 Grande physical model. Colorado State University, Engineering Research Center, Bureau of  
824 Reclamation Technical Service Center.  
825

826 Seabergh, W. C., Cialone, M. A., and Stauble, D. K. (1997). Impacts of inlet structures on channel  
827 location. *Coastal Engineering Proceedings*, 1(25). doi: 10.9753/icce.v25.%p  
828

829 Seabergh, W. C., and Kraus, N. C. (2003). Progress in Management of Sediment Bypassing at  
830 Coastal Inlets: Natural Bypassing, Weir Jetties, Jetty Spurs, and Engineering Aids in Design, *Coastal  
831 Engineering Journal*, 45, 533-563. doi: 10.1142/S0578563403000944  
832

833 Siefken, S., Ettema, R., Posner, A., Baird, D., Holste, N., Dombroski, D. E., et al. (2021). Optimal  
834 Configuration of Rock Vanes and Bendway Weirs for River Bends: Numerical-Model Insights.  
835 *Journal of Hydraulic Engineering*, 147. doi: 10.1061/(ASCE)HY.1943-7900.0001871  
836

837 Singhvi, A., Luijendijk, A. P., and van Oudenhoven, A. P. E. (2022). The grey – green spectrum: A  
838 review of coastal protection interventions. *Journal of Environmental Management*. 311, 114824. doi:  
839 10.1016/j.jenvman.2022.114824  
840

841 Smolders, S., João Teles, M., Leroy, A., Maximova, T., Meire, P., and Temmerman, S. (2020).  
842 Modeling Storm Surge Attenuation by an Integrated Nature-Based and Engineered Flood Defense  
843 System in the Scheldt Estuary (Belgium). *J. Mar. Sci. Eng.* 8, 27. doi: 10.3390/jmse8010027  
844

845 Sutton-Grier, A. E., Wowk, K., and Bamford, H. (2015). Future of our coasts: The potential for  
846 natural and hybrid infrastructure to enhance the resilience of our coastal communities, economies,  
847 and ecosystems. *Environmental Science & Policy*. 51, 137-148. doi: 10.1016/j.envsci.2015.04.006  
848

849 Tomiczek, T., Sciaudone, E. J., Velasquez-Montoya, L., Smyre, E. J., Wargula, A., Fawcett, K., et al.  
850 (2022). Investigation of Barrier Island Highway and Marsh Vulnerability to Bay-Side Flooding and  
851 Erosion. *Journal of Marine Science and Engineering*. 10, 734. doi: 10.3390/jmse10060734  
852

853 Toso, C., Madricardo, F., Molinaroli, E., Fogarin, S., Kruss, A., Petrizzo, A., et al. (2019). Tidal inlet  
854 seafloor changes induced by recently built hard structures. *PloS one*, 14(10), e0223240. doi:  
855 10.1371/journal.pone.0223240  
856

857 USACE (U.S. Army Corps of Engineers). (1995). *Design of Coastal Revetments, seawalls and*  
858 *bulkheads*. EM-1110-2-1614. Vicksburg, MS: U.S. Army Corps of Engineers Engineer Research  
859 and Development Center.  
860

861 USACE (U.S. Army Corps of Engineers). (2002). *Coastal Engineering Manual*. Washington, DC:  
862 USACE.  
863

864 USACE (U.S. Army Corps of Engineers). (2001). Manteo (Shallowbag) Bay North Carolina.  
865 Supplement No. 2 Final supplement No. III. Environmental Impacts Statement. USACE Wilmington  
866 District.  
867

868 U.S. Department of Agriculture, Forest Service, National Technology and Development Program.  
869 (2003). *A Soil Bioengineering Guide for Streambank and Lakeshore Stabilization*. FS-683P. San  
870 Dimas, CA.  
871

872 Velasquez-Montoya, L., and Overton, M. F. (2017). Impacts of seasonal forcings on the  
873 hydrodynamics of Oregon Inlet, NC. *Coastal Dynamics*, Helsingør, Denmark.  
874

875 Velasquez-Montoya, L., Overton, M. F., and Sciaudone, E. J. (2020). Natural and anthropogenic-  
876 induced changes in a tidal inlet: Morphological evolution of Oregon Inlet. *Geomorphology*. 350,  
877 106871. doi: 10.1016/j.geomorph.2019.106871  
878

879 Velasquez-Montoya, L. Sciaudone, E. J., Harrison R. B., and Overton, M. F. (2021). Land cover  
880 changes on a barrier island: Yearly changes, storm effects and recovery periods. *Applied Geography*.  
881 135, 102557. doi: 10.1016/j.apgeog.2021.102557  
882

883 Vila-Concejo, A., Ferreira, O., Morris, B. D., Matias, A., and Dias, J. M. A. (2004). Lessons from  
884 inlet relocation: examples from Southern Portugal. *Coastal Engineering*. 51, 967-990. doi:  
885 10.1016/j.coastaleng.2004.07.019  
886

887 Wang, P. and Beck, T. (2012). Morphodynamics of an anthropogenically altered dual-inlet system:  
888 John's Pass and Blind Pass, west-central Florida, USA. *Marine Geology*. 291-294, 162-175. doi:  
889 10.1016/j.margeo.2011.06.001  
890

891 Wargula, A., Sciaudone, E., Velásquez-Montoya, L., Fawcett, K., Amodeo, M., Smyre, E., et al.  
892 (2021). Marsh Erosion Processes near a Coastal Highway on the Outer Banks, NC. *GEO-EXTREME*  
893 2021, Savannah, Georgia.

894  
895 Webb, B., Dix, B., Douglass, S., Asam, S., Cherry, C., and Buhring, B. (2019). Nature-Based  
896 Solutions for Coastal Highway Resilience: An Implementation Guide. Report FHWA-HEP-19-042,  
897 229.  
898  
899 Wentworth, C. K. (1922). A scale of grade and class terms for clastic sediments. *The Journal of*  
900 *Geology*. 20, 377-392.  
901  
902 Westerink, J. J., Luettich, R. A., Feyen, J. C., Atkinson, J. H., Dawson, C., Roberts, H. J., et al.  
903 (2008). A basin to channel scale unstructured grid hurricane storm surge model applied to southern  
904 Louisiana. *Monthly Weather Review*. 136, 833–864. doi: 10.1175/2007MWR1946.1  
905  
906 Wilber, P. (1992). Thin-layer disposal: Concepts and terminology. *Environmental Effects of*  
907 *Dredging Information Exchange Bulletin D-92-1*. Vicksburg, MS: U.S. Army Engineer Waterways  
908 Experiment Station.  
909  
910 Willmott, C. J. (1981). On the validation of models. *Physical Geography*. 2. 184-194. doi:  
911 10.1080/02723646.1981.10642213  
912  
913 Winkler, M. F. (2003). Defining Angle and Spacing of Bendway Weirs. Technical Report, CHETN-  
914 IX-12. Vicksburg, MS: U.S. Army Corps of Engineers Engineer Research and Development Center.

## 915 **1 Data Availability Statement**

916 The numerical model outputs presented in this study are available on request from the corresponding  
917 author.

918

919 **Figure Captions**

920 Figure 1. Study Area. (A) Location of the Outer Banks of North Carolina relative to the East Coast of  
921 the United States. (B) The Outer Banks with the hydrodynamic and wave model domains indicated in  
922 black solid and black dashed-dot lines, respectively. (C) Oregon Inlet, where blue shades indicate  
923 depths in meters relative to NAVD88.

924 Figure 2. (A) Water levels relative to NAVD88, (B) wave heights, and (C) wind speed boundary  
925 conditions used for the 30-day simulation period versus time. Colors indicate the heading of the  
926 waves and winds.

927 Figure 3. Coastal protection alternative (red highlights) on bathymetry (blue color contours) and the  
928 existing island shape (black outline) for (A) Seawall, (B) Bendway Weirs, (C) Terminal Groin  
929 Extension, (D) Jetties, where the dashed red line indicates the new position of central channel, the  
930 dotted black line indicates the area of the sedimentation basin, and the yellow line indicates the  
931 position of the weir (E) Channel Relocation, where dashed line indicates new flood channel position  
932 and dotted line indicates filled region (old channel) (F) Island Restoration.

933 Figure 4. Box-and-whisker plots of depth-averaged along-channel velocity versus present condition  
934 and alternative at the south flood channel. Negative velocities indicate ebb flows, while positive  
935 velocities indicate flood flows. The horizontal red line indicates the median velocity. The vertical  
936 length of the blue boxes indicates the 25th and 75th percentiles of velocity. The black whiskers  
937 extend to the maximum and minimum velocities, excluding outliers, which are represented with red  
938 plus symbols.

939 Figure 5. Depth-averaged along-channel velocity in the “South” location near the shoreline (Figure 1)  
940 during the present condition (red line) and under coastal protection alternatives (black points) versus  
941 time. Positive velocity is to the southeast (flooding), negative velocity is to the northeast (ebbing).  
942 Alternatives include the (A) terminal groin extension, (B) jetties, (C) channel relocation, and (D)  
943 island restoration; seawall and bendway weir alternatives are not shown.

944 Figure 6. Box-and-whisker plots of depth-averaged along-channel velocity versus present condition  
945 and alternatives at the (A) main channel, (B) north flood channel, and (C) center flood channel.  
946 Negative velocities indicate ebb flows (bay to ocean direction), while positive velocities indicate  
947 flood flows (ocean to bay direction). The horizontal red line indicates the median velocity. The  
948 vertical length of the blue boxes indicates the 25th and 75th percentiles of velocity. The black  
949 whiskers extend to the maximum and minimum velocities.

950 Figure 7. Difference in depth-averaged velocity for the present conditions and for the (A, B) terminal  
951 groin extension and (C, D) jetties during (A, C) maximum ebb and (B, D) maximum flood. Red and  
952 blue colors indicate reduced and increased velocity, respectively, relative to present conditions.

953 Figure 8. Difference in depth-averaged velocity for the present conditions and for the (A, B) channel  
954 relocation and (C, D) island restoration during (A, C) maximum ebb and (B, D) maximum flood. Red  
955 and blue colors indicate reduced and increased velocity, respectively, relative to present conditions.

956

957 **Tables**

958 Table 1. Coastal protection alternatives with advantages and disadvantages of their use near tidal inlets. Note that this list  
 959 does not include challenges related to local permitting or economic considerations.

<b>Alternative</b>	<b>Intended Purpose</b>	<b>Advantages</b>	<b>Disadvantages</b>
Seawall	Prevent flow-sediment contact in order to stop erosion at a shoreline or bank.	Stop channel encroachment into the back-barrier beach/marsh. Little maintenance unless damaged by storm events or scour. Minimizes the effects of wave action on the shoreline.	Potential impact to adjacent beaches and shorelines by interfering with longshore transport (Dean and Dalrymple, 2002). Does not facilitate creation of additional habitat and reduces the intertidal zone required for marsh survival. Vulnerable to scour.
Bendway Weirs	Slow down currents along the exterior bank of a curved channel.	Suitable for deep channels. Reduces uni-directional flow velocities against the exterior side of river bends. Could create feeding and habitat for certain fish species (Kinzli and Myrick, 2009).	Flow velocities tend to increase near the tip of the structure causing scour (Lyn and Cunningham, 2010; Siefken et al., 2021). Mostly used in rivers, not tested in tidal inlets. Could have negative impacts on submerged aquatic vegetation.
Terminal Groin Extension	Slow down currents by blocking tidal flows and possibly trap sediments.	Can be attached to existing revetment structures. Little maintenance unless damaged by storm events or scour.	Potential impact to adjacent beaches and shorelines by interfering with longshore transport. Vulnerable to scour. Could have negative impacts on tidal habitats.
Jetties	Redirect flows at the inlet to keep a main channel open and slow down currents away from the central channel.	Commonly used in tidal inlets. Stabilizes the inlet channel and ensures navigation in the central part of the inlet.	Interrupt longshore transport along the ocean shoreline, creating the need for sediment bypassing mechanisms. Mostly intended for channel stabilization and navigation rather than for estuarine shoreline protection.
Channel Relocation	Redirect flows at the inlet to slow down flow velocities near erosional hotspots.	Have been successfully used in tidal inlets (Vila-Concejo et al., 2004). Beneficial use of dredged materials. Provides opportunity for habitat restoration. Uses a combination of dredging and natural inlet processes to redirect strong currents away from eroding shoreline.	Requires regular maintenance dredging to maintain intended profile. Impacts existing shoals and islands and their associated habitat. Potential impacts on navigation routes.
Island Restoration	Rebuild lost land and widen the barrier island.	Beneficial use of dredged materials from navigation channels. Potential habitat creation and enhancement.	Requires regular maintenance dredging to maintain intended profile. Impacts existing shoals and islands and their associated habitat. Potential impacts on existing navigation routes.

961 Table 2. Effectiveness categories for coastal protection alternatives based on percent duration below the erosion threshold

**Effectiveness of Alternatives Percent time along-channel velocity is below the erosion threshold, 0.20 m/s**

Least Effective	< 50%
Moderately Effective	50% to 80%
Highly Effective	> 80%

962  
963  
964

Table 3. Depth-averaged along-channel comparison in the south flood channel

Alternative	Relative Difference (%)	Percent time below Erosion Threshold (%)	Effectiveness
Seawall	7	47	Least Effective
Bendway Weirs	8	49	Least Effective
Terminal Groin Extension	73	100	Highly Effective
Jetties	34	74	Moderately Effective
Channel Relocation	92	100	Highly Effective
Island Restoration	100	100	Highly Effective

965

966 Table 4. Coastal protection alternatives with their effects on velocities within the inlet system.

Alternative	Effects along estuarine shoreline	Effects on other channels and shoals
Seawall	Minimum effects in flow reduction/increase.	Minimum effects in the overall hydrodynamics of the inlet.
Bendway Weirs	Minimum effects in flow reduction/increase.	Minimum effects in the overall hydrodynamics of the inlet.
Terminal Groin Extension	Third most effective alternative at reducing velocities in the south flood channel and along the shoreline	Increases velocities on the northern half of the flood delta and reduces velocities on the ebb delta.
Jetties	Reduces velocities in the south flood channel	Has the most significant effects on the overall hydrodynamics of the inlet. Changes velocities in all channels and throughout the ebb and flood deltas.
Channel Relocation	Second most effective alternative at reducing velocities in the south flood channel and along the shoreline	Increases velocities in the delta and creates different flow patterns in the flood delta with flow increase in the center.
Island Restoration	Most effective alternative at reducing velocity along the original shoreline	Increases velocities at the edge of the “restored” shoreline.

967

# APPENDIX F

# APPENDIX F

## Field Data Database File Descriptions

Data	File Name	Data Collection Method/ Instrument	Data type (spatial or temporal)	Data Format (GIS, text file, figure)	Location	Start Date and End Date	Datum and Units	Notes	Data Collector
Shoreline survey	20210308_sl	Trimble R12	spatial	GIS	Whole survey area	20210308-20210308	NAD83 State Plane NC ft NAVD88 ft	Modified to include shoreline classifications	NCSU
Shoreline survey	20210503_sl	Trimble R1	spatial	GIS	Whole survey area	20210503	NAD83 State Plane NC ft	Modified to include shoreline classifications	NCSU
Shoreline survey	20210908_sl	Trimble R12	spatial	GIS	Whole survey area	20210908	NAD83 State Plane NC ft NAVD88 ft	Modified to include shoreline classifications	NCSU
Shoreline survey	20211026_sl	Trimble R12	spatial	GIS	Whole survey area	20211026	NAD83 State Plane NC ft NAVD88 ft	Modified to include shoreline classifications	NCSU
Shoreline survey	20211123_sl	Trimble R12	spatial	GIS	Whole survey area	20211123	NAD83 State Plane NC ft NAVD88 ft	Modified to include shoreline classifications	NCSU
Shoreline survey	20200622_sl	Trimble R12	spatial	GIS	Whole survey area	20200622	NAD83 State Plane NC ft NAVD88 ft	Modified to include shoreline classifications	NCSU
Shoreline survey	20191113_sl	Trimble R10	spatial	GIS	Whole survey area	20191113	NAD83 State Plane NC ft NAVD88 ft	Modified to include shoreline classifications	NCSU
Shoreline survey	20191125_sl	Trimble R10	spatial	GIS	Whole survey area	20191125	NAD83 State Plane NC ft NAVD88 ft	Modified to include shoreline classifications	NCSU

Shoreline survey	20200812_sl	Trimble R12	spatial	GIS	Whole survey area	20200812	NAD83 State Plane NC ft NAVD88 ft	Modified to include shoreline classifications	NCSU
Wrackline survey	20210503_wk	Trimble R12	spatial	GIS	Whole survey area	20210503	NAD83 State Plane NC ft NAVD88 ft		NCSU
Wrackline survey	20210308_wk	Trimble R12	spatial	GIS	Whole survey area	20210308	NAD83 State Plane NC ft NAVD88 ft		NCSU
Wrackline survey	20210908_wk	Trimble R12	spatial	GIS	Whole survey area	20210908	NAD83 State Plane NC ft NAVD88 ft		NCSU
Wrackline survey	20211026_wk	Trimble R12	spatial	GIS	Whole survey area	20211026	NAD83 State Plane NC ft NAVD88 ft		NCSU
Wrackline survey	20211123_wk	Trimble R12	spatial	GIS	Whole survey area	20211123	NAD83 State Plane NC ft NAVD88 ft		NCSU
Wrackline survey	20200812_wk	Trimble R12	spatial	GIS	Whole survey area	20200812	NAD83 State Plane NC ft NAVD88 ft		NCSU
Bathymetry	20191011_low soundings_grid	Single beam echosounder connected to a Z boat	spatial	GIS	Whole survey area	20191011	GCS NAD83 m NAVD88 m		Michael Grillot, NHERI
Bathymetry	20190507_bathy_tidecorrected_NAVD88	Deeper sonar	spatial	textfile	Whole survey area	20190507	GCS NAD 83 m NAVD88 m		USNA
Bathymetry	20191011_hisound_contours	Single beam echosounder connected to a Z boat	spatial	GIS	Whole survey area	20191011	GCS NAD83 m NAVD88 m		Michael Grillot, NHERI
Bathymetry	20191011_his	Single beam	spatial	GIS	Whole	20191011	GCS NAD83 m		Michael Grillot,

	oundings_grid	echosounder connected to a Z boat			survey area		NAVD88 m		NHERI
Bathymetry	20210420_bathy_contours	Kayak with echosounder	spatial	GIS	Whole survey area	20210420	UTM Zone 18N m NAVD88 m		Dr. Peter Traykovski Woods Hole Oceanographic Inst.
Bathymetry	202104_bathy_grid	Kayak with echosounder	spatial	GIS	Whole survey area	20210420	UTM Zone 18N m NAVD88 m		Dr. Peter Traykovski Woods Hole Oceanographic Inst.
Currents	20191008_Currents	Signature 1000 ADCP mounted to boat	Temporal & spatial	textfile	Tidal channel various locations	20191008	meters/sec		USNA/NCDOT/NCSU
Currents	2020_Aquadoppp	Aquadoppp ADCP	temporal	textfile	Deployed in stationary mount in channel	20200826 - 20201001	meters/sec		USNA/NCDOT/NCSU
Currents	2020_Signature	Signature 1000 ADCP	temporal	textfile	Deployed in stationary mount in channel	20200826 - 20201001	meters/sec		USNA/NCDOT/NCSU
Currents	Transect_1_D AV_Ebb	Signature 1000 ADCP mounted to boat	Temporal & spatial	textfile	Tidal channel Transect 1 (north)	20211028	meters/sec	Depth averaged velocity components on ebb at Transect 1	USNA/NCDOT
Currents	Transect_1_D AV_Flood	Signature 1000 ADCP mounted to boat	Temporal & spatial	textfile	Tidal channel Transect 1 (north)	20211026	meters/sec	Depth averaged velocity components on flood at Transect 1	USNA/NCDOT
Currents	Transect_2_D AV_Ebb	Signature 1000 ADCP mounted to boat	Temporal & spatial	textfile	Tidal channel Transect 2 (middle)	20211028	meters/sec	Depth averaged velocity components on ebb at Transect 2	USNA/NCDOT
Currents	Transect_2_D	Signature	Temporal	textfile	Tidal	20211026	meters/sec	Depth averaged	USNA/NCDOT

	AV_Flood	1000 ADCP mounted to boat	& spatial		channel Transect 2 (middle)			velocity components on flood at Transect 2	
Currents	Transect_3_D AV_Ebb	Signature 1000 ADCP mounted to boat	Temporal & spatial	textfile	Tidal channel Transect 3 (south)	20211028	meters/sec	Depth averaged velocity components on ebb at Transect 3	USNA/NCDOT
Currents	Transect_3_D AV_Flood	Signature 1000 ADCP mounted to boat	Temporal & spatial	textfile	Tidal channel Transect 3 (south)	20211026	meters/sec	Depth averaged velocity components on flood at Transect 3	USNA/NCDOT
Water Levels	North Transect HOBO at Wrackline	HOBO	temporal	textfile	Stationary deployment near wrackline	20210308 - 20211028	NAVD88 meters		USNA/NCSU
Water Levels	North Transect HOBO on Marsh Edge	HOBO	temporal	textfile	Stationary deployment near marsh edge (north side)	20210308 - 20211028	NAVD88 meters		USNA/NCSU
Water Levels	South Transect HOBO on Marsh Edge	HOBO	temporal	textfile	Stationary deployment near marsh edge (south side)	20210308 - 20211028	NAVD88 meters		USNA/NCSU
Water Levels	2019_Marsh	TruBlue 255	temporal	textfile	Stationary deployment in marsh	20191011 - 20191022	meters	Depth	USNA/NHERI
Water Levels	2019_Piling	TruBlue 255	temporal	textfile	Stationary deployment at piling	20191026 - 20191109	meters	Mean-subtracted water level	USNA/NHERI
Water Levels	2019_Shoreline	TruBlue 255	temporal	textfile	Stationary deployment near shoreline	20191011 - 20191110	meters	Mean-subtracted water level	USNA/NHERI

Water Levels	2020_MarshNorth	HOBO	temporal	textfile	Stationary deployment Marsh North	20200826 - 20201001	NAVD88 meters		USNA/NCSU
Water Levels	2020_MarshSouth	HOBO	temporal	textfile	Stationary deployment Marsh South	20200622 - 20201001	NAVD88 meters		USNA/NCSU
Water Levels	2020_Piling	HOBO	temporal	textfile	Stationary deployment at piling	20200622 - 20201001	meters	Mean-subtracted water level	USNA/NCSU
Water Levels	2020_ShorelineSouth	HOBO	temporal	textfile	Stationary deployment near south shoreline	20200622 - 20201001	meters	Mean-subtracted water level	USNA/NCSU
Water Levels	2020_ShorelineNorth	HOBO	temporal	textfile	Stationary deployment near north shoreline	20200826 - 20201001	meters	Mean-subtracted water level	USNA
Field Notes	20200622_field_notes			PDF	Whole survey area	20200622			NCSU
Field Notes	20200812_field_notes			PDF	Whole survey area	20200812			NCSU
Field Notes	20200826_field_notes			PDF	Whole survey area	20200826			NCSU
Field Notes	20191113_fieldnotes			PDF	Whole survey area	20191113			NCSU
Field Notes	20191125_fieldnotes			PDF	Whole survey area	20191125			NCSU
Sediment	201910_dunepilotsedimentsummary	Grab sampler, mastersizer	spatial	XLSX	Whole survey area	201910	GCS NAD83, micrometer		USNA/NCSU

Sediment	201910_sed_d10	mastersizer	spatial	GIS	Whole survey area	201910	GCS NAD83, micrometer		USNA/NCSU
Sediment	201910_sed_d50	mastersizer	spatial	GIS	Whole survey area	201910	GCS NAD83, micrometer		USNA/NCSU
Sediment	201910_sed_d90	mastersizer	spatial	GIS	Whole survey area	201910	GCS NAD83, micrometer		USNA/NCSU
Location Map	201910_Water Level_Sensor_Locations		spatial	GIS	Whole survey area	201910	GCS WGS 1984		NCSU/USNA
Location Map	201910_Land SedSamples_WLsensors		image	PNG	Whole survey area	201910		Figure image	NCSU/USNA
Location Map	20200622_Locations		spatial	GIS	Whole survey area	20200622	NAD 83 State Plane NC ft		NCSU
Location Map	20200622_InstrumentLocMap		image	JPG	Whole survey area	20200622		Figure image	NCSU
Location Map	2021DeploymentsLocationMap		image	JPG	Whole Survey Area	20210308-20210923		Figure image	USNA
Location Map	20210308_wlgauges_locations		spatial	GIS	Whole survey area	20210308	NAD83 State Plane NC ft		NCSU

Location Map	20210923_wl_tilt_gauges_locations		spatial	GIS	Whole survey area	20210923	GCS WGS 84		NCSU/USNA
Plant ID Guides	Plant_Identification_Guides		document	PDF		2019			NCSU
Soundside Flooding Events	Historic_Soundside_Flooding_events		temporal	XLSX	Whole survey area	2019-2021			NCSU
Geodatabase	RP2020-09Data.mdb		spatial	GIS	Whole survey area	2019-2021		Geodatabase containing all GIS files from the project (enumerated above)	NCSU

